11 May 2007 | S10

Science

AAAS

Systems that set the standard, software that's a step ahead.

Lead the way with a Stratagene personal QPCR system featuring enhanced MxPro™ QPCR Software.

Our Mx3000P® and Mx3005P™ personal quantitative PCR (QPCR) Systems combine an advanced optical system with powerful data analysis to give you complete flexibility at an affordable price. Our open platform design supports traditional and advanced applications as well as newly emerging QPCR chemistries. In addition, our MxPro™ QPCR Software combines leading edge data analysis algorithms with intuitive organization designed for ultimate ease-of-use.

- **Four- or five-color systems to best fit your research needs**
- **96-well thermal block with temperature uniformity of +/-0.25°C**
- **New MxPro™ QPCR Software with optional features for 21 CFR Part 11 compatibility**

Need More Information? Give Us A Call:

Stratagene US and Canada
Order: 800-424-5444 x3
Technical Service: 800-894-1304 x2

Stratagene Japan K.K.
Order: 3-5821-8077
Technical Service: 3-5821-8076

Stratagene Europe
Order: 00800-7000-7000
Technical Service: 00800-7400-7400

www.stratagene.com

STRATAGENE

Genetic Data Management and Analysis System

Introducing the Rosetta Syllego™ system, a genetic data management and analysis solution. The path to breakthrough science just became more straightforward. With the Rosetta Syllego system, you can better plan and execute genetic studies and ensure high-quality data to prevent loss of time in downstream analyses. It also helps you connect relevant genotypic and phenotypic study data and catalog these data and analysis results for drawing solid conclusions. All so you can focus on what really matters—advancing your research and drug development programs. Go to **www.rosettabio.com/syllego** for more information.

ROSETTA
BIOSOFTWARE

1.800.737.6583 (U.S.)
+1.206.926.1220 (Outside the U.S.)
sales@rosettabio.com

GE Healthcare

ÄKTA™

100,000 scientists working with proteins believe in ÄKTA, UNICORN and wizards.

To 100,000 scientists worldwide, ÄKTA™ sets the standard in protein purification. All systems in the ÄKTAdesign™ family work with intelligent UNICORN™ software, which makes it easy to control every stage of your purification process. But we're never content to stand still. The result is products like ÄKTAxpress™, which can solve low expression and double-tagged protein purification challenges, and ÄKTApurifier™, a time-saving automated protein purification system that can be configured to suit your personal application and workflow needs.

By continually developing technology that can turn your scientific ideas into reality, we're bringing science to life and helping transform healthcare.

We call it Protein Separations Re-imagined.

Discover the legendary purification power of UNICORN and ÄKTA, visit www.gehealthcare.com/akta

imagination at work

GE Healthcare Bio-Sciences AB, a General Electric Company.
Björkgatan 30, 751 84 Uppsala, Sweden

GE09-06. First printed 2006

Volume 316, Issue 5826

COVER

A bat, *Glossophaga soricina*, in flight within a wind tunnel. The air velocity field induced by the wingbeat is shown by superimposed arrows and to scale. The reconstructions of the wake produced by bat flight, reported on page 894, have features that are not observed in the wakes of similarly sized birds.

Image: L. C. Johansson, M. Wolf, and A. Hedenström

DEPARTMENTS

EDITORIAL

NEWS OF THE WEEK

NEWS FOCUS

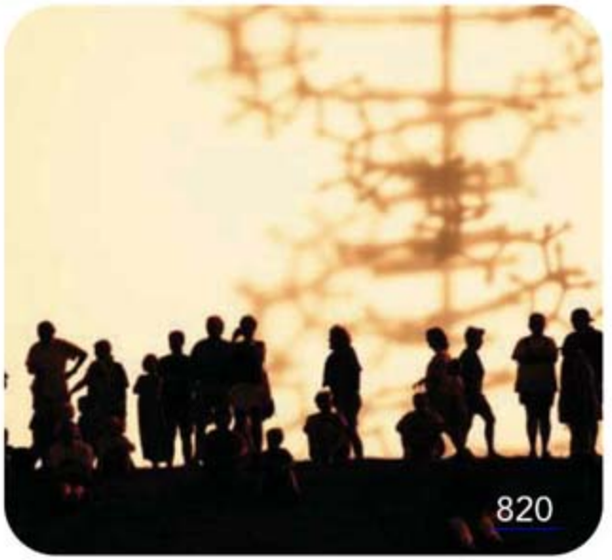

LETTERS

BOOKS *ET AL.*

POLICY FORUM

PERSPECTIVES

838

CONTENTS continued >>

QIAcube — pure efficiency

New

Winner of the New Product Award (NPA) Designation of the Association for Laboratory Automation (ALA) 2007

reddot design award winner 2007

reddot design award
product design 2007

- Eliminate manual processing steps
- Continue to use trusted QIAGEN spin-column kits
- Free up your time with affordable, automated sample preparation
- Purify DNA, RNA, or proteins from up to 12 samples per run
- Standardize your results and increase your productivity

Contact QIAGEN today or visit www.qiagen.com/MyQIAcube .

QIAGEN®

Sample & Assay Technologies

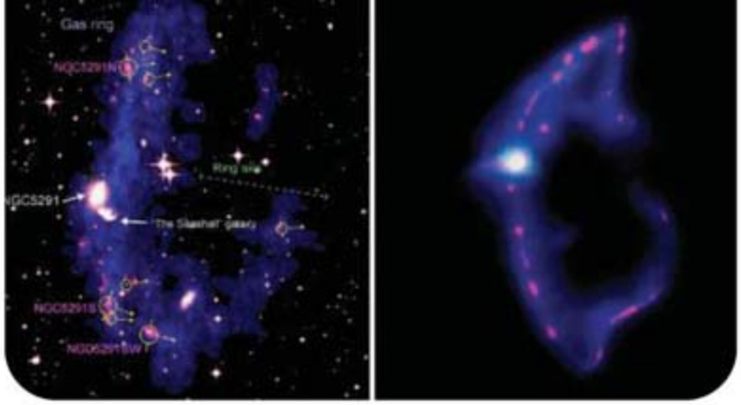

SCIENCE EXPRESS

www.sciencexpress.org

ASTROPHYSICS

Missing Mass in Collisional Debris from Galaxies
F. Bournaud et al.
The motion of gas clouds in dwarf galaxies shows that they surprisingly contain dark matter, perhaps unseen cold molecular gas that could be more common than thought.
10.1126/science.1142114

PERSPECTIVE: Proteasomes Keep the Circadian Clock Ticking
D. Gatfield and U. Schibler
10.1126/science.1144165

POLICY FORUM: Tropical Forests and Climate Policy
R. E. Gullison et al.
10.1126/science.1136163

CLIMATE CHANGE

Marine Radiocarbon Evidence for the Mechanism of Deglacial Atmospheric CO_2 Rise
T. M. Marchitto, S. J. Lehman, J. D. Ortiz, J. Flückiger, A. van Geen
Carbon-14 dates from a sediment core imply that Pacific deep waters stored CO_2 during glacial times and then vented it as deglaciation started, accelerating the temperature rise.
10.1126/science.1138679

PERSPECTIVE: Deglaciation Mysteries
R. F. Keeling
10.1126/science.1142326

REVIEW

BREVIA

RESEARCH ARTICLES

REPORTS

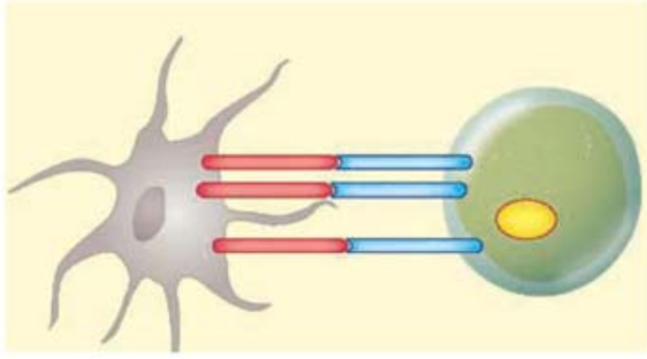

840 & 860

CONTENTS continued >>

Uncover apoptosis: a sensitive and sensible approach

Invitrogen BioSource™ phosphoELISA™ assays for studying apoptosis

Apoptosis, or programmed cell death, is essential to the development, immunological competence, and homeostasis of living things. It has become one of the most widely researched cell processes in biology, with over 1,200 articles published monthly in the past year alone.

Induction of apoptosis unfolds a cascade of events that triggers the activation of effector caspase proteases. Caspase proteases then cleave poly (ADP-ribose) polymerase (PARP), a 116 kDa nuclear protein typically involved in DNA damage detection and repair, between Asp214 and Gly215. This cleavage produces the p85 and p25 fragments, effectively eliminating DNA repair by PARP during apoptosis and committing the cell to the apoptotic pathway (Figure 1).

Many assays designed for examining apoptosis rely upon the activation of caspases. However, caspase proteases are rapidly degraded, making them difficult to detect and often overlooked by existing methods. Fortunately, there are other targets available for measuring apoptotic activity. Since PARP cleavage plays a significant role in apoptosis, PARP, p25, and p85 are ideal markers for these assays.

Invitrogen's Cleaved PARP [214/215] phosphoELISA™ Kit is designed to detect and quantify ultrasensitive levels of the human PARP p85 fragment. Conveniently packaged as a ready-to-use kit, it provides sensitive quantitative results in only four hours. In fact, the Cleaved PARP [214/215] phosphoELISA™ Kit can detect apoptosis in as few as 50–100 cells, making it 100x more sensitive than caspase-3 protease assays (Figure 2) and 10x more sensitive than western blot detection (Figure 3).

Now you can decisively uncover apoptotic activity in your experiment with the Cleaved PARP [214/215] phosphoELISA™ Kit. To learn more and find additional apoptosis-related products, visit www.invitrogen.com/biosource. Your search for apoptosis solutions is over.

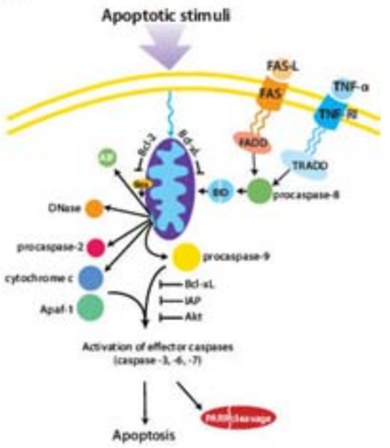

Figure 1—Pathway of PARP cleavage by caspases.

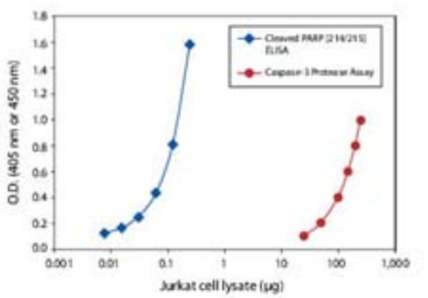

Figure 2—Sensitivity comparison of the Cleaved PARP [214/215] phosphoELISA™ Kit to a caspase-3 protease assay. Jurkat cells were treated with 1 µM staurosporine for 3 hours. Cell extracts were prepared. Cell lysates were serially diluted and analyzed with the Cleaved PARP [214/215] phosphoELISA™ Kit (Cat. no. KHO0741) and Caspase-3 Colorimetric Kit (Cat. no. KHZ0021). The amount of cell lysate assayed was plotted against the corresponding O.D. signal.

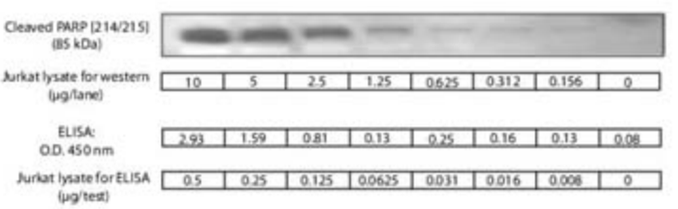

Figure 3—Detection of cleaved PARP [214/215] by ELISA and western blot. Jurkat cells were treated with staurosporine. The amounts of cell lysate used in western blotting and ELISA are indicated. Different amounts of cell lysate were used due to the much higher sensitivity of ELISA. The bands shown in the western blotting data were developed using rabbit anti–cleaved PARP [214/215] (Cat. no. 44-698G) and an alkaline phosphatase–conjugated anti–rabbit IgG followed by chemiluminescent substrate and autoradiography.

Science

REPORTS *CONTINUED...*

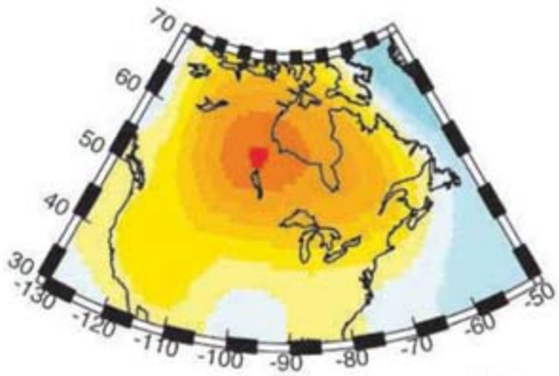

881

904

AAAS
ADVANCING SCIENCE, SERVING SOCIETY

SCIENCE (ISSN 0036-8075) is published weekly on Friday, except the last week in December, by the American Association for the Advancement of Science, 1200 New York Avenue, NW, Washington, DC 20005. Periodicals Mail postage (publication No. 484460) paid at Washington, DC, and additional mailing offices. Domestic individual membership and subscription (51 issues): $142 ($74 allocated to subscription). Domestic institutional subscription (51 issues): $710; Foreign postage extra: Mexico, Caribbean (surface mail) $55; other countries (air assist delivery) $85. First class, airmail, student, and emeritus rates on request. Canadian rates with GST available upon request, GST #1254 88122. Publications Mail Agreement Number 1069624. **Printed in the U.S.A.**

Change of address: Allow 4 weeks, giving old and new addresses and 8-digit account number. **Postmaster:** Send change of address to AAAS, P.O. Box 96178, Washington, DC 20090–6178. **Single-copy sales:** $10.00 current issue, $15.00 back issue prepaid includes surface postage; bulk rates on request. **Authorization to photocopy** material for internal or personal use under circumstances not falling within the fair use provisions of the Copyright Act is granted by AAAS to libraries and other users registered with the Copyright Clearance Center (CCC) Transactional Reporting Service, provided that $18.00 per article is paid directly to CCC, 222 Rosewood Drive, Danvers, MA 01923. The identification code for *Science* is 0036-8075. *Science* is indexed in the *Reader's Guide to Periodical Literature* and in several specialized indexes.

CONTENTS continued >>

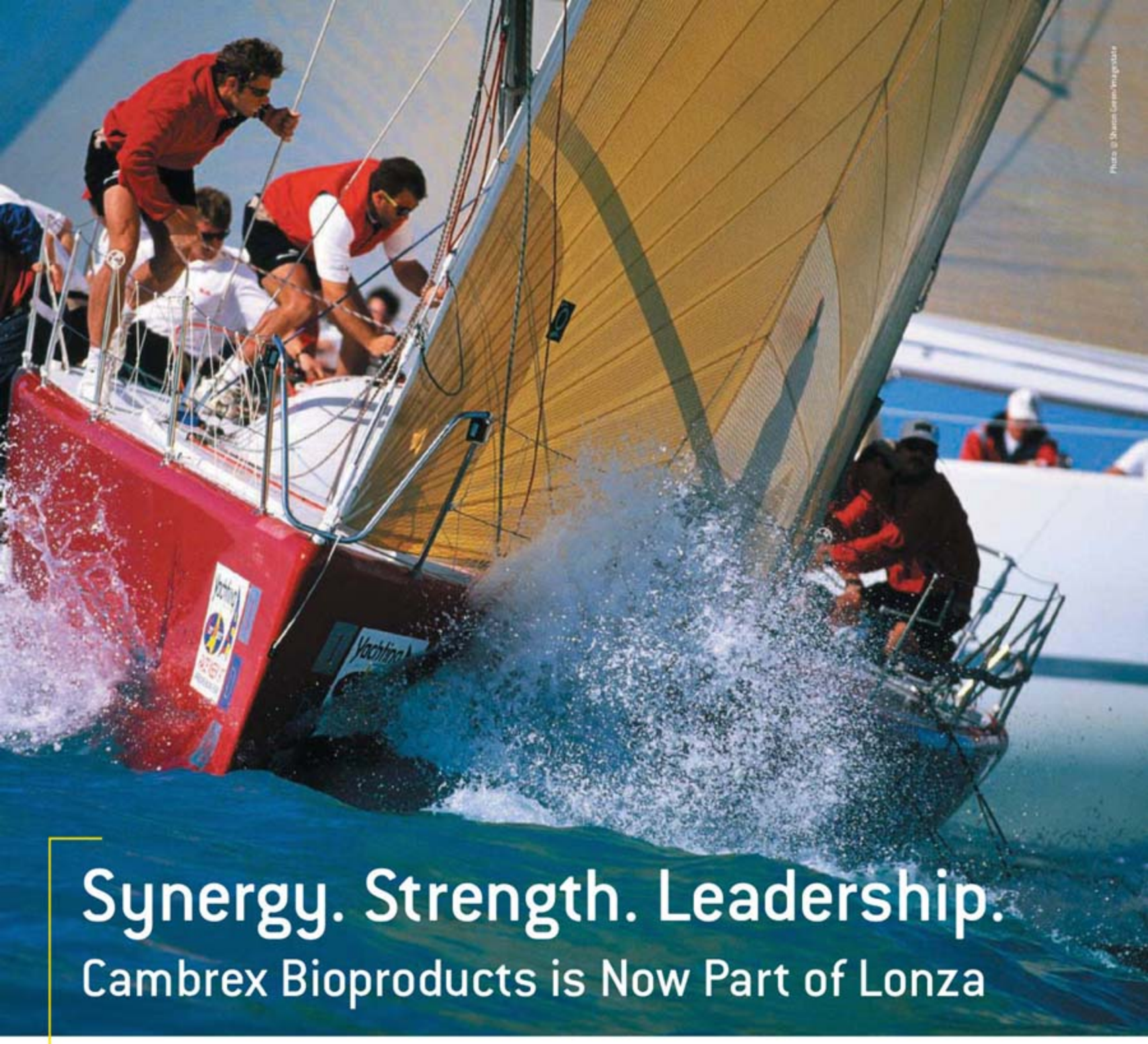

Synergy. Strength. Leadership.

Cambrex Bioproducts is Now Part of Lonza

Following the acquisition of Cambrex Bioproducts, Lonza is now your leading supplier of cutting edge products for cell and molecular biology, including:

- Clonetics® & Poietics™ Primary Cells & Media
- BioWhittaker® Media & Sera
- MycoAlert® Mycoplasma Detection Assays
- SeaKem®, NuSieve® & MetaPhor® Agarose

We offer the same dedicated sales, marketing, customer service and technical support teams you know – and the quality and reliability you trust. Visit www.lonzabioscience.com/bioproducts to find out more about our research products.

US 800-638-8174 or 301-898-7025 • Europe 32 (0) 87 321 611
www.lonza.com

Lonza

Eta Carinae—a prime supernova candidate.

SCIENCENOW

www.sciencenow.org DAILY NEWS COVERAGE

Star Goes Out Big Time
Astronomers track a new kind of supernova, the brightest ever recorded.

Ancient Australians Were a People Apart
Genetic evidence confirms Aborigines lived in isolation for thousands of years.

Trick Three-Planet Orbit Remains True
Einstein's theory of gravity permits weird figure-8 orbit, at least temporarily.

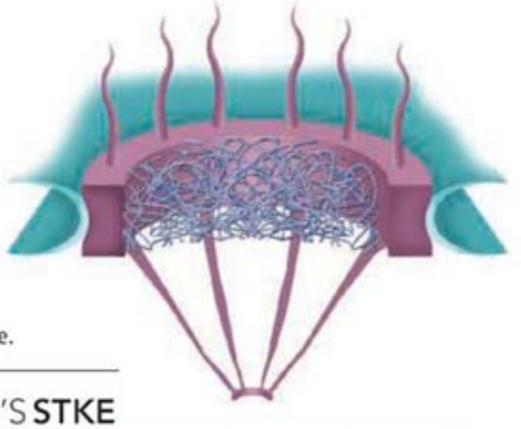

The nuclear pore.

SCIENCE'S STKE

www.stke.org SIGNAL TRANSDUCTION KNOWLEDGE ENVIRONMENT

PERSPECTIVE: Extrasynaptic NMDA Receptors Reshape Gene Ranks
I. Medina
Activation of synaptic or extrasynaptic NMDARs produces different gene expression profiles, which may explain their distinct roles in neuronal survival and death, respectively.

PERSPECTIVE: The Regulation of Nuclear Membrane Permeability by Ca^{2+} Signaling—A Tightly Regulated Pore or a Floodgate?
K. Török
Do calcium signals lead to specific or nonspecific increases in the permeability of the nuclear pore complex?

FORUM: Combining Simulation Techniques to Create a Model
J. Shillcock
Follow this ongoing discussion of mesoscopic models for spatial mechanisms of cell signaling.

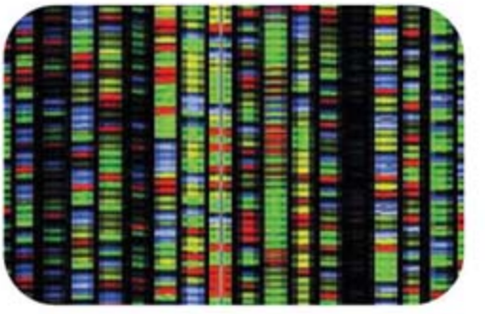

A molecular geneticist studies bygone eras.

SCIENCE CAREERS

www.sciencecareers.org CAREER RESOURCES FOR SCIENTISTS

CANADA: Opening Minds to Ancient Times
A. Fazekas
Molecular evolutionary geneticist Hendrik Poinar says collaboration and communication are keys to his success.

FRANCE: Still Learning
E. Pain
At age 33, Julia Kempe has four postgraduate degrees and tenure, but she has refused to settle down.

US: Opportunities—More School?
P. Fiske
Should a Ph.D. scientist get a master's degree in business administration?

US: From the Archives—Be Honorable and Strategic
C. Golde
In negotiating an academic job, knowing what you need helps make a compelling case.

CREDIT (SCIENCE CAREERS): NATIONAL SCIENCE FOUNDATION

Separate individual or institutional subscriptions to these products may be required for full-text access.


2005/06


2002/03


2000/01


1998/99


1996/97


1995


1993/94


1992


1990/91


1988/89


1986/87


1985/86


1983/84


1982/83


1981/82


1980/81


1979


1978


1975/76

2007/08 NEB catalog & technical reference is now available.

in a word, essential.

www.neb.com

NEW ENGLAND BioLabs® Inc.
the leader in enzyme technology

New England Biolabs Inc.
240 County Road, Ipswich, MA 01938 USA 1-800-NEB-LABS Tel. (978) 927-5054 Fax (978) 921-1350 info@neb.com
Canada Tel. (800) 387-1095 info@ca.neb.com • **China** Tel. 010-82378266 beijing@neb-china.com
Germany Tel. 0800/246 5227 info@de.neb.com • **Japan** Tel. +81 (0)3 5669 6191 info@neb-japan.com
UK Tel. (0800) 318486 info@uk.neb.com
For a complete list of international offices, please visit www.neb.com

Magnetic Misalignment >>

The two Voyager spacecraft detected a series of radio sources that lie just beyond the heliopause, the outer extent of the solar wind–inflated bubble that encases the solar system. These radio sources may originate from the intersection of an interplanetary shock with the heliopause, but model studies have required assumptions about the direction of the interstellar magnetic field in this region. The orientation of the local field introduces asymmetries that affect the location of radio emission and the streaming direction of ions from the termination shock of the solar wind. Others have assumed that the magnetic field is aligned with the galactic plane, as it is on large scales in the Milky Way. However, by comparing a magneto-hydrodynamic model of the heliosphere with Voyager observations, **Opher *et al.*** (p. 875; see the Perspective by **Jokipii**) show that locally the interstellar magnetic field is misaligned by 60° to 90° relative to the galactic plane.

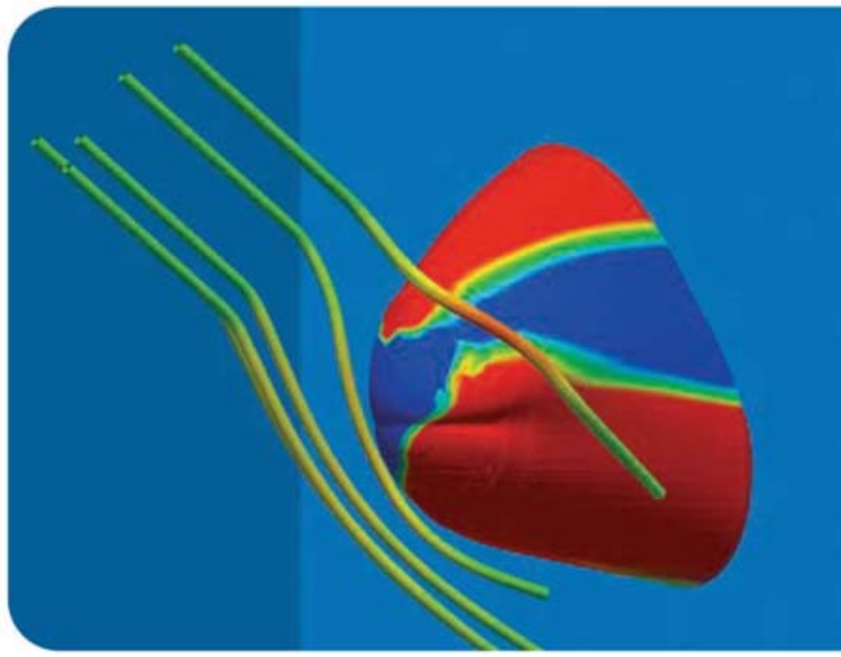

Pairing Up But Not Condensing

When equal populations of fermions of opposite spin states come together, they can be expected to pair and condense into a macroscopically coherent state, such as a superfluid. What happens when the initial populations are unequal? **Schunck *et al.*** (p. 867; see the news story by **Cho**) look at conditions of strong population imbalance using clouds of fermionic gases. Pairing of the atoms occurs, but condensation of the pairs into the superfluid state is suppressed by the imbalance, even down to the lowest temperatures.

Fighting Desertification

Drylands host more than one-third of the world's population, including many of the poorest inhabitants of developing nations. These areas are likely to be impacted disproportionately by global warming, but efforts to stem outcomes such as desertification are hampered by a limited understanding of the interconnectivity of dryland ecosystems and human social systems. **Reynolds *et al.*** (p. 847) offer a framework for a more integrative approach to understanding dryland development and combating desertification, with particular emphasis on constructing solutions that synthesize scientific, management, and policy concerns.

CREDITS (TOP TO BOTTOM): COURTESY OF OPHER, STONE, AND GOMBOSI; REYNOLDS *ET AL.*

Foggy Fallout

Titan's orange haze is caused by a smog of organic molecules created in its atmosphere. Some of the heavier red-brown organic molecules, called tholins, are thought to precipitate onto Titan's surface. It has been thought that tholins form at stratospheric heights in Titan's lower atmosphere, but **Waite *et al.*** (p. 870; see the Perspective by **Atreya**) show that they form at much higher altitudes (about 1000 kilometers). Analysis of data taken by the Cassini spacecraft shows that a series of chemical reactions transform simple organic molecules (such as methane and nitrogen molecules) into much larger molecules (with masses of 80 to 350 daltons). Eventually, these molecules form organic molecules as heavy as 8000 daltons that also bear a negative charge.

Crumbing Carbonates

As earthquakes propagate, their actions may actively weaken previously stable faults through changes in the rocks at high velocity. **Han *et al.*** (p. 878; see the Perspective by **Madariaga**) demonstrate experimentally that frictional heating causes dramatic fault weakening in Carrara marble. At the sliding fault interface, heat causes the marble to decompose into fine particles tens of nanometers in size that make it more slippery. Such effects could make earthquakes rupture more easily in carbonate rocks.

Ice, the Mantle, and Canadian Gravity Lows

Terrestrial gravity above a point on Earth can vary with changes in the amount or density of underlying mass. In northern Canada, a large depression of the continental craton has created a region of anomalously low gravity. This topographic low may be the remnants of the depression made by the Laurentide Ice Sheet, in the case of incomplete rebound of the crust (glacial isostatic adjustment, or GIA) after the melting of the ice sheet at the end of the Last Glacial Maximum, or the result of active downwelling of the mantle. **Tamisiea *et al.*** (p. 881) examine 4 years of data from the Gravity Recovery and Climate Experiment (GRACE) satellites and conclude that GIA has contributed 40 to 50% of the gravity anomaly over the area. They also infer that the Laurentide Ice Sheet had two large domes during the Last Glacial Maximum, rather than only one as some studies have suggested.

Masterful Decisions

In the immune system, B and T lymphocytes develop via distinct pathways from common bone marrow progenitors, and the signaling protein Notch plays a crucial role in deciding T cell fate determination. **Maeda *et al.*** (p. 860; see the Perspective by **Maillard and Pear**) now find that a proto-oncogene called *LRF* represses this

Continued on page 795

www.roche-applied-science.com

Introducing Our Second Generation Genome Sequencing System

Genome Sequencer FLX

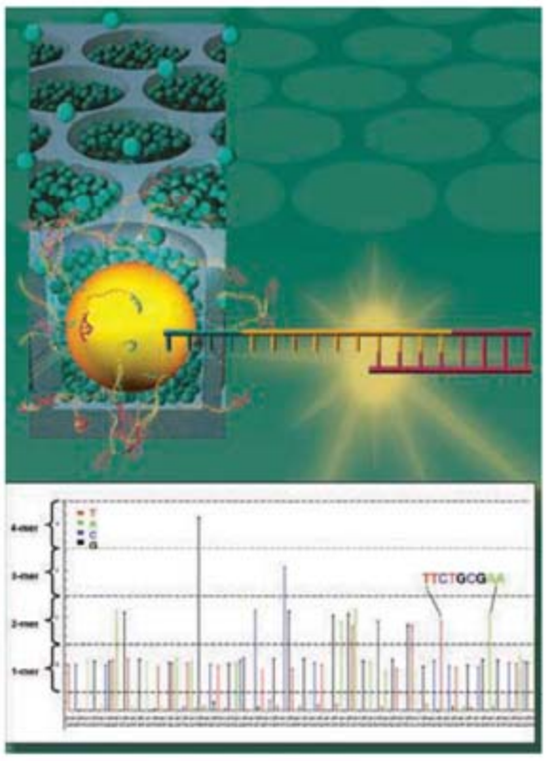

Be First to the Finish with...

- Increased read lengths averaging 200 to 300 bases per read
- Throughput of more than 400,000 reads per run
- High single-read accuracy greater than 99.5% over 200 bases
- Consensus-read accuracy greater than 99.99%

...more Flexibility and more Applications.

Visit ***www.genome-sequencing.com*** to learn about the expanding number of peer-reviewed publications appearing weekly.

454 LIFE SCIENCES

Roche Diagnostics

Roche Diagnostics GmbH
Roche Applied Science
68298 Mannheim
Germany

Continued from page 793

Notch signal and in so doing induces progenitors to undergo a B cell developmental program. Thus, *LRF* may act as a master regulator in the cell fate decision that generates the two main arms of the adaptive immune system.

IP_4 Recruits Signaling Proteins

Inositol phosphates are important intracellular second messengers in eukaryotic cells. In particular, higher-order inositol polyphosphates regulate a range of biological processes, from chromatin remodeling to calcium signaling. **Huang *et al.*** (p. 886, published online 5 April; see the Perspective by **Irvine**) now report that inositol 1,3,4,5-tetrakisphosphate (IP_4) plays an unexpected role in T cells by modifying a well-established protein recruitment pathway. Soluble IP_4 in the cell was found to lock onto pleckstrin homology domains that regulate the recruitment of signaling proteins to the cell membrane for activation during T cell development.

Genetic Factor in Obesity

To be considered robust, genetic association studies must be confirmed in more than one independent set of subjects. **Frayling *et al.*** (p. 889, published online 12 April; see the 13 April news story by **Kaiser**) present a genome scan of DNAs from a large case-control study for type 2 diabetes and identify a common genetic variant associated with obesity and a risk of being overweight. These findings of were confirmed in 12 additional cohorts, among a total of 38,759 individuals. On average, individuals homozygous for the high-risk allele weighed nearly 3 kilograms more than individuals homozygous for the low-risk allele. The effect was consistent across samples, across ages (from 7 years upward), across genders, and irrespective of diabetes status.

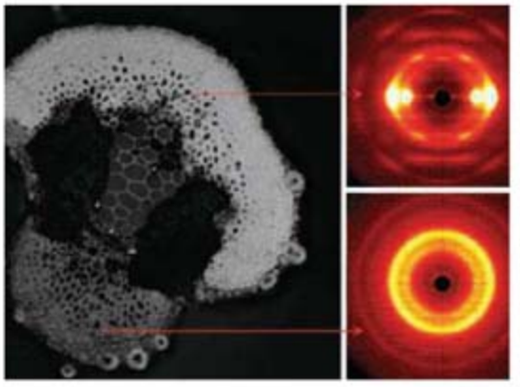

CREDIT: ELBAUM ET AL.

Awns and Seed Dispersal

Awns are pointed projections on the seeds of wheat and other grasses that play a role in the dispersal of seeds in the air and on the ground. **Elbaum *et al.*** (p. 884) show how changes in humidity lead to bending of the awns as the result of moisture-induced changes in the arrangement of the awn's cellulose fibrils. In turn, the bending of the awns not only pushes the seed along the ground, but can even lead to the active burial of the seed, which presumably improves the chances of germination.

Bat Flight Control

When animals fly, their wings produce a vortex wake that can provide clues about the aerodynamic forces they generate. **Hedenström *et al.*** (p. 894; see the cover) describe unusual aerodynamic features of the wake topology for the small bat species *Glossophaga soricina*, using digital particle image velocimetry that captures the movement of fog particles in the wake of flying animals. The two wings generate separate vortices, interlinked by vortex structures shed from the body. During the upstroke the outer (hand) part of the wing generates negative lift, while the inner part of the wing (arm) generates positive lift. Different parts of the wing produce extra vortices in the wake, which differ significantly from the wakes produced by birds.

Subliminal Motivation

Humans are normally aware of their motivation, such as during athletic training or studying for an exam. Can motivation also be unconscious, such that a person is unable to report the goals or rewards that drive a particular behavior? **Pessiglione *et al.*** (p. 904, published online 12 April) developed an incentive force task using either one penny or one pound as a reward. The coins were displayed at different durations so that they were either consciously or subliminally perceived. Using functional magnetic resonance imaging and measuring a range of other physiological parameters, the authors found that even when the subjects were not consciously aware of the size of the reward, they nonetheless exerted more force in association with higher stakes.

Louise M. Slaughter has represented New York's 28th Congressional District since 1986 and is chair of the U.S. House Committee on Rules. She has an MS degree in Public Health.

Your Genes and Privacy

THE GENETIC INFORMATION NONDISCRIMINATION ACT (GINA) LANGUISHED IN past Congresses for 12 years. But finally, new leadership in the House of Representatives has given the bill its best chance to become law since its introduction in 1995. On 25 April, GINA passed the House by a vote of 420 to 3. The act will prohibit health insurers from denying coverage or charging higher premiums to a healthy individual solely because they possess a genetic predisposition to develop a disease in the future. It will also bar employers from using genetic information in hiring, firing, job placement, or promotion decisions.

Over time, the need for GINA has only grown. We stand on the verge of some of the most stunning breakthroughs in modern medical history. The completion of the sequencing of the human genome enables researchers to identify genetic markers for a variety of chronic health conditions, offering a new approach to treat and prevent diseases. But without federal safeguards in place, the promise of genetic research will not be realized. Fear is the obstacle that must be overcome: fear that our personal genetic information could be abused and prevent us from getting the health insurance we need and the jobs we want. To benefit from gene-based medicine, the public's fear of genetic discrimination must be eliminated, and Congress has a responsibility to help allay the public's concerns.

Instances of genetic discrimination in the United States have already occurred. In the 1970s, many African-Americans were denied jobs, educational opportunities, and insurance based on their status as carriers of sickle cell anemia. In 2000, the Burlington Northern Santa Fe Railroad performed genetic tests on employees without their knowledge during an attempt to undermine a worker's compensation claim by proving that carpal tunnel syndrome has a genetic basis. And in 2004, a U.S. Department of Health and Human Services committee heard powerful testimony from victims of workplace and insurance discrimination. As a result of cases like these, public concern is palpable: In a 2006 survey, 66% of respondents reported worries about storage of and access to their genetic information, 72% agreed that the government should establish laws and regulations to protect the privacy of their genetic information, and 85% said that employers would use such information to discriminate unless current law was amended.

Genetic discrimination is, of course, inherently unjustifiable and illogical. Having a genetic predisposition to a disease in no way guarantees that it will develop, and virtually all of us have some bad genes that could potentially manifest in illness. As a result, discrimination based on one's genetic makeup alone could logically be extended into a form of discrimination against everyone. But what is more, the unease the public feels concerning how their genetic information will be used has a deeply negative impact on public health. If individuals are afraid of suffering discrimination at the hands of employers and insurance companies, they will be less likely to get genetic tests and receive needed preventative treatment. In the cases of breast or colon cancer, this could mean life or death.

Perhaps worst of all, genetic research is being stifled. Large samples of individuals must participate in genetic research studies to make them valid, and potential participants will hesitate if they fear losing their jobs or health insurance. Francis Collins, head of the National Human Genome Research Institute, and James Watson called attention to this problem in a 2003 *Science* editorial, writing that genetic discrimination will "slow the pace of the scientific discovery that will yield crucial medical advances" by resulting in studies based on "a self-selected group that could skew research results."

The responsibility of Congress to address the threat posed by genetic discrimination makes GINA's recent passage in the House significant. Because similar bills have already been approved by the Senate on two previous occasions, and because President Bush supports the proposal, its future looks bright. On the day that GINA is signed into law, an insidious form of discrimination will disappear, opening the door to a field of scientific research that holds as much promise as any in medical history.

– Louise M. Slaughter

10.1126/science.1144588

CREDIT: JANE ADES, NHGRI

One FailSafe™ PreMix is guaranteed to work.

Keep a dozen on hand for your PCR challenges

Using a unique blend of thermostable enzymes and a set of 12 standardized premixes, optimization of any PCR reaction is quick, easy and reproducible.

The FailSafe™ PCR System Amplifies—

- Up to 85% GC-rich templates
- Any templates up to 20 kb
- Multiplex PCR, consistently
- Low copy number templates

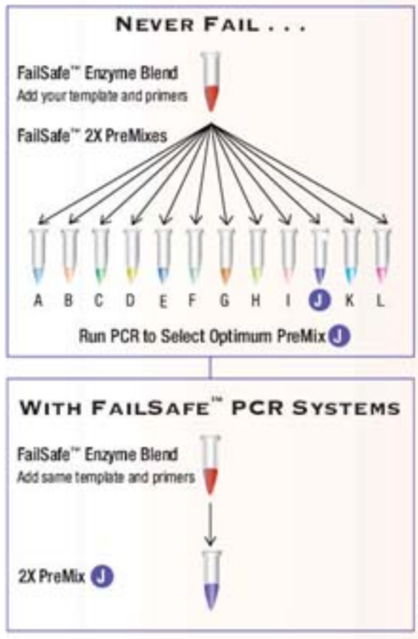

Amplification of an 80-85% GC-rich region of the human fragile X gene. PCR was performed using the FailSafe™ PCR System. Lanes A-L show the amplification products resulting from PCR using the 12 FailSafe PCR PreMixes. M, molecular weight marker. Optimal amplification was obtained with FailSafe PCR PreMix J.

Start using FailSafe and get your PCR to work
the *first time and every time.*

EPICENTRE offers a money-back guarantee for successful PCR with one or more PreMix. If you're not happy, you don't pay.

To order yours, go to **www.EpiBio.com**
and enter QuickInfo code: **FSA28**

EPICENTRE® Biotechnologies

EDITED BY GILBERT CHIN AND JAKE YESTON

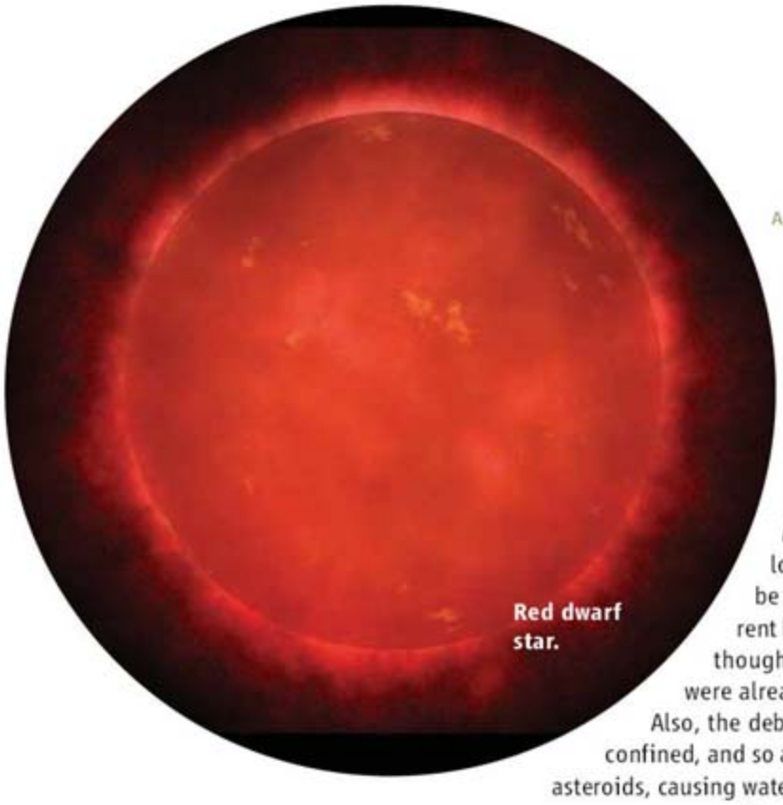

Red dwarf star.

ASTRONOMY

Not So Cozy

Habitable Earth-like planets must form just close enough to their parent star for liquid water—and hence life—to exist on their surfaces. Any closer and surface water would be boiled off; any further and it would freeze. Moreover, stars must be at least as long-lived as the Sun for habitable planets to form around them. Red dwarfs offer possible suitable sites: They are both the most common type of star in the Milky Way and also, being smaller than the Sun, exceptionally long-lived. However, Lissauer argues that red dwarfs may not be so hospitable after all. Because red dwarfs are faint, their current habitable zones lie very close to the star. Billions of years ago, though, the star would have been much hotter, and so if a planet were already in place then, its volatiles would have evaporated quickly. Also, the debris left over from disks around such star systems is relatively confined, and so any planets would have been buffeted by collisions with many asteroids, causing water and volatiles to be lost. — JB

Astrophys. J. **660**, L149 (2007)10.1111/j.1469-8137.2007.02103.x (2007).

ATMOSPHERIC SCIENCE

Sourcing Methane

Methane is a powerful trace greenhouse gas, second in importance only to carbon dioxide, and exerts an important influence on climate and atmospheric chemistry. Both anthropogenic and natural sources contribute substantially to the global methane budget. Recently, Keppler *et al.* claimed that terrestrial plants could produce large amounts of methane in aerobic conditions, an unexpected finding that, if true, would necessitate a major revision of our understanding of the methane cycle. Dueck *et al.* measured aerobic methane emissions from six different terrestrial plant species by employing a carbon-isotopic labeling technique for quantification. They found no evidence for substantial methane emission in any of the species, either instantaneously by continuous flow measurements or over the course of 6 days. They thus concluded that terrestrial plants are not an important source of aerobically produced methane on a global scale. — HJS

Nature **439**, 187 (2006); *New Phytol.* 10.1111/j.1469-8137.2007.02103.x (2007).

MICROBIOLOGY

Building from the Inside Out

The evolutionary origins of complex organs, which in their current state of assembly feature many distinct components that apparently have no function in isolation, have long been debated. Liu and Ochman have unraveled the history of the origins of bacterial flagella by using a phylogenetic profiling method applied across whole genome sequences to identify a set of 24 core genes in the common ancestor of bacteria. The members of this core set were probably derived from a single gene that had undergone a combination of successive duplication, loss, transfer, and diversification events. The evolution of the flagellar components apparently followed the present-day order of assembly, with the oldest proteins (the rotary motor) being those proximal to the bacterial inner membrane and the most recent (the filament monomers) being the most distal. Hence, the flagellum probably started life as a simple proton-driven transporter that evolved into a more elaborate secretory apparatus—of a sort still found in bacteria today in the form of the type III secretion system—and finally into the self-secretory motility organelle of modern species. — CA

***E. coli* flagella.**

Proc. Natl. Acad. Sci. U.S.A. **104**, 7116 (2007).

PSYCHOLOGY

Pas des Yeux

A dialogue, though generally understood to be a conversation between two people, allows for much more than the mere exchange of verbal information. Linguistic (for example, syntax) and nonlinguistic (for example, body postures) telltales develop and become synchronized as people talk and listen. Visual attention is another dimension in which behavior can become coordinated as when a listener's gaze is directed toward an object of mutual interest by pointing.

Richardson *et al.* show that the eyes of conversants—who are looking at the same scene but are not within sight of each other—tracked the same objects within the scene for several seconds, starting from the time at which the speaker began to fixate on the object before talking about it and including the time taken by the listener to saccade to the object after hearing what the speaker had begun to say. Another important contribution to the coordination of visual attention comes from having a common ground of understanding. Conversants looking at a Salvador Dalí painting were more likely to exhibit synchronized eye movements if they had previously heard the same introduction, either to the painting itself or to Dalí's life, as compared to pairs of conversants in which one had heard about the painting and the other about his life. — GJC

Psychol. Sci. **18**, 407 (2007).

Continued on page 801

CREDITS (TOP TO BOTTOM): NASA; CDC/PEGGY S. HAYES

Solved!

INNOVATION @ WORK

Innovative Solutions for Ion Channel Research

Puzzled over who will meet your ion channel research needs? Look no further. We have the most extensive line of innovative products for ion channel research.

- Subunit selective antibodies
- Toxins
- Inhibitors and activators
- RNAi libraries
- PCR/Amplification Reagents, Quantitative PCR, Real-time PCR
- Cloning Systems, kTransfection Reagents, Competent Cells, Expression Vectors
- Cell Culture Media, Supplements, Growth Factors

Sigma is the Solution.

Visit sigma.com/ionchannelsolutions for more information.

Sigma also offers these convenient online tools for your research:

Antibody Explorer
sigma.com/antibody

Sigma-RBI Handbook of Receptor Classification and Signal Transduction
sigma.com/ehandbook

Pathfinder Interactive Pathways
sigma.com/pathfinder

sigma.com

Accelerating Customers' Success through Leadership in **Life Science, High Technology** and **Service**

SIGMA-ALDRICH CORPORATION • BOX 14508 • ST. LOUIS • MISSOURI 63178 • USA

SIGMA®

Continued from page 799

CHEMISTRY

Shaped by a Protein

Hydrogels consist of water-soluble cross-linked polymers that can change properties such as their degree of swelling in response to changes in temperature, acidity, or ionic strength. Murphy *et al.* explored the use of a protein, calmodulin, as the active component of their gel systems. In the presence of calcium ions, calmodulin adopts an extended dumbbell shape that collapses upon the binding of certain ligands. The authors engineered a calmodulin variant with the tyrosine residues at the ends of the dumbbell motif replaced by cysteines. The two cysteine residues were separated by 50 Å in the extended configuration but only by 15 Å in the collapsed form. The engineered calmodulin was then incorporated through reaction of the cysteine side chains into a poly(ethylene glycol) (PEG) hydrogel. By treatment with a peptide ligand and subsequent washing, the incorporated protein could be cycled repeatedly between the two conformations, leading to an overall gel volume change on the order of 10 to 20%. Although this change is comparatively small in the hydrogel context, the authors note that the system was far from optimized, and that there are more than 200 well-characterized protein motions that might be adapted into functional gels. — MSL

Calmodulin hydrogel.

CREDIT: MURPHY ET AL., ANGEW. CHEM. INT. ED. 46, (2007)

Angew. Chem. Int. Ed. **46**, 3066 (2007).

CELL BIOLOGY

Full to Bursting

Peroxisomes are membrane-bounded intracellular organelles that carry out important oxidative reactions in lipid metabolism. In order to adequately supply daughter cells, peroxisomes must multiply and divide throughout the cell cycle. Guo *et al.* have examined the maintenance and division of peroxisomes in yeast—specifically, how peroxisomal membrane lipids and proteins are dynamically and spatially regulated during the cell cycle. They find that as peroxisomes mature, they accumulate larger quantities of the enzymes involved in lipid metabolism. One of these, acyl-CoA oxidase, is primarily localized to the matrix (the interior of the peroxisome) in immature organelles but is partly found in association with the inner surface of the peroxisomal membrane in mature organelles. Once at the membrane, acyl-CoA oxidase binds to the protein Pex16p; this interaction activates the transformation of endogenous lipids into components that induce bending of the outer leaflet of the membrane, which, in turn, activates peroxisomal membrane proteins that mediate division of the organelle. Thus, peroxisomes have an internal sensing mechanism that triggers their own multiplication as they grow. — SMH

J. Cell Biol. **177**, 289 (2007).

Science stke AAAS

www.stke.org

<< Just the Right Amount of Guidance

Dysfunctional signaling by the neurotransmitter serotonin (5-HT) is associated with psychiatric illnesses such as anxiety disorders and depression. These conditions may reflect abnormal signaling at synapses in the adult brain or changes that have occurred during brain development, when serotonin is present and influences pathfinding by thalamocortical neurons. Bonnin *et al.* provide mechanistic insight into how changes in serotonin signals can disrupt axon migration. In cultured explants from the dorsal thalamus of mice, axons are normally attracted to HEK-293 cells that have been engineered to express the axon guidance protein netrin-1. But when the explants were treated with serotonin, the axons reversed their response and were repelled from cells producing netrin-1. This response was caused by decreased synthesis of the second messenger cAMP in the serotonin-stimulated dorsal thalamus neurons. Pharmacological inhibition of the cAMP-dependent protein kinase could reproduce the effect of serotonin, whereas activation of the kinase blocked the serotonin effect. To show the importance of this effect in vivo, the authors used targeted electroporation in developing mouse embryos, thereby causing the cells of the dorsal thalamus to express either more serotonin receptors (to enhance signaling) or fewer receptors (to limit signaling). Increasing and decreasing serotonin signaling produced opposite effects, and both manipulations caused abnormal migration trajectories of the thalamus axons. Thus, the authors propose that developmental abnormalities in serotonin signaling—either too much or too little—may alter the circuitry of thalamocortical axons and may contribute to mental health disorders. — LBR

Nat. Neurosci. **10**, 588 (2007).

SPOTLIGHT: SINGAPORE

Renowned Cancer Researcher Sir David Lane Leads the Singapore Institute of Molecular and Cell Biology

Sir David Lane is one of the scientists credited with the landmark discovery of the tumor suppressor protein p53. His research focuses on the study of this protein, including ways to use the p53 system to develop new treatments for cancer. In 2004, Sir David was named the Executive Director of the Singapore Institute of Molecular and Cell Biology (a research institute of the Agency for Science, Technology and Research, A*Star). Previously, he was Director of the Cancer Research UK Cell Transformation Research Group and Professor of Oncology at the University of Dundee in Scotland. He founded the biotechnology company Cyclacel Ltd., and was named "Emerging Entrepreneur of the Year" by the Entrepreneurial Exchange in 2001. Sir David was knighted by the Queen of England in 2000 in recognition of his contributions to cancer research.

Q&A

What did discovery of the p53 tumor suppressor gene mean for the field of oncology?

It led to the realization that there was a common step in human cancer, and it created a major field of work. More than 40,000 papers have now been published on p53, and the pathway has been shown to be critical in protecting us from developing cancer. The finding that p53 is activated by cellular stress has greatly enhanced our understanding of cancer as a disease of defective signaling. It is also leading to major new efforts in drug discovery.

What recent developments in your laboratory are you excited about?

We have recently made great progress discovering new isoforms of p53 that regulate its activity in development, and we are especially excited about using the Zebra fish system to study p53. This allows powerful new genetic methods to be applied to some of the most difficult problems in the field. Also, our new studies in developing small molecules drugs to modulate the p53 pathway are exciting. These experiments make us increasingly optimistic about a new generation of anti-cancer drugs emerging from the p53 field.

Tell us about IMCB, A*STAR's Institute of Molecular and Cell Biology?

IMCB was founded in 1987. It is a great international institute with investigators from 20 or more countries all working together. Our major research areas are in cell biology, developmental biology cancer and infectious disease. We now have more than 40 research teams and several support laboratories. The Institute's scientists publish in the top journals and IMCB won the Nikkei prize for innovation in 2000.

What do you hope to accomplish in your role as IMCB's executive director?

I have two main goals. Excellence comes first, and I am delighted by our very successful international recruitment of senior staff over the last couple of years. This proves that

the IMCB is internationally competitive at the highest level. My second goal is to bridge the gap between invention and application. With the great resources of the Biopolis, we will be able to take our discoveries closer to market, enhancing their chance of success.

Does Singapore present unique opportunities for cancer research in general and your work in particular?

I have never had better resources or more freedom to do my work. We have superb facilities and we have been able to recruit very hard-working and dedicated young scientists to work and train with us. The Zebra fish expertise is outstanding at IMCB, and this has been further enhanced by Neal Copeland and Nancy Jenkins' arrival, which gives us a world-leading position in cancer genetics using mouse models.

Are there particular aspects of Singapore's biomedical sciences hub—the Biopolis—that will help drive the process of scientific discovery forward?

The key factor is the focus it represents. You are constantly meeting people from other institutes and from the industrial companies at the site. It's a real critical mass. It has also become a focal point for meetings and international visitors. This creates great buzz, which creates a vital atmosphere that nurtures innovation and discovery. It's wonderful to sit out in the evening in one of the bars or restaurants at the Biopolis and swap ideas with other scientists.

What else about Singapore drew you to work there?

I was very interested in how Singapore works. It seems so efficient compared to most countries and I wanted to understand how this is managed. It also seemed a very exciting thing to do, to live in another country and experience something of Asia. I really love the people here. Singaporeans are very kind and welcoming, and it's a great cultural mix.

Are there other areas of research in Singapore that you find especially significant?

Some of the work on stem cells looks very promising, and it's a great field. I am excited by the push in immunology because I did my PhD in that subject. I am very impressed by the work of Genome Institute of Singapore in high throughput analysis of gene expression and in expression signatures for disease analysis. The Institute of Bioengineering and Nanotechnology and the Bioprocessing Technology Institute are also making big contributions, with fascinating work on new materials and on cell production.

Who are some of the biomedical scientists working today you particularly admire?

The list is very long! Nobel Laureate Sydney Brenner, who helped set up IMCB in 1987, has been wonderful to interact with and has great insight into how to create an environment for innovation. Neal Copeland and Nancy Jenkins, Philip Ingham and Jean Paul Thiery—our new recruits to IMCB—all have truly amazing track records and very hot new results. And this is just to mention a few.

www.sciencemag.org

Science

1200 New York Avenue, NW
Washington, DC 20005
Editorial: 202-326-6550, FAX 202-289-7562
News: 202-326-6581, FAX 202-371-9227

Bateman House, 82-88 Hills Road
Cambridge, UK CB2 1LQ
+44 (0) 1223 326500, FAX +44 (0) 1223 326501

Subscription Services For change of address, missing issues, new orders and renewals, and payment questions: 866-434-AAAS (2227) or 202-326-6417, FAX 202-842-1065. Mailing addresses: AAAS, P.O. Box 96178, Washington, DC 20090-6178 or AAAS Member Services, 1200 New York Avenue, NW, Washington, DC 20005

Institutional Site Licenses please call 202-326-6755 for any questions or information

Reprints: Author Inquiries 800-635-7181
Commercial Inquiries 803-359-4578

Permissions 202-326-7074, FAX 202-682-0816

Member Benefits Bookstore: AAAS/BarnesandNoble.com bookstore www.aaas.org/bn; Car purchase discount: Subaru VIP Program 202-326-6417; Credit Card: MBNA 800-847-7378; Car Rentals: Hertz 800-654-2200 CDP#343457, Dollar 800-800-4000 #AA1115; AAAS Travels: Betchart Expeditions 800-252-4910; Life Insurance: Seabury & Smith 800-424-9883; Other Benefits: AAAS Member Services 202-326-6417 or www.aaasmember.org.

science_editors@aaas.org	(for general editorial queries)
science_letters@aaas.org	(for queries about letters)
science_reviews@aaas.org	(for returning manuscript reviews)
science_bookrevs@aaas.org	(for book review queries)

Published by the American Association for the Advancement of Science (AAAS), *Science* serves its readers as a forum for the presentation and discussion of important issues related to the advancement of science, including the presentation of minority or conflicting points of view, rather than by publishing only material on which a consensus has been reached. Accordingly, all articles published in *Science*—including editorials, news and comment, and book reviews—are signed and reflect the individual views of the authors and not official points of view adopted by the AAAS or the institutions with which the authors are affiliated.

AAAS was founded in 1848 and incorporated in 1874. Its mission is to advance science and innovation throughout the world for the benefit of all people. The goals of the association are to: foster communication among scientists, engineers and the public; enhance international cooperation in science and its applications; promote the responsible conduct and use of science and technology; foster education in science and technology for everyone; enhance the science and technology workforce and infrastructure; increase public understanding and appreciation of science and technology; and strengthen support for the science and technology enterprise.

Information for Authors

See pages 120 and 121 of the 5 January 2007 issue or access www.sciencemag.org/feature/contribinfo/home.shtml

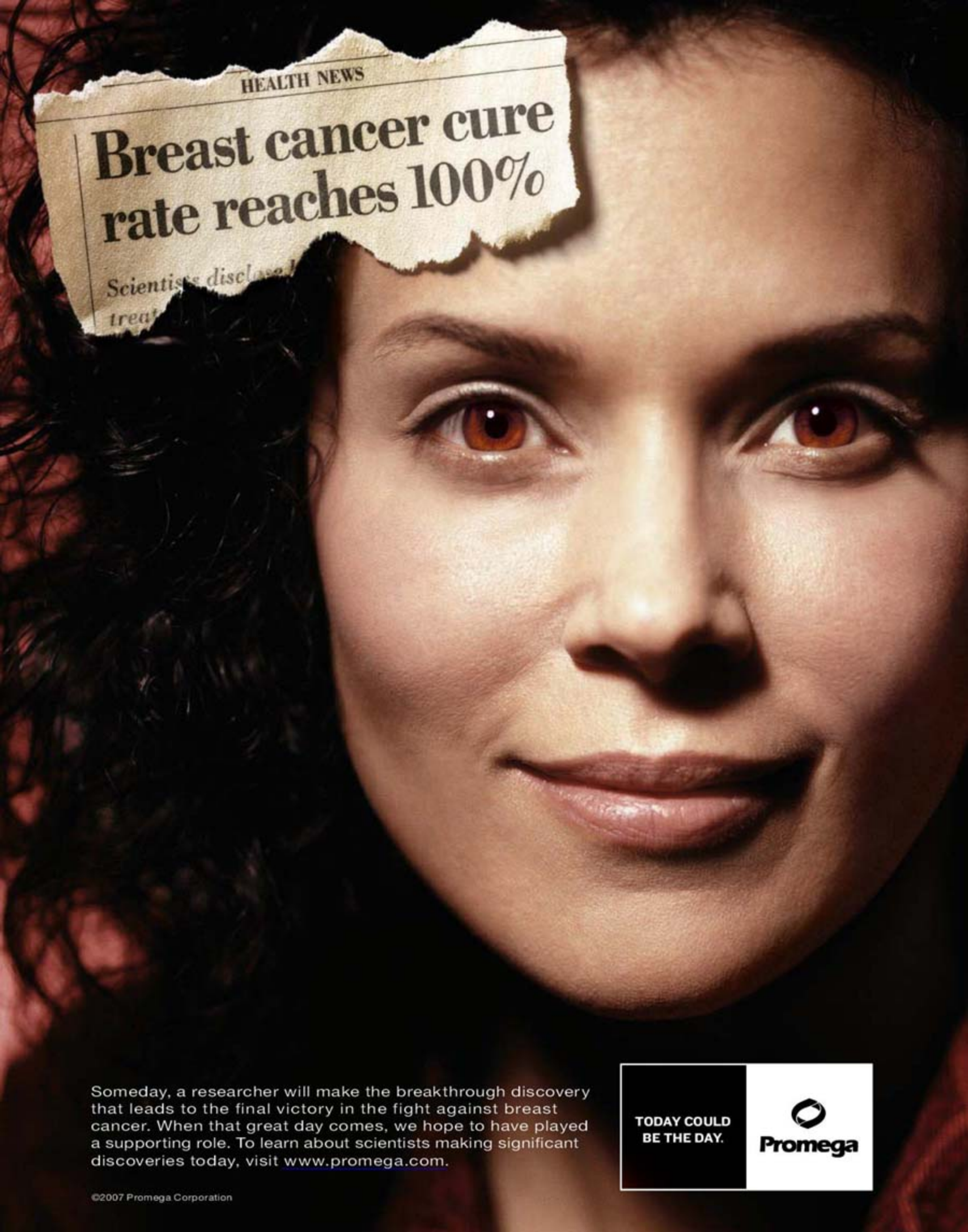

Someday, a researcher will make the breakthrough discovery that leads to the final victory in the fight against breast cancer. When that great day comes, we hope to have played a supporting role. To learn about scientists making significant discoveries today, visit www.promega.com.

TODAY COULD BE THE DAY.

Promega

Perfect

Thermo
SCIENTIFIC

The world leader in
analytical instrumentation.

Some things just go great together. Like the merger forming Thermo Fisher Scientific. We've always been in the lab together, now we've created the world leader in serving science.

Our new brand – Thermo Scientific – stands for superior analytical instruments and workflow solutions spanning sample preparation, sample analysis, diagnostics and data interpretation.

Complements

Fisher Scientific

The world leader in laboratory supply and services.

Our famous Fisher Scientific brand stands for choice and convenience, as well as a complete range of quality products and services delivered when and where they're needed.

Thermo Fisher Scientific will lead to new and better technologies for research, analysis, discovery and diagnostics. New ways to help customers make the world healthier, cleaner and safer.

www.thermofisher.com 1-800-678-5599

ThermoFisher SCIENTIFIC

Hard Facts About Our Planet

NET WATCH

One knock against Wikipedia and other user-written resources is that you don't know whether an article was penned by an authority or some high school dropout living in his parents' basement. By handing the writing and editing over to experts, the Encyclopedia of Earth aims to provide that accountability. The reference is the centerpiece of the new Earth Portal, sponsored by the nonprofit National Council for Science and the Environment in Washington, D.C.

The 150 or so authors—who include Ph.D.s, teachers, lawyers, and other specialists—had to submit their credentials for approval, and their work is vetted by an editor conversant with the field. You can browse the more than 2000 articles to learn how the body expels toxins and why the global "dust budget," a tally of how much dust enters and leaves the atmosphere, is important for climate forecasting. Earth Portal also offers a news section and a discussion forum. >> www.earthportal.org

Belugas on the Brink

The belugas of Alaska's Cook Inlet are a genetically distinct population that has probably been isolated for several thousand years. Now the numbers of these toothed white whales (*Delphinapterus leucas*) have dwindled to only 302. They are likely to disappear within the century unless the federal government lists them as endangered, says the National Marine Fisheries Service, which proposed the listing on 19 April.

"We don't have a fix yet on why these belugas are declining," says Rod Hobbs, a marine mammal biologist at the National Marine Mammal Laboratory in Seattle, Washington. Possible causes are pollution, habitat loss, or a shortage of salmon, their preferred food.

As recently as the 1980s, an estimated 1300 belugas swam in the inlet. Subsistence hunting by native Alaskans took its toll, but tighter hunting regulations put in place in 1999 did not stop the population from shrinking—by more than 4% a year. "We thought the whales would have shown signs of recovery by now," says Hobbs, but hunting seems only to have "masked the real problem." He notes that hunters have also reported a decrease in the belugas' blubber content.

More-detailed studies of the whales are planned. Once they are listed as endangered, hunting will be banned, and a recovery plan will be developed to bring back the population to about 780 animals.

Earliest America

IN A CEREMONY LAST WEEK IN WASHINGTON, D.C., the German government turned over a map known as "America's Birth Certificate" to the Library of Congress, which has purchased it for $10 million from a German prince. Created in 1507 by Martin Waldseemüller, it's the first map to feature the name "America" and the first to identify the Pacific Ocean as a separate body of water. This map, printed from 12 wooden plates, is believed to be the only remaining copy.

Chinese Orchid Craze

At an orchid show last month in Shaoxing, eastern China, a plant sold for about $175,000 (1.35 million yuan). The record-breaking sale gave a glimpse of a little-noted offshoot of the Asian economic boom: Orchids in China "are like Dutch tulip bulbs in the 17th century," says William Rhodehamel of the Hoosier Orchid Co. in Indianapolis, Indiana.

The Chinese export (or smuggle out) many of their 1200 native orchid species. But there's only one brand they themselves get excited about, says botanist Holger Perner, an orchid expert at Huanglong National Park in Sichuan. That's the Oriental cymbidium, valued since the time of Confucius. Nowadays, Perner says, dealers will speculate with "super cymbidiums," buying a hot specimen as the price is rising and making millions from selling pieces of the multiplying plant.

Priciest of all are strange-looking plants—not necessarily favored by the Western eye—that result from natural mutations in the wild. "In order to find a single rare mutant, entire populations are stripped from the wild country-wide," says Perner. In China, few plant species are protected, and it is legal to collect most orchids in the wild. A new law to protect cymbidiums is in the works.

High-value orchid under scrutiny at national orchid fair in Yunnan Province in 2005.

CREDITS (TOP TO BOTTOM): LIBRARY OF CONGRESS; JUPITER IMAGES; HOLGER PERNER

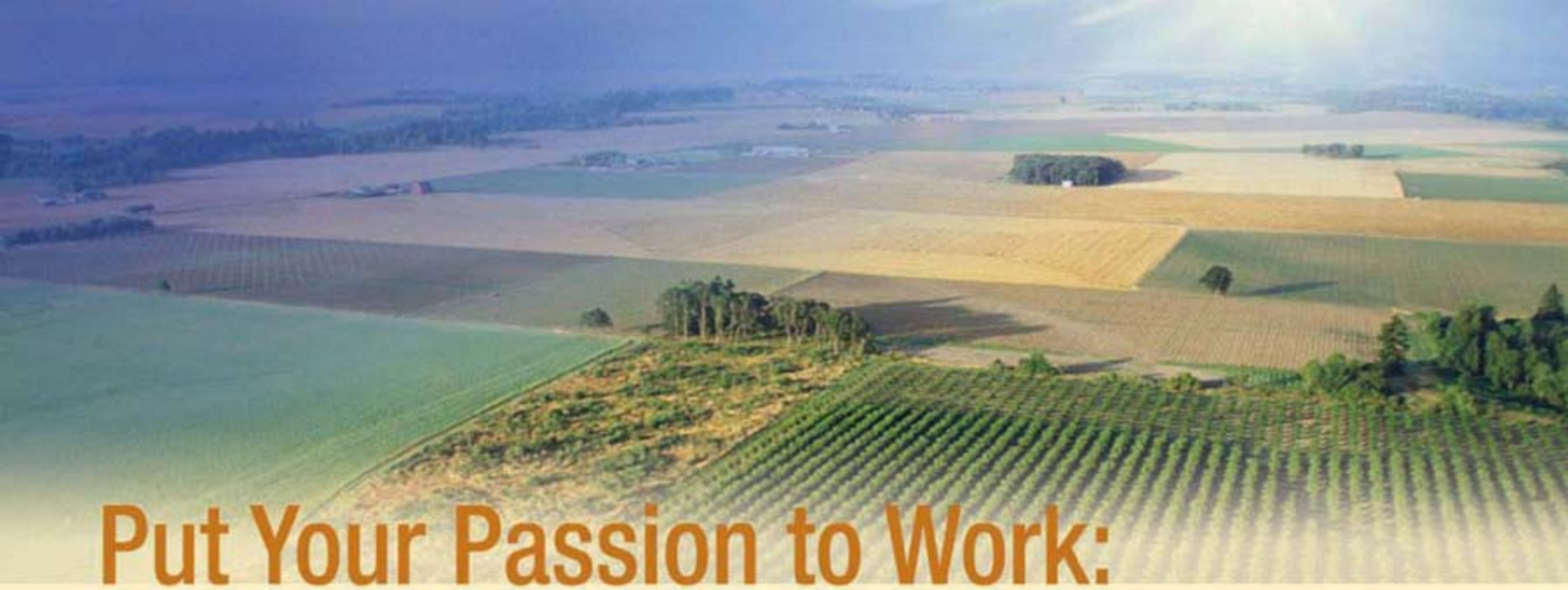

Put Your Passion to Work:

THE MONSANTO EXPERIENCE

At Monsanto, we're passionate about using science and technology to improve agriculture. We invest about $1.5 million a day to look for and bring to market the innovative technologies that our customers tell us make a difference. It's research that's about more than just biotechnology. We use many tools – like genomics, conventional and molecular breeding, crop analytics, animal productivity, chemistry and biotechnology – to bring forward new products to answer our customers' needs, in turn, providing benefits to not only the farmer, but processors and consumers, as well.

At Monsanto, we believe in -

INNOVATION IN AGRICULTURE

Advanced science and innovative technology are at the heart of our company. We are committed to developing science based solutions to make our farmer customers more productive and profitable. Our employees are making a difference by feeding the world while preserving the environment.

EXCELLENCE

People at Monsanto are driven to do extraordinary things and are dedicated to being the best in our industry.

GREAT WORKING RELATIONSHIPS

Monsanto is team based with highly qualified professionals sharing knowledge, creating a great place to work and allowing employees to take ownership for results.

To learn more about Monsanto, our passion and our opportunities, visit **www.monsanto.com**.

Come grow with us.

MONSANTO

imagine™

Monsanto values diversity and is an equal opportunity affirmative action employer. M/F/D/V

EDITED BY YUDHIJIT BHATTACHARJEE

Money Matters

GIFT OF HISTORY. Physicists working in industrial labs invented the transistor, the silicon microchip, and numerous other technologies we take for granted. Now, the stories of those pioneers will be recorded, thanks to a brother's gift.

To honor former Executive Director Marc Brodsky, 68, the American Institute of Physics (AIP) is raising an endowment to finance the recording of oral histories from prominent industrial physicists. Much of the $90,000 collected so far came from Marc's brother Julian in a gift unveiled at Marc's retirement party in March. "I don't know how they kept it a secret," Marc says. "I was supposed to know everything that was going on [at AIP]." Marc (right in photo) worked at IBM for 25 years before joining AIP in 1993, and under his guidance, AIP began collecting such interviews in 2002. That effort will now continue indefinitely.

"I know Marc has very much enjoyed his stay at AIP, and I thought this was an appropriate way to commemorate him," says Julian, 73, who co-founded the Comcast cable television company. Julian knows the value of oral history: In 1991, a fire destroyed Comcast's archives, prompting company officials to interview dozens of longtime Comcast employees.

FOLLOW-UP

STOPGAP. The California Institute for Regenerative Medicine (CIRM) has decided that two interim heads can do the work of former president Zach Hall until it finds a permanent replacement for him.

Hall stepped down on 30 April, more than a month ahead of schedule, citing his health and a "contentious" debate over the timetable for a $222 million construction program (*Science*, 27 April, p. 526). On 2 May, the governing board divided up Hall's job, giving "co-equal" appointments to Chief Financial Officer Lorraine Hoffman and Director of Scientific Activities Arlene Chiu. Hoffman, who joined CIRM last November, has an extensive background in both housing and finance. Neurobiologist Chiu, recruited 2 years ago from the National Institutes of Health, will serve as interim chief scientific officer.

The board plans public hearings on the controversial construction program. The search continues for Hall's replacement.

MOVERS

IN A NEW SPACE. When the United Kingdom's Royal Institution began refurbishing its historic headquarters in central London in early 2006, Richard Catlow, head of RI's famed Davy Faraday Laboratory, moved his research group to University College London (UCL). But it emerged last month that the inorganic chemist and his team members had decided to stay at UCL. Their shift leaves RI Director Susan Greenfield with the challenge of filling a lab once home to luminaries including chemist Humphrey Davy, electromagnetic pioneer Michael Faraday, and crystallographers William and Lawrence Bragg.

Over the past couple of decades, the lab has concentrated on solid state chemistry, most recently under Catlow's directorship. For the past 10 years, Catlow's group has worked closely with UCL colleagues. "Our work has become more UCL-centric, and it made sense to consolidate here," explains Catlow, who has headed UCL's chemistry department for the past 5 years.

POLITICS

FISHED OUT. A Bush Administration official criticized for heavily editing scientific reports on endangered species resigned last week from the Department of the Interior (DOI). Julie MacDonald, deputy assistant secretary for Fish, Wildlife, and Parks and a civil engineer by training, had pressured scientists at the Fish and Wildlife Service to weaken protection for species, according to DOI's inspector general, which last month also concluded that she had violated federal rules by leaking internal agency documents to lobbyists (*Science*, 6 April, p. 37).

MacDonald resigned the same day that Senator Ron Wyden (D–OR), citing concerns about her actions, put a hold on the pending confirmation of her boss, Lyle Laverty. Wyden hasn't yet released the hold, however. "It is not an isolated incident, and he wants some assurances that this won't happen again," says a spokesperson. Francesca Grifo of the Union of Concerned Scientists recommends that DOI ensure that its scientists get a final review of their work and says it should increase transparency.

On Campus >>

OPENING UP. German physicist Romano Rupp of the University of Vienna in Austria has become the first non-Chinese person to be named science dean at a Chinese university. Next month, Rupp will take charge of the Teda School of Applied Physics at Nankai University in Tianjin.

Rupp's appointment is part of a housecleaning by Nankai's new president, structural biologist Rao Zihe, who is replacing 14 of the university's 22 deans. Rupp, who has been a visiting professor at Teda for many years, says his appointment "sends a signal that positions at Nankai are fully open to the international community of researchers." Three of the nine deans already announced are expatriate Chinese from the United States, whereas the others are homegrown.

Rupp, who studies optical storage and neutron physics, will retain his current job as a physics professor and divide his time between Vienna and Tianjin.

Got a tip for this page? E-mail people@aaas.org

CREDITS (TOP TO BOTTOM): VIVIAN BRODSKY; SOURCE: RICHARD CATLOW; SOURCE: ROMANO RUPP

Dustup over generic drugs
816

After the French election
819

All smiles. Demonstrators outside the IPCC meeting reflected the mellow mood of negotiations inside.

CLIMATE CHANGE

IPCC Report Lays Out Options for Taming Greenhouse Gases

BANGKOK—Reining in climate change won't bankrupt the world economy and won't require technological miracles. But we'll have to start soon. That is the mostly upbeat conclusion from Working Group III of the Intergovernmental Panel on Climate Change (IPCC), which met behind closed doors for 3 days last week here in the Thai capital.

The fruit of the working group's labor is a 35-page document that lays out options—and their price tags—for reducing greenhouse gas emissions to head off catastrophic climate change. The most ambitious plan, which would stabilize greenhouse gas levels in the atmosphere (measured in equivalents of CO_2) below 535 parts per million (ppm), would come with an estimated 3% decrease in global gross domestic product (GDP) by 2030 compared to business as usual. Less ambitious targets come cheaper. The easiest option—aiming for under 710 ppm, 50% higher than the current atmospheric concentration of long-lived greenhouse gases of 460 ppm—could yield a small net gain for the global economy.

The report—the executive summary written by 33 of the several hundred contributing authors of a review of major economic modeling studies due to be released in September—concludes that getting from today's greenhouse gas–intensive economy to any of these targets is achievable with currently available tools such as shifting to alternative energy sources, boosting energy efficiency, and reducing deforestation, coupled with a suitable mix of caps, taxes, and economic incentives. But other scientists warn that reality will present harder choices than the models suggest. "The only reason for economists to make forecasts is to make astrologers look good," says Martin Hoffert, a physicist at New York University who has criticized earlier IPCC studies.

Last-ditch editing

Reaching consensus on these take-home messages was easier than expected. Media reports had predicted bitter disputes between IPCC member countries. For example, China was expected to insist on softening statements that might suggest that its fast-growing and fossil-fueled economy might need to be slowed, whereas the United States was expected to bully for nuclear power. But in fact, says Dennis Tirpak, a climate policy analyst who heads the climate change unit at the Organisation for Economic Co-operation and Development in Paris and one of the summary's authors, "the atmosphere was quite civilized."

China did put its foot down—over the adjective used to characterize the scientific evidence behind estimates of the cost of achieving emissions targets. China urged that the quality be downgraded from "high" to "medium." The motivation was "only to protect the scientific integrity of the IPCC," says co-author Dadi Zhou, a climatologist and deputy director of the Energy Research Institute in Beijing. Others who spoke with *Science* agree. "China had a valid point, and we adopted it," says co-author Jayant Sathaye, an energy policy analyst at Lawrence Berkeley National Laboratory in California.

In the end, only two short passages in the report fell short of unanimous approval. One was four lines stating that with a price of $50 for a ton of emitted CO_2, nuclear energy would be cost-effective in providing nearly a fifth of global electricity—with the caveat that "safety, weapons proliferation and waste remain as constraints." Even that cautious endorsement sparked what Sathaye calls an "adrenaline-fueled" discussion ending with firmly anti-nuclear Austria insisting on a footnote saying that it "could not agree with this statement." The other sticking point was a passage on forestry, which drew fire on technical grounds from a delegate from Tuvalu.

The final result is a document that strikes a far more optimistic tone than did the previous three mitigation reports. At least, that was the mood of the IPCC's buoyant press release, which has been echoed by the media since its release.

Climate crystal ball

But hidden within the text of the report are abundant references to uncertainties and caveats that have gone largely unmentioned.

For one, many scientists are muttering, the report is only as good as its models. To explore mitigation options, the IPCC uses two distinct strategies. Bottom-up models break the economy down into sectors and predict how different mixes of technologies will cut carbon emissions in each. Top-down models simulate whole economies to compare how different global strategies, such as carbon ▶

CREDIT: PORNCHAI KITTIWONGSAKUL/AFP/GETTY IMAGES

Gene hunters' new tool
820

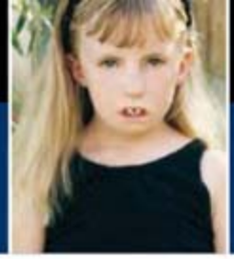

A syndrome without smiles
826

Meanwhile, Back in Washington …

After playing a minor role for years in the U.S. Senate's Energy and Natural Resources committee, a molecule had a coming-out last week: carbon dioxide. The committee was drafting a bill meant to broaden energy independence, including measures on ethanol production, energy efficiency, and carbon sequestration.

But when a Republican senator from coal-rich Wyoming proposed a measure to boost the production of fuel made from gasified coal, panel Chair Jeff Bingaman (D–NM) balked. Concerned that the technology was unproven and could release too much CO_2 into the atmosphere, he asked Democratic members—even those from other coal-rich states, such as newly elected Jon Tester of Montana—to hold the line against the measure. The amendment failed on a party-line vote. Tester said he could support the technique later but that storing carbon emitted from coal-to-liquid facilities was a priority. "The carbon issue is that important," he said.

The skirmish "shows how global climate change has arrived as an issue in the debate on energy" in Washington, D.C., says Jim Presswood, a lobbyist for the Natural Resources Defense Council. Last year, when the Republican party controlled Congress, the amendment probably would have passed, Presswood says. But when Democrats took over in January, they made climate change a top priority, and the new speaker of the House of Representatives, Nancy Pelosi (D–CA), set 4 July as a target deadline to pass a House bill that would cap U.S. emissions of greenhouse gases.

Since then, several factors have fallen into place: One longtime opponent of carbon limits, Democratic Representative John Dingell of Michigan, is listening, with a series of hearings on the idea. And the Edison Electric Institute, which represents American utilities, recently signaled its openness to emission limits—provided they cover all industries and include price controls. President George W. Bush's emphasis on research and voluntary measures no longer holds sway.

But 4 months into their rule, Democrats are beginning to realize that the new mood in Congress won't translate into new laws overnight. Pelosi has pushed back her timeline as efforts to pass a carbon bill have collided with international implications and state interests—most importantly, coal. Some observers are already saying that major new policies will have to wait until after next year's presidential election.

For sure, science is getting a different reception on Capitol Hill. ▶

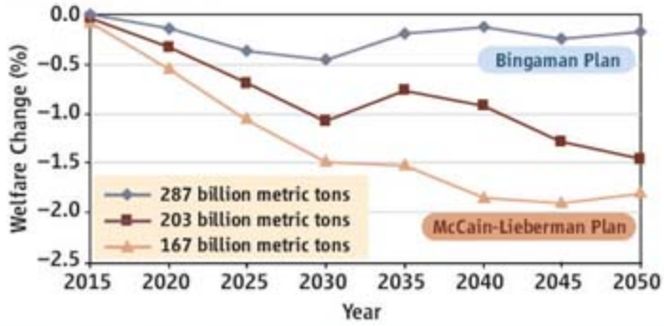

Price club. MIT modeling studies suggest that policies placing different limits on greenhouse gas emissions will have varying impacts on the average U.S. citizen's wealth. Figures are cumulative amounts emitted between 2015 and 2050.

taxes or fixed greenhouse-gas stabilization targets, will play out through market forces. Each approach has its drawbacks. Bottom-up models tend to ignore economics, whereas top-down models smooth over the differences between regions and sectors. In 2001, the two approaches were often at odds. The good news, says Sathaye, is that "for the first time, the range of results from bottom-up and top-down models are starting to converge." However, enormous wiggle room remains.

One problem is that bottom-up models don't cope well with lifestyle: the preferences that drive people to choose one mix of technologies over another. For example, the report suggests that a broad portfolio of alternative energy sources, such as solar and biofuels, could cut projected annual CO_2 emissions in the year 2030 by 5 to 7 gigatons at no cost at all, thanks to savings in energy efficiency. But that conclusion is misleading, says author Richard Richels, an economic modeler at the Electric Power Research Institute in Palo Alto, California, because it ignores the implicit cost of making people choose something they don't want. "If it's advantageous, why aren't people doing it?" Richels asks.

Since 2001, researchers have worked to make the models more realistic by incorporating such "market feedback," says Billy Pizer, an economist with Resources for the Future in Washington, D.C., who co-authored a related chapter in the full mitigation report. But it's one thing to account for people's illogical behavior and quite another to persuade them to change it. "It's stuff that pays for itself that people don't do," he says.

Steady progress has been made with top-down models, says Jae Edmonds of the College Park, Maryland, office of the Pacific Northwest National Laboratory. The modelers are now accounting for more regional details, such as the availability of land area for biofuels and the potential for storing coal-plant carbon emissions underground. They have also expanded the models to include emissions of greenhouse gases other than CO_2, such as methane. Doing so has lowered the top-down estimates of mitigation costs. "The reason is that you have other opportunities to reduce ▶

CREDITS (TOP TO BOTTOM): MIT; J. BOHANNON/SCIENCE

Continued from page 813

Hearings by at least 15 panels since January have touched on everything from the environmental impacts of expanding biofuel production to the effects a cap would have on Detroit's automakers. Climate scientist Stephen Schneider of Stanford University in Palo Alto, California, says the "cordial" and inquisitive atmosphere of the three hearings at which he has testified this year are a welcome contrast to the previous "20 years of combat on the Hill" he's endured, much of it over the very existence of the problem. Longtime foes of carbon restrictions are laying down arms. "My view is changing, as is the view of much of the energy industry," Representative Rick Boucher (D–VA) said in February, crediting the "deeply solidified" scientific consensus.

After years of relatively sporadic hearings about confronting climate change, aggressive lobbying by industry, nonprofit activists, and scientists has fueled more than 100 legislative proposals on the topic—about a dozen with mandatory emissions limits. But the deluge of new input "doesn't necessarily make it simpler to get things done," says David Hunter, an aide to Senator Susan Collins (R–ME).

Right now the most aggressive emissions limit proposal in Congress belongs to Representative Henry Waxman (D–CA), who wants to cut U.S. emissions 83% from current levels by 2050. A recent analysis by researchers at the Massachusetts Institute of Technology (MIT) suggests that the measure would cut the average citizen's available income by about 2% by 2050. It would yield an approximate 460 parts per million (ppm) level of CO_2 in the atmosphere if China and India begin by 2025 to cut their emissions and by 2050 to stabilize them. That level, roughly 20% higher than today's, would still mean "additional warming of twice to three times [what] we have seen over the last century," the MIT study concluded.

But few believe that bill can fly now, as a less aggressive approach, pushed by senators Joe Lieberman (D–CT) and John McCain (R–AZ), failed in 2005, attracting only 38 votes. So others, including Bingaman, have sought consensus by setting the emission bars lower. Bingaman's carbon-trading proposal includes a so-called safety valve that limits the price that industry and, subsequently, consumers must pay for emitting CO_2. The MIT analysis predicts that Bingaman's approach would cost citizens only 0.5% of available income by 2050 while holding CO_2 in the atmosphere to about 490 ppm.

Some lawmakers say it's crucial to pass some bill—even a flawed one—soon. Early U.S. action, they argue, could spur the crucial participation by India and China in an emissions-control regime. "If we take 10 years to get started, the problem will be harder to deal with then," says Representative Tom Udall (D–NM). But others, including editors at the left-leaning *New Republic* magazine, have urged the Democrats not to accept compromises for the sake of expedience. "There won't be many chances to get this right, and Democrats will need to wait until they can go for broke," a March editorial declared.

Privately, lobbyists on each side of the issue say that only a committed president can muster the political force to broker a deal. Presidential contenders such as John Edwards, senators McCain and Barack Obama (D–IL), have championed forceful proposals to contain greenhouse gas emissions. Meanwhile, the timeline is the one thing that's becoming clear: "It'll take a ways to pass comprehensive greenhouse legislation," says Hunter.

–ELI KINTISCH

emissions," says Sathaye. For example, a landfill emitting methane can be cheaper to deal with than a coal plant, but such advantages were lost in previous simulations.

But top-down models can still run aground on the shoals of international politics. One rosy prediction is that an imposed cost of $100 per ton of CO_2—equivalent to an extra $1 per gallon at the pumps—could yield a cut of 17 to 26 gigatons of CO_2 by 2030, as much as 38% of estimated emissions under a fairly carbon-intensive forecast. But this assumes that the whole world participates in carbon trading and that markets are free and transparent. Given current Indian and Chinese wariness towards carbon caps, says Pizer, "that's not politically likely."

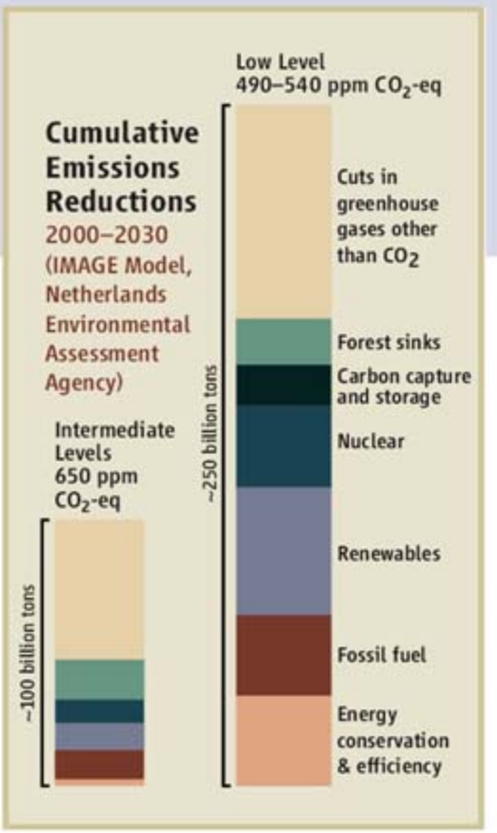

Diet plan. The IPCC report drew on models that calculated global portfolios of emissions reductions needed to reach various target levels of greenhouse gases in the atmosphere.

Spin control

Now that the debate over the content of the 1000-page Fourth Assessment Report is done, the battle is shifting to its interpretation. Many IPCC scientists say they are uneasy with the optimistic spin put on the report. "I think something that is being underplayed … is the scale of the mitigation challenge," says Brian O'Neill, a climate policy modeler at the International Institute for Applied Systems Analysis in Vienna, Austria, who contributed to a chapter on mitigation scenarios. "To limit warming to something near the European Union's stated goal of 2°C, global emissions have to peak within the next decade or two and be cut by 50% to 80% by midcentury." That's a tall order, O'Neill says—and it could get a lot taller if global temperatures turn out to be more sensitive to increases in greenhouse gases than the IPCC has been assuming. "My point is not that there should be more gloom and doom," says O'Neill, but "a message that says that we have to stay below 2°C, but don't worry, it will be easy and cheap, just doesn't add up."

Other researchers say the report's insistence that current mitigation strategies can suffice gives short shrift to future research. That's a mistake, says Hoffert: "It is ludicrous to think a greenhouse-gas emissions price, cap, or tax alone will get you to stable concentrations of [greenhouse gases]." New technologies will be critical, he says, and unless policymakers pave the way with measures such as a gradually increasing carbon tax, they will not be competitive. And Richels fears that if the takeaway message is that mitigation is cheap, societies "may not be as motivated to invest in the future" for such research.

Overall, the question of whether mitigation is "affordable"—be it 0.3% or 3% of global GDP—is "a difficult one to answer," says Sathaye. But some say that when stakes are overwhelmingly high, purely economic reasoning misses the boat. "What did World War II cost us economically?" asks Hoffert. "Does the question even make sense?" **–JOHN BOHANNON**

With reporting by Eli Kintisch.

CREDIT: ADAPTED FROM THE IPCC FOURTH ASSESSMENT REPORT

PHYSICS

All Paired Up but Unable to Flow, Atoms Strain Key Conceptual Link

Day leads to night, life leads to death, winter leads to spring; some things necessarily imply others. So it has seemed in physics: At very low temperatures, certain particles pair, and when they do, the pairs inevitably gang up to form a "superfluid" that flows without resistance. That explains how electrons glide through superconductors, how atoms of helium-3 form a liquid with no viscosity, and perhaps, how neutrons circulate through neutron stars. But an experiment reported on page 867 breaks the pairing-to-superfluidity connection. Atoms in an ultracold gas can pair but do not flow without resistance, even at temperatures approaching absolute zero, physicists report.

"If they have found a [zero temperature] state that has pairing but no superfluidity, that would be revolutionary," says Mohit Randeria, a theorist at Ohio State University in Columbus. But he cautions that it's too early to rewrite the physics texts.

How atoms and other quantum particles behave depends on how they spin. Particles can have only certain fixed amounts of spin, and those with an integer multiple of a basic amount called Planck's constant are known as bosons. They are sociable particles that at low temperature can crowd into a single jumbo quantum wave, which is the key to superfluidity. In contrast, particles with an extra half bit of spin are known as fermions and are loners. No two identical fermions can occupy the same quantum wave or state.

Fermions can get together, however, if they form loose overlapping pairs that act like bosons. In a superconductor, an electron spinning in one direction pairs with another spinning the opposite way, and atoms in ultracold gases can pair similarly. But what happens when the particles spinning one way outnumber those spinning the other way?

To find out, Christian Schunck, Wolfgang Ketterle, and colleagues at the Massachusetts Institute of Technology in Cambridge studied puffs of lithium-6 atoms. In previous work, they tested for superfluidity by rotating the clouds and looking for whirlpools called vortices, which are sure signs of a flowing quantum wave (*Science*, 23 December 2005, p. 1892). They fiddled with the ratio of up-spinning and down-spinning atoms and found that superfluidity persisted until the ratio reached about 85:15, with the pairs forcing the leftover up atoms to the cloud's edge. Larger mismatches quashed the superfluidity.

But in the new experiment, the team has found that even when the ratio is skewed

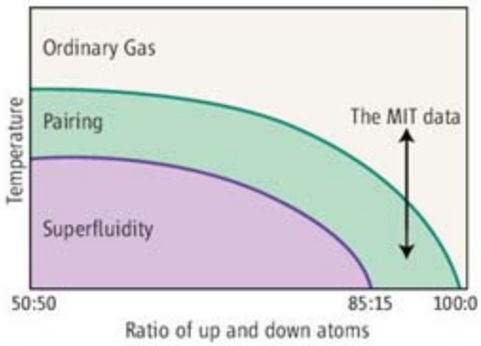

Disconnect. When the up-spinning atoms greatly outnumber the down-spinning ones, the atoms still pair, but they do not form a superfluid.

enough to prevent superfluidity, the atoms still pair. The researchers used radio waves to pop the down-spinning atoms into an entirely different quantum state. As they lowered the temperature, they had to increase the energy of the waves by a particular amount. That's exactly what should happen if the atoms pair and extra energy is needed to break the pairs apart, Ketterle says.

The finding appears to clash with a theorem which states that fermions that do not form a superfluid cannot pair either. "What we really need now is a rethinking of pairing," says Rudolf Grimm, an experimenter at the University of Innsbruck in Austria. But theorist Kathryn Levin of the University of Chicago in Illinois says the theorem "just doesn't apply" because it relies on assumptions that aren't valid for the strongly interacting atoms.

Even so, the experiment marks a "triumph," Randeria says. He notes that at smaller mismatches, Ketterle and colleagues see the atoms pair above the temperature at which superfluidity is known to set in. Some physicists have argued that the electrons in high-temperature superconductors form such "preformed pairs," but this experiment provides far clearer evidence, Randeria says. In that much at least the coupling between pairing and superfluidity is unraveling. **–ADRIAN CHO**

CREDIT: PRESTON HUEY/SCIENCE

SCIENCESCOPE

Transgenic Hay Mowed

A federal court extended a ban on planting of genetically engineered alfalfa last week. Alfalfa that has been altered to tolerate applications of the herbicide glyphosate will only be allowed back on the market after the U.S. Department of Agriculture (USDA) finishes a detailed environmental impact study. USDA says that could take 2 years.

The agency approved so-called Roundup Ready alfalfa in 2005, but 3 months ago, the U.S. District Court in San Francisco, California, ruled that the study should have come first (*Science*, 16 March, p. 1479). The judge in the case, Charles Breyer, imposed a temporary ban on planting in March and last week made the order permanent.

USDA will now examine the risk that increasing use of glyphosate will produce glyphosate-resistant weeds, as well as the economic impact on farmers of cross-pollination between conventional and genetically engineered alfalfa plants, especially those grown to produce seed. Several alfalfa seed producers in Idaho have reported finding traces of the Roundup Ready gene in stocks of conventional seed. In last week's decision, Breyer wrote that "such contamination is irreparable environmental harm." John Turner, an official with the USDA office that regulates transgenic crops, said that the judge "is asking questions that we haven't had to answer before," but he called the assignment "doable." USDA is considering hiring outside experts to help with the study.

–DAN CHARLES

A Commission Before Munitions

A House defense panel wants the Bush Administration to slow down its plans to build a new nuclear weapon. Last week, it voted to cut $45 million from the president's $88 million request for research on the Reliable Replacement Warhead (RRW) and use some of the money for more study.

The proposed blue-ribbon commission would "create a public discussion about future requirements for nuclear weapons," said Representative Ellen Tauscher (D–CA). Some opponents were hoping for more: "The subcommittee is taking a 'go slow' approach on the RRW rather than the 'no go' approach the program deserves," says a spokesperson for the Union of Concerned Scientists.

Now the focus shifts to a House spending panel, where chair Peter Visclosky (D–IN) has made known his doubts. The Senate's position is less clear. **–ELI KINTISCH**

AIDS DRUGS

Brazil, Thailand Override Big Pharma Patents

Executing a much-repeated threat, Brazil on 4 May broke sharply with big pharma and for the first time signed a "compulsory license" that allows the country to make or import a generic version of a patented anti-HIV drug. Brazilian President Luiz Inácio Lula da Silva, who signed the decree in a televised ceremony, took this step shortly after Thailand decided on similar action with the same drug—efavirenz—and two others. "Many other countries will likely follow suit," predicts economist James Love, who runs Knowledge Ecology International, a think tank in Washington, D.C. Love has urged developing countries to issue compulsory licenses, which are permitted by World Trade Organization rules for noncommercial uses of patented drugs, especially if they involve public health.

Lifeline. As more patients fail to respond to front-rank anti-HIV drugs, the demand grows for inexpensive, next-generation therapies.

Efavirenz is used by nearly 65,000 of the 170,000 people in Brazil now receiving free treatment from the government. Merck offered earlier in the week to cut the price from $580 per patient per year to $400, but Brazil noted that a generic version would reduce costs to about $165—saving the country an estimated $30 million this year alone. In a statement, Merck said it was "profoundly disappointed" by the decision and warned that the "expropriation of intellectual property sends a chilling signal to research-based companies," contending that they "cannot sustain a situation in which the developed countries alone are expected to bear the cost for essential drugs." But Pedro Chequer, the former head of Brazil's AIDS program who now works for the Joint United Nations Programme on HIV/AIDS, says, "I am really proud of this wonderful political decision."

Thailand faced similar praise and criticism when it issued compulsory licenses for efavirenz in November and then again in January for the anti-HIV drug lopinavir/ritonavir (made by Abbott Laboratories of Abbott Park, Illinois) and the blood thinner clopidogrel (made by Sanofi-Aventis of Paris, France). "Thailand's move has stirred up a hornet's nest," says Jon Ungphakorn, a former Thai senator who strongly backs his government's actions.

To the astonishment of Ungphakorn and many others in Thailand, Abbott announced on 14 March that it was pulling applications it had pending to register seven new medicines for sale in Thailand. Then on 30 April, the Office of the U.S. Trade Representative cited Thailand's issuing of compulsory licenses as one reason for elevating the country to the dreaded Priority Watch List, a U.S. government warning to countries that it judges do not adequately protect intellectual property, which can drive away foreign investment and impact export tariffs. "It's surprising that the reactions have been so harsh to a move that is perfectly legal," says Ungphakorn. "What the United States and Abbott have done to Thailand is to send a message to the whole developing world: 'Don't you dare carry out compulsory licenses, or there will be retaliation.'"

Merck and Abbott say they do not understand why Thailand has yet to accept their latest offers. Merck says it will sell efavirenz to the country for $237.25 per patient per year—a "no profit" price that Brazil said it would have agreed to—while Abbott reduced the price of lopinavir/ritonavir from $2200 to $1000 per patient per year. (Sanofi-Aventis, which sells clopidogrel in Thailand for about $800 per patient per year, did not reply to an interview request.)

Lawyer Sean Flynn, an intellectual-property expert at American University in Washington, D.C., who supports Thailand's and Brazil's actions, says the countries ideally would like to create competition among generic manufacturers to drive prices as low as possible. And Flynn flatly dismisses the "tired" argument that R&D would be harmed by these compulsory licenses, stressing that the drugs were not initially made for developing countries. "They were created for the European and U.S. markets, and that's where the incentive comes from to invest in developing them," contends Flynn, adding that patent holders also receive some royalties from drugs sold under compulsory licenses.

Abbott has taken the brunt of the criticism. AIDS advocates in particular have protested its plans to withdraw the registration of its new drugs, including a heat-stable form of lopinavir/ritonavir that's badly needed in Thailand. "Patients are being penalized," charges Paul Cawthorne, head of the Thai mission for Médecins Sans Frontières. "It's disgusting and completely unethical." Such criticism is misguided, counters Abbott spokesperson Dirk van Eeden: "The Thai government said it will not buy it, so why is there a need for us to register it?" he asks.

Although a handful of countries have issued compulsory licenses for AIDS drugs without kicking up much of a fuss, all involved older, first-generation drugs. Now the second-line treatments are at stake. Economist Love adds that big pharma feels threatened that this movement could go beyond AIDS to heart disease and other ailments. "There's a big push in Thailand to do it for everything," says Love.

Merck notes that it "remains flexible and committed to exploring a mutually acceptable agreement" with Brazil, and Thailand on 14 May plans to hold a meeting with Merck, Abbott, and Sanofi-Aventis to attempt again to negotiate lower prices for their products.

–JON COHEN

CREDIT: ADREES LATIF/REUTERS

GENDER EQUITY

Women Are Scarce in New NAS Class

The number of women elected this year to the U.S. National Academy of Sciences (NAS) is the smallest since 2001 and fewer than half the number chosen in 2005. Only 12% of the new class of 72 announced last week (www.nas.edu) are women, compared to levels approaching 25% earlier in the decade. The dismal showing has prompted criticism from some quarters that NAS is backing away from efforts to promote gender equality. But NAS officials say the meager crop simply reflects the persistent dearth of women at the highest levels of science.

"I am amazed that the number is so low," says Jong-on Hahm, who until 2005 served as director of NAS's Committee on Women in Science and Engineering and is now a research professor with the Women's Leadership Program at George Washington University in Washington, D.C. "They seem to have stopped paying attention to the issue."

Not so, counters Ralph Cicerone, who became NAS president in 2005. He says this year's total of nine women "is an unpleasant surprise" because activity aimed at increasing women's representation within the academy "is probably at an all-time high." The academy has been encouraging its members to identify eminent female scientists in their fields and generate "fuller lists" of candidates, says Cicerone. He says he cannot point to a specific reason why the number dipped, however, and the academy has no plans to dissect this year's process.

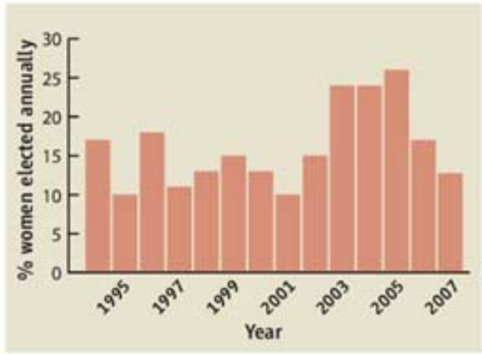

Wrong direction. The number of women elected to NAS this year has taken a tumble compared with recent classes.

But Cicerone says the general underrepresentation of women in the academy is no mystery. "Even though the number of women entering science has been increasing over the years, we are seeing a lagging effect in the composition of the membership, … since it usually takes 25 years or more of research past Ph.D. to achieve the accomplishment required to be elected to the academy," he explains.

Critics aren't persuaded by that argument. "It's the nomination process and sometimes the selection process that fails women," says Nora Berrah, a physicist at Western Michigan University in Kalamazoo and co-chair of the American Physical Society's Committee on the Status of Women in Physics. "Women do not lobby to be nominated, and perhaps we should do it. Also, often the selection process does not have enough women in it." Berrah is disappointed that only one of the nine new members is from the physical sciences and mathematics. NAS officials would not disclose the composition of the committee that chose nominees in that category, but it was unlikely to have been more than the academy's overall tally of 10% women.

Although they receive 43% of U.S. Ph.D. degrees awarded in the natural sciences, women face several barriers that prevent "a normal career progression," says Donna Nelson, a chemist at the University of Oklahoma, Norman. For example, she says, graduate students are sometimes discouraged from selecting a female professor as an adviser, and female professors are sometimes denied access to specialized lab equipment. Similar barriers were documented in a 1999 Massachusetts Institute of Technology study (*Science*, 12 November 1999, p. 1272). Nelson says such a climate hinders a woman's ability to assemble the necessary credentials.

Cicerone says academy members "are keen to do more" to expand the pipeline as well as identify more women candidates. One suggestion is to find rising stars early in their careers and mentor them so as to increase their chances of being elected down the road. "We hope this year's number is just a temporary lull," he says.

–YUDHIJIT BHATTARCHARJEE

BUDGET POLICY

U.S. Science Adviser Tells Researchers to Look Elsewhere

Hardheaded realist or apologist for the Bush Administration? That's what some U.S. researchers were asking themselves last week after presidential science adviser John Marburger said they needed to rely more on nonfederal funding—in particular philanthropy and industry—to expand the scientific enterprise because Congress and the White House cannot keep up with the type of budgetary growth needed to capitalize on scientific opportunities. Several university lobbyists discounted the advice, however, saying those other sectors can't fill the gap that would be left if federal support lags.

Marburger argued his case last week at the annual Science and Technology Forum, the largest gathering of the year for policy analysts, sponsored by AAAS (which publishes *Science*). He said that competing societal priorities have held science to a constant slice of the federal pie for the past 40 years (see graph), and that it is unrealistic to expect legislators to grant larger, sustained increases. "I haven't seen any evidence of an increased top line for science," he told *Science* after his 3 May speech. "I think that's wishful thinking."

The same slice. The share of U.S. discretionary spending going to research hasn't changed much since the days of the Apollo program.

SOURCES: NAS; AAAS, FROM 2008 U.S. BUDGET REQUEST

Marburger spoke glowingly of philanthropies willing to support basic research, citing the Kavli Foundation's network of institutes in the physical sciences (*Science*, 21 January 2005, p. 340), the myriad medical charities and patient advocacy groups, and university partnerships with industry. But many in the audience later referred to that support as "drops in the bucket" and felt Marburger was simply defending the Administration's policies.

"Yes, when you cut taxes and create a deficit and spend hundreds of billions of ▶

dollars on an unpopular war, it leaves you with precious little to spend on anything else," fumed Michael Lubell of the American Physical Society. "I don't expect to see any real changes until after the 2008 election."

Part of Marburger's comments were aimed at pending legislation that would authorize large increases at several science agencies (*Science*, 4 May, p. 672). "People probably wonder why Marburger is not more enthusiastic about these authorizations," the science adviser said in an interview. "I appreciate the desire of Congress to do this, and I feel uncomfortable criticizing them. But it's unrealistic to expect it to happen."

His dark analysis also applies to the flattening of the National Institutes of Health budget after its 5-year doubling ended in 2003, which he says created an increased research capacity that the federal government cannot support. Referring to the communities' expectations of continued robust increases, he said in his speech that "I cannot see how such an expansion can be sustained by the same business model that led to its creation. The new researchers will either find new ways to fund their work, or they will leave the field."

Michael Rodemeyer, a former longtime Democratic congressional science aide, acknowledges that "it's politically hard" to shift spending toward science but disagrees with Marburger that there is any "iron law" fixing its share of domestic spending. But Dan Sarewitz, another former aide now at Arizona State University in Tempe, thinks that Marburger's underlying message is valid. "It's certainly reasonable to complain that the current Administration's priorities have recklessly wasted the budgetary surplus and made it impossible to make important discretionary investments," says Sarewitz. "But if this is true for science, then it's true for other areas. … So which ones would science like to go up against?"

–JEFFREY MERVIS

BIODIVERSITY

The Ultimate Life List

Hands up if you've heard this before: An ambitious new project promises to create an online compendium of all 1.8 million or so described species. It can already claim participation by premier institutions, a wad of start-up cash, and huzzahs from biodiversity guru Edward O. Wilson. Although some confess to a wary sense of déjà vu, taxonomists hope that the Encyclopedia of Life (EOL) can provide the long-awaited comprehensive species catalog. Even enthusiasts agree that it faces some tall hurdles, however, such as signing up curators and getting permission to use copyrighted material.

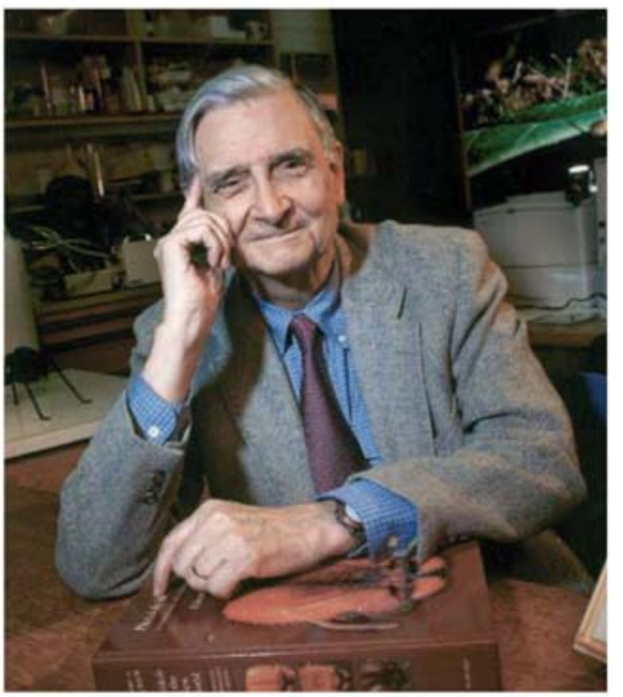

Electronic ark. E. O. Wilson's idea for a Web-based encyclopedia containing all the species on Earth is now ready for launch.

CREDIT: JIM HARRISON/HARVARD UNIVERSITY

Announced this week, EOL involves big names in biodiversity research, including Harvard University and the Smithsonian Institution, and has garnered $12.5 million from the John D. and Catherine T. MacArthur Foundation and the Alfred P. Sloan Foundation. Its plan envisions posting Web pages for each known species. EOL will also provide access to original species descriptions by teaming with the Biodiversity Heritage Library, which is digitizing the pre-1923 taxonomic literature on which the copyright has expired.

Pages on 50,000 species should be ready by the end of 2008, with 700,000 to 1 million species online by 2011, says EOL's newly appointed executive director, James Edwards. He estimates that the work will take 10 years and cost $70 million to $100 million. A separate group is developing a European equivalent, known as SpeciesBase, and the two projects will swap information.

If EOL sounds familiar, that's because its brief overlaps with those of several efforts, notably the All Species Foundation, whose chair promised to deliver a Web site for every species (*Science*, 26 October 2001, p. 769). That project is defunct, but others have managed to cover slices of biodiversity. At one end of the spectrum is the Catalogue of Life, which houses bare-bones taxonomic data—the equivalent of name, rank, and serial number—for more than 1 million species. At the opposite end are lush sites such as FishBase and AlgaeBase, which home in on specific groups and offer illustrated pages on individual species.

EOL will follow both approaches but differs from these projects in automating information collection. Software will pluck data from FishBase, Catalogue of Life, and other Web sources—a "mashup" in Internet parlance. But EOL will be a curated mashup, with experts crafting a home page for each species that records its classification, alternative names, distribution, habitat, diet, and so on. Users will have the opportunity to build additional wiki-style pages, determining what content to include and who gets to contribute, Edwards says. Birdwatchers could flock together to post sighting records, for example, while molecular biologists might add gene expression data.

Researchers praise the EOL's vision but fret about the execution. "The exercise is only worthwhile if it's more accurate and better coordinated than what's already available on the Internet," says Frank Bisby, a taxonomist at the University of Reading in the U.K. and co-director of the Catalogue of Life. Even getting the names right for the poorly studied groups that contain much of biodiversity is a challenge, says Joel Cracraft, curator of ornithology at the American Museum of Natural History in New York City.

Obtaining permission to use post-1923 literature is also an issue, says Donat Agosti, an American Museum of Natural History entomologist who works in Bern, Switzerland. Edwards says that EOL is negotiating with scientific societies and publishers. Although some deals are in the offing, none has yet been announced, he says.

–MITCH LESLIE

Facing off. Both Nicolas Sarkozy and his opponent Ségolène Royal stressed the importance of science to France, but Sarkozy proposed more radical reforms.

FRENCH SCIENCE

Researchers Await Changes—and Clashes—After Sarkozy's Victory

PARIS—"We're in mourning," laments Cécile Wandersman, head of a research unit at the Pasteur Institute. "For me, this is a great hope," says Jean-Robert Pitte, president of the Université Paris-Sorbonne. Both were talking about this week's election of right-wing politician Nicolas Sarkozy as France's next president.

As the contrasting comments indicate, Sarkozy's victory and his conservative agenda have divided the scientific community, just as it has French society as a whole. Known for tough talk on law and order, immigration, and morality, the former interior minister is mistrusted and reviled by the left—including many in the academic world. Wandersman, for instance, scoffs at Sarkozy's promise to raise research spending to 3% of gross domestic product by 2012. But to Pitte and many others, his agenda for change—including a shakeup of the higher education system as early as this summer—are just what France's sclerotic research scene needs.

Research had played a larger-than-usual role in this election with both Sarkozy, who chairs the Union for a Popular Movement (UMP), and his rival, Socialist Party candidate Ségolène Royal, promising to increase science and higher education budgets. That was a victory in itself, says Jules Hoffmann, president of the French Academy of Sciences: "Research has never been this high on the agenda before."

But the candidates' opinions diverged on how to address the malaise in French research and the long-running problems at the country's universities. Science and higher education don't mix well in France, because most research takes place at mammoth government institutions such as the National Centre for Scientific Research (CNRS) rather than at the universities. A highly centralized administration system means universities are relatively powerless to set their own agendas; they also suffer from the fact that the smartest young minds typically attend the so-called grands écoles, which train France's professional and political elite but carry out little research.

Royal's answer to these woes centered on 10% annual budget increases and revoking the most controversial elements of a research reform bill that President Jacques Chirac's government had introduced last year (*Science*, 10 March 2006, p. 1371). In contrast, Sarkozy offered more radical reforms that would move the country's education system closer to the Anglo-Saxon model. He has said he will introduce a law within 6 months that would offer universities much more autonomy—for instance, to manage their own budgets and set recruitment and research policies.

Clear winner. Nicolas Sarkozy received 53% of the votes during the second round of the election.

Sarkozy has also suggested turning the big research bodies such as CNRS into U.S.-style granting agencies that would reward proposals rather than employ scientists—a controversial shift in a country where science usually means a government job for life. To carry out those promises, Sarkozy's UMP will have to retain its majority in the National Assembly during elections next month; polls suggest it will.

Sarkozy's plans have alarmed Sauvons la Recherche (SLR), a left-leaning movement that brought thousands of researchers to the streets in 2004 to protest cuts to science budgets by the Chirac government. Nine days before the runoff, SLR called on its members to vote for Royal. Sarkozy seems intent on rushing his higher education plan through Parliament without proper consultation by the scientific community, says SLR President Bertrand Monthubert. Turning France's research organizations into funding agencies would create more uncertainty for investigators and make science careers even less attractive, he says: "What works in Britain or the U.S. doesn't necessarily work in France."

But Pitte argues that more autonomy for universities is "absolutely needed"—and he hopes Sarkozy will go further. Universities should have the right to raise tuition fees and to select the best students rather than admitting everyone who qualifies, says Pitte. Those reforms go against France's egalitarian streak and are bound to trigger protests, he admits; his own Sorbonne was paralyzed for over a month last year by student revolts that eventually brought down a labor law already adopted by Parliament. This time, says Pitte, "I hope the government will be courageous and hard."

Bernard Bobe, an economist at the Ecole Nationale Supérieure de Chimie in Paris, notes that Sarkozy, like Royal, has failed to address the old split between universities and grands écoles. What's more, he is not convinced that the research and education system will be a high priority for Sarkozy, who has announced ambitious plans on a raft of other issues. France's science system has proven extremely resistant to reform, Bobe notes; "I think Sarkozy has the courage, but I'm not sure he has the ambition" to succeed where others have failed.

–MARTIN ENSERINK

CREDITS (TOP TO BOTTOM): CLAUDE PARIS/AP; BENOIT TESSIER/REUTERS

Closing the Net on Common Disease Genes

Huge data sets and lower cost analytical methods are speeding up the search for DNA variations that confer an increased risk for diabetes, heart disease, cancer, and other common ailments

AFTER YEARS OF CHASING FALSE LEADS, gene hunters feel that they have finally cornered their prey. They are experiencing a rush this spring as they find, time after time, that a new strategy is enabling them to identify genetic variations that likely lie behind common diseases. By scanning the genomes of thousands of people and comparing the sick with the healthy, biologists are uncovering markers for DNA sequences they believe clearly increase the risk of type 2 diabetes, cancer, heart disease, inflammatory bowel disease, and other debilitating ailments.

Their new tool, known as the genome-wide association (GWA) study, derives its power from the Human Genome Project and the more recent Haplotype Map that catalogs human genetic variation. The hunt has been sped along as well by the plummeting cost of gene scanning and by efficient gene-chip technologies available only in the past 2 years.

What sets these studies apart from earlier gene discoveries claimed for the same diseases is that the new associations are statistically far more powerful and highly unlikely to be due to chance. Researchers are also confident about a flurry of new results because they've been recorded again and again in populations studied by independent teams. Fueling the excitement is a sense of surprise: "Most of these genes were not on anybody's candidate gene list," says David Cox, chief scientific officer of Perlegen Sciences in Mountain View, California, which uses whole-genome scanning to identify drug targets. Cox recently co-authored a paper identifying a new genetic variant that raises heart disease risk and has another in the pipeline on breast cancer. He and many others expect the discoveries to point toward novel biology worth exploring.

At the same time, this wave of GWA studies is studded with caveats. Although many agree that the findings are real, few scientists believe that they should be quickly put to clinical use—for example, to evaluate a person's risk of having a heart attack. Scientists haven't sorted out how these genes might interact with the environment, or how lifestyle changes might modulate the risk they confer. "There's going to be some scrambling to catch up on the clinical side," says Nancy Cox, a human geneticist at the University of Chicago in Illinois.

Furthermore, these first studies may have identified only the strongest associations, with many more genes still to be dug up. Finding them will likely require an unusual degree of cooperation in this intensely competitive field.

Uncommon beginnings

The new discoveries mark a major break with the past in part because their sweep is so broad. Traditionally, geneticists focused on single genes with potent effects, typically looking at large families riddled with rare diseases, such as cystic fibrosis or Huntington's disease or inherited forms of cancer. By tracking a small number of genetic markers that were linked to disease in such families, researchers successfully homed in on the culpable gene that causes disease.

These family "linkage" studies lacked the power to pick up genetic variants that have a modest effect or that may interact with environmental exposures, however. And yet it is these variants, which may raise risk by 50% or less, that could play a key role in common, complex diseases. (The exception is work by deCODE Genetics in Reykjavik, which has used linkage methods and a proprietary database containing information on much of Iceland's adult population to find some common disease genes.)

As an alternative to traditional linkage studies, researchers have tried searching for "candidate genes" known to play a role in some biologic process, such as insulin production. They looked for associations between mutations in these candidates and common diseases. Hundreds of studies have reported such associations. But few have been reproduced more than once or twice.

The new strategy that's blossomed this spring has fundamentally altered the gene-

CREDIT: GETTY IMAGES

hunting landscape. Rather than work with a few thousand genomic markers, scientists are now using gene chips that can scan an individual's DNA sample for anywhere from 100,000 to 500,000 or more single-base changes. Known as single-nucleotide polymorphisms (SNPs), these changes are selected to reflect patterns of common genetic diversity. Such high SNP density makes it much easier to detect culprit DNA changes. In addition, because the cost of using such chips has dropped sharply, scientists can test DNA from thousands of people, adding power to their studies.

By compiling the SNPs from every DNA sample in a database, and comparing the SNPs in, say, heart attack patients to those in healthy people, it's possible to discern even subtle genetic signals that contribute to blocked arteries. The signals in GWA studies, emanating from a SNP or set of SNPs, don't necessarily mean that the SNPs themselves are influencing disease but rather that they're located in or near the problem DNA.

Still, "one size never fits all," and other strategies will still be necessary to identify the DNA behind disease, says Kathleen Merikangas, a genetic epidemiologist at the National Institute of Mental Health in Bethesda, Maryland. For example, GWA studies cannot discern rare variants or extra copies of genes, which can have a strong effect on physiology.

Gene bonanza

The list of diseases and traits examined with GWA began as a trickle 2 years ago with a highly touted paper on macular degeneration; it hit on a new gene in severely affected patients. Last October came a study that identified a gene involved in memory, and in December yet another gene surfaced that, depending on the version inherited, increased the risk of Crohn's disease—an inflammatory bowel disorder—by as much as 56%, or decreased it by 74%, in one group tested. All three studies have since been replicated.

This year, the results began to come fast and furiously. In the first week of April, a new gene variant involved in prostate cancer and confirmation of a second were described in *Nature Genetics*. This new variant appears to raise the risk of prostate cancer by 58%, and in combination with other variants, including five in the same region discovered with a different technique, could explain a large proportion of cases in African Americans, according to the researchers who found them.

Late April brought a trio of online papers in *Science* that presented three novel diabetes gene variants; the studies also confirmed a handful of other findings, including a gene involved in controlling body weight that was published weeks earlier. Last week, two independent reports were published, also online in *Science*, of a genetic variant associated with heart disease that, in the one-quarter of Caucasians tested who carry two copies, increases the chance of a heart attack by more than 50%.

"There is a great deal of excitement, because everyone realizes the field is changing so fast," says Judy Cho, who led the group that found the Crohn's gene and directs the inflammatory bowel disease center at Yale University.

The pace, most believe, will only quicken. The Wellcome Trust Case Control Consortium, a collaboration of 24 human geneticists in the United Kingdom, will soon report findings on seven diseases studied with GWA, including bipolar disorder, rheumatoid arthritis, and hypertension. Papers on type 1 diabetes and breast cancer are nearing publication; the latter will report similar findings to prostate cancer, says co-author Bruce Ponder of Cancer Research UK Cambridge Research Institute—a handful of new genes that slightly raise risk.

Clinical questions

What do all these discoveries mean for medicine? With the notable exception of the macular degeneration gene variant, which raises disease risk about two to three times in those with one copy, most of the genes found so far boost risk only incrementally. Although a 50% increase may sound substantial, in absolute terms it's modest. For example, says Ponder, a 60-year-old woman's breast cancer risk is 3%. If she carries two copies of the most potent breast cancer variant found by his group, which makes her 1.6 times more likely to develop breast cancer, her overall risk increases to just 4%.

It's also unclear how lifestyle modifications affect the total risk these variants confer—in other words, whether someone can use the information to lower disease risk, say, by exercising or dieting. On the other hand, if the gene is common, it may have a major impact on disease prevalence across a population, notes Merikangas. Although the risk may not be worrisome for an individual, a gene with modest effects may account for many cases of disease.

These concepts are difficult to convey to patients. "There is a complete disconnect" between what the general public expects from susceptibility genes for diseases such as these, says Cox of Perlegen, and how they should be applied clinically. "The public … really loves the concept of personalized medicine," says Cox. "They don't understand, and I don't think we've explained, that having something that's statistically meaningful does not mean having something that's clinically relevant to them."

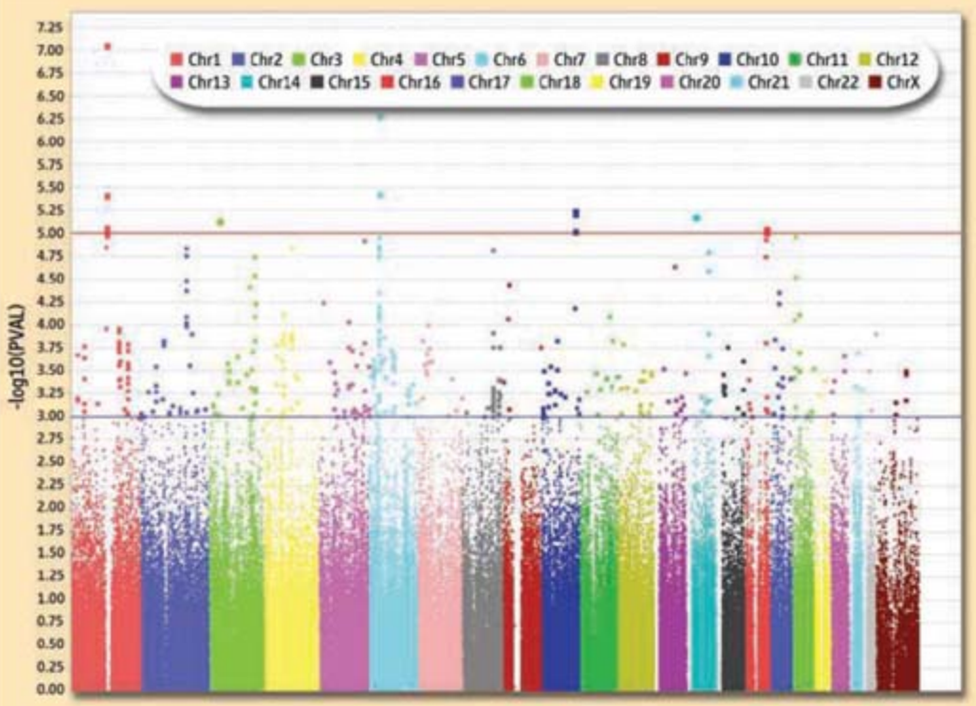

Rising to the top. In a genome-wide association study for type 2 diabetes, 386,731 genetic markers, shown here by chromosome, pop up. Those above the higher line appeared to be significantly associated with disease.

CREDIT: THE DIABETES GENETICS INITIATIVE/BROAD INSTITUTE OF MIT/HARVARD/LUND UNIVERSITY/NOVARTIS

Still, many predict that companies will jump at offering "risk predictors" directly to consumers. DeCODE has already released a test for *TCF7L2*, the highest-risk diabetes gene, which increases the chance of disease by about 40% among those with one copy tested so far, and plans to offer a test for the heart disease marker. But most academic researchers say they need to know more about how these variants cause disease before diagnostic tests like this one can be useful. "I'm not at all enthusiastic about rushing out to test people in the clinic" for these genes, says David Altshuler of the Broad Institute in Cambridge, Massachusetts, who helped lead one of the teams studying diabetes.

For many biologists, interest focuses not only on risk assessment but also on a longer-term clinical application: better understanding diseases and designing improved treatments to combat them. "The exciting part to us is, it's opening up completely new hypotheses," says Lon Cardon of the University of Oxford, a collaborator in the Wellcome Trust consortium.

Many of the new results point to genes in unsuspected stretches of the genome, or to regulatory regions between genes, ignored by studies focusing on candidate genes. Members of one of the teams that described new variants for type 2 diabetes, for example, at the start of the project compiled a list of 1000 candidate genes they thought they might find. None of the nine variants the group detected were on that original list, says Altshuler.

The findings could also point researchers in new directions, to pathways not previously contemplated as drug targets. For example, the newly discovered heart disease variant falls in the same region on chromosome 9 as one of the new diabetes variants. "This is a stunner," says Francis Collins, head of the National Human Genome Research Institute in Bethesda, Maryland, who helped lead one of the diabetes teams, because it could help explain why some people are vulnerable to both diabetes and heart disease.

The next wave

To unravel the deeper biology, scientists need to find still more susceptibility genes and understand how they interact. "We need to now understand what happens if you have three risk alleles, or five, or seven," says Thomas Hughes, who collaborated with Altshuler and is global head of diabetes and metabolism research at the drug company Novartis. Some could enhance or, alternatively, neutralize the effects of others, notes Stephen Chanock of the National Cancer Institute in Bethesda, Maryland. But finding this second wave of disease variants will be much tougher, because their effects will likely be smaller—and will require massive data sets in order to be detected, researchers say.

Many scientists say that the best way to speed progress is by sharing data fresh from the genotyping labs, even before it's been analyzed for gene-disease associations. But pooling data is more complicated than it sounds. One problem is that researchers may have to track down people who provided their DNA to a study to get their consent to have it distributed widely. DeCODE CEO Kári Stefánsson, who says the company's informed consent agreement could preclude data sharing, has another concern: He argues that because investigators have often collected data on clinical measures using different methods, pooling the data could lead to spurious associations. "It may be extraordinarily misleading," he says.

But the reality is that many common disease gene variants will likely go undiscovered without large collaborative efforts. The three diabetes teams, for example, were able to firmly pin down markers only because they shared their data, says Hughes. "Things that were deeply buried in our [gene] list … start to shine when you pool them with larger and larger populations," he notes. Cho, the Crohn's researcher, admits that she and her colleagues rushed their first, potent gene into print, but now she realizes that "we have to combine forces with other people" to find the rest.

The culture is already changing. For instance, the investigators who lead the National Institutes of Health (NIH)–sponsored Framingham Heart Study will make available later this year SNP data and clinical information with identifying information removed on 9000 residents of Framingham, Massachusetts, who have participated in the decades-long health study. And the Wellcome Trust consortium, which draws on existing cohorts in the U.K., already provides SNP data on controls to other researchers and later this summer will add data on subjects with diseases. To his surprise, says Cardon, "we didn't find any [investigators] who did not want to [contribute]."

Hoping to encourage such sharing, NIH expects to issue a new data-release policy in a few months that will request that any U.S. investigator receiving funding for GWA studies deposit their data sets in a central repository. (Only results of genetic analyses will be posted publicly; the SNP data on individuals, which could in theory be used to identify a person, will be available to qualified investigators who agree not to distribute it publicly.)

The proposed NIH policy, which will also restrict patenting, will ask that data be submitted as quickly as possible but provide a window—perhaps 9 months—to allow the original investigators to publish on it first.

Scientists expect that this first round of GWA genetic discoveries will taper off in a year or two as they begin the slow, hard work of untangling what these genetic variants do. But among many biomedical researchers, there is a sense that the field of genomic medicine has entered a new phase, one that will finally test the promise of the Human Genome Project. "Are we on the threshold of something?" says Neil Risch, a human geneticist at the University of California, San Francisco. "I think so."

–JENNIFER COUZIN AND JOCELYN KAISER

Selected Genome-Wide Scan Results

DISEASE	PUBLICATION DATE	SAMPLE SIZE*	GENES OR VARIANTS FOUND	APPROXIMATE INCREASED RISK FOR HOMOZYGOTES†
Macular degeneration	2005	1700	1 new gene	400% to 600%
Inflammatory bowel disease	2006	4500	1 new gene	120%
Prostate cancer	2007	17,500	2 variants in same region (1 new)	123%
Obesity	2007	38,700	1 new gene	67%
Type 2 diabetes	2007	32,500	9 variants (3 new)	80%
Heart disease	2007	41,600	1 new variant	25% to 40%

* Cases and controls including replicates. † For highest risk variant.

Brownout. With warmer winters, mountain pine beetles have chewed through millions of hectares of forests in British Columbia.

CREDIT: NATURAL RESOURCES CANADA, CANADIAN FOREST SERVICE

ECOLOGY

Back to the No-Analog Future?

Fossil pollen and climate models suggest a messy world in 2100, as surviving species reshuffle into entirely new combinations, creating "no-analog" ecosystems

Fly over northern Indiana, and you'll see a quilted landscape of corn and soybeans, punctuated by glacial lakes. The gelatinous mud in those lakes has preserved plenty of fossil pollen, from which paleoecologists have reconstructed a record of the region's past. Now, that same fossil pollen is providing a glimpse into Earth's ecological future—and it's not a pretty picture.

It suggests that, if the climate changes over the next 100 years as current models predict, surviving species throughout much of Earth's land area will not simply migrate north and south en masse as unchanging communities, as Charles Darwin once believed. Instead, they are likely to be reshuffled into novel ecosystems unknown today. If that view is even partly correct, then the task of preparing for, or even predicting, the ecological effects of climate change just got a whole lot harder.

Analyses over the past several decades have shown that during the last North American ice age, as the Laurentide Ice Sheet retreated into Canada 17,000 to 12,000 years ago, the region from Minnesota to Ohio to Tennessee supported a forest of spruce, sedge, oak, ash, and hophornbeam—an ecosystem that simply doesn't exist today, despite the fact that all of those species still survive. These odd communities—called "no analog" ecosystems because no modern counterparts for them exist—likely arose from odd combinations of climate variables such as precipitation, temperature, and seasonal variations that also don't exist today, say John Williams of the University of Wisconsin, Madison, and Stephen Jackson of the University of Wyoming in Laramie.

Williams helped demonstrate the connection between no-analog communities and climate during his Ph.D. work at Brown University in the late 1990s, when he compared pollen and climate records for dozens of field sites across the eastern United States. That result, published in 2001, piqued Williams's interest in whether climate change over the next century might lead to a similar type of ecosystem reshuffling—and whether these changes could be predicted. "It was a logical next step," says Williams, "to think about the future."

To find out, Williams and Jackson teamed up with John Kutzbach, a climate modeler at the University of Wisconsin, Madison. They have analyzed the outputs of standard climate models to try to map geographic areas that are likely to experience novel climates, which in turn could result in no-analog communities. In a paper published online in the *Proceedings of the National Academy of Sciences* (*PNAS*) on 27 March, they project that by 2100, depending on which climate scenario and model they use, 4% to 39% of the world's land area will experience combinations of climate variables that do not currently exist anywhere on the globe. Areas with these novel climates are likely to develop no-analog ecosystems.

Jackson, Kutzbach, and Williams fed two standard greenhouse scenarios into their models: the pessimistic A2 scenario, in which CO_2 concentrations reach 850 parts per million (ppm) by 2100, and the more optimistic B1 scenario, in which CO_2 climbs to 550 ppm. They divided the world's landmasses into grid cells measuring 2.8° latitude by 2.8° longitude and, for each cell, looked at what the models predict for four climate variables: mean summer temperature, mean winter temperature, mean summer precipitation, and mean winter precipitation.

For each spot on the map, they compared the forecast climate in 2100 with baseline climate from 1980 to 1999. To test whether these forecast climate changes would be sufficient to reshuffle ecosystems, they compared them with variations in climate that underlie different ecosystems in the same geographic area today (for example, deciduous forest and pine forest).

Not only will novel climates appear, according to the analysis, but existing climates will disappear for 4% to 48% of the world's land area. In other words, the conditions that now exist in these areas will not be found anywhere in the world by 2100. These globally disappearing climates signal the likelihood for significant ecological disruption, if not necessarily no-analog ecosystems. "This is a conservative analysis," says Jackson. "If we added more climate variables, we'd probably end up with more disappearing and novel climates."

New climates are expected to cause ecosystem reshuffling as individual species, constrained by different environmental factors, respond differently. One tree may be limited by summer rains that hold back seedling recruitment, for instance, whereas another species may be limited by winter freezes that control insect pests. Some species may migrate up-latitude or up-elevation, while others stay put. An ecosystem might see many species vanish—but also new arrivals.

Williams and colleagues project that the tropics, including Amazonia, will see the most pronounced no-analog climates, with rising temperatures pushing these already-warm areas outside of any climates currently known today. Soaring temperatures combined with drought could selectively kill taller, canopy-forming trees—rapidly transforming ecosystems by increasing sunlight and drying at ground level.

Within North America, the team predicts that the southeastern United States will see no-analog climates, driven by a selective rise in summer temperatures. The result could be increased wildfires in forests that are poorly adapted to fire, leading to rapid opening of the canopy unless those forests are managed aggressively.

"I applaud their work," says William Hargrove, a landscape ecologist at Oak Ridge National Laboratory in Tennessee. "We've seen an explosion of climate-change models turning out results, but I don't see as much work on the prognostic impact of these results on ecosystems." In

"I feed my cells Lifeline™ Media. I wouldn't consider anything else."

LIFELINE®
CELL TECHNOLOGY

"I care about my cells and need them to thrive. The people at Lifeline Cell Technology understand and care about my cells too. Their cell culture experience dates back to the 1980's, to the introduction of Normal Human Cell Systems. Their philosophy is to provide quality-tested products that are guaranteed to perform. Best of all, their technical staff is accessible and knowledgeable."

At Lifeline Cell Technology we produce Stem Cell and Primary Cell products for your research. Stem Cell products include Mitomycin C Treated Fibroblasts with Serum Free Medium and ags-Neural Stem Cells, *a unique cellular model of stroke*. Try our primary human cell products, including Endothelial Cells, Dermal Fibroblasts, Serum Free or Low Serum Media, Growth Factors and Reagents. Lifeline products are consistently manufactured and rigorously tested.

To learn about our products, please visit lifelinecelltech.com or call us at 301.845.7787. We'll be pleased to help you with your research needs and give you the specialized attention you and your cells deserve.

Call Lifeline Technical Service and Sales at 301.845.7787
or visit lifelinecelltech.com for more information.
Lifeline Cell Technology – 10 East Frederick Street – Walkersville, MD 21793

INTERNATIONAL STEMCELL CORPORATION

a similar exercise, published in 2005, Hargrove and colleagues mapped changes in seven climate variables across the United States. They predicted a higher rate of vanishing climates by 2100 than did Williams, Jackson, and Kutzbach. Hargrove attributes some of this difference to the fact that his team considered not only climate but also other ecologically relevant variables, such as soil type and landscape topography. "If you consider only climate," says Hargrove, "you may underestimate the magnitude of ecological change."

One of the biggest issues raised by novel and disappearing climates is whether species whose preferred climates disappear locally can migrate to other areas where suitable climates still persist. As described in *PNAS*, Williams, Jackson, and Kutzbach performed a second analysis examining this very question. For each point on the map where the climate changes by 2100, they examined the surrounding areas to determine whether the current climate would persist elsewhere within a 500-km radius. Imposing this constraint increased the proportion of disappearing climates to 14% to 85% of the world's land area, depending on the climate scenario and model.

Migration corridors are often proposed as a strategy to facilitate the movement of species in response to climate change; but this analysis suggests that often there may be no suitable refugia nearby. "Even if these species can migrate quickly enough," says Jackson, "they may effectively have nowhere to go."

Rapid shifts in the pollen record lead some people to predict that future changes could be sudden as well. Some argue that it's already happening, with droughts across the Southwestern United States between 2000 and 2005 killing over 80% of adult piñon trees in some stands, drastically altering the piñon-juniper woodlands. If drought frequency increases in the Southwest, as some climate models predict, then other species could seize the niche vacated by those dead piñons, permanently altering the landscape's canopy structure, hydrology, and fire regime. "It's going to be interesting to see what happens there in the next 20 years," says Jackson. "This ecosystem may or may not come back."

Others remain circumspect. Craig Allen, a landscape ecologist who observed the die-offs firsthand from the U.S. Geological Survey's (USGS's) Jemez Mountains Field Station in New Mexico, points out that the proximate cause of most piñon mortality was beetle infestation. That means many juvenile trees survived, and these could restore piñon populations within decades if further droughts don't intervene.

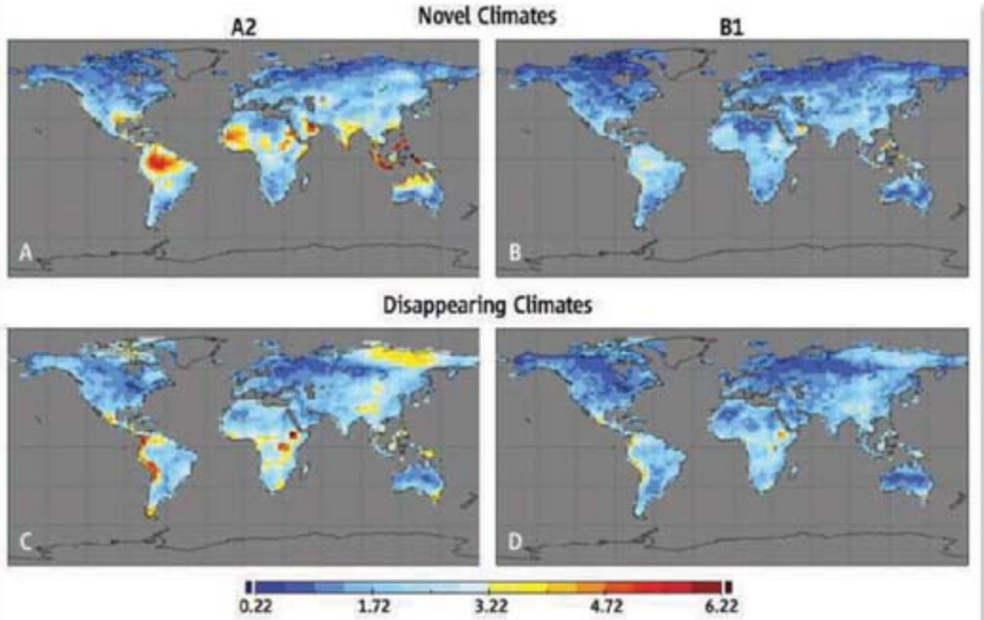

Brave new world. Pessimistic (A2) and optimistic (B1) greenhouse scenarios predict that novel climates will appear across the tropics by 2100, while current climate types disappear in the tropics and the higher latitudes. Color scale represents degree of difference from current climate, with yellow-orange-red indicating significantly different climate by 2100 and substantial risk for developing no-analog ecosystems.

CREDIT: WILLIAMS *ET AL.*, *PNAS* 104, 14 (2007)

The prospect of novel climates has people rethinking traditional goals such as maintaining native ecosystems. "That's probably going to be impossible," says Nathan Stephenson, a research ecologist at the USGS Western Ecological Research Center in Three Rivers, California. "But what you can still do, even if you can't maintain native communities, is potentially maintain regional biodiversity and ecosystem functions."

Nowhere is this point of view more evident than in the management of forests—where human intervention has always been heavy. In British Columbia, climate-related surges in mountain pine beetles and fungus have browned millions of hectares of trees in recent years. Ecologists there are thinking about how to maintain a forest that will provide reliable watersheds, wildlife habitat, and lumber supplies into the future. The solution could involve planting different mixtures of tree species or replanting forests using seed stock from warmer areas, says Del Meidinger, an ecologist with the British Columbia Ministry of Forests and Range in Victoria. "You have to plant something that will survive now but will still grow well into the future" in a changed climate, says Meidinger.

Land managers would love to predict how ecosystems will reorganize, what sorts of no-analog communities might emerge, and which species will dominate. Ecologists have produced niche models that predict species' future geographic distributions based on climates in their current locations. But that approach may break down when it comes to future no-analog climates, says Williams. "You're limited by what you can observe today," he says. "It's a real problem for making ecological forecasts for climates that are outside the current range of observation."

One promising approach to making better forecasts is to base them on experimentally determined physiology. Ronald Neilson, a bioclimatologist with the Forest Service's Pacific Northwest Research Station in Corvallis, Oregon, is developing such a model. It predicts drought-induced mortality and fire by calculating how much leaf area can be supported by local moisture levels, based on measured rates of leaf water loss. "What we're simulating at the moment is plant functional types," says Neilson. "We want to get to the species level."

This year, Neilson and Michael Loik of the University of California, Santa Cruz, will take the first step in that direction. They'll begin a seedling transplantation study to measure the physiological tolerances of a single species: Jeffrey pine, in the eastern Sierra Nevada of California. It's an effort-intensive approach, to be sure, but understanding the implications of a no-analog future might require no less.

–DOUGLAS FOX

Douglas Fox is a freelance science writer based in northern California.

Stern countenance. Tim McCaughan says his condition leads people to take him more seriously than he intends.

CREDIT: MIKE AHLERS/CNN

NEUROLOGICAL DISORDERS

The Mystery of the Missing Smile

Genetic studies and an ineffective abortion drug have provided some of the few clues researchers have about a rare disorder that hampers facial expressions

BETHESDA, MARYLAND—People can't always tell when Tim McCaughan is joking. Several years ago, a recently hired colleague congratulated him on a promotion, saying she was sure it was well-deserved. "Well, how would you know?" McCaughan quipped, playfully suggesting that maybe he didn't deserve the promotion after all. But his face didn't convey that he was joking, and the woman thought he was being a jerk. McCaughan has a rare neurological condition called Möbius syndrome that limits his ability to smile and make other facial expressions.

"People often take me much more seriously than I really am," says McCaughan, a senior producer at CNN who oversees the news network's coverage of the White House. He eventually managed to smooth things over with his colleague, who became his wife a few years later. "I'm still living that one down," he says.

McCaughan's case of Möbius syndrome is on the milder side of a wide spectrum. Many people have more extensive facial paralysis that impairs their speech and causes difficulties with eating. Limb deformities such as clubfoot often accompany Möbius syndrome. And for some unknown reason, autism appears to be far more common in people with the syndrome than in the general population.

An international group of neurologists, geneticists, and other specialists gathered here recently for the first scientific conference* on this mysterious congenital disorder. They explored possible genetic and environmental triggers, discussed potential treatments, brainstormed research strategies, and hashed out a consensus set of diagnostic criteria. "This is really at such an early stage," says John Porter, a program director at the National Institute of Neurological Disorders and Stroke, one of the meeting's sponsors. The meeting was a good start, but cracking the biology of Möbius syndrome isn't going to be easy, Porter says. "I think the mechanistic insights are going to take a while."

Frozen faces

The syndrome is named for Paul Julius Möbius, a German neurologist who published an early description of it in 1888. (He was also the grandson of August Ferdinand Möbius, the mathematician of Möbius strip fame.) According to a statement developed at the conference, the syndrome's defining characteristics are facial weakness and impaired ability to move the eyes to the side—symptoms that are present at birth and don't worsen with age. Researchers estimate that Möbius syndrome occurs in 1 of every 50,000 live births, affecting boys and girls equally often.

The core symptoms of Möbius syndrome point to defects in two cranial nerves: the abducens nerve, which innervates the lateral rectus muscles that rotate the eyes toward the side of the head; and the facial nerve, which innervates the muscles of the face. Yet, there doesn't seem to be a single neuropathological signature of the disorder.

At the conference, George Padberg, a neurologist at the University Medical Center in Nijmegen, the Netherlands, described magnetic resonance imaging studies he and colleagues have done to visualize the nervous system in people with Möbius syndrome, as well as findings from electrophysiological tests of nerve function. This work has revealed a variety of defects. In some patients, the cranial nerves appear to be damaged or even missing. Others have abnormalities in the brainstem that include—and often extend beyond—the region where the abducens and facial nerves originate. Based on these and other findings, Padberg suspects that Möbius syndrome results from genetic miscues that derail the embryonic development of the brainstem.

But the search for the relevant genes has yielded little fruit so far. The rarity of the disorder, coupled with the fact that only about 2% of cases are inherited, makes it difficult to find a sufficient number of subjects for genetic linkage studies, says Ethylin Wang Jabs, a geneticist at Johns Hopkins University in Baltimore, Maryland. The complexity of the disorder and lack of precise diagnostic criteria have also complicated matters, Jabs says. Padberg's group, for example, has published studies identifying regions of chromosome 3 and chromosome 10 as likely loci of genes related to inherited Möbius syndrome in two Dutch families, but other researchers point out that individuals in these families lack the eye-movement irregularities necessary to qualify as true cases of Möbius syndrome. (Padberg now agrees.)

Now that there's a more precise definition of the disorder, the next step for finding Möbius genes, Jabs and others say, will be to create a central database in which researchers can share clinical and genetic data on Möbius patients. Jabs has started a database that now includes clinical data and/or DNA samples from 89 people with Möbius syndrome and more than 100 relatives, and other research teams have similar data.

Researchers are also looking to related disorders and mouse models of brain develop-

* Moebius Syndrome Foundation research conference, 24–25 April 2007.

ment for clues. At the conference, Elizabeth Engle, a pediatric neurologist at Children's Hospital Boston, described her team's research on several inherited neurological conditions that share symptoms with Möbius syndrome. Athabascan brainstem dysgenesis syndrome (ABDS), named for the Native American population in which it was first described in 2003, causes impaired lateral eye movements and sometimes facial weakness as well. Similar symptoms had been reported in mice lacking a gene called *Hoxa1*, one of a family of genes that guide embryonic development. People with ABDS inherit a truncated copy of the human version of the gene, *HOXA1*, Engle and colleagues reported in 2005 in *Nature Genetics*. It's possible that spontaneous mutations in *HOXA1* could be involved in Möbius syndrome, Engle says, but so far no one has looked. Jabs has been screening her Möbius patients for mutations in two other *Hox* genes, *HOXB1* and *HOXB2*, based on findings of facial nerve abnormalities in mice lacking these genes. So far, however, nothing has turned up.

Misoprostol is typically used in the first trimester of pregnancy, and in the sample of Möbius children Ventura has worked with, misoprostol exposure occurred on average about 40 days after conception.

Some researchers have proposed that Möbius syndrome can result from a transient interruption in fetal blood circulation, and Ventura and others think the misoprostol findings fit with that idea. One possibility is that uterine contractions evoked by the drug disrupt fetal blood supply during a crucial stage of development, causing neural circuits in the brainstem to be permanently miswired.

Other researchers are exploring the apparent link between Möbius syndrome and autism. Research teams from Sweden, Canada, and Brazil reported at the conference that roughly a third of their Möbius patients have autism spectrum disorders; teams from the United States and the Netherlands reported autism rates of 5% or less, however. One possibility is that the miswiring of the brainstem that occurs in Möbius syndrome somehow predisposes people to autism. Another, more speculative hypothesis is that the limited facial expressions in infants with Möbius syndrome hinder social interactions early in life, thereby stunting the development of the brain's social circuitry and leading to social impairments characteristic of autism.

"We have evolved to use our faces as a primary means of communication, both through speech and facial expressions," says Karen Schmidt, a biological anthropologist at the University of Pittsburgh in Pennsylvania who studies facial behavior. An infant with Möbius syndrome is less able to smile and interact with others, and many children with Möbius syndrome are shunned by their peers. The long-term effects of such relative social deprivation could be substantial, Schmidt says.

Unfortunately, there's little help for the neurological symptoms of Möbius syndrome. One dramatic exception is "smile surgery" developed by plastic surgeon Ronald Zuker at the Hospital for Sick Children in Toronto, Canada. At the conference, Zuker described the 8-hour procedure, which he has performed in hundreds of children since the late 1980s. Zuker's team transplants a small piece of muscle from the patient's thigh to the face and positions it so that it will raise the upper lip when it contracts. To innervate the transplanted muscle, the surgeons usually reroute a nerve that innervates the masseter, the muscle that raises the lower jaw during chewing. Initially, the patients need to think about clamping their jaws to fire the nerve and elicit a smile, Zuker says, but with time the smile becomes more automatic.

Zuker showed several before-and-after videos that revealed striking differences. One boy, when asked to smile prior to surgery, could only muster an expression that looked closer to a grimace or frown, the corners of his mouth moving slightly sideways and downward. After surgeries on both sides, his smile was unmistakable, and he even seemed to modulate it according to whether he actually felt like smiling or was merely indulging the cameraman for the umpteenth time.

Still, smiles aren't for everyone—at least not all the time. McCaughan, whose work at CNN has given him the opportunity to travel with and interview several U.S. presidents over the years, says his condition sometimes works in his favor. "I'd say I've got the best deadpan in the business when asking a question." **–GREG MILLER**

CREDIT: COURTESY OF LORI THOMAS

Something to smile about. Möbius syndrome robbed Chelsey Thomas of a smile (*left*); plastic surgeons gave her a new one in two stages.

A troubling drug problem

Garbled genes aren't the only way to get Möbius syndrome. Since the mid-1990s, dozens of cases of Möbius syndrome have been linked to misoprostol, a drug commonly used by women in Brazil to induce abortion. Elective abortion is illegal in Brazil, but misoprostol is cheap and widely available, says pediatric ophthalmologist Liana Ventura of Fundação Altino Ventura, a medical charity in Recife, Brazil. Although misoprostol is used in three-quarters of abortion attempts in Brazil, it is not particularly effective: Up to 80% of pregnancies continue to term, and about 20% of those result in an infant with Möbius syndrome, Ventura says.

LETTERS

edited by Etta Kavanagh

"Overshoot" Scenarios and Climate Change

IF IT IS DESIRABLE TO REMAIN BENEATH LOW LEVELS OF ATMOSPHERIC CARBON DIOXIDE concentrations, and if W. S. Broecker ("CO_2 arithmetic," Policy Forum, 9 Mar., p. 1371) is correct that this will be difficult to achieve by systematic emission reductions alone, then radical thinking across a broad range of options is required.

So far, the scientific community has considered climate change under plausible scenarios of technical and economic futures without any explicit action to curb emissions. However, if followed, such a scenario could take us into the territory of dangerous climate change (*1*), to which society would need to adapt. The community has also considered what emissions pathways would be needed to avoid crossing unacceptable or "dangerous" levels. These lead to the eventual stabilization of climate, but invariably require massive reductions in fossil fuel burning, starting soon. The latter places a burden on the current and next few generations, while the former leaves the potentially huge problem of dealing with the adverse effects of climate change to future generations. The balance of taking action now and the consequences of no action are an area of active debate [e.g., (*2*)].

It is against this dilemma that the concept of "overshoot" scenarios is emerging in which atmospheric concentrations and/or associated temperature increases could temporarily exceed target levels (such as the 2°C warming favored by the European Union) before declining to stabilization. In this scenario, emissions would be reduced less severely in the short term, but more severely later on (possibly using carbon capture technology), when compared to a nonovershooting scenario. As such, "overshoot" could be a conscious policy that removes some of the burden of mitigation from the present generations while protecting future generations from exposure to the most severe impacts. However, it comes with the inherent risk that the climate might enter a state from which recovery becomes impossible. The risks associated with "overshooting" and reversibility in climate change on practical time scales remain an open research question requiring urgent attention.

"If emissions targets are not met, or if the impacts of climate change are greater than expected, we might well find ourselves in the position of having a greenhouse gas level that is 'dangerous'..."
—Huntingford and Lowe

If emissions targets are not met, or if the impacts of climate change are greater than expected, we might well find ourselves in the position of having a greenhouse gas level that is "dangerous," thus accidentally following an overshoot scenario. In this case, the capability to draw CO_2 from the atmosphere might be highly desirable.

CHRIS HUNTINGFORD[1] AND JASON LOWE[2]

[1]Centre for Ecology and Hydrology, Wallingford, Oxfordshire, OX10 8BB, UK. [2]Met Office Hadley Centre, Reading Unit, Meteorology Building, Berkshire RG6 6BB, UK.

References

1. H. J. Schellnhuber, W. Cramer, N. Nakicenovic, T. Wigley, G. Yohe, Eds., *Avoiding Dangerous Climate Change* (Cambridge Univ. Press, Cambridge, 2006).
2. N. Stern, *The Economics of Climate Change: The Stern Review* (Cambridge Univ. Press, Cambridge, 2007).

CO_2 Emissions: A Piece of the Pie

IN HIS POLICY FORUM "CO_2 ARITHMETIC" (9 Mar., p. 1371), W. S. Broecker uses the idea of a permissible cumulative CO_2 emissions "pie" to conceptualize the allocation of future emissions among the world's nations. The size of the pie is determined by the target for atmospheric CO_2 concentration stabilization; the higher the target level, the larger the pie. To calculate the size of the pie for different stabilization levels, Broecker notes that, for every 4 Gt of carbon emitted

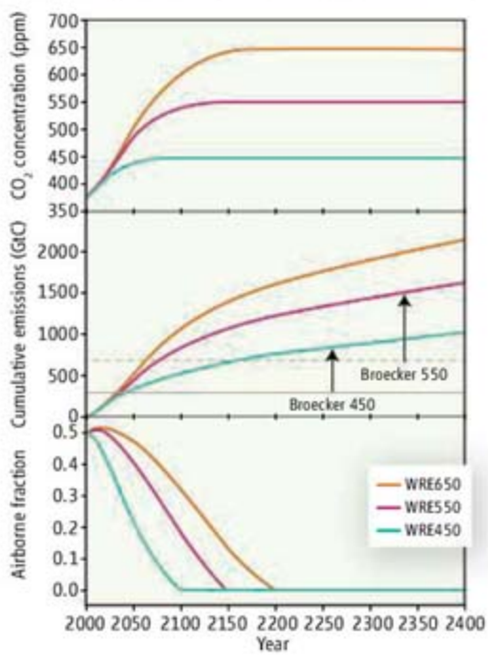

(**Top**) WRE concentration stabilization profiles (*1*) stabilizing at 450 ppm (in 2100), 550 ppm (in 2150), and 650 ppm (in 2200). (**Middle**) Corresponding cumulative emissions from mid-2007. Emissions are the sum of fossil and land-use change emissions. The horizontal lines show the allowable cumulative emissions given by Broecker for the 450 and 550 ppm stabilization cases. Arrows show how much larger the corrected cumulative emissions are compared with the Broecker estimates. (**Bottom**) Airborne fractions (change in atmospheric loading per unit of total emissions) for the three stabilization cases. Broecker assumes that the airborne fraction will remain constant at the present value (around 0.5).

today, atmospheric CO_2 concentration increases by about 1 ppm. This corresponds to a current airborne fraction (i.e., the change in atmospheric loading per unit of total emissions) of about 0.5. He then assumes that this value for the airborne fraction can be applied to future concentration stabilization scenarios; i.e., he assumes that every 1 ppm of concentration increase relative to today increases the size of the pie by 4 Gt of carbon. This assumption is incorrect and leads to a serious underestimate of the size of the pie.

A more credible estimate of permissible future emissions is shown in the accompanying figure, based on the standard WRE concentration stabilization profiles updated from (*1*). The figure shows the concentration profiles for stabilization at 450, 550, and 650 ppm, levels chosen here purely for illustrative purposes. Corresponding emissions (middle panel) are calculated with an inverse version of the MAGICC carbon cycle model (*2*), which accounts for both CO_2 fertilization and climate feedbacks on the carbon cycle. Climate feedbacks are important because, for any given stabilization profile, they reduce the allowable emissions significantly below those that would be implied if climate feedbacks were ignored. It can be seen that Broecker's estimates of total cumulative emissions are much less than those calculated by the carbon cycle model. The model also shows that cumulative emissions continue to rise for centuries after concentration stabilization. This reflects a continuing and only slowly decreasing flux of CO_2 into the oceans, in turn arising from the very long time that it takes for equilibrium between the atmosphere and ocean to be reestablished.

The reason why Broecker's estimates are so low is because of his constant airborne fraction assumption. Although this is a useful approximation when CO_2 emissions are increasing, it cannot be applied to stabilization cases where emissions must eventually decrease. That this assumption is incorrect in such cases is clear from the fact that, at stabilization, the airborne fraction must drop to zero. The decline in airborne fraction from the present value of around 0.5 to zero at stabilization is shown in the bottom panel of the figure.

The primary objective of Article 2 of the United Nations Framework Convention on Climate Change is stabilization of atmospheric greenhouse gas concentrations. Describing a CO_2 concentration stabilization target in terms of an allowable cumulative emissions "pie" that must be divided amongst nations in some equitable manner is an elegant way of visualizing this objective. Through this image, Broecker's Policy Forum provides a useful service, which, in principle, may help policy-makers construct policies that are more scientifically well founded than, for example, the Kyoto Protocol. It is unfortunate that Broecker has underestimated the size of the pie and ignored the fact that the size of the pie changes over time. Nevertheless, even with the much larger pie derived here, the message that the emissions requirements of the pie present a formidable technological challenge to society remains an important policy implication.

TOM M. L. WIGLEY

National Center for Atmospheric Research, Boulder, CO 80307–3000, USA.

References

1. T. M. L. Wigley, R. Richels, J. A. Edmonds, *Nature* **379**, 240 (1996).
2. T. M. L. Wigley, S. C. B. Raper, *Science* **293**, 451 (2001).

Response

WIGLEY IS CERTAINLY CORRECT IN HIS ASSERtion that on a time scale of several hundred years, the size of the carbon pie would be considerably greater than my estimate of 720 Gt of carbon. The reason is that, as the CO_2 content of the atmosphere approaches stabilization, ocean uptake becomes ever more important. But during the transition period (now to 2075 A.D.) when the world is struggling to reduce its CO_2 emissions, the permissible net CO_2 emissions would be on the order of 720 Gt of carbon or, using the ocean model adopted by Wigley, 900 Gt of carbon (see figure below).

Then, as Wigley points out, over the following 200 years (2075 to 2275 A.D.), another 720 or so Gt could be added without any substantial increase in the atmosphere's CO_2 content. I purposefully avoided the long term because my goal was to show, in a simple way, that, if an upper limit of 560 ppm were set and if the carbon pie was divided according to population, the rich countries would face a monumental emission-reduction task.

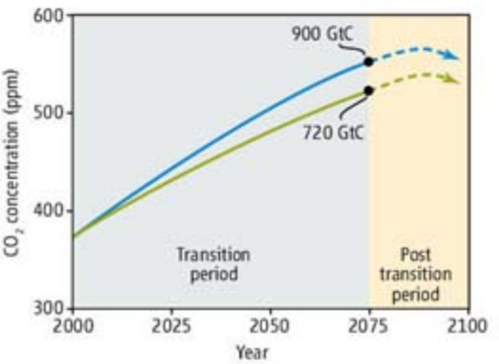

On the basis of Wigley's model, the release of 720 Gt of carbon during the transition period from 2000 to 2075 A.D. would raise the atmosphere's CO_2 content to 520 ppm. To bring it to 560 ppm during the same period would allow approximately 25% more CO_2 to be released to the atmosphere.

With regard to the post-2075 world, I suspect that to quell the continuing rise in sea level driven by the melting of the polar ice caps, there would be a desire to bring the atmosphere's CO_2 content back down at a rate far faster than offered by the ocean. If, as I deem necessary, CO_2 capture from the atmosphere is to become a major player, then in the post-2075 A.D. world, it would be used to accomplish this drawdown.

Hence, although useful during the 75-year or so period of transition from business-as-usual CO_2 emissions to no net CO_2 emissions, the carbon-pie concept will have little value in the posttransition period.

Once it is stabilized, I suspect that CO_2 capture from the atmosphere will be used not only to compensate ongoing CO_2 emissions but also to draw down the atmosphere's CO_2 content.

WALLACE S. BROECKER

Lamont-Doherty Earth Observatory of Columbia University, Palisades, NY 10964–8000, USA.

Biobanking Primer: Down to Basics

COLLECTION AND STORAGE OF BIOLOGICAL samples for genetic research are increasing (*1*). The implications of biobanking go well beyond the participant to the family and include general findings about discrete subpopulations (*2*). Research personnel and members of Research Ethics Boards (REBs) share responsibility for obtaining informed consent and ensuring the protection of participants and the confidentiality of personal genetic and other medical and sociodemographic information (*3*). Do they have the necessary expertise to fulfill these responsibilities? They need to be aware of new normative frameworks that address ethical issues in population-based genetics research (*4*) and to understand that guiding principles in traditional medical ethics might not be sufficient (*5*). Several studies have noted variability in the way REBs evaluate a given research protocol, running the gamut from approval without condition to refusal (*3*, *6*, *7*). Ongoing training for those involved in biobanks should be a fundamental institutional priority to obtain appropriate informed consent from participants.

Receive a free TaqMan® Low Density Array Upgrade and 20 Free TaqMan® Array cards*
Visit 7900HT.com to learn more.

Proven Performance in Labs Everywhere. Customized for Yours.

Applied Biosystems 7900HT Fast Real-Time PCR System Meets Your Changing Needs.

The gold standard in real-time PCR
Used by researchers all over the world and referenced in hundreds of journals, the Applied Biosystems 7900HT Fast Real-Time PCR System is the recognized gold standard in real-time PCR.

Interchangeable blocks
Configurable and highly flexible, the 7900HT Fast System offers user-interchangeable thermal cycling blocks, cycling times as low as 35 minutes and automated plate loading/unloading for higher throughput.

The world's largest collection of assays
Choose from over 2 million TaqMan® Gene Expression, Genotyping and miRNA Assays.

Easy, pre-loaded assays in a micro fluidic card format
For the ultimate in ease-of-use, order your assays pre-loaded in the 384-well TaqMan® Low Density Array.

To see how the 7900HT Fast System meets your changing research needs, visit www.7900HT.com

Applied Biosystems

* Receive a Low Density Array Upgrade and 20 Free TaqMan® Low Density Array cards with the purchase of an Applied Biosystems 7900HT Fast Real-Time PCR System. This offer cannot be combined with other promotions or discounts. Offer valid until March 31, 2006. Void where prohibited. This offer is for US customers only — International customers please inquire with your local sales office. Other restrictions may apply. All prices exclude any applicable delivery and/or local tax. Please contact your local Sales Representative for other details of this offer. http://www.7900HT.com

Three essential elements must be addressed. First, the principal investigator (PI) must ensure that research personnel are competent to provide simplified, yet complete, information when recruiting participants for biobanking studies.

Second, REBs must provide training specific to biobanking. Institutions should provide funds permitting this ongoing training for researchers, as well as REBs, where the requirement for expertise is essential. Those needing biobanks should contribute financially to relevant ethics training. This could be made mandatory for research personnel.

Third, the study population should be involved. The PI, working with the REB, needs to ensure that they are well informed about the research and biobanks. This partnership would help to bridge the gap between two entities that are often more like adversaries, rather than partners with the same objectives. This three-pronged strategy underpins the principles of the 2003 International Declaration on Human Genetic Data of UNESCO, article 24 (*8*).

In light of the increasing interest in biobanking, training of REBs and research personnel should be part of the mission of every institution to ensure a more coherent process in obtaining informed participation. Such training would be applicable to many innovative initiatives.

CHRISTIANE AURAY-BLAIS[1]* AND JOHANE PATENAUDE[2]

[1]Service of Genetics, Department of Pediatrics, Faculty of Medicine and Health Sciences, Université de Sherbrooke, Sherbrooke, QC, Canada J1H 5N4. [2]Department of Surgery, Faculty of Medicine and Health Sciences, Université de Sherbrooke, Sherbrooke, QC, Canada J1H 5N4.

*To whom correspondence should be addressed. E-mail: christiane.auray-blais@usherbrooke.ca

References

1. Creation and Governance of Human Genetic Research Databases (OECD Publishing, Paris, 2006) (www.oecd.org/dataoecd/61/49/37647362.pdf).
2. German National Ethics Council, Opinion on biobanks for research (2004) (see www.ethikrat.org).
3. C. Auray-Blais, J. Patenaude, *BMC Med. Ethics* **7**, 1 (2006).
4. B. M. Knoppers, R. Chadwick, *Nat. Rev. Genet.* **6**, 75 (2005).
5. J. E. Lunshot, *Nat. Rev. Genet.* **7**, 162 (2006).
6. P. Glasziou, I. Chalmers, *Br. Med. J.* **328**, 121 (2004).
7. J. de Champlain, J. Patenaude, *J. Med. Ethics* **32**, 530 (2006).
8. UNESCO, International Declaration on Human Genetic Data, 2003) (see www.unesco.org/confgen/2003/genetic/).

CORRECTIONS AND CLARIFICATIONS

Reports: "Picobiliphytes: a marine picoplanktonic algal group with unknown affinities to other eukaryotes" by F. Not *et al.* (12 Jan., p. 253). There were two errors on page 253. In the abstract, the second sentence is incorrect. It should read, "A distinct picoplanktonic algal group, initially detected from 18S ribosomal DNA (rDNA) sequences, was hybridized with rRNA-targeted probes, detected by tyramide signal amplification–fluorescent in situ hybridization, and showed an organelle-like body with orange fluorescence indicative of phycobilins." In the author affiliations, an institution (CSIC) was missing from Ramon Massana's affiliation. It should be Institut de Ciències del Mar, CSIC, Passeig Marítim de la Barceloneta 37-49, 08003 Barcelona, Spain.

Letters to the Editor

Letters (~300 words) discuss material published in *Science* in the previous 3 months or issues of general interest. They can be submitted through the Web (www.submit2science.org) or by regular mail (1200 New York Ave., NW, Washington, DC 20005, USA). Letters are not acknowledged upon receipt, nor are authors generally consulted before publication. Whether published in full or in part, letters are subject to editing for clarity and space.

Now Available!
Custom panels in smaller, 10-card order sizes.

384 Wells. Preloaded for TaqMan® Performance.

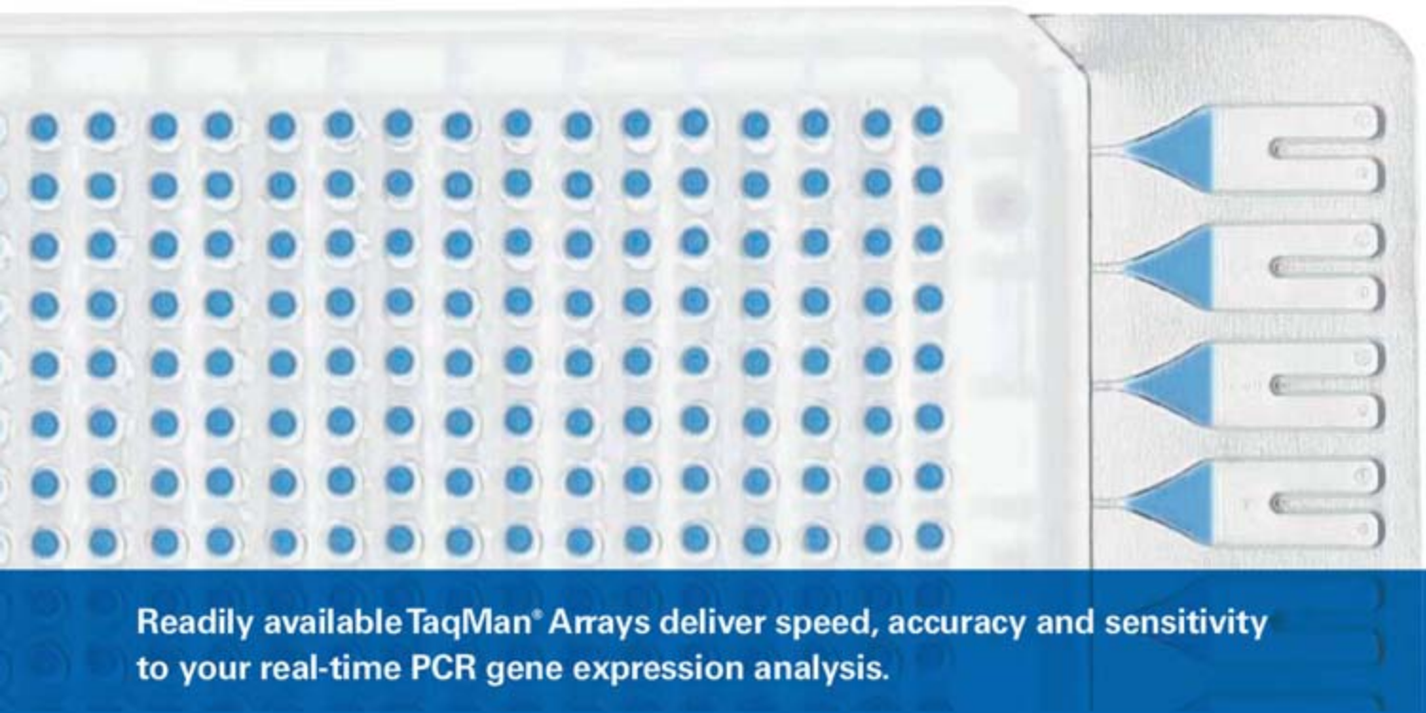

Readily available TaqMan® Arrays deliver speed, accuracy and sensitivity to your real-time PCR gene expression analysis.

TaqMan® Low Density Array Gene Signature Panels are readily available, expertly-designed, focused gene sets that don't require liquid handling robots or complex pipetting to use. Simply add your cDNA and TaqMan® Universal PCR Master Mix into the eight sample ports of this micro fluidic card and instantly run 384 real-time PCR reactions on the 7900HT Fast Real-Time PCR System. The Gene Signature Panels come pre-loaded with TaqMan® Gene Expression Assays, so you get the accuracy, reproducibility, and specificity that only TaqMan® Assays can provide. It's the fast and affordable way to validate microarray hits and screen pathways and biomarkers without the worry and difficulty associated with 96-well plates or individual tubes.

Order from the growing portfolio of TaqMan® Low Density Array Gene Signature Panels:

- Human or Mouse GPCR Panel
- Human or Mouse Immune Panel
- Human, Mouse, or Rat Endogenous Control Panel
- Human Protein Kinase Panel
- Human Apoptosis Panel
- Human ABC Transporter Panel

More panels will be available soon! Register to receive new Gene Signature Panel product announcements or suggest a panel of your own at tlda.appliedbiosystems.com

The perfect combination: the TaqMan Low Density Array and Applied Biosystems 7900HT Fast Real-Time PCR System.

Applied Biosystems

PHILOSOPHY OF SCIENCE

The World of Science

Peter Lipton

Nobody thinks current science is the complete truth; nobody thinks current science is just a story unconstrained by evidence. But almost every intermediate position has its supporters.

Many philosophers of science think that although the whole truth and nothing but the truth is an asymptote, science is producing objective and increasingly comprehensive descriptions of a largely invisible world. Other philosophers would not go this far. Some would insist that even our best scientific theories are only models, whose job it is to generate accurate predictions, not to reveal a hidden reality. Some are depressed by the graveyard of discarded theories that litter the history of science, theories that were predictively successful for a time but that we now know to be fundamentally mistaken. The claim that today's science has finally gotten on the right track may sound like whistling in the dark.

Most philosophical retreats from the full-blooded truth view take one of two forms: partial truth or constructivism. On partial truth approaches, we should believe only certain aspects of our best theories. Perhaps we should only believe what those theories say about observables, or about abstract structures, or about concrete entities. Constructivism is more subtle. Here what is to be adjusted is not how much truth we claim, but our conception of what it means to be true. Perhaps what theories in the natural sciences describe is not a world entirely independent of us, but rather a world that is partially structured by our own conception of it.

The most famous version of constructivism comes from the great 19th-century philosopher Immanuel Kant. He held that there is indeed a world of "things in themselves," but because of its radical independence from human thought, that is a world we can know nothing about. By contrast, the "phenomenal" world that science describes is a world partially constituted by us. The phenomenal world is a joint product of the things in themselves and the structuring activity of the mind. And according to Kant we bring a lot to the party. The human contribution to the phenomenal world includes space, time, and causation.

A more recent proponent of a version of constructivism is Thomas Kuhn. Like Kant, Kuhn held that the world described by science is a world partially constituted by cognition. But whereas Kant held that there is only one form the human contribution could take, Kuhn argued that the contribution changes as science changes. Kuhn is Kant on wheels.

Constructivism is not easy to understand. In what sense do scientists constitute the world they study? What is the human element in, say, baryons? Kuhn attempted to clarify his constructivism in terms of taxonomies. According to him, the things in themselves do not come predivided into natural kinds. It is the scientists who have to divide things up. Thus while talk of baryons is talk of something in the world, the category is given by scientists, not by the joints of nature.

Kant explained his constructivism differently, appealing to properties such as colors, properties that already seem anthropocentric. Colors are not quite identified with human color experiences, but they are taken to be defined in terms of those experiences. To say that the ball is red is to say that it is disposed to cause us to have red experiences. Thus colors are not in our heads (and the ball is colored even in the dark), but they are defined in terms of what goes on in our heads. Kant's claim was that all the properties that science deploys are like that.

Hue circle. There is no simple linear relationship between wavelength and color.

Ronald Giere's clear and engaging book *Scientific Perspectivism* develops a version of constructivism. Like Kant, Giere (an emeritus professor of philosophy at the University of Minnesota) explains his position with colors. He points out that they cannot easily be identified with objective properties such as surface spectral reflectances because of the existence of metamers. Different reflectances may correspond to the same color. Color must rather be seen as the product of an interaction between surface and perceiver, and this makes colors irreducibly perspectival. Like Kant, Giere wants to extend his picture of colors to all of science. Scientific descriptions capture only selected aspects of reality, and those aspects are not bits of the world seen as they are in themselves, but bits of the world seen from a distinctive human perspective.

Scientific Perspectivism

by Ronald N. Giere

University of Chicago Press, Chicago, 2006. 168 pp. $30, £19. ISBN 9780226292120.

In addition to the color example, Giere articulates his perspectivism by appeal to maps and to his own earlier and influential work on scientific models. Maps represent the world, but the representations they provide are conventional, affected by interest, and never fully accurate or complete. Similarly, scientific models are idealized structures that represent the world from particular and limited points of view. According to Giere, what goes for colors, maps, and models goes generally: science is perspectival through and through.

Constructivists deny the "view from nowhere." Science can only describe the world from a human perspective. Objectivists claim that, on the contrary, there is such a view. You can't think without thinking, but it does not follow that what you are thinking about—baryons, say—must somehow include the thinker. Objectivists hold on to the idea that the world has its own structure, which science reveals.

Giere's book makes a serious case for constructivism, but those with strong objectivist inclinations will not be moved. For one thing, in spite of his best efforts and the excellent philosophical company he keeps, the constructivist position remains somewhat obscure. The notion of a physical world that emerges from the interaction of the objective and the subjective is difficult to grasp, even if you are a philosopher. And although Giere's arguments for constructivism are serious and provocative, they have uncertain force. Scientific descriptions surely are incomplete and affected by interest, but these are features the objectivist can take on board. Completeness and objectivity are orthogonal. Maybe in the end constructivism is true, or as true as a constructivist can consistently allow. Nevertheless, the thought that the world has determinate objective structures is almost irresistible, and Giere has not ruled out the optimistic view that science is telling us something about them.

The reviewer is in the Department of History and Philosophy of Science, Cambridge University, Free School Lane, Cambridge CB2 3RH, UK. E-mail: Peter.Lipton@kings.cam.ac.uk

10.1126/science.1141366

SOCIAL SCIENCE

The Child as Scientific Object

Emily D. Cahan

For anyone wishing to understand the ways in which the child sciences emerged from a matrix of science and social relevance, Alice Boardman Smuts's *Science in the Service of Children, 1893–1935* is an excellent place to begin. The academic and professional fields we know today as developmental psychology, child-centered pedagogy, child psychiatry, and policy studies related to children were among those born in this formative period. In weaving a tapestry of scientific, social, institutional, and professional histories, Smuts provides the first comprehensive narrative of the child sciences in the initial third of the previous century.

Science in the Service of Children, 1893–1935

by Alice Boardman Smuts

Yale University Press, New Haven, CT, 2006. 395 pp. $55. ISBN 9780300108972.

Written in an engaging style, the book (based on the author's 1995 dissertation at the University of Michigan) richly details the movements that enabled scientific child study to gain a foothold in American science and society. Drawing on archives from around the nation as well as interviews with as many early voices as was possible, Smuts describes the roles of female social reformers, philanthropists, and "progressive" scientists who established new institutions and new ways of looking at children. The book celebrates the work of scientists, practitioners, and a largely female cadre of social reformers, all of whom helped to define what Swedish social commentator Ellen Key described in 1909 (*1*) as "the century of the child."

Claiming that the "revolution in child study is a neglected chapter in American history," Smuts unravels the history of three distinct but related approaches: child guidance, sociological studies, and research in child development. She views the three approaches not as isolated efforts but as parts of a broad movement that shared a common goal: "the discovery of new knowledge about children in order to better serve both children and the nation." It was thought that the science of child development would, in the traditions of the Enlightenment and the spirit of the Progressive Era, be used as an instrument of individual and social reform. Scientific child study would occupy a strategic place in the design of practices, programs, and policies for children. Accepting the positivistic framework of the times, people assumed that research in child development was free of the "taint" of values. Smuts's book celebrates the triumph of science over sentiment and caprice but leaves critical discussions of the limitations of such science to others.

In the last quarter of the 19th century—on the heels of the Darwinian revolution and in the midst of massive social changes (including but not limited to industrialization, urbanization, and immigration)—people in the United States and abroad began to look at and see children differently. Children were moving out from the home into the public worlds of urban streets and schoolrooms, and there was trouble. Children labored in the streets, some peddled newspapers, and some committed mild to moderate crimes. Charity workers observed increasing numbers of homeless orphans and children working 12-hour days in sweatshops. Recitation dominated educational instruction, children were cooped up in urban schoolrooms with no ventilation, and there was no public space in which kids could play. Social reformers and journalists (such as the photographer Jacob Riis) drew the public's attention to the conditions in which children lived on the streets or in squalid, unsafe, and overcrowded tenements. People with common sense and humanitarian ideals indicted these conditions and called for reform.

In the 1880s and 1890s, there was little secular wisdom to guide people toward sound judgments about designing programs, practices, and policies for children. Reformers sought answers to countless relevant questions: How many hours could a child work without suffering physical or emotional distress? How old should a child be before undertaking work or formal schooling? What should the average child know about the world? How do children relate to one another in social groups? How many words does an average four-year-old know? What is the value of children's play? What should we teach young children? Efforts to understand children's lives and mentalities existed well before this time, but they were scattered and heterogeneous, with few of the trappings of conventional science—little sense of shared purpose or methods, and little shared theoretical framework outside of evolutionary theory. Smuts describes how the child sciences and professions took form as graduate and professional schools proliferated. Most important, unlike their cousin experimental psychology, child study and developmental psychology did not spring forth from either philosophy or science. Rather, they emerged out of a matrix of scientific, social, and humanitarian ideals.

The child sciences whose origins Smuts recounts have been a positive force in modern societies by helping us to design environments appropriate for children. Developmental psychology, for example, has contributed to children's television, preschool programs, and instructional strategies for science and math education; it has helped us create and evaluate important policies such as Head Start. These designs inevitably lead to questions of value, questions—such as what constitutes "good" development—that the empirical norms of experimental science cannot on their own answer. This slippage from science to values is not a sign of an immature science, nor is it the removable error of inadequate methods. Rather, it is inherent in the very subject of children, their development and welfare. If we don't question the limitations of the child sciences or make our values explicit, then we run the risk of relying on the false claims of scientism and the hubris of using current findings to define our values. By bringing together an enormous amount of information from scattered sources, Smuts's history offers an excellent foundation for further work in the history of scientific study of the child.

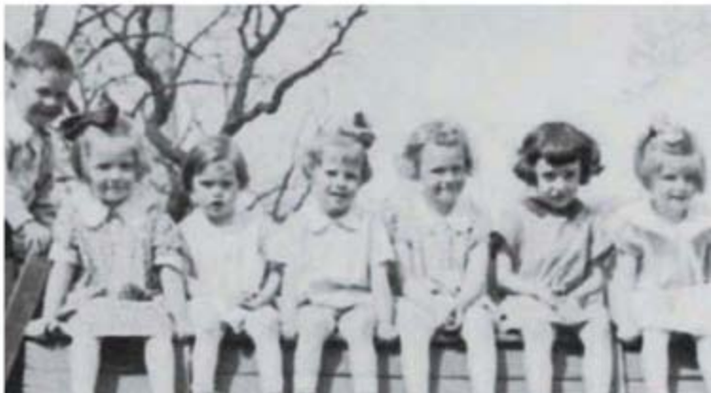

Study subjects. Children at the University of Minnesota's Nursery School Laboratory (established in 1925).

CREDIT: COURTESY UNIVERSITY OF MINNESOTA INSTITUTE OF CHILD DEVELOPMENT

The reviewer is in the Department of Human Development, Wheelock College, 200 The Riverway, Boston, MA 02215, USA. E-mail: ecahan@wheelock.edu

Reference

1. E. K. S. Key, *The Century of the Child* (Putnam's, New York, 1909).

10.1126/science.1136576

MEDICINE

Reestablishing the Researcher-Patient Compact

Well-intentioned regulations protecting privacy are denying important information to patient subjects. Advances in information technology mean that a better approach to clinical research is possible.

Isaac S. Kohane,[1,2,3]* Kenneth D. Mandl,[1,2,3] Patrick L. Taylor,[2,4] Ingrid A. Holm,[2,5] Daniel J. Nigrin,[1,2,3] Louis M. Kunkel[2,5,6]

In the name of privacy and protection of study subjects, the research community has, albeit with good intentions, broken the historical doctor-patient compact, distorting an ideal of information exchange that might inform subjects of health risks or benefits (*1*, *2*). To minimize privacy risks in genomic research, investigators and institutional review boards (IRBs) construe that federal regulations require anonymized data. This disallows communicating pertinent results back to subjects. Such results could help the subjects and would justify the beneficence of that research (*3*). When large cohorts are enrolled for genomic and clinical characterization (*4*–*6*), both sides agree not to reconnect findings from the aggregated data or to infer meaning or insight for a specific patient, or to make that knowledge available to the patient. The scientific motivation behind this mutual commitment never to communicate or identify has origins in the evolution of modern study design (*7*). It has coincided with the growth of grass-roots privacy concerns, the enactment of Health Insurance Portability and Accountability Act (HIPAA) (*8*), the Office of Human Research Protection (OHRP) procedures, and state laws to protect genetic information misuse (*9*–*13*). Yet this intentional failure of communication may be detrimental.

Consider the scenario: In 5000 patients with diabetes mellitus, one subject has an incidental finding of the expression of a fusion gene indicative of early malignancy. Genome-wide polymorphism studies reveal a variant in 40 others that predicts benefit from a recently approved medication. To follow up, the IRB must either sanction reidentification or notify the entire cohort, unnecessarily alarming some (*14*). This scenario will become more common as more genetic signatures are linked with pertinent phenotypes. Further, this highlights only one of several opportunities (*15*) missed because of an understandable but overreaching paternalism.

The advent of genome-scale measurements and health information technologies allows us to reconnect patient subjects and researchers in a manner respectful of regulations and privacy concerns and to maximize potential benefit to the public and the individual in the course of research. A solution must anonymize information while making discoveries available to participants who "tune in." Although seemingly paradoxical, it is comparable to UHF/VHF television. To "participate," an individual buys a television and privately decides when and what he watches. In the research analogy, a subject's "programming" is a product of her own information and the aggregated study results. Her reception of research results depends on whether she "tunes in" to the broadcast.

We propose a collaborative clinical research regime, the Informed Cohort (see figure, page 837). IC subjects are enrolled at their health-care institution through an extensive informed consent process. If they choose, subjects provide additional clinical information and biospecimens, typically a blood sample, for high-throughput measurements. In addition to the usual concerns regarding comprehension, transparency, and coercion, the consent process must mirror the dynamic quality of the subjects' changing involvement over time—contributing more information or withdrawing at will. Although IRBs may absorb the additional responsibility, we propose giving crucial oversight functions to an independent IC Oversight Board (ICOB), responsible for communicating study information back to patients. The ICOB multidisciplinary team (geneticists, statisticians, ethicists, patients, and communications experts) deals with complex issues—what information is worthy of communication and how best to communicate it, for example.

At enrollment, subjects are given a Web-based, interoperable personally controlled health record (PCHR) (*16*–*18*). In our model of PCHR design, (*16*) individual records are encrypted, preventing compelled third-party disclosures (*19*), for example, by subpoena. Only the patient can decide to whom personally identified information will be disclosed and under what circumstances (*20*–*22*). Thus, each patient owns an integrated copy of his or her traditional record data plus high-throughput genome-scale measurements made on his or her own biomaterials. For example, she may consent to share a part of her PCHR data, which is then anonymized and entered into a population database. Her data can be studied in an IRB- and HIPAA-compliant manner across topics including population genomics, public health, medication effects, and quality of care. Data can be shared with appropriate parties including biomedical researchers and public health authorities. Under no circumstances would there be an attempt to contact or to discover the identity of the patient. Anonymized data-gathering can be a dynamic process for longitudinal studies of individuals (*23*).

The IC design allows patients to be contacted as necessary and as desired by each patient. As shown in the figure, each PCHR has an "agent," the listener. The agent has a dedicated purpose: to intercept broadcasts over the Internet from the health-care system with information regarding patients with particular characteristics and to determine whether the described characteristics match the patient the agent serves. For example, does the DNA polymorphism or diagnostic category match the content of the patient's record? These broadcasts are not targeted to any specific patient, and only under two conditions does the agent notify the patient of the broadcasts: if the patient has allowed this agent listener function to be turned on at all (it can be turned off at any time), and if she has allowed further notification from the health-care system in a particular clinical or genomic domain that is available to her as an electronic checklist.

Researchers at any given time may make a discovery pertaining to a class of patients with a particular characteristic or set of genomic markers and may want to alert those patients about clinical implications, request more information, obtain more genomic material, or perform other measurements.

[1]Center for Biomedical Informatics, [2]Department of Pediatrics, Harvard Medical School, Boston, MA 02115, USA. [3]Children's Hospital Informatics Program at the Harvard–MIT Division of Health Sciences and Technology, Cambridge, MA 02139, USA. [4]Office of the General Counsel, [5]Program in Genomics, and [6]Howard Hughes Medical Institute at Children's Hospital Boston, Boston, MA 02115, USA.

*Author for correspondence. E-mail: isaac_kohane@harvard.edu

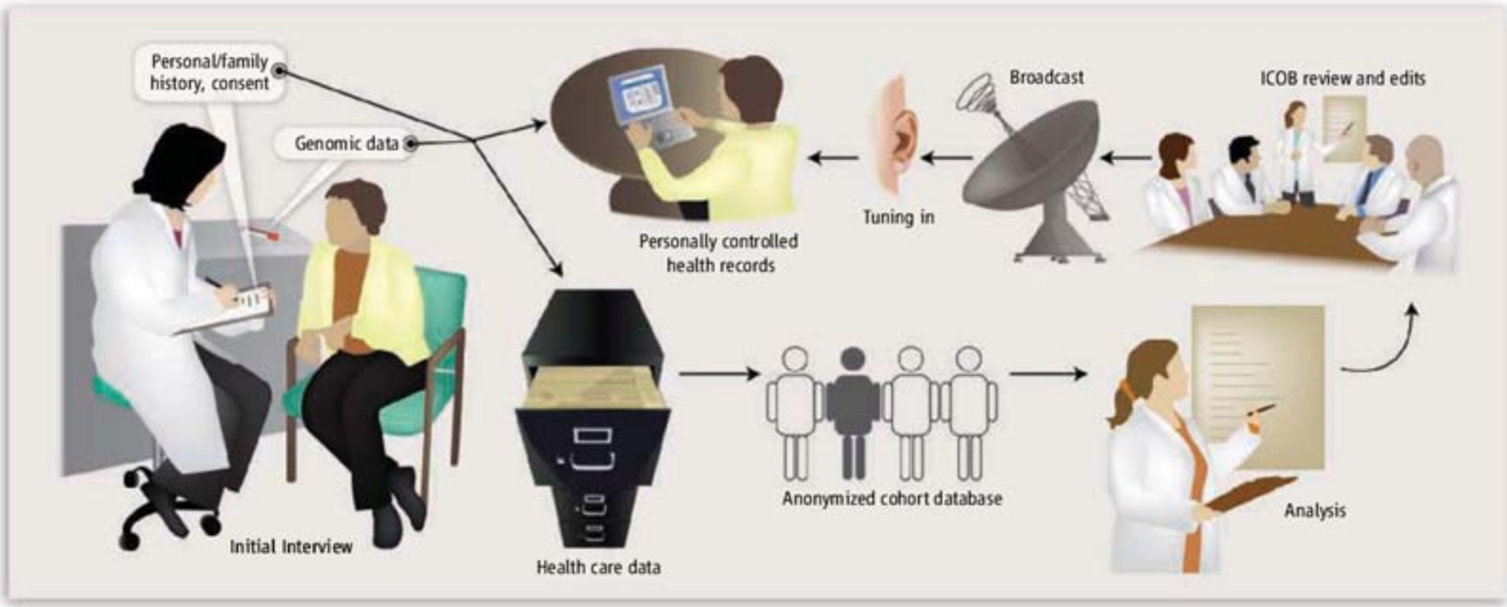

However, researchers do not know who the patient is and so broadcast to the system of the IC—conditional on the ICOB editorial process and approval—a description of the kind of patients that they are seeking to contact. The agent's "decisions" are the product of the subject's stated categorical preferences for information and the ICOB's study-specific determination about what information can be effectively communicated in a manner sensitive to subjects' health literacy. All IC agents that are turned on will intercept all such broadcasts and determine whether the characteristics, of the patient, genomic or clinical, match the characteristics of the patients described in the broadcast. The agent listens for information pertaining, for example, to a particular single-nucleotide polymorphism (SNP) and scans the PCHR for the presence of that SNP. The notification appears to the patient much as an e-mail does.

Because the IC protects privacy through anonymization, but permits direct benefit to participating subjects, it is ethically superior to the status quo. It enables patients as partners in research rather than passive, disenfranchised purveyors of biomaterials and data. Further, this procedure is feasible using today's technology and does not breach current regulations. In addition, because it is built around PCHRs interacting with a national electronic health network, it could have markedly amplified research potential, offering dramatically greater accessibility for properly authorized researchers across multiple health-care institutions.

Several questions remain unanswered and require careful analysis in ways that might vary by population and geography. How can the IC work for individuals with poor health literacy? What about individuals without effective and private access to networked computers? What is the level of certainty or the expected benefit to the patient that should inform ICOB about what should be broadcast to the IC and when? Some of these questions cannot be answered in the abstract and will require detailed review by experts in each instance.

If the IC is more than a thought experiment, what will it take to realize this proposal and what are the anticipated resources required? Many of the technical hurdles have been overcome. Commodity-priced, genome-wide common variant assays are available now. Early versions of personal health records, once a futuristic concept (*24*), are in the hands of thousands of patients through diverse implementations at the Veterans Administration (*25*), hospitals (*26*), and managed-care organizations. More investment will be required in health-care settings and staffing for effective and safe support of study participants. Moreover, this investment is within the range of leading academic medical centers where this model can be debugged and made more efficient and affordable for wider adoption. Indeed, the leadership at Children's Hospital Boston has committed itself to piloting the IC in several clinics. Undoubtedly, there will be unanticipated technical, legal, and sociological challenges, and we anticipate a vigorous debate within the biomedical community.

References and Notes

1. P. A. Schulte, K. Ringen, *Am. J. Public Health* **74**, 485 (1984).
2. J. M. Last, *J. Clin. Epidemiol.* **44** (suppl. 1), 95S (1991).
3. National Commission for the Protection of Human Subjects of Biomedical and Behavioral Research, *The Belmont Report: Ethical Principles and Guidelines for the Protection of Human Subjects of Research* (Department of Health, Education, and Welfare, Washington, DC, 1979).
4. National Institutes of Health (NIH), "Request for Information (RFI): Proposed Policy for Sharing of Data obtained in NIH supported or conducted Genome-Wide Association Studies (GWAS)" (NOT-OD-06-094, NIH, Bethesda, MD, 2006); http://grants.nih.gov/grants/guide/notice-files/NOT-OD-06-094.html.
5. A. Regaldo, *Wall Street Journal*, 7 June 2006, p. B1.
6. C. T. Hall, *San Francisco Chronicle*, 15 February 2007, pp. B3.
7. H. M. Marks, *The Progress of Experiment: Science and Therapeutic Reform in the United States, 1900–1990* (Cambridge History of Medicine, Cambridge Univ. Press, New York, vol. 11, 1997), 258 pp.
8. Pub. L. 104-191 (1996).
9. Office for Human Research Protection, "Issues to consider in the research use of stored data or tissues" (Department of Health and Human Services, Washington, DC, 1997); www.hhs.gov/ohrp/humansubjects/guidance/reposit.htm.
10. P. A. Roche, G. J. Annas, *N. Engl. J. Med.* **355**, 545 (2006).
11. Association for the Accreditation of Human Research Protection Programs, "Accreditation Standard(s) II.6.A and II.6.B." (Association for the Accreditation of Human Research Protection Programs, 2006); www.aahrpp.org/www.aspx?PageID=27.
12. National Human Genome Research Project, "Genetic Discrimination: Legislation on Genetic Discrimination" (NIH, 2006); www.genome.gov/10002077.
13. National Conference of State Legislatures (NCSL), "Genetics tables: State genetic privacy laws" (NCSL, Washington, DC, 2006); www.ncsl.org/programs/health/genetics/prt.htm.
14. I. S. Kohane *et al.*, *JAMA* **296**, 212 (2006).
15. I. S. Kohane, R. B. Altman, *N. Engl. J. Med.* **353**, 2074 (2005).
16. W. W. Simons, K. D. Mandl, I. S. Kohane, *J. Am. Med. Inform. Assoc.* **12**, 47 (2005).
17. P. C. Tang , J. S. Ash, D. W. Bates, J. M. Overhage, D. Z. Sands, *J. Am. Med. Inform. Assoc.* **13**, 121 (2006).
18. G. DeBor *et al.*, *J. Healthc. Inf. Manag.* **20**, 63 (2006).
19. M. A. Rothstein, M. K. Talbott, *JAMA* **295**, 2882 (2006).
20. D. H. Gustafson *et al.*, *Am. J. Prev. Med.* **16**, 1 (1999).
21. S. M. Miller *et al.*, *J. Health Commun.* **10** (suppl. 1), 119 (2005).
22. B. Adida, I. S. Kohane, *BMC Genomics* **7**, 93 (2006).
23. C. Quantin *et al.*, *Int. J. Med. Inform.* **49**, 117 (1998).
24. Guardian Angel: Personal Lifelong Active Medical Assistant, www.ga.org.
25. J. B. Perlin *et al.*, *Am. J. Manag. Care* **10**, 828 (2004).
26. S. N. Weingart, D. Rind, Z. Tofias, D. Z. Sands, *J. Am. Med. Inform. Assoc.* **13**, 91 (2006).

10.1126/science.1135489

OCEAN SCIENCE

Biomixing of the Oceans?

André W. Visser

Although the idea that small swimming organisms could change the ocean's circulation has attracted attention, their movements do not cause enough mixing.

Every now and then, an idea comes along that is so appealing, it seems bad manners to challenge it. Biomixing—the action of swimming organisms in mixing the world's oceans—is one such idea that has gained recent purchase. If correct, biomixing has far-reaching consequences for our understanding of the oceans. But can swimming organisms actually achieve significant mixing? Central to this question is their mixing efficiency.

Biomixing is certainly an engaging notion. For instance, at the global scale, it suggests that billions of small organisms paddling away in the deep oceans stir cold deep water upward, thus contributing to global circulation (*1*) and climate. At more local scales, it suggests that schools of krill and other marine animals (*2*) plough the thermocline, mixing nutrient-rich water upward and thereby fertilizing their own feeding grounds. Swimming organisms do seem to dissipate substantial amounts of mechanical energy. There are even observations showing considerably elevated dissipation rates in the wake of a migrating school of krill (*3*). The case for biomixing thus seems to be compelling.

However, in these studies, the dissipation of mechanical energy is equated with mixing. Yet, most of the biomixing is purportedly achieved by small but numerous zooplankton with diameters of 1 cm or less. Can mechanical energy at these small scales achieve any substantial mixing (that is, increase the potential energy of the water column) before it is dissipated as heat?

Turbulence in the oceans is generated by a variety of mechanisms, including tides, winds, and swimming animals. It cascades energy from large scales to ever smaller scales, where it is eventually dissipated. Turbulence is effective in mixing because it is active over a range of scales; stretching and folding of the fluid at large scales facilitates molecular diffusion at smaller scales.

The efficiency of turbulence in mixing a stratified water column is expressed by Γ, the ratio of the change in potential energy to the work done. Mixing efficiency is controlled by three parameters: the integral frequency L (the scale at which turbulent kinetic energy is imparted to the flow), the rate of turbulent energy dissipation ε (equivalent to the rate of work done), and the buoyancy length scale N (a measure of the stratification of the water column). The latter two parameters can be conveniently combined as the buoyancy length scale $B = (\varepsilon/N^3)^{1/2}$. Theoretical considerations (*4*, *5*) and observations (*6*, *7*) indicate that when $L \geq B$, the mixing efficiency is at its maximum. However, when $L < B$, the mixing efficiency can be orders of magnitude less (see the figure).

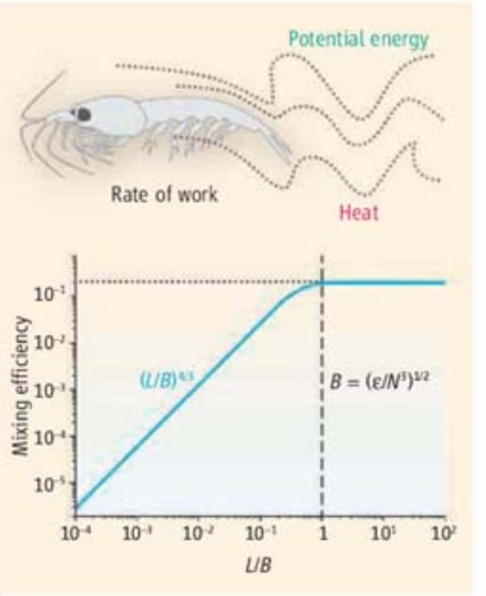

The efficiency of mixing. (**Top**) The turbulent kinetic energy generated by a swimming animal dissipates either as heat or in increasing the potential energy of a stratified water column. (**Bottom**) The mixing efficiency Γ (that is, the proportion of kinetic energy that goes into potential-energy increase) is a function of the integral length scale L and the buoyancy length scale B. For a swimming animal, L is the size of the animal itself. Small animals tend to be much less efficient at mixing than larger animals, depending on the ratio L/B. For animals of a given size (that is, L), mixing efficiency decreases as dissipation rate increases, either because individual animals swim faster or because they aggregate in denser assemblages.

The net dissipation rate due to an assemblage of swimming organisms depends on the power expended per individual and the number of individuals per unit volume (*2*). Thus, the dissipation rate ε of a school of krill—assuming a body length of 1 to 1.5 cm, a swimming speed of 5 to 10 cm s^{-1}, and a number density of 5000 individuals m^{-3}—is equal to 10^{-5} to 10^{-4} W kg^{-1}, consistent with observations (*3*). How much mixing does this represent?

An organism of a given body size λ cannot inject energy into a flow at length scales larger than itself. Thus $L \approx \lambda$, consistent with observations for grid-generated turbulence (*8*). The buoyancy frequency for the surface ocean is typically 10^{-2} s^{-1} or less, so that the buoyancy length scale associated with the above measurements is 3 to 10 m, and the corresponding mixing efficiency $\Gamma = 10^{-4}$ to 10^{-2}. Hence, only 1% at most of the mechanical energy dissipated by the swimming school of krill and other marine animals actually goes into mixing. The dissipation rate measured in the wake of a dense assemblage of swimming organisms may indeed be considerably higher than that associated with oceanic turbulence, but it does not necessarily follow that the corresponding mixing is also proportionally higher.

The case for biomixing as an important component of the meridional overturning circulation is fraught with the same problem. Considering tides and winds alone, there is an apparent shortfall of ~1 TW in the energy budget driving this circulation (*9*, *10*). The oceanic biosphere captures solar energy at a rate of ~63 TW (*1*, *11*). If only a small percentage of this captured solar energy makes its way into mechanical energy of swimming, the energy budget can apparently be closed. One terawatt corresponds to an average dissipation rate of 10^{-9} W kg^{-1} in the deep oceans, where the buoyancy frequency is typically 10^{-3} s^{-1} or less (*12*). Thus, a mean buoyancy length scale for the deep ocean is 1 m or greater. However, most of the biomass of the oceans is concentrated in small organisms such as copepods ($\lambda \approx 1$ mm). The efficiency of these organisms in mixing is only 10^{-3}. It is only when one comes to larger, but much less abundant, organisms, such as fish and marine mammals, that the mixing efficiency approaches its maximum.

Dissipation is the end product of turbulence. It is also the most readily measured turbulence parameter in the ocean. However, important aspects of turbulence—such as mixing—also depend on the larger scales of

The author is at the Technical University of Denmark, Danish Institute for Fisheries Research, Department of Marine Ecology and Aquaculture, Kavalergaarden 6, DK-2920 Charlottenlund, Denmark. E-mail: awv@difres.dk

turbulent motion (*13*, *14*). By whatever means one approaches the calculation of biomixing of the oceans, one will always be confronted by the fact that the mixing efficiency of small organisms is extremely low. Most of the mechanical energy they impart to the oceans is dissipated almost immediately as heat. There may be a case to be made for biomixing by larger animals on a local scale, but their relatively low abundance means that they are unlikely to be important contributors to global circulation.

References and Notes

1. W. K. Dewar *et al.*, *J. Mar. Res.* **64**, 541 (2006).
2. M. E. Huntley, M. Zhou, *Mar. Ecol. Prog. Ser.* **273**, 65 (2004).
3. E. Kunze, J. F. Dower, I. Beveridge, R. Dewey, K. P. Bartlett, *Science* **313**, 1768 (2006).
4. S. A. Thorpe, *The Turbulent Ocean* (Cambridge Univ. Press, Cambridge, UK, 2005).
5. The rate at which potential energy increases due to turbulent mixing is KN^2, where K is the turbulent diffusivity. The ratio KN^2/ε defines the mixing efficiency Γ, the fraction of total energy that goes into mixing. The remaining $(1 - \Gamma)\varepsilon$ is the rate at which turbulent kinetic energy is dissipated as heat, and an energy balance requires that $\varepsilon = KN^2 + (1 - \Gamma)\varepsilon$. Turbulent diffusivity can be estimated from Richardson's law, $K \approx [(1 - \Gamma)\varepsilon L^4]^{1/3}$. The form of the mixing efficiency as a function of the integral length scale L and the buoyancy scale $B = (\varepsilon/N^3)^{1/2}$ thus follows: $\Gamma \approx \Gamma_0$ for $L \geq B$, and $\Gamma = (L/B)^{4/3}$ for $L < B$. Theoretically, Γ_0 can approach 1, although observations indicate that it is close to 0.2 (*15*, *16*).
6. C. R. Rehmann, J. R. Koseff, *Dyn. Atmos. Oceans* **37**, 271 (2004).
7. R. E. Britter, in *Turbulence and Diffusion in Stable Environments*, J. C. R. Hunt, Ed. (Clarendon, Oxford, 1985), pp. 3–13.
8. K. Yoon, Z. Warhaft, *J. Fluid Mech.* **215**, 601 (1990).
9. W. Munk, C. Wunsch, *Deep-Sea Res.* **45**, 1977 (1998).
10. C. Wunsch, *Nature* **405**, 743 (2000).
11. M. J. Behrenfeld, P. G. Falkowski, *Limnol. Oceanogr.* **42**, 1 (1997).
12. M. Dengler, D. Quadfasel, *J. Phys. Oceanogr.* **32**, 1165 (2002).
13. L. F. Richardson, *Proc. R. Soc. London Ser. A* **110**, 709 (1926).
14. A. Okubo, *Deep-Sea Res.* **18**, 789 (1971).
15. T. R. Osborn, *J. Phys. Oceanogr.* **10**, 83 (1980).
16. N. S. Oakey, *J. Phys. Oceanogr.* **12**, 256 (1982).

17. This study was supported by the Danish Research Agency (grant 21-03-0299).

10.1126/science.1141272

PLANETARY SCIENCE

A Local Wiggle in the Turbulent Interstellar Magnetic Field

Conflicting measurements of the magnetic field outside the solar system now make sense.

J. R. Jokipii

Recent observations, both remotely and in situ with the Voyager space probes, are clearing away some of the mystery about the interstellar magnetic field that lies just outside the solar system. On page 875 of this issue, Opher *et al.* (*1*) report a new analysis showing that previous measurements of the field (*2*, *3*), initially indicating quite different fields, are in fact consistent with each other [also suggested by Gurnett *et al.* (*4*)]. Also, it now seems clear that the very local interstellar magnetic field points in a quite different direction from that obtained from numerous previous ground-based measurements, which were averages over large distances. This discrepancy can now be understood as a natural consequence of fluid turbulence in the interstellar medium, in which the magnetic-field direction changes dramatically over shorter scales than could be measured previously. The insights gained will help researchers better understand the interstellar medium and the nature of its interaction with the plasma environment around the Sun.

A stream of ionized particles—the solar wind—is continuously emitted by the Sun and has carved out a bubble in the interstellar plasma, called the heliosphere, which extends outward from the Sun more than 100 astronomical units (AU) (1 AU is the distance from the Sun to Earth) in all directions. The ionized regions of the interstellar gas and its magnetic field are largely excluded from this bubble. This local interstellar magnetic field, immediately outside of the heliosphere, is an important factor in determining the interaction of the interstellar medium with the heliosphere. The interaction determines, among other things, the effects of the heliosphere on the galactic cosmic rays, an important part of Earth's environment in space.

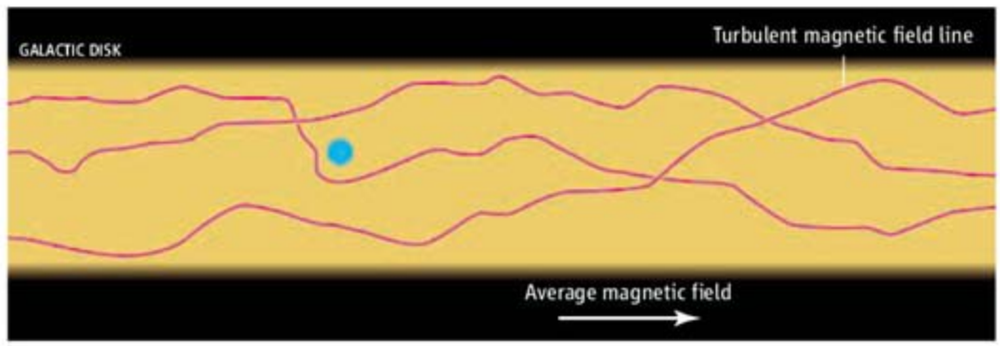

Local disturbance. Schematic illustration of the braided and intertwined turbulent interstellar magnetic field. The average magnetic field is parallel to the plane of the galactic disk, and the filled blue circle represents the heliosphere, where the local magnetic field has a pronounced deviation from the average.

Until recently, observations of the interstellar plasma and magnetic field were restricted to effects averaged over long lines of sight to distant objects, corresponding to spatial scales of tens of parsecs (1 parsec, or pc, is 3×10^{18} cm, or 200,000 AU), more than a thousand times the scale of the heliosphere. These observations yielded accurate information about the interstellar plasma and the magnitude and direction of the magnetic field, but the spatial resolution was limited by the averaging to scales of several parsecs or more (*5*).

From these measurements, the magnetic field was found to be approximately in the galactic plane, along a spiral arm. However, there is a complication: The interstellar medium is turbulent, with pronounced fluctuations of fluid parameters such as density, with a coherence scale (typical scale of the largest fluctuations in the turbulence) on the order of 1 to 10 pc (*6*, *7*). Because the interstellar plasma is a hydromagnetic fluid, there is no electric field in the frame of the fluid and the magnetic field is dragged with the plasma motions. As a result, plasma flows and magnetic field should vary on similar scales.

The author is in the Department of Planetary Sciences, University of Arizona, Tucson, AZ 85721, USA. E-mail: jokipii@lpl.arizona.edu

Therefore, it is reasonable to expect that the very local interstellar magnetic field differs considerably from the averages over several parsecs, as is now confirmed by Opher *et al.* (*1*).

Observational evidence for this difference in magnetic-field directions, obtained from the observed deflection of interstellar hydrogen, was reported by Lallement *et al.* (*2*), which allowed them to infer the plane of the interstellar magnetic field. These results were not consistent with the earlier results of Kurth *et al.* (*3*) obtained with Voyager radio wave data, which suggested a direction of the local magnetic field nearly parallel to the galactic plane. Subsequently, Gurnett *et al.* (*4*) pointed out that the Voyager data were also consistent with the Lallement *et al.* result. The analysis of Opher *et al.* establishes that the local magnetic field is at a large angle to the large-scale average field, finally reconciling the various observations.

The source of the confusion is turbulence, and its existence in the ambient interstellar medium has been known for decades (*6*–*10*). Turbulence is a phenomenon whereby large-scale fluid flow breaks down into random fluctuations and eddies and does not flow smoothly. Turbulence in Earth's atmosphere can often be seen mixing the smoke downwind from a smokestack or a fire.

Turbulent fluid flow is fundamentally irregular and random, and can be described only in terms of its statistical properties, such as mean fluctuation scale and square of the fluctuation velocity. In the interstellar plasma, it is found that the mean square of the change of turbulent density and magnetic field between two points varies as the ⅔ power of the separation distance, from small scales of thousands of kilometers to the coherence scale of several parsecs. A similar scaling of the turbulent flow velocity is seen in other naturally occurring turbulent flows such as in Earth's oceans and atmosphere, planetary atmospheres, and in the solar wind. One may conclude that the observed substantial difference between the large-scale average magnetic field and the locally observed field is an expected consequence of interstellar turbulence. The figure illustrates, schematically, the inferred turbulent magnetic field.

The analysis by Opher *et al.* has also improved our understanding of the effects of the interstellar magnetic field on the interaction of the interstellar medium with the heliosphere. A decade ago, simulations (*11*, *12*) showed that the local magnetic-field direction may be important in determining the shape of the heliosphere. If the local interstellar magnetic field is canted at an angle to the interstellar plasma flow direction onto the heliosphere, the magnetic field can push the heliosphere to one side and induce a global lateral asymmetry. Opher *et al.* use simulations, combined with comparison with Voyager 1 and 2 energetic-particle observations, to further constrain the direction and magnitude of the interstellar magnetic field and the consequent lateral asymmetry of the heliosphere.

Voyager 1, having crossed the solar-wind termination shock in December 2004, is now exploring the heliosheath (that region of subsonic outward flow between the termination shock and the interstellar plasma). Voyager 2, yet to cross the termination shock, is following Voyager 1, but moving in a different direction and currently some 20 AU closer to the Sun. Continued measurements from Solar and Heliospheric Observatory (SOHO) and the launch of the Interstellar Boundary Explorer (IBEX) next year will provide improved remote observations of the interaction of the interstellar medium with the heliosphere. These in situ and remote measurements should continue the remarkable recent expansion of our knowledge of the very local interstellar medium, the solar system's home in space, and its interaction with the heliosphere.

References

1. M. Opher, E. C. Stone, T. I. Gombosi, *Science* **316**, 875 (2007).
2. R. Lallement *et al.*, *Science* **307**, 1447 (2005).
3. W. S. Kurth, D. A. Gurnett, *J. Geophys. Res.* **108** 8027 (2003).
4. D. A. Gurnett, W. S. Kurth, I. S. Cairns, J. Michell, in *AIP Conference Proceedings* (American Institute of Physics, College Park, MD, 2006), vol. 858, pp. 129–134.
5. P. Frisch, *Space Sci. Rev.* **72**, 599 (1995).
6. L. C. Lee, J. R. Jokipii, *Astrophys. J.* **206**, 735 (1976).
7. S. R. Spangler, A. H. Minton, *Astrophys. J.* **458**, 194 (1996).
8. S. Chandrasekhar, G. Munch, *Astrophys. J.* **115**, 103 (1952).
9. J. R. Jokipii , E. N. Parker, *Astrophys. J.* **159**, 799 (1969).
10. J. W. Armstrong, B. J. Rickett, S. R. Spangler, *Astrophys. J.* **443**, 209 (1995).
11. N. Pogorelov, T. Matsuda, *J. Geophys. Res.* **10**, 237 (1998).
12. R. Ratikewicz *et al.*, *Astron. Astrophys.* **335**, 363 (1998).

10.1126/science.1141628

IMMUNOLOGY

Keeping a Tight Leash on Notch

Ivan Maillard and Warren S. Pear

A signaling pathway in bone marrow progenitor cells leads to T cell development unless a cellular factor intervenes and turns them toward a B cell fate.

Although multiple hematopoietic progenitor cells in the bone marrow have the potential to develop into T cells, they only do so after progenitors leave the bone marrow and reach the thymus. By contrast, B cells are produced primarily in the bone marrow. The key molecular determinant of the B versus T cell fate decision is signaling by the membrane protein Notch. Simply put, Notch signaling in progenitors drives T cell development at the expense of B cell development (*1*–*3*). On page 860 of this issue, Maeda *et al.* (*4*) identify a factor that is required to block Notch signaling in bone marrow progenitor cells, allowing their development into B cells. The factor is encoded by *LRF* (leukemia/lymphoma-related factor, previously known as *Pokemon*), a gene whose dysregulated expression can lead to cancer (causing it to be designated an oncogene). This newly identified role for LRF indicates that Notch signaling is actively repressed in certain physiological conditions.

The thymus expresses an abundance of ligands that activate Notch, in particular the Delta-like family member Dll-4 (*5*, *6*). This environment is thus conducive to high-intensity signaling by Notch in progenitor cells that arrive from the bone marrow (*7*). The B cell fate of progenitors in the bone marrow has been attributed to the absence of such high-intensity Notch signals, although it has not been clear whether limited ligand availability or other factors might explain the low levels of Notch signaling in these cells. The findings of Maeda *et al.* identify LRF as an important new member in the list of molecules that can inhibit Notch and show that Notch signals are actively repressed in bone marrow

I. Maillard is in the Division of Hematology-Oncology, Abramson Family Cancer Research Institute, University of Pennsylvania School of Medicine, Philadelphia, PA 19104, USA. W. S. Pear is in the Department of Pathology and Laboratory Medicine, Abramson Family Cancer Research Institute and Institute of Medicine and Engineering, University of Pennsylvania School of Medicine, Philadelphia, PA 19104, USA. E-mail: wpear@mail.med.upenn.edu

hematopoietic progenitors.

LRF belongs to the POK (POZ/BTB and Krüppel) family, a group of proteins that includes PLZF (promyelocytic leukemia zinc finger), BCL6 (B cell lymphoma 6), and Th-POK. All function in hematolymphoid development, and several play a role in oncogenic transformation (*8*–*11*). POK proteins contain an amino-terminal POZ/BTB domain that mediates homodimerization and interaction with other proteins, and a carboxyl-terminal Krüppel-type zinc finger domain that binds to DNA.

Maeda and colleagues previously identified a central role for LRF in oncogenic transformation, in which it cooperates with several proto-oncogenes and decreases expression of the tumor suppressor protein p19 (ARF) (*8*). In the current work, they studied the physiological function of LRF in hematopoiesis. Mice lacking LRF in the bone marrow had a profound block in early B cell development that could not be overcome by ectopic expression of potent B lineage–specific transcription factors, such as EBF (early B cell factor). Concurrently, LRF-deficient progenitors gave rise to T cells in the bone marrow through a thymus-independent T cell developmental pathway. Because this phenotype mimics the effect of constitutive Notch signaling (*2*), the authors investigated the effects of LRF loss on Notch signaling. They found that LRF-deficient multipotent hematopoietic progenitors had increased expression of multiple Notch-regulated genes (including *Hes1*, *Deltex1*, *Notch3*, and *pTCRa*), suggesting that Notch signaling had been activated. These findings indicate that LRF blocks (or at least substantially reduces) Notch signaling in bone marrow hematopoietic progenitors, even if they are exposed to Notch ligands in their immediate environment (see the figure). Whether any residual low-intensity signaling is linked to a physiological function of Notch in controlling hematopoietic stem cell self-renewal and differentiation remains controversial.

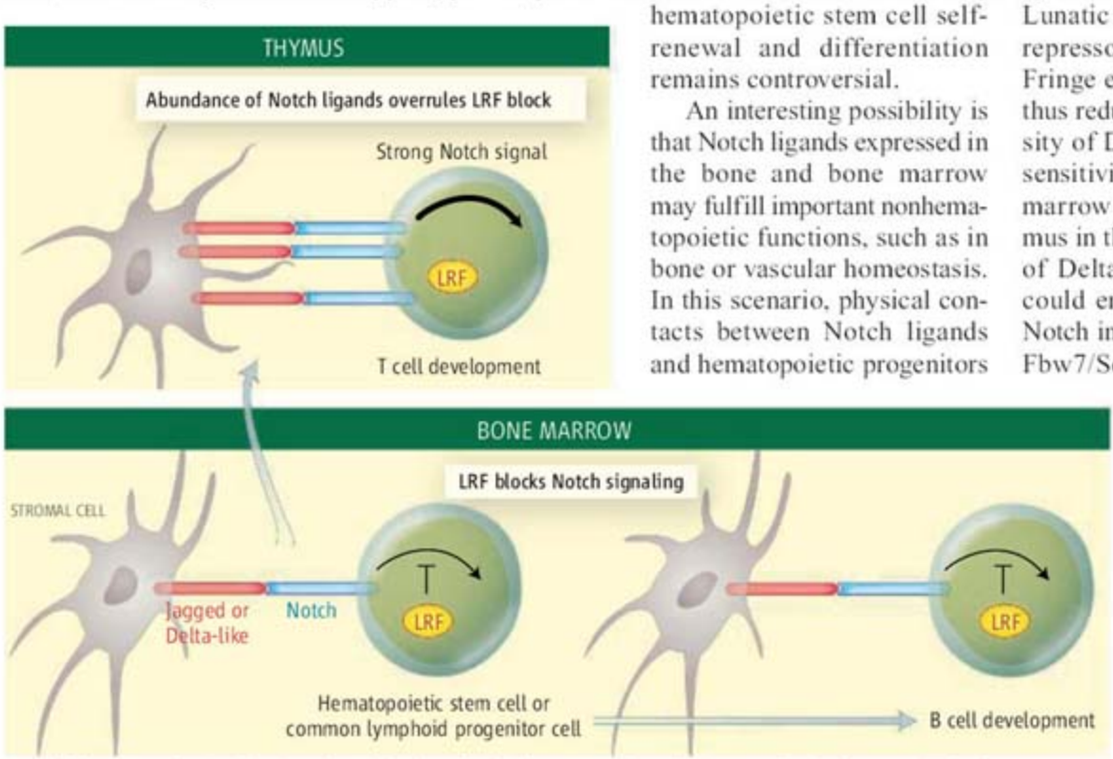

Notch block. Notch signaling is reduced by the cellular factor LRF, thus allowing B cell development in the bone marrow. In the absence of LRF-inhibitory activity, progenitor cells develop into T cells in the thymus.

An interesting possibility is that Notch ligands expressed in the bone and bone marrow may fulfill important nonhematopoietic functions, such as in bone or vascular homeostasis. In this scenario, physical contacts between Notch ligands and hematopoietic progenitors in the bone marrow cavity would naturally occur, and LRF may ensure that hematopoietic stem cells and their progeny in the bone marrow maintain the potential to develop into multiple lineages in an environment that may continually support high-intensity Notch signaling.

How, then, does Notch signaling occur in LRF-expressing lymphoid progenitors in the thymus? Potentially, high concentrations of Notch ligands in the thymus overcome LRF-mediated Notch inhibition. Alternatively, LRF activity may be repressed. This could be fleshed out by studying the regulation and function of LRF at early stages of T cell development.

Although Maeda *et al.* show that LRF blocks Notch signaling, where it acts in the Notch signaling pathway is not known. Notch signaling is initiated after its interaction with a ligand. This leads to successive proteolytic cleavage steps including intramembrane proteolysis by a γ-secretase complex. This event releases the intracellular domain of Notch into the cytoplasm and ultimately to the nucleus, where it activates transcription upon binding to the transcription factor CSL (CBF1/RBP-J/Suppressor of Hairless/Lag-1) and to the transcriptional coactivator Mastermind.

There are multiple steps in this pathway that might be regulated by LRF. For example, signaling via Delta-like ligands is enhanced by the expression of the glycosyltransferase Lunatic Fringe (*12*). As a transcriptional repressor, LRF could decrease Lunatic Fringe expression by the progenitor cells, thus reducing their sensitivity to a low density of Delta-like ligands. Such decreased sensitivity could be important in the bone marrow but would be overcome in the thymus in the presence of a high concentration of Delta-like ligands. Alternatively, LRF could enhance the effects of intracellular Notch inhibitory proteins, such as Numb or Fbw7/Sel10, effectively reducing Notch signaling. In addition, proteins containing POZ/BTB domains can interact with E3 ubiquitin ligase complexes to target proteins for degradation (*13*). Because the Notch intracellular domain undergoes rapid turnover by proteasomal degradation, LRF could potentially participate in this process, thereby attenuating Notch signaling.

The role of LRF as a Notch inhibitor is seemingly at odds with the description of *LRF* as a dominant oncogene in T cell lymphoblastic leukemia (*8*), given that most human and mouse T cell tumors contain activating mutations in *Notch1* (*14*). There may be several explanations for this apparent paradox. First, not all T cell tumors have Notch mutations and/or are Notch dependent (*14*, *15*); the presence of Notch mutations and Notch dependence have not been examined in LRF tumors. Second, activating mutations in *Notch1* may overcome LRF-mediated suppression. For example, mutations in the Notch heterodimerization domain cause ligand-independent cleavage, which would render the effects of LRF on ligand sensitivity irrelevant. Alternatively, carboxyl-terminal Notch mutations increase nuclear Notch activity, which might override LRF's effects on Notch degradation.

The work by Maeda *et al.* provides new insights for understanding the molecular mechanisms underlying early lymphoid cell development. Determining the precise

CREDIT: P. HUEY/SCIENCE

mechanism of LRF action may lead to new opportunities to inhibit Notch for therapeutic purposes. Because LRF is broadly expressed, it will also be interesting to determine whether this factor influences Notch signaling at other stages of hematolymphoid development, and in tissues such as the vasculature, gut, brain, and skin, where Notch function is critical. This versatility of Notch, and the ubiquity of its signaling pathway components, require its tight regulation to achieve specificity. LRF appears to keep Notch on just such a tight leash.

References

1. F. Radtke *et al.*, *Immunity* **10**, 547 (1999).
2. J. C. Pui *et al.*, *Immunity* **11**, 299 (1999).
3. I. Maillard, T. Fang, W. S. Pear, *Annu. Rev. Immunol.* **23**, 945 (2005).
4. T. Maeda *et al.*, *Science* **316**, 860 (2007).
5. V. Besseyrias *et al.*, *J. Exp. Med.* **204**, 331 (2007).
6. K. Heinzel, C. Benz, V. C. Martins, I. D. Haidl, C. C. Bleul, *J. Immunol.* **178**, 858 (2007).
7. A. Sambandam *et al.*, *Nat. Immunol.* **6**, 663 (2005).
8. T. Maeda *et al.*, *Nature* **433**, 278 (2005).
9. T. Maeda, R. M. Hobbs, P. P. Pandolfi, *Cancer Res.* **65**, 8575 (2005).
10. R. Perez-Torrado, D. Yamada, P. A. Defossez, *Bioessays* **28**, 1194 (2006).
11. X. He *et al.*, *Nature* **433**, 826 (2005).
12. I. Visan et al., *Immunol. Rev.* **209**, 76 (2006).
13. L. Pintard *et al.*, *Nature* **425**, 311 (2003).
14. A. P. Weng *et al.*, *Science* **306**, 269 (2004).
15. Z. Guo *et al.*, *Blood* 10.1182/blood-2006-11-059071 (22 February 2007)

10.1126/science.1143336

GEOPHYSICS

Slippery When Hot

Laboratory experiments provide a possible explanation for why friction between rocks does not impede the slippage that leads to earthquakes.

Raul Madariaga

Most earthquakes in Earth's crust are caused by fast slip on preexisting faults. Slip on faults explains well the emission of seismic waves, but it does not address how friction between rocks is overcome, especially at the fast rates at which earthquakes slip. On page 878 of this issue, Han *et al.* (*1*) address this question in a laboratory experiment.

The authors studied friction at high speeds between two precut cylindrical bars of Carrara marble cut along a section perpendicular to the axis of the cylinder. They found that friction decreases as a result of rapid, localized heating produced by high slip rates. Calcite, the main constituent of marble, decomposes into small particles of lime (CaO), forming a narrow zone of powder (called fault gauge) and producing a substantial amount of CO_2. The reduction in friction is so dramatic that when the slip rate increases beyond about 50 cm/s, the fault effectively slips freely. Marble is not the typical rock lining seismic faults, but nevertheless the authors attribute the reduction in friction to low-strength minerals like talc. The work provides new insight into friction at high speeds that may help to solve some long-standing puzzles in earthquake science, but it also raises questions regarding the scaling of stresses in seismic ruptures.

Early kinematic models of seismic slip on faults did not take into account the frictional properties of the fault, because seismic radiation could be computed independently of the actual stresses that operated on the fault. These models were highly successful and led to a broad understanding of earthquake kinematics. In the early 1970s, seismologists realized that friction had a fundamental role in determining the dynamics of earthquakes. Yet the actual properties of friction remained elusive, because experiments on rock friction could only be done at speeds of less than 1 mm/s, whereas earthquake slip occurs at rates closer to 1 m/s.

The most basic information about rock friction was found by Byerlee (*2*), who showed that static friction (the resistance to the initiation of slip on the fault) varied between 0.6 and 0.8 times the confining pressure (the pressure that holds the rocks together in the deep Earth) for almost all

The author is in the Laboratoire de Géologie, CNRS–Ecole Normale Supérieure, 24 rue Lhomond, 75231 Paris Cedex 05, France. E-mail: madariag@geologie.ens.fr

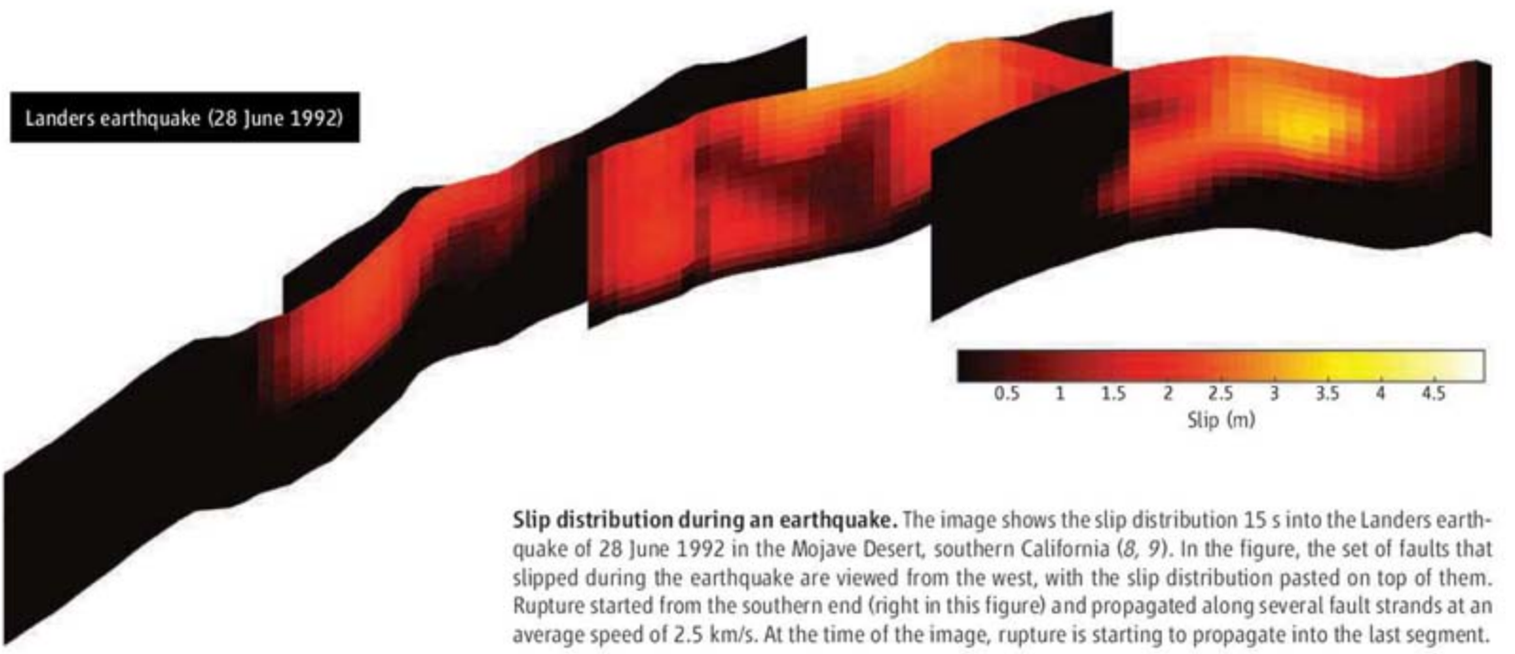

Slip distribution during an earthquake. The image shows the slip distribution 15 s into the Landers earthquake of 28 June 1992 in the Mojave Desert, southern California (*8*, *9*). In the figure, the set of faults that slipped during the earthquake are viewed from the west, with the slip distribution pasted on top of them. Rupture started from the southern end (right in this figure) and propagated along several fault strands at an average speed of 2.5 km/s. At the time of the image, rupture is starting to propagate into the last segment.

rock samples. These results led to the slip-weakening model, in which friction was assumed to decrease as slip on the fault increased. The key model parameter was the slip-weakening distance (the amount of slip required to reduce friction at high speeds). This phenomenological model avoided the difficult question of the origin of friction.

Mechanical studies of rocks in the late 1970s provided the first experimental evidence that steady-state friction indeed decreased logarithmically with slip rate. Friction also depends on several parameters representing the state of the slipping surface (*3*). In these experiments, designed to understand friction at low slip rates, the slip-weakening distance is very small, on the order of a fraction of 1 mm.

In the past 15 years, seismologists were able to study in detail several major earthquakes in the United States, Japan, Turkey, and Taiwan. The slip-weakening distances inferred for these events were several orders of magnitude longer than those observed in rate-and-state friction experiments. A simple scaling argument explains the long slip distances. Earthquakes are similar for a broad range of scales, at least from magnitudes of about 4 to 8; the single scaling variable appears to be the length of the fault. If this is the case, then slip-weakening distances must scale with earthquake size; otherwise, either large earthquakes would all propagate with rupture speeds higher than that of shear waves, or small events could never occur because of the high frictional resistance of the faults. Han *et al.* find that slip weakening occurs on scales on the order of a meter, a value that is very close to the slip-weakening distances observed in earthquakes of magnitude around 7. A numerical simulation of the Landers earthquake of 28 June 1992 in California (see the figure) required slip weakening distances of several tens of centimeters, similar to those observed by Han *et al.*

The experiments by Han *et al.* show that friction is very sensitive to slip rate. Large slip-rate weakening favors the creation of rupture pulses instead of long cracks. In pulses (*4*), slip occurs in a narrow zone that follows the rupture front; this is a very efficient way to propagate seismic slip while maintaining a high average stress on the fault. The results reported by Han *et al.* may also help to explain the "San Andreas Fault paradox": There is no observed increase in heat flow near the fault, which means either that the fault is very weak during slip, producing very little heat, or that friction is high but heat is evacuated by fluid flow (*5*).

The experiments also raise several questions. The most obvious is that they were done at a fixed slip rate, whereas earthquakes are intrinsically transient phenomena, with slip rate increasing from zero to speeds on the order of 1 m/s when the rupture front arrives, finally decreasing to zero as the fault heals. It remains unclear whether the friction law derived in this work applies to transient slip of short duration.

By far the most important question concerns scaling. Han *et al.* carried out their experiments at confining pressures of 7.3 MPa. Will the same friction law apply at the much higher confining pressures that prevail in seismogenic zones? Seismic data have shown that slip rates are proportional to stress drop (the difference between the static and dynamic friction). Stress drops in the experiments were on the order of 7 MPa at the confining pressure of 13 MPa. Extrapolating to the depths where earthquakes occur, this implies stress drops at least an order of magnitude greater than those observed. Furthermore, the experiments were done on marble; the results may be different for the silicate rocks found at 10 km depth.

Thermal weakening is not the only mechanism that may reduce friction at high slip rates; melting (*6*) is another example. Furthermore, direct application of the results reported by Han *et al.* actual fault zones depends on the assumption that slip is concentrated on a narrow band. Recent experiments on sand have shown (*7*) that slip bands tend to form outside the main slip zones as fault zones evolve toward large accumulated slip. We are only at the beginning stages of a fresh understanding of fast frictional processes in earthquakes.

References

1. R. Han, T. Shimamoto, T. Hirose, J.-H. Ree, J. Ando, *Science* **316**, 878 (2007).
2. J. D. Byerlee, *Pure Appl. Geophys.* **116**, 615 (1978).
3. J. H. Dieterich, *J. Geophys. Res.* **84**, 2161 (1979).
4. T. H. Heaton, *Phys. Earth Planet. Inter.* **64**, 1 (1990).
5. C. H. Scholz, *Geology* **28**, 163 (2002).
6. G. Di Toro, T. Hirose, S. Nielsen, G. Pennacchioni, T. Shimamoto, *Science* **311**, 647 (2006).
7. G. Chambon, J. Schmittbuhl, A. Corfdir, *J. Geophys. Res.* **111**, 10.1029/2003JB00273 (2006).
8. H. Aochi, R. Madariaga, E. Fukuyama, *Geochem. Geophys. Geosyst.* **4**, 1020 (2003).
9. S. Peyrat, K. B. Olsen, R. Madariaga, *J. Geophys. Res.* **106**, 20467 (2001).

10.1126/science.1142332

PLANETARY SCIENCE

Titan's Organic Factory

Sushil Atreya

Researchers have identified molecules in the atmosphere of one of Saturn's moons that are responsible for its smog-like haze.

Since its discovery by Christiaan Huygens in 1655, Saturn's large moon Titan has intrigued scientists, not the least because its surface is blanketed by thick haze. This haze plays an important role in warming Titan's nitrogen atmosphere, preventing its condensation and subsequent removal. However, the most important aspect of Titan's haze may be its composition. It has long been suspected that the haze results from complex organic molecules, perhaps even prebiotic molecules (*1*). Now, close flybys of Titan by the Cassini spacecraft reveal that such molecules may indeed be forming. On page 870 of this issue, Waite *et al.* (*2*) report identification of benzene, along with both positively and negatively charged organic ions. Heavy molecules formed from these ions eventually produce Titan's upper haze layers and are expected to contribute substantially to the total haze content of the atmosphere.

Unlike the other moons in the solar system, Titan has a massive atmosphere, consisting of 95% nitrogen and 5% methane. Chemical processes are initiated by the break-up of these gas molecules by solar radiation and charged particle collisions (see the figure). Even though Titan receives only 1% of the solar ultraviolet flux that Earth does, and is bombarded by charged particles from Saturn's magnetosphere only some of the time, this energy is sufficient for photochemistry to proceed efficiently. Simple hydrocarbons—such as ethane, acetylene, and diacetylene—and nitriles, such as hydrogen cyanide (HCN) and cyanogen (C_2N_2) form readily. Somewhat

The author is in the Department of Atmospheric, Oceanic, and Space Sciences, University of Michigan, Ann Arbor, MI 48109, USA. E-mail: atreya@umich.edu

more complex molecules such as propane, butane, polyacetylenes, and cyanoacetylene follow from these simpler units (*3*). Researchers believed that the haze seen on Titan by Voyager 1 and Voyager 2 during 1980–1981 was the result of condensation of many of these molecules and polymers of polyynes and HCN (*3*), somewhat similar to the formation of urban photochemical smog on Earth.

That is where things stood until a tentative detection of a few parts per billion of benzene (C_6H_6) by the Infrared Space Observatory (ISO) in 2003 (*4*). Wilson *et al.* proposed recombination of propargyl (C_3H_3) molecules (which are derived from acetylene) with each other to explain the observations (*5*). Benzene is key to the formation of polycyclic aromatic hydrocarbons (PAHs) through a continued sequence of hydrogen atom removal and acetylene addition (*6*, *7*). Conversion from gas phase to particulates occurs when the PAHs reach a high mass of about 2000 daltons (1 dalton is the atomic mass unit equal to 1/12 the mass of the carbon atom), and ultimately soot forms, like the exhaust from diesel trucks. PAHs were predicted in laboratory simulation experiments of Titan (*8*), and models showed PAH polymers to be the largest contributors to Titan's haze (*9*).

The conventional photochemical process leading up to PAHs begins with the dissociation of methane some 600 to 800 km above Titan's surface. However, measurements with the Ion Neutral Mass Spectrometer (INMS) on Cassini (*2*) show that benzene must be forming in the thermosphere-ionosphere region also, well above Titan's normal photochemical regime. Moreover, the benzene is found to be at a concentration of parts per million, some 1000 times as high in mole fraction as the stratospheric value from the ISO and the Cassini Composite Infrared Spectrometer. Thus, the benzene abundance in the (lower density) thermosphere is comparable to its abundance in the (higher density) stratosphere.

What is the cause for this high benzene concentration? A previously neglected mechanism of ion-molecule reactions seems to be at work. Although charge-exchange reactions to produce simple one- and two-carbon ions, such as CH_5^+ and $C_2H_5^+$ were known in the past (*10*), no one recognized that the chemistry in the ionosphere could proceed to more complex molecules. Waite *et al.* (*2*) show that heavier ions, including $C_6H_7^+$ are formed through a sequence of subsequent charge-exchange reactions of the above ions with ambient neutral molecules such as acetylene and diacetylene. Benzene results from electron recombination of $C_6H_7^+$ in the ionosphere. The ion-molecule reactions proceed much more efficiently than those between neutrals in the atmosphere below. This can explain why the ionospheric benzene mole fraction is enormous. With so much benzene around, a large production of PAHs in the ionosphere cannot be far behind.

The detection reported by Waite *et al.* of heavy positive ions up to 350 daltons and negative ions up to 8000 daltons by Cassini Plasma Spectrometer (CAPS) (*2*) implies that ion-molecule reactions may be producing more complex ions than just $C_6H_7^+$ even as the PAHs form and grow in Titan's ionosphere. However, there is no way to positively identify the composition of such molecules from the CAPS spectra. Chemical models do not help either, because the appropriate laboratory chemical kinetics data are lacking. Thus, to conclude that the ions seen by CAPS are massive organic molecule precursors to haze or haze itself is speculative. However, considering the likely chemical pathways to the formation of such molecules, the unexpectedly large mole fraction of benzene in the ionosphere, the presence of haze layers at high altitudes, and the total atmospheric aerosol content, this speculation may be close to reality.

The picture emerging from the work of Waite *et al.* and previous studies is that both the ionosphere and the neutral atmosphere below play important roles in the formation of complex organic molecules. These molecules are precursors to haze. Very few molecules survive condensation below Titan's cold tropopause (70.4 K). As a result, aerosols have been snowing down onto the surface of Titan over the past 4.5 billion years. If left alone, they could accumulate to a depth of hundreds of meters. However, the rain of methane is expected to wash some of the deposit into lake beds or river basins. Nevertheless, relatively large quantities are expected to survive intact on the surface.

The combined CAPS and INMS observations (*2*) allow a glimpse of the composition of these aerosols. Unfortunately, their low concentrations mean that chemical identification of the more complex of these molecules is beyond the capability of most instruments. Yet there is hope for detection of complex species on the surface where the

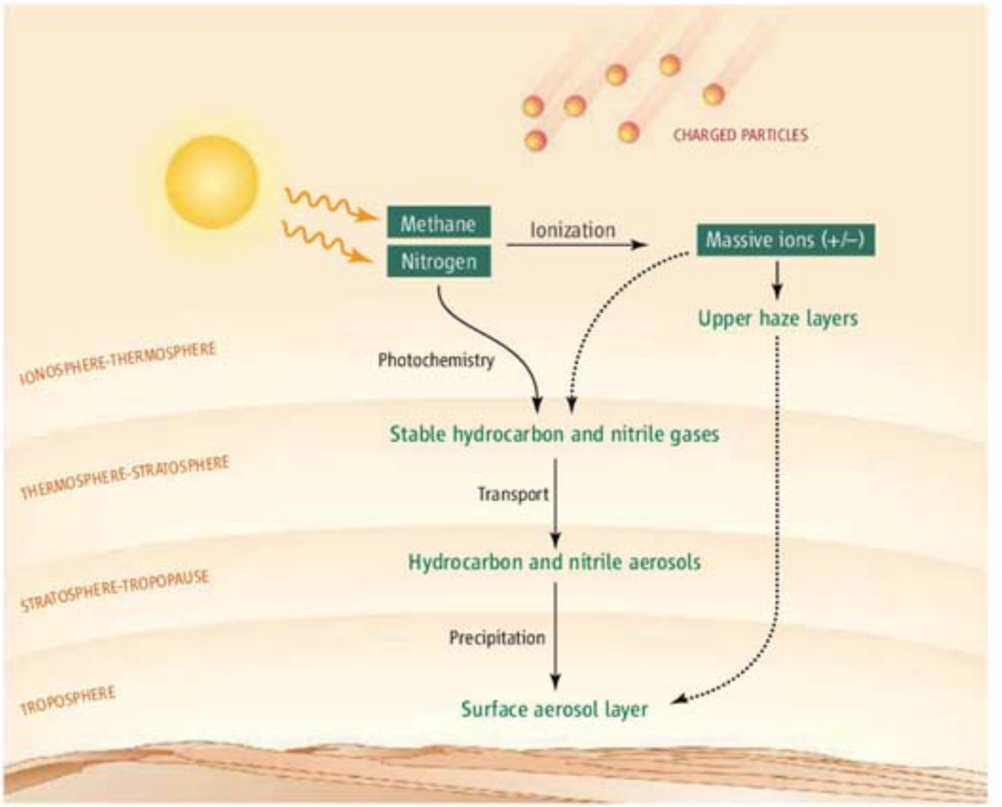

Haze formation. Ultraviolet radiation from the sun and charged particles from Saturn's magnetosphere initiate photochemical reactions of nitrogen and methane in Titan's ionosphere-thermosphere region (~1000 km altitude) and these reactions can extend into the lower stratosphere (~200 km). The hydrocarbon and nitrile products begin condensing below ~200 km down to the tropopause (~40 km). These aerosols eventually precipitate out of the troposphere and accumulate on Titan's surface together with aerosols from the upper layers. [Adapted from (*12*)]

CREDIT: ADAPTED BY P. HUEY/SCIENCE

atmospheric aerosols accumulate. Indeed, the Huygens Gas Chromatograph Mass Spectrometer (part of a probe launched from the Cassini spacecraft) found Titan's surface material to be a rich mixture of molecules (*11*). The Huygens team has made a tentative identification of benzene and cyanogen among other volatiles, even though the same molecules are not yet seen in the mass spectra during descent, most likely due to their low abundance in the atmosphere below 146 km where the data were taken.

A complete chemical analysis of the surface material, including isotopes, should be a key focus of any future missions to Titan. This is because Titan's surface composition is expected to reflect to a large extent the composition of molecules originating from its atmosphere and ionosphere, but in substantially greater concentration than that in their production region. Who knows, we may yet find those elusive prebiotic molecules.

References and Notes

1. C. Sagan *et al.*, in *Saturn*, T. Gehrels, Ed. (Univ. Arizona Press, Tucson, 1984), pp. 788–807.
2. J. H. Waite Jr., *et al.*, *Science* **316**, 870 (2007).
3. Y. L. Yung *et al.*, *Astrophys. J. Suppl.* **55**, 465 (1984).
4. A. Coustenis *et al.*, *Icarus* **161**, 383 (2003).
5. E. H. Wilson *et al.*, *J. Geophys. Res.* **108(E2)**, 5014, 10.1029/2002JE001896 (2003).
6. H. Wang, M. Frenklach, *Combust. Flame* **110**, 173 (1997).
7. C. W. Bauschlicher Jr., A. Ricca, *Chem. Phys. Lett.* **326**, 283 (2000).
8. C. Sagan *et al.*, *Astrophys. J.* **414**, 399 (1993).
9. E. H. Wilson, S. K. Atreya, *J. Geophys. Res.* **109**, E06002, 10.1029/2003JE002181 (2004).
10. S. K. Atreya, *Atmospheres and Ionospheres of the Outer Planets and their Satellites* (Springer-Verlag, New York–Berlin, 1986), pp. 183–186.
11. H. B. Niemann *et al.*, *Nature* **438**, 779 (2005).
12. S. K. Atreya *et al.*, *Planet. Space Sci.* **54**, 1177 (2006).

13. This work was supported by the NASA Cassini-Huygens and Planetary Atmospheres programs.

10.1126/science.1141869

CELL SIGNALING

The Art of the Soluble

New information about the synthesis and function of inositol phosphates shows that they may have wider and more important effects than previously realized.

Robin Irvine

Since the 1980s, inositol lipids have captured more attention than inositol phosphates as important cellular signaling molecules, even though it was an inositol phosphate—inositol 1,4,5-trisphosphate (IP_3)—that was assigned a definitive cellular function first (*1*). Two papers recently published in *Science* (*2*, *3*) and one that appears in this issue (*4*) go a long way toward redressing this balance and establish (*4*) a new relationship between the lipids and their soluble counterparts.

In most eukaryotic cells, IP_3 is phosphorylated by a sequence of enzymes (kinases) to produce inositol hexakisphosphate (IP_6; see the figures) (*5*, *6*). Remarkably, phosphorylation does not stop there but continues to produce mono- and bis-pyrophosphorylated inositol phosphates [properly called PP-IP_5 and $(PP)_2$-IP_4, but loosely termed IP_7 and IP_8, respectively]. A number of potential functions have been assigned to IP_7, including DNA recombination, vacuolar morphology, gene expression, protein phosphorylation, and telomere length (*6*).

One way in which such functions for IP_7 have been determined is by studying the phenotypes resulting from deletion of *Kcs-1*, the gene that encodes IP_6 kinase in the budding yeast *Saccharomyces cerevisiae*. However, the recent *Science* paper by Mulugu *et al.* (*2*) shows that we've been aware of only half the IP_7 story. The authors revisited a puzzling finding that yeast lacking *Kcs-1* still make IP_7 (*7*). The great investigative strength of yeast is the ability to manipulate its genetics, but sometimes you have to do things the hard, biochemical way. Mulugu *et al.* combined both approaches, forging through protein purification and then a screen of 40 potential yeast proteins, to identify a second, novel IP_6 kinase. This enzyme turns out to be encoded by a gene that, in the fission yeast *Schizosaccharomyces pombe*, is functionally linked to a protein complex (ARP) and the actin cytoskeleton to control cell shape and integrity.

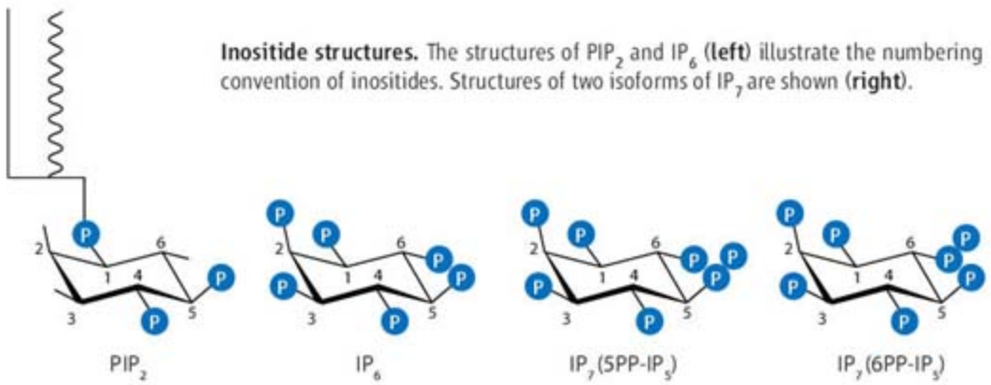

Inositide structures. The structures of PIP_2 and IP_6 (**left**) illustrate the numbering convention of inositides. Structures of two isoforms of IP_7 are shown (**right**).

This new IP_6 kinase (called Vip1 in *S. cerevisiae* and Asp1 in *S. pombe*) is found in all eukaryotes and has a kinase domain and a phosphatase domain, the latter of which has an unknown role. Mulugu *et al.* used elegant structure-based threading software to identify key residues in the enzyme that they then mutated to generate forms lacking kinase activity. They show that it is indeed the ability of Vip1/Asp1 to make IP_7 that is essential to its contribution to yeast cellular integrity, growth, and morphology.

But why are there two IP_6 kinases? Mulugu *et al.* show by nuclear magnetic resonance that each kinase makes a different IP_7 isomer. Kcs-1 makes 5PP-IP_5, but Vip1 synthesizes 4/6PP-IP_5—that is, IP_7 with a pyrophosphate in the 4 or 6 position. Although 4PP-IP_5 and 6PP-IP_5 cannot be distinguished by nuclear magnetic resonance (*5*), it is likely to be 6PP-IP_5, the form identified in the slime mold *Dictyostelium discoideum* (*8*). This discovery enabled the researchers to solve another long-standing mystery—the identity of an IP_7 kinase that makes IP_8. When added together, the two IP_6 kinases synthesized IP_8 in vitro. In short, either IP_6 kinase can make IP_8, but each needs the right substrate—an IP_7 made by the other kinase.

Another important function for IP_7 comes out of the accompanying *Science* paper by Lee *et al.* (*3*). Budding yeast stop growing when deprived of phosphate, a result of the inactivity of a cyclin/cyclin-dependent kinase (CDK) complex that con-

The author is in the Department of Pharmacology, University of Cambridge, Cambridge CB2 1PD, UK. E-mail: rfi20@cam.ac.uk

sists of three proteins, Pho80, 81, and 85. Through an arduous purification, the authors determined that IP_7 is required for maintaining the inactive state of this complex. The CDK inhibitor Pho81 is the likely effector protein (and receptor) for IP_7, but which IP_7? The one made by Kcs-1 or by Vip1? The genetic evidence points unambiguously to Vip1. Moreover, Lee *et al.* show that 4/6PP-IP_5 is more efficacious than 5PP-IP_5 in inactivating the CDK-Pho complex in vitro. This is the first isomer-specific molecular action of an IP_7 linked to a physiological response, and as such, IP_7 becomes a bona fide second messenger.

On page 886 of this issue (*4*), Huang *et al.* solve an older mystery—the physiological function for inositol 1,3,4,5-tetrakisphosphate (IP_4). Since its discovery (*9*), the issue of whether IP_4 is a signaling molecule has been controversial and confusing (see the figure) (*5*). For example, depending on the system, IP_4 blocks or promotes net calcium entry into cells (*10*, *11*).

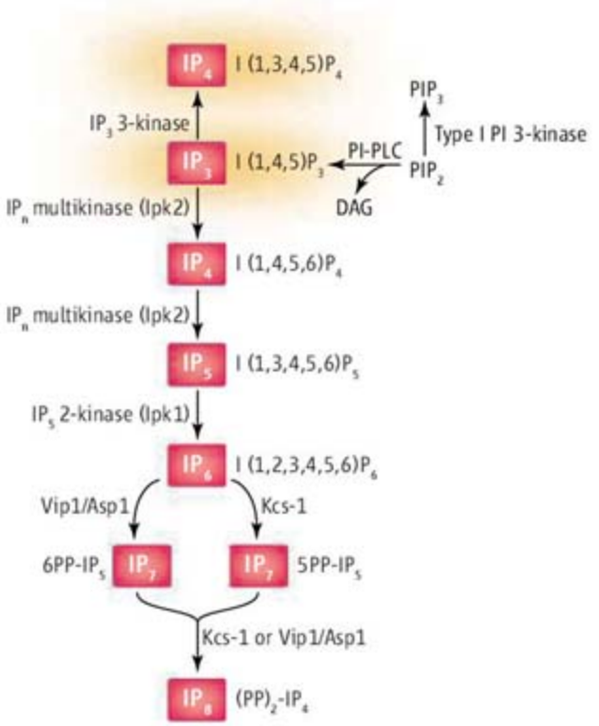

Inositide kinases. The metabolic relationships among inositides. Yeast nomenclature is also shown; yeast has no type I PI 3-kinase, and IP_3 3-kinase is found only in metazoans. The IP_3 and IP_4 isomers highlighted in gold are discussed here. DAG, diacylglycerol.

This confusion is exacerbated by the uncertain nature of an IP_4 receptor. IP_4 is the polar head group of phosphatidylinositol 3,4,5-trisphosphate (PIP_3; see the figures), an inositol lipid that governs many aspects of cellular physiology (*12*). Because any PIP_3 effector protein (there are now about 20) must distinguish PIP_3 from its precursor, phosphatidylinositol 4,5-bisphosphate (PIP_2), it must recognize PIP_3's polar head group, which is IP_4. Thus, any PIP_3 effector might be expected to bind IP_4 and indeed, those PIP_3 effectors that have been studied in vitro do precisely that. So IP_4 binding is not a good criterion for identifying putative IP_4 effectors.

Three years ago, Huang and colleagues determined that a mouse with defective T cell development had a mutation in the gene encoding an isoform of the enzyme IP_3 3-kinase (*13*). Contemporaneously, another group found the same phenotype by generating a transgenic mouse lacking the same IP_3 3-kinase (*14*). Now Huang *et al.* have dissected out where the problem lies. The developmental defect is due to insufficient activation of phosphoinositide phospholipase C (PI-PLC), the enzyme that splits PIP_2 into IP_3 and diacylglycerol. It turns out that by activating protein kinase C, diacylglycerol drives T cell development.

So what molecular event that activates PI-PLC is missing in these mutant mice? In T cells, activation of the relevant (γ) isoform of PI-PLC depends on its phosphorylation by the enzyme Itk. Itk localization depends on PIP_3 in the membrane. Huang *et al.* convincingly demonstrate that when T cells from mutant mice lacking IP_3 3-kinase are stimulated, PIP_3-dependent recruitment of Itk to the plasma membrane does not occur because it requires obligatory help from IP_4. As with all well-characterized PIP_3 effectors, Itk binds PIP_3 through its pleckstrin homology (PH) domain. Huang *et al.* show that low (physiological) concentrations of IP_4 promote binding of Itk's PH domain to PIP_3 in vitro. The precise mechanism by which IP_4 promotes this interaction is not fully elucidated yet, but given that the authors also show that Itk oligomerizes (likely forms dimers) through its PH domain, it may be a simple allosteric effect. In other words, IP_4 binds to one Itk monomer and increases the affinity of another for PIP_3. At high IP_4 concentrations, dissociation of Itk from PIP_3 occurs, as one might expect from direct competition between IP_4 and PIP_3.

The tale becomes more intriguing because Huang *et al.* discovered two other proteins whose PH domains exhibit IP_4-promoted binding to PIP_3. One is already a promising IP_4 effector, $GAP1^{IP4BP}$ (*15*, *16*), unique among known PIP_3-binding proteins in being constitutively bound to the plasma membrane. Arguably more provocative, however, is the other protein, a kinase called Tec. This is a well-established PIP_3 effector (*17*) but there has been no hint that it might be regulated by IP_4. This observation leads to the sightly unnerving question: Do all PIP_3 effectors show the same behavior?

One possibility is Btk, the B cell equivalent of Itk. In looking at B cell signaling in the same mutant mice, Miller *et al.* (*11*) found that B cell development and proliferation are both compromised. Moreover, in the mutant B cells, PI-PLCγ activity is slightly decreased. However, things are never so simple, because the authors were unable to detect compromised tyrosine phosphorylation of Btk in vitro, so it is unclear whether recruitment of Btk (or another PIP_3 effector) to the B cell membrane by PIP_3 requires physiological input from IP_4.

In considering this fascinating new relationship between PIP_3 and IP_4, how much PIP_3 is needed for IP_4 to be effective in vivo? Unstimulated cells can contain a physiologically significant concentration of PIP_3 (*18*). Could there be circumstances where events hitherto believed to be entirely under PIP_3 control may be partly, or even mostly, under the influence of its soluble counterpart? After so long in the shadows, it seems that IP_4 is coming into the limelight, and may be in for an exciting time.

References

1. H. Streb *et al.*, *Nature* **306**, 67 (1983).
2. S. Mulugu *et al.*, *Science* **316**, 106 (2007).
3. Y.-S. Lee *et al.*, *Science* **316**, 109 (2007); published online 5 April 2007 (10.1126/science.1138684).
4. Y. H. Huang *et al.*, *Science* **316**, 886 (2007); published online 5 April 2007 (10.1126/science.1138684).
5. R. F. Irvine, M. J. Schell, *Nat. Rev. Mol. Cell Biol.* **2**, 327 (2001).
6. J. D. York, *Biochim. Biophys. Acta* **1761**, 552 (2006).
7. S. J. York *et al.*, *J. Biol. Chem.* **280**, 4264 (2005).
8. T. Laussmann *et al.*, *Biochem. J.* **322**, 31 (1997).
9. I. R. Batty, S. R. Nahorski, R. F. Irvine, *Biochem. J.* **232**, 211 (1985).
10. L. Changya *et al.*, *FEBS Lett.* **251**, 43 (1989).
11. A. T. Miller *et al.*, *Nat. Immunol.* **8**, 514 (2007).
12. B. Vanhaesebroeck *et al.*, *Annu. Rev. Biochem.* **70**, 535 (2001).
13. B. G. Wen *et al.*, *Proc. Natl. Acad. Sci. U.S.A.* **101**, 5604 (2004).
14. V. Pouillon *et al.*, *Nat. Immunol.* **4**, 1136 (2003).
15. P. J. Cullen *et al.*, *Nature* **376**, 527 (1995).
16. G. E. Cozier *et al.*, *J. Biol. Chem.* **275**, 28261 (2000).
17. M. G. Tomlinson *et al.*, *J. Biol. Chem.* **279**, 55089 (2004).
18. W. D. Heo *et al.*, *Science* **314**, 1458 (2006); published online 8 November 2006 (10.1126/science.1134389).

10.1126/science.1143339

Global Desertification: Building a Science for Dryland Development

James F. Reynolds,[1]* D. Mark Stafford Smith,[2] Eric F. Lambin,[3] B. L. Turner II,[4] Michael Mortimore,[5] Simon P. J. Batterbury,[6] Thomas E. Downing,[7] Hadi Dowlatabadi,[8] Roberto J. Fernández,[9] Jeffrey E. Herrick,[10] Elisabeth Huber-Sannwald,[11] Hong Jiang,[12] Rik Leemans,[13] Tim Lynam,[14] Fernando T. Maestre,[15] Miguel Ayarza,[16] Brian Walker[2]

In this millennium, global drylands face a myriad of problems that present tough research, management, and policy challenges. Recent advances in dryland development, however, together with the integrative approaches of global change and sustainability science, suggest that concerns about land degradation, poverty, safeguarding biodiversity, and protecting the culture of 2.5 billion people can be confronted with renewed optimism. We review recent lessons about the functioning of dryland ecosystems and the livelihood systems of their human residents and introduce a new synthetic framework, the Drylands Development Paradigm (DDP). The DDP, supported by a growing and well-documented set of tools for policy and management action, helps navigate the inherent complexity of desertification and dryland development, identifying and synthesizing those factors important to research, management, and policy communities.

Drylands cover about 41% of Earth's land surface and are home to more than 38% of the total global population of 6.5 billion (*1*, *2*). Some form of severe land degradation is present on 10 to 20% of these lands [medium-confidence conclusion of (*2*)] (*3*), the consequences of which are estimated to affect directly some 250 million people in the developing world, an estimate likely to expand substantially in the face of climate change and population growth (*4*). The United Nations has periodically focused on desertification and drylands, notably adopting the Convention to Combat Desertification (CCD) in 1992 (*3*) and designating 2006 as the International Year of the Desert and Desertification.

One contribution of the CCD was to enshrine a definition of desertification as "land degradation in arid, semi-arid, and dry subhumid areas resulting from various factors, including climatic variations and human activities," that is, encompassing both biophysical and social factors (*5*). However, the CCD and related efforts receive comparatively little exposure in the popular and scientific media (*6*), in part because of the absence of a focused international science program (*7*). Advances in various aspects of science relevant to drylands and community development practices in recent years suggest a common framework for managing dryland systems.

The DDP presented here centers on the livelihoods of human populations in drylands, and their dependencies on these unique ecosystems, through the study of coupled human-environmental (H-E) systems (*8*). The DDP responds to recent research and policy trends (Fig. 1) that link ecosystem management with human livelihoods in order to best support the large, and rapidly expanding, populations of dryland dwellers (*9*). The DDP represents a convergence of insights and key advances drawn from a diverse array of research in desertification, vulnerability, poverty alleviation, and community development (Table 1).

Research and practice in these fields have increasingly converged on a set of five general lessons concerning the condition and dynamics of H-E systems as they apply to sustainable development in drylands. (i) Both researchers and practitioners need to adopt an integrated approach: Ecological and social issues are fundamentally interwoven, and so are the options for livelihood support and ecological management. (ii) There needs to be a heightened awareness of slowly evolving conditions: Short-term measures tend to be superficial and do not resolve persistent, chronic problems nor deal with continual change. (iii) Nonlinear processes need to be recognized: Dryland systems are not in equilibrium, have multiple thresholds, and thus often exhibit multiple ecological and social states. (iv) Cross-scale interactions must be anticipated: Problems and solutions at one scale influence, and are influenced by, those at other scales. (v) A much greater value must be placed on local environmental knowledge (LEK): Its

Fig. 1. The focus on global drylands is shifting from an emphasis on negative images of desertification (upper: drought-stricken cattle on an eroded grassland in central Australia. Photo: M. Stafford Smith) to a more forward-looking perspective concerning human livelihoods, based on interactions between and among human activities and natural-world processes (lower: farmer spraying organic pesticide on domesticated quinoa in southern Bolivia. Photo: J. Reynolds). Either way, great challenges to the future security of some 250 million people remain (*4*).

[1]Nicholas School of the Environment and Earth Sciences and Department of Biology, Post Office Box 90328, Duke University, Durham, NC 27708, USA. [2]Commonwealth Scientific and Industrial Research Organisation (CSIRO) Sustainable Ecosystems, Post Office Box 284, Canberra, ACT 2602, Australia. [3]Université Catholique de Louvain, B-1348 Louvain-la-Neuve, Belgium. [4]Graduate School of Geography and George Perkins Marsh Institute, Clark University, Worcester, MA 01610, USA. [5]Drylands Research, Cutters' Cottage, Glovers' Close, Milborne Port, Sherborne DT9 5ER, UK. [6]School of Social and Environmental Enquiry, University of Melbourne, Melbourne, VIC 3010, Australia. [7]Stockholm Environmental Institute, Oxford Office, 266 Banbury Road, Oxford OX2 7DL, UK. [8]Institute for Resources, Environment and Sustainability, University of British Columbia, Vancouver, BC V6T 1Z4, Canada. [9]Facultad de Agronomía and Instituto de Investigaciones Fisiológicas y Ecológicas, Universidad de Buenos Aires/CONICET (Consejo Nacional de Investigacione, Científicas y Técnicas), Buenos Aires C1417DSE, Argentina. [10]U.S. Department of Agriculture–Agricultural Research Service, Jornada Experimental Range MSC 3JER, Box 30003, New Mexico State University, Las Cruces, NM 88003–8003, USA. [11]Instituto Potosino de Investigación Científica y Tecnológica, Camino a la Presa San José 2055, San Luis Potosí, S.L.P. 78216, México. [12]Department of Geography, University of Hawaii at Manoa, Honolulu, HI 96822, USA. [13]Environmental Systems Analysis Group, Wageningen University, Post Office Box 47, 6700 AA Wageningen, the Netherlands. [14]CSIRO Sustainable Ecosystems, PMB PO, Aitkenvale, Qld 4814, Australia. [15]Universidad Rey Juan Carlos, Área de Biodiversidad y Conservación, Escuela Superior de Ciencias Experimentales y tecnológicas, C/ Tulipán s/n, Móstoles, 28933 Spain. [16]CIAT (International Center for Tropical Agriculture)–Honduras, Edificio de DICTA en la Secretaria de Agricultura y Ganaderia, Tegucigalpa, Honduras.

*To whom correspondence should be addressed. E-mail: james.f.reynolds@duke.edu

practice is central to the management of most drylands but is often undervalued.

Template for a New Science

Building on earlier efforts (*10*), we synthesize and formalize these lessons more explicitly in the DDP. The issues that the DDP principles highlight arise from a suite of biophysical and socioeconomic features that together constitute a "drylands syndrome," such that dryland populations are among the most ecologically, socially, and politically marginalized populations on Earth (*11*). Sustainable development in drylands is determined by five key features of the drylands syndrome (noted as ds-1 to ds-5 below), which dominate the dynamics of H-E systems.

Dryland syndrome. Drylands—which include arid, semi-arid, and dry subhumid areas—are by definition (*12*) areas where precipitation is scarce and typically more-or-less unpredictable (ds-1: high variability). High air temperatures, low humidity, and abundant solar radiation result in high potential evapotranspiration. Many dryland soils contain small amounts of organic matter and have low aggregate strength (ds-2: low fertility). Both tillage and grazing by domesticated animals can quickly have major impacts, so drylands are sensitive to degradation (*1*, *2*). These and other biophysical features have profound social and economic implications.

Compared to mesic areas, and a few major desert cities notwithstanding, the human populations of drylands are usually sparser (ds-3: sparse populations), more mobile, more remote from markets (ds-4: remoteness), and distant from the centers (and priorities) of decision-makers (ds-5: distant voice). It is also harder to deliver services efficiently, and institutional arrangements devised in other regions may be dysfunctional when imposed on drylands. As a result, dryland populations tend to lag behind populations in other parts of the world on a variety of economic and health indices, even controlling for "ruralness" (*2*), with higher infant mortality, severe shortages of drinking water, and much lower per capita gross national product.

Principles of the DDP. The DDP consists of five principles (Table 2), which are based on the aforementioned lessons but that are also consistent with the dryland syndrome.

Principle 1. Dryland H-E systems are coupled, dynamic, and coadapting, with no single target equilibrium point (*13*). They are the coevolved product of complex interactions between biophysical (e.g., climate, soil, biota) and

Table 1. Selected fields of activity relevant to dryland development, showing some key advances in research and lessons for management and policy over the past two decades, and which provide the basis for the new synthesis presented in Table 2. P1 to P5 indicate how the specific advances and lessons foreshadow principles 1 to 5 and their implications as given in Table 2.

Fields of activity	Some key advances in drylands research	Some key lessons learned for drylands practitioners
Desertification and rangelands ecology: Understanding the biophysical (*59, 60*) and socioeconomic (*61*) drivers of dryland degradation, as part of global environmental change research	Many case studies of chronic dryland degradation—caused by interactions between biophysical and social drivers—have been documented [e.g., land uses that exhaust available water resources or are unsuited to highly variable precipitation regimes (*62*)]. The debate about drylands being disequilibrium systems has been resolved in favor of a more dynamic, nonequilibrium view (*13*). [→P1, P2, P3]	Desertification is the emergent outcome of a suite of social and biophysical causal factors, with pathways of change that are specific in time and place (*23*). Poor resource management is compounded by weak institutions, poorly implemented technologies, or exploitative economic and political systems [thus emphasizing links between coupled H-E systems (*63*)]. [→P1, P2]
Vulnerability: Understanding the integrated environmental, social, economic, and political exposure of human welfare to a range of potentially harmful perturbations (*64*)	Vulnerability involves multiple stressors across multiple temporal and spatial scales, and emerges from the interactions of social actors, the environment, and institutions (*65*). Thresholds of critical risks are dynamic in space and time and are rooted in historical structural causes [e.g., construction of wells during a severe drought in the Sahel interrupted herd movements, creating new vulnerabilities (*22*)]. [→P1, P3, P4]	Expansion of cropping into rangelands during wet periods changes system thresholds and often results in crises and environmental collapse when dry conditions return, e.g., the 1930s U.S. Dust Bowl (*66*) and "sandification" in China's Ordos Plateau (*31*). With adequate preparedness, early-warning systems can reduce the human toll of natural hazards and livelihood-based measures can reduce longer-term vulnerability [e.g., community adaptation to drought in Kordofan, Sudan (*67*)]. [→P2, P3]
Poverty alleviation: Elucidates human welfare–land degradation relationships (*68*)	"Poverty trap" thresholds exist (*69*) from which it is difficult for individuals and households to extract themselves without outside intervention. Livelihood diversification, which is increasingly promoted in drylands, reduces dependence on highly variable natural resources (*2*). [→P2, P3]	Development schemes in drylands justified as alleviating poverty have often been driven by divergent, higher-level political or economic objectives [e.g., forced relocation of Ethiopian Highlands peoples after the 1980s famine (*70*)]. Low productivity often means that interregional flows of labor, capital, and skills (e.g., by migration to urban or more humid areas) are needed to sustain poverty reduction in drylands. [→P3, P4]
Community-driven development: Seeks to enlarge the role of local communities in policy and to strengthen local autonomy in governance (*71*)	"Top-down" development policies often contradict local practices and undermine sustainable development [e.g., conflicts between state and local perspectives on burning in Mali (*72*)]. Community-driven management, though more sensitive to local conditions and knowledge, is not a universal solution (*73*). [→P4, P5]	An increased role for local communities and land users is needed for win-win (environment-development) outcomes (*74*) requiring rights to participate and capacity-building initiatives. Proper engagement of local people (and local environmental knowledge) with scientists (and scientific knowledge) can contribute to sustainable management (*75*, *76*). [→P5]

human (e.g., demographic, economic, institutional) subsystems (*14*), complete with a history and geography, and are constantly changing in response to both external (e.g., climate, prices) and internal (e.g., feedbacks between soil nutrients and plant growth, a farmer's economic decisions regarding land use) drivers. An example of the coevolution of H-E systems is provided by Mortimore and Harris (*15*) for the Kano Close-Settled Zone in Nigeria, covering the period 1962 to 1996 (*16*). Given this scenario, approaches to development must simultaneously consider both biophysical and socioeconomic dimensions of the dryland system in question [key implication 1 (ki-1) in Table 2] (*17*). Trends in soil fertility or biodiversity, for example, must be linked to factors such as labor, settlement patterns, and livelihood system dynamics, and vice versa, with appropriate temporal and spatial definitions (*18*).

Principle 2. The critical dynamics of dryland systems are determined by "slow" variables, both biophysical and socioeconomic [as exemplified by the coevolution of the coupled H-E systems of Maradi, Niger (Box S1, supporting online text)]. Slow variables (e.g., soil fertility, household capital wealth) have lengthy turnover times and are thus useful for gaining insights into long-term H-E changes, resource collapses, potential surprises, and new opportunities (*19*). The vagaries of precipitation, pest outbreaks, and other strongly fluctuating variables characteristic of drylands tend to generate noise, making such "fast" variables with relatively rapid turnover times (e.g., crop yield, household disposable cash) poor indicators of land degradation or the need for intervention (*17*). Nevertheless, both research and human exploitation of resources are often based on relatively fast variables (*19*), which for drylands has confused the debate about strategic development needs (*20*, *21*).

Given the complex, multivariate structure of H-E systems, it is important to recognize that not all variables carry equal weight (*17*). It is often possible to identify combinations of interrelated variables that can be grouped together as syndromes of degradation (*22*), thus simplifying analysis and intervention (ki-2, Table 2) (*23*).

Principle 3. Slow variables possess thresholds that, if crossed, cause the system to move into a new state or condition. The importance of thresholds is widely recognized in both the ecological and socioeconomic literature (*24*) and, although this usually focuses on one, dominant "shift," Kinzig *et al.* (*25*) show that most regional-scale systems have a number of actual or potential regime shifts, in different domains (ecological, social, economic) and at different scales, such that one shift may trigger or preclude others. Thresholds may vary as a function of internal dynamics at other scales, and in some instances can be deliberately altered. For example, the provision of piped water or solar cookers in remote villages can dramatically alter the income threshold at which women have spare time to invest in small business or education by reducing the time taken to collect water or fuel (*26*).

Table 2. Principles of the Drylands Development Paradigm, with a brief overview of their importance vis-à-vis the five main components of the dryland syndrome (ds-1 to ds-5, see text) and their implications for research, management, and policy. [Based on Stafford Smith and Reynolds (*77*)] H-E, human-environmental systems; LEK, local environmental knowledge.

Principles	Why important in drylands	Links to dryland syndrome (ds-1 to ds-5)	Key implications (ki) for research, management, and policy
P1: H-E systems are coupled, dynamic, and coadapting, so that their structure, function, and interrelationships change over time.	The close dependency of most drylands livelihoods on the environment imposes a greater cost if the coupling becomes dysfunctional; variability caused by biophysical factors as well as markets and policy processes, which are generally beyond local control, means that tracking the evolving changes and their functionality is relatively harder and more important in drylands.	ds-1: variability; ds-4: remoteness	ki-1: Understanding dryland desertification and development issues always requires the simultaneous consideration of both human and ecological drivers, and the recognition that there is no static equilibrium "to aim for."
P2: A limited suite of "slow" variables are critical determinants of H-E system dynamics.	Identifying and monitoring the key slow H and E variables is particularly important in drylands because high variability in "fast" variables masks fundamental change indicated by slow variables.	ds-1: variability	ki-2: A limited suite of critical processes and variables at any scale makes a complex problem tractable.
P3: Thresholds in key slow variables define different states of H-E systems, often with different controlling processes; thresholds may change over time.	Thresholds particularly matter in drylands because the capacity to invest in recovering from the impacts of crossing undesirable thresholds is usually lower per unit (area of land, person, etc); and, where outside agencies must be called upon, the transaction costs of doing so to distant policy centers are usually higher.	ds-1: variability; ds-2: low productivity; ds-4: remoteness; ds-5: distant voice	ki-3: The costs of intervention rise nonlinearly with increasing land degradation or the degree of socioeconomic dysfunction; yet high variability means great uncertainty in detecting thresholds, implying that managers should invoke the precautionary principle.
P4: Coupled H-E systems are hierarchical, nested, and networked across multiple scales.	Drylands are often more distant from economic and policy centers, with weak linkages; additionally, regions with sparse populations may have qualitatively different hierarchical relationships between levels.	ds-3: sparse population ds-4: remoteness; ds-5: distant voice;	ki-4: H-E systems must be managed at the appropriate scale; cross-scale linkages are important in this, but are often remote and weak in drylands, requiring special institutional attention.
P5: The maintenance of a body of up-to-date LEK is key to functional coadaptation of H-E systems.	Support for LEK is critical in drylands because experiential learning is slower where monitoring feedback is harder to obtain (owing to more variable systems, larger management units, in sparsely populated areas) and, secondarily, where there is relatively less research.	ds-1: variability; ds-3: sparse population	ki-5: The development of appropriate hybrid scientific and LEK must be accelerated both for local management and regional policy.

As an H-E system moves further from some desirable condition or state, the cost of intervention to "return" the system to that condition also increases. Sudden changes or nonlinearities associated with thresholds (e.g., run-off from overland flow to gullies; labor withdrawn due to war or out-migration) tend to amplify the costs of intervention (ki-3, Table 2). In impoverished drylands, these costs are further exacerbated by economic limits to local investment capacity, thus triggering the call for external resources that further increase transaction costs in remote areas [examples in (*17*, *27*)] (*28*).

Principle 4. The involvement of multiple stakeholders, with highly differing objectives and perspectives, illustrates the need to pay attention to the multilevel, nested, and networked nature of H-E systems. Operating hierarchically and across scales, linkages between stakeholders embed the system in question within others (*10*, *29*). Such scale issues are especially important in drylands because so many of them are sparsely occupied and remote, e.g., from city-based agencies or company headquarters, which weakens political and economic empowerment (*30*). In addition, slow variables at one scale of interest are affected by slow and fast variables operating at other scales, such that interventions at one scale generally alter the system at the next [e.g., (*31*)].

However, not every problem need be viewed as encompassing all scales of concern. Berkes and Jolly (*32*), for example, argue that short-term coping mechanisms are displayed at the household and individual scales, whereas long-term adaptive strategies, such as change in cultural values, are expressed at broader scales. In general, intervention on, and management of, a particular process must occur at the appropriate scale (ki-4, Table 2). For example, inasmuch as management is affected by institutions (rules of governance), the two should be scale-matched (*33*).

Principle 5. The key to maintaining functional coadaptation of coupled H-E systems is an up-to-date body of "hybrid" environmental knowledge that integrates local management and policy experience with science-based knowledge, all of which must be mediated through an effective institutional framework. Local environmental knowledge, which encompasses a wide range of activities, may develop rapidly or over generations (*34*) and has served long-persisting groups well [e.g., native Americans (*35*)].

In the modern world, however, the traditional role of LEK is threatened by rapid changes in both biophysical (e.g., exotic-species introductions, shifts in climate) and socioeconomic (e.g., population growth, changing technologies, new economic demands) drivers. Furthermore, in the variable environments of drylands, especially those subject to climate change, acquiring new LEK through learning from experience is particularly slow, so identifying new alliances of local and science-based knowledge systems to speed up this acquisition is particularly important (*27*) (ki-5, Table 2). Examples of the products of such alliances include local climate forecasts (*36*) and soil classifications (*37*).

Application of the DDP

The DDP serves two purposes: One is conceptual, providing a holistic synthesis of the disparate lessons drawn from previous work on desertification and development (Table 1) in the setting of the unique features of drylands (the dryland syndrome); the other is practical, providing a template whereby each of the five principles (Table 2) can be thoroughly examined and tested in case studies.

Other complex, integrated approaches to environment and development issues that have been entertained in the past, such as farming systems research [e.g., (*38*, *39*)], have faced the genuine difficulties that researchers, managers, and policy-makers have with tackling complexity. To address the global problem of desertification realistically, an integrative approach is required, not only because of synergy between elements of coupled H-E systems (*14*), but also because programmatic and policy concerns about each have implications that often conflict if treated individually (*21*). The real challenge that the DDP aims to satisfy is to develop efficient and effective approaches to understanding complex H-E interactions in drylands, while respecting and recognizing the capacity of local communities and policy-makers to deal with their complexity.

The DDP is being tested by the ARID*net* network (*40*) with interdisciplinary workshops of 15 to 25 participants. To date, ARID*net* workshops have addressed local questions of land degradation in rural, dryland H-E systems in Bolivia, Mexico (*41*) (Box S3), and Honduras (*42*). The DDP is most effective when conceptualizing and framing local issues, and their potential solutions, because it is open to the many different lenses through which dryland use and development are viewed by multiple stakeholders. In these workshops, the implementation phase was found to be most challenging, requiring that all stakeholders jointly work through the DDP principles, agreeing on the specific implications of each. The Mexican and Honduran case studies revealed that it is necessary to allow people to explore problems in their own words and gradually work specific issues into the DDP framework.

Dryland development issues occur also in more developed countries. In Australia, for example, the Desert Knowledge initiative (*43*) seeks sustainable livelihoods and viable desert settlements, and in the United States, the Central Arizona–Phoenix Long Term Ecological Research project (*44*) seeks to understand the relation between land-use decisions and ecological consequences. These projects share the long-term goal of improving dryland ecosystems and regional economies and, building on DDP-like analyses, seek economic livelihoods that may emerge from sustainable use of dryland environments yet reach out successfully to markets beyond these regions.

The DDP does not purport to represent an exhaustive set of programs, tools, and approaches for dryland development. In fact, in recent years there has been substantial improvement in the suite of toolsets available to the policy, management, and research communities concerned with dryland development [e.g., (*2*, *45*–*49*)]. Rather, the DDP serves as an analytical framework through which specific problems may be identified and opportunities implemented with greater insight. We are confident that further application and testing of the DDP through case studies will lead to continued refinement of a parsimonious set of theoretical, systems-oriented principles for analyzing dryland development issues in any particular region of the world, to the betterment of the 2.5 billion people who live in drylands globally.

References and Notes

1. GLP, Global Land Project—Science Plan and Implementation Strategy" [IGBP (International Geosphere Biosphere Program) Report No. 53/International Human Dimensions Programme Report No. 19, IGBP Secretariat, Stockholm, 2005]; www.globallandproject.org/documents.shtml.
2. MEA, *Millennium Ecosystem Assessment—Ecosystems and Human Well-Being: Desertification Synthesis* (World Resources Institute, Washington, DC, 2005).
3. UNCCD, United Nations Convention to Combat Desertification, Elaboration of an International Convention to Combat Desertification in Countries Experiencing Serious Drought and/or Desertification, Particularly in Africa" (U.N. Doc. A/AC.241/27, 33 I.L.M. 1328, United Nations, 1994).
4. The precise numbers of the dryland population affected by desertification is contentious (*50*), but 250 million is a widely cited approximation (*2*, *3*). For comparison, the Global Fund estimates annually 1 million deaths and 300 to 500 million new infections for malaria, 3 million deaths and 40 million new infections for AIDS/HIV, and 2 million deaths and 8 million new infections for tuberculosis (www.theglobalfund.org).
5. There has been extensive debate concerning definitions of desertification and degradation (*51*). Although the CCD definition is now formalized internationally, a summary of the debate is given in (*10*, *52*).
6. In a search of *Science* for July 1996 through June 2006, "climat* change" appears in 634 titles/abstracts, and "biodiversity" (or "biological diversity") appears in 211, whereas "desertification" (and biophysical forms of "degradation") appears in only 4. Meanwhile, the Convention on Climate Change occurs in 7 abstracts, the Convention on Biological Diversity occurs in 4, and the CCD appears in 1. Similar findings are true for *Nature*.
7. We suggest that in the past this has been exacerbated by a polarization of the research and practitioner communities over the phenomena and processes of study, including tensions between environmental and development agendas and conceptual differences between top-down, expert-driven managerial solutions and bottom-up, local knowledge and capacity-building approaches (*53*). Such polarizations and differences are now ameliorating.
8. We use H-E interactions to encompass a broad interpretation of the mutual interactions between and among human activities and natural-world processes—an emerging field of science that has evolved in response to the need to elucidate complex relationships between sustainable resource use by humans and their environment (*54*). Also termed "social-ecological

systems" by The Resilience Alliance (www.resalliance.org/1.php), H-E systems are more complex than the binary nature of these terms implies (*25*). Hence, developing a predictive understanding of them is a major challenge for modern science (*55*), a challenge that is particularly accentuated in drylands.

9. This represents a shift in attitude, from an emphasis on mainly negative aspects of desertification (drought, famines, poverty), to a more positive focus on alternative livelihoods and sustainability (*56*, *57*).
10. J. F. Reynolds, D. M. Stafford Smith, Eds., *Global Desertification: Do Humans Cause Deserts?* (Dahlem Workshop Report 88, Dahlem Univ. Press, Berlin, 2002).
11. S. Khagram, W. C. Clark, D. F. Raad, *J. Hum. Dev.* **4**, 289 (2003).
12. N. J. Middleton, D. S. G. Thomas, Eds., *World Atlas of Desertification* (U.N. Environment Programme, Edward Arnold, New York, ed. 2, 1997).
13. L. Gillson, M. T. Hoffman, *Science* **315**, 53 (2007).
14. K. A. Galvin, P. K. Thornton, J. R. de Pinho, J. Sunderland, R. B. Boone, *Hum. Ecol.* **34**, 155 (2006).
15. M. Mortimore, F. Harris, *Land Use Policy* **22**, 43 (2005).
16. In a sandy dryland area of ~2500 km^2 around Kano, Nigeria, changes in a H-E system from the 1960s to the 1990s were driven by a 25% decline in average annual rainfall and by an increase in rural population densities from 140 to >220 km^2.
17. R. Fernández *et al.*, in *Global Desertification: Do Humans Cause Deserts?*, J. F. Reynolds, D. M. Stafford Smith, Eds. (Dahlem Univ. Press, Berlin, 2002), pp. 297–323.
18. A. Warren, S. Batterbury, H. Osbahr, *Global Environ. Change* **11**, 79 (2001).
19. S. R. Carpenter, M. G. Turner, *Ecosystems* **3**, 495 (2000).
20. D. Schroter *et al.*, *Science* **310**, 1333 (2005).
21. B. L. Turner II, *Geogr. J.* **163**, 133 (1997).
22. T. E. Downing, M. Lüdeke, in *Global Desertification: Do Humans Cause Deserts?*, J. F. Reynolds, D. M. Stafford Smith, Eds. (Dahlem Univ. Press, Berlin, 2002), pp. 233–252.
23. H. J. Geist, E. F. Lambin, *Bioscience* **54**, 817 (2004).
24. B. Walker, J. A. Meyers, *Ecol. Soc.* **9**, 3 (2004); www.ecologyandsociety.org/vol9/iss2/art3.
25. A. Kinzig *et al.*, *Ecol. Soc.* **11**, 20 (2006); www.ecologyandsociety.org/vol11/iss1/art20/.
26. C. A. Sullivan, *World Dev.* **30**, 1195 (2002).
27. P. F. Robbins *et al.*, in *Global Desertification: Do Humans Cause Deserts?*, J. F. Reynolds, D. M. Stafford Smith, Eds. (Dahlem Univ. Press, Berlin, 2002), pp. 325–355.
28. In wealthy economies, there are enough resources for technological-managerial intervention to compensate for declines in critical variables of the H-E system (e.g., through large-scale water transport) or to shift the entire dryland-use system (e.g., suburban expansion of the American Sunbelt) (*58*).
29. L. H. Gunderson, C. S. Holling, Eds., *Panarchy: Understanding Transformations in Human and Natural Systems* (Island Press, Washington, DC, 2002).
30. S. Batterbury *et al.*, in *Global Desertification: Do Humans Cause Deserts?*, J. F. Reynolds, D. M. Stafford Smith, Eds. (Dahlem Univ. Press, Berlin, 2002), pp. 357–385.
31. H. Jiang, in *Global Desertification: Do Humans Cause Deserts?*, J. F. Reynolds, D. M. Stafford Smith, Eds. (Dahlem Univ. Press, Berlin, 2002), pp. 181–196.
32. F. Berkes, D. Jolly, *Conserv. Ecol.* **5**, 18 (2001); www.consecol.org/vol5/iss2/art18.
33. E. Ostrom, J. Burger, C. B. Field, R. B. Norgaard, D. Policansky, *Science* **284**, 278 (1999).
34. N. J. Turner, M. B. Ignace, R. Ignace, *Ecol. Appl.* **10**, 1275 (2000).
35. G. P. Nabhan, *Ecol. Appl.* **10**, 1288 (2000).
36. C. J. Stigter, Z. Dawei, L. O. Z. Onyewotu, M. Xurong, *Clim. Change* **70**, 255 (2005).
37. E. Barrios *et al.*, *Geoderma* **135**, 248 (2006).
38. M. Tengo, K. Belfrage, *Ecol. Soc.* **9**, 4 (2004); www.ecologyandsociety.org/vol9/iss3/art4.
39. A. M. Ridley, P. M. Mele, C. R. Beverly, *Soil Biol. Biochem.* **36**, 1213 (2004).
40. ARID*net* is an international network (Box S2) established to conduct case studies of dryland H-E systems, the goal of which is to facilitate field-level interactions between researchers, local stakeholders (farmers, landowners, developers), and decision-makers.
41. E. Huber-Sannwald, F. T. Maestre, J. E. Herrick, J. F. Reynolds, *Hydrol. Process.* **20**, 3395 (2006).
42. Millions of rural poor in the subhumid and semi-arid regions of Guatemala, Honduras, Nicaragua, and El Salvador face severe food deficits and poor opportunities for generating income to improve their livelihoods. The Quesungual Slash and Mulch Agroforestry System (QAS) was developed as a development strategy to improve rural livelihoods in the Lempira Department, Honduras, and has now been adopted by more than 6000 farmer households. This alternative to slash-and-burn agriculture builds strongly on local knowledge to deliver a doubling in crop yields and cattle-stocking rates and considerable reduction in costs associated with agrochemicals and labor, as well as much improved resilience to droughts and cyclones thanks to enhanced landscape water-holding characteristics. To examine the QAS in the context of the DDP framework, an ARID*net* workshop (13 to 20 November 2005)—involving 20 natural and social scientists working in conjunction with local communities and decision-makers—conducted a systematic analysis of long-term sustainability in the Candelaria region of Lempira. An analysis of findings showed that increased rates of soil erosion associated with inappropriate management practices in southern Honduras and northern Nicaragua can push these hillside agroecosystems across hydrologic thresholds (principle 3 in Table 2, i.e., P3; P1 to P5 and ki-1 to ki-5 refer to principles 1 to 5 and key implications 1 to 5, respectively, in Table 2) when coarse-textured surface horizons are lost. Intervention costs rise nonlinearly (ki-3) for both biophysical (soil profile development) and socioeconomic reasons (more-motivated farmers emigrate in early stages of yield decline) (P1, ki-1). The QAS, based on local environmental knowledge (P5), effectively addresses the key slow biophysical variables (soil depth and forest cover) by increasing the stability over time of the fast biophysical (soil moisture availability) and socioeconomic variables (income is diversified with fuelwood and tree-crop production) (P2). The system is supported by an extensive set of government and nongovernment relationships at multiple levels (P4, ki-4). The DDP analysis, and the development of related conceptual models, helped workshop participants identify the key factors and processes addressed by the QAS (P5). For another example, from Mexico, see Box S3.
43. P. Wand, M. Stafford Smith, in Proceedings of the Australian Rangelands Society 13th Bienniel Conference, Alice Springs, 5 to 8 July 2004 (Australian Rangelands Society, Adelaide, 2004), pp. 15–22.
44. N. B. Grimm, C. L. Redman, *Urban Ecosyst.* **7**, 199 (2005).
45. G. Mansuri, V. Rao, *World Bank Res. Obs.* **19**, 1 (2004).
46. B. Campbell, J. Hagmann, A. Stroud, R. Thomas, E. Wollenberg, *Navigating Amidst Complexity: Guide to Manage R&D Interventions for Improving Livelihoods and the Environment* (Center for International Forestry Research, Bogor, Indonesia, 2006).
47. S. Gillespie, "Scaling Up Community-Driven Development: A Synthesis of Experience" (Discussion Paper No. 181, International Food Policy Research Institute, Washington, DC, 2004).
48. M. Winslow, B. I. Shapiro, R. Thomas, S. V. R. Shetty, "Desertification, Drought, Poverty and Agriculture: Research Lessons and Opportunities" [Joint publication: International Center for Agricultural Research in the Dry Areas (ICARDA), the International Crops Research Institute for the Semi-Arid Tropics (ICRISAT), and the United Nations Convention to Combat Desertification's (UNCCD) Global Mechanism, Rome, Italy, 2004].
49. R. Thomas *et al.*, in *Combating Desertification: Sustainable Management of Marginal Drylands (SUMAMAD)* (UNESCO, Paris, Shiraz, Iran, 2004), pp. 80–93.
50. P. Dobie, "Poverty and the Drylands," The United Nations Development Programme, Office to Combat Desertification and Drought (2001).
51. D. S. G. Thomas, *J. Arid Environ.* **37**, 599 (1997).
52. J. F. Reynolds, in *Encyclopedia of Biodiversity*, S. Levin, Ed. (Academic Press, San Diego, CA, 2001), vol. 2, pp. 61–78.
53. S. M. Herrmann, C. F. Hutchinson, *J. Arid Environ.* **63**, 538 (2005).
54. T. Dietz, E. Ostrom, P. C. Stern, *Science* **302**, 1907 (2003).
55. V. Grimm *et al.*, *Science* **310**, 987 (2005).
56. U.N. Environment Programme, "Deserts and Drylands," *Our Planet* 17, no. 1 (2006); www.ourplanet.com/.
57. Niamey Declaration, "From Desert to Oasis" Workshop, Niamey, Niger (September 2006); www.oasisglobal.net/symposium_files/declaration.html.
58. J. X. Kasperson, R. E. Kasperson, B. L. Turner II, *Regions at Risk: Comparisons of Threatened Environments*, UNU Studies on Critical Environmental Regions (United Nations Univ. Press, Tokyo, 1995).
59. W. H. Schlesinger *et al.*, *Science* **247**, 1043 (1990).
60. A. Warren, *Trans. Inst. Br. Geogr.* **20**, 193 (1995).
61. P. Hiernaux, M. D. Turner, in *Global Desertification: Do Humans Cause Deserts?*, J. F. Reynolds, D. M. Stafford Smith, Eds. (Dahlem Univ. Press, Berlin, 2002), pp. 135–148.
62. J. Puigdefábregas, *Land Degrad. Dev.* **9**, 393 (1998).
63. F. T. Maestre, J. F. Reynolds, E. Huber-Sannwald, J. Herrick, D. M. Stafford Smith, in *Dryland Ecohydrology*, P. D'Odorico, A. Porporato, Eds. (Kluwer, Dordrecht, Netherlands, 2006), pp. 315–332.
64. H. G. Bohle, T. E. Downing, M. J. Watts, *Global Environ. Change* **4**, 37 (1994).
65. B. L. Turner II *et al.*, *Proc. Natl. Acad. Sci. U.S.A.* **100**, 8074 (2003).
66. M. H. Glantz, N. S. Orlovsky, *Desertificat. Control Bull.* **9**, 15 (1983).
67. T. E. Downing, *die Erde* **133**, 363 (2002).
68. M. Leach, R. Mearns, Eds., *The Lie of the Land: Challenging Received Wisdom on the African Environment* (Heinemann, Portsmouth, NH, 1996).
69. J. D. Sachs *et al.*, in *Brookings Papers on Economic Activity 1*, W. C. Brainard, G. L. Perry, Eds. (Brookings Institution, Washington, DC, 2004), pp. 117–240.
70. H. Kloos, A. Aynalem, *GeoJournal* **19**, 113 (1989).
71. S. Alkire *et al.*, in *PRSP (Poverty Reduction Strategy Papers) Source Book*, J. Klugman, Ed. (World Bank, Washington, DC, 2002), pp. 301–332.
72. P. Laris, *Hum. Ecol.* **30**, 155 (2002).
73. M. B. Lane, G. McDonald, *J. Environ. Plan. Manage.* **48**, 709 (2005).
74. C. Reij, I. Scoones, C. Toulmin, Eds., *Sustaining the Soil: Indigenous Soil and Water Conservation in Africa* (Earthscan Publications, London, 1996).
75. G. Gilchrist, M. Mallory, F. Merkel, *Ecol. Soc.* **10**, 20 (2005); www.ecologyandsociety.org/vol10/iss1/art20.
76. M. D. Turner, P. Hiernaux, *Landscape Ecol.* **17**, 367 (2002).
77. D. M. Stafford Smith, J. F. Reynolds, in *Global Desertification: Do Humans Cause Deserts?*, J. F. Reynolds, D. M. Stafford Smith, Eds. (Dahlem Workshop Report 88, Dahlem Univ. Press, Berlin, 2002), pp. 403–424.
78. We acknowledge the participants and support staff of the 88th Dahlem workshop (Berlin, 2001), especially the contributions of N. Abel, P. Hiernaux, and C. Vogel to the concepts presented here. We thank L. Hein, I. M. Rao, D. Walker, R. Virginia, C. Vogel, and R. Thomas for critical reviews. D.M.S.S. is supported by the Australian Government Cooperative Research Centres Programme through the Desert Knowledge CRC and by CSIRO. J.F.R. is supported by research award Humboldt-Forschungspreis (Humboldt Foundation, Bonn) and the Department of Plant Ecology (University of Bayreuth). ARID*net* is funded by the U.S. NSF, Research Coordination Networks (grant 0234186).

Supporting Online Material

www.sciencemag.org/cgi/content/full/316/5826/847/DC1
Boxes S1 to S3

10.1126/science.1131634

Imaging of Single Organic Molecules in Motion

Masanori Koshino,[1,2] Takatsugu Tanaka,[3] Niclas Solin,[3] Kazutomo Suenaga,[1,2]* Hiroyuki Isobe,[3,4]*† Eiichi Nakamura[1,3]*

Progress in fluorescent imaging has afforded remarkably specific views of the structural dynamics of single large biomolecules (*1*). However, translating such advances to the scale of small-molecule chemistry has proven challenging. For organic compounds, spectroscopic and diffractive techniques have recently furnished detailed time-resolved pictures of structural evolution averaged over large ensembles (*2*). In principle, if small molecules could be confined within an adequate field of view, transmission electron microscopy (TEM) would offer sufficient resolving power to measure three-dimensional structural dynamics at the single-molecule level. However, the assumed high sensitivity of hydrocarbons to damage by electron impact has discouraged previous exploration of this method (*3*–*5*). We report herein the observation, with near-atomic resolution, by TEM of a single small organic molecule either at rest or translating within a single-wall carbon nanotube (CNT).

We chose for this proof-of-principle study molecules **1** to **4**, containing hydrocarbon chains covalently attached to an *ortho*-carborane end group [Fig. 1A; $C_2B_{10}H_{12}$, circa (ca.)-0.8-nm diameter], which serves as a tag for identification by its characteristic shape.

As the molecular container, we chose a mixture of CNTs with diameters of 0.9 to 1.2 nm, from which we could combinatorially investigate size matching between the host and the guest. The guest molecules were introduced by vaporization at 160°C in vacuum into CNTs that had been oxidatively perforated. Room-temperature TEM (120 kV, 2.4 Å resolution) was applied with 0.5-s electron irradiation imaging intervals, followed by 1.6-s periods of charge-coupled device data readout time.

The single-chain molecule **1** in 0.9-nm-diameter CNTs was entirely immobilized, and its head and tail structure was clearly visualized (Fig. 1B and fig. S1). Comparison of the experimental images [1.6 ± 0.1 (SD) nm length] with simulation (1.7 nm) indicated that the hydrocarbon chain adopts a fully stretched conformation (Fig. 1, C and D). The measured image contrast between the head and tail structures was 1:1.05 ± 0.27 (SD) (Fig. 1E), which agrees very well with the 1.04 value obtained by simulation (fig. S1). Electron energy loss spectroscopy (EELS) analysis supported the presence of carborane (fig. S2). Molecules **2**, **3**, and **4** in narrow CNTs were identified in a similar manner (fig. S1).

Molecules **2** and **4** may be trapped in ca.-1.2-nm-diameter CNTs, because one of their hydrocarbon tails appears to stick to the CNT wall (e.g., the tail of **2** sticks at the position shown by the red arrow in Fig. 1F) and serves as a hinge for the thermal motion of the intertwined hydrocarbon chains. The sticking phenomenon is probably due to interaction of the chain terminus with a defective area, such as a hole or an oxidized portion of the CNT wall. Molecule **4** in Fig. 1G (models in Fig. 1, H and I; figs. S4 and S5; and movies S1 and S2) changed its conformation in a stepping manner from one conformation (e.g., at 0 s) to another (6.3 s) twice during the first 20 s and then shifted to further different conformations afterward (33.6 s). Molecules loosely trapped in ca.-1.2-nm-diameter CNTs translated back and forth without changing their molecular orientations but with frequent stepwise speed changes from 0 (i.e., sticking) to over 10 nm/s (figs. S6 and S7 and movie S3). The sticking may be reversible (movie S3). These results highlight the unanticipated utility of TEM for single-molecule chemical analysis relevant to fundamental reactivity as well as to engineering applications, such as tribology and gas absorption and storage in activated carbon.

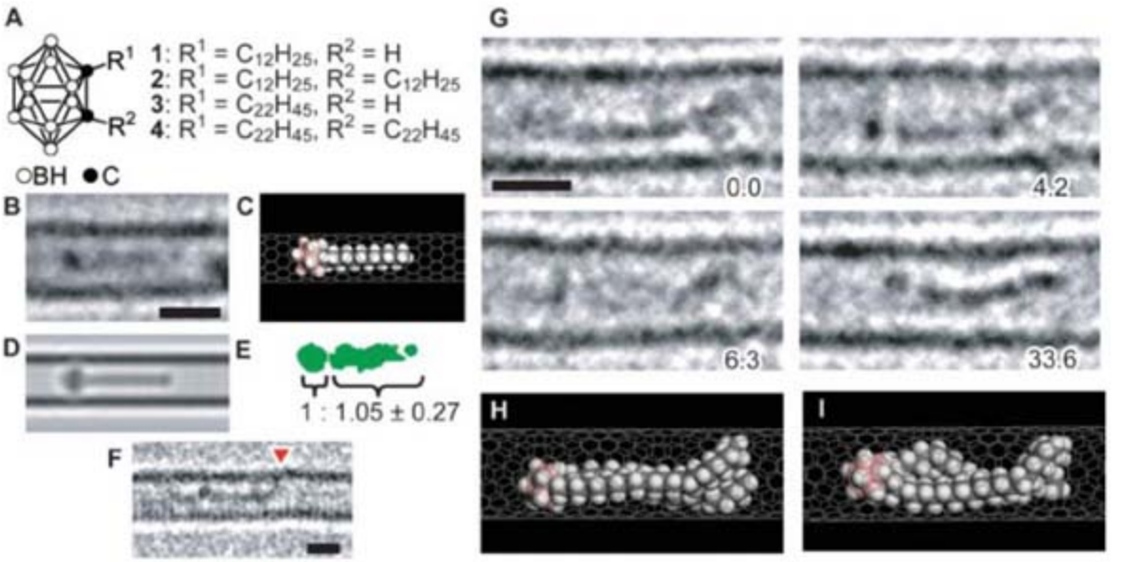

Fig. 1. (**A**) Molecules **1** to **4**. (**B**) TEM image of **1** in a CNT. Scale bars indicate 1 nm. (**C** and **D**) Model of **1** in CNT and simulation of its micrograph. Hydrogen, white; boron, pink; and carbon, gray. (**E**) Molecular image and digitized image contrast ratio of **1** obtained by subtracting the background contrast from (B). (**F**) TEM image of **2** sticking to a tube defect indicated by a red arrow (movie S3). (**G**) Experimental images of the intertwined hydrocarbon chains of **4** at consecutive times in seconds. (**H** and **I**) Models of **4** at 4.2 s and 6.3 s, respectively.

References and Notes

1. Special issue on Biological Imaging, S. M. Hurtley, L. Helmuth, Eds., *Science* **300** (4 April 2003).
2. J. Zheng, K. Kwak, J. Xie, M. D. Fayer, *Science* **313**, 1951 (2006).
3. R. F. Egerton, P. Li, M. Malac, *Micron* **35**, 399 (2004).
4. Z. Liu *et al.*, *Phys. Rev. Lett.* **96**, 088304 (2006).
5. R. M. Smith, *Understanding Mass Spectra* (Wiley, Hoboken, NJ, ed. 2, 2005).

6. This work was partially supported by Kakenhi (Houga, 18655012) and the Center of Excellence (COE) program provided by the Ministry of Education, Culture, Sports, Science, and Technology. We thank K. Yamanouchi for helpful discussion. N.S. thanks the Knut och Alice Wallenbergs stiftelse (Stockholm, Sweden) for a postdoctoral fellowship.

Supporting Online Material

www.sciencemag.org/cgi/content/full/1138690/DC1
Materials and Methods
Figs. S1 to S7
Movies S1 to S3

11 December 2006; accepted 8 February 2007
Published online 22 February 2007;
10.1126/science.1138690
Include this information when citing this paper

[1]Exploratory Research for Advanced Technology (ERATO), Nakamura Functional Carbon Cluster Project, Japan Science and Technology Agency (JST), Hongo, Bunkyo-ku, Tokyo 113-0033, Japan. [2]Research Center for Advanced Carbon Materials, National Institute of Advanced Industrial Science and Technology (AIST), Higashi, Tsukuba, Ibaraki 305-8565, Japan. [3]Department of Chemistry, University of Tokyo, Hongo, Bunkyo-ku, Tokyo 113-0033, Japan. [4]Precursory Research for Embryonic Science and Technology (PRESTO), JST, Hongo, Bunkyo-ku, Tokyo 113-0033, Japan.

*To whom correspondence should be addressed. E-mail: suenaga-kazu@aist.go.jp (K.S.); isobe@mail.tains.tohoku.ac.jp (H.I.); nakamura@chem.s.u-tokyo.ac.jp (E.N.)
†Present address: Department of Chemistry, Tohoku University, Aoba-ku, Sendai 980-8578, Japan.

You could be next

Yes, it *can* happen to you:
If you're a young scientist making inroads in neurobiology research, the next Eppendorf and *Science* Prize for Neurobiology could be yours!

This annual research prize recognizes accomplishments in neurobiology research based on methods of molecular and cell biology. The winner and finalists are selected by a committee of independent scientists, chaired by the Editor-in-Chief of *Science*. Past winners include post-doctoral scholars and assistant professors.

To be eligible, you must be 35 years of age or younger. If you're selected as this year's winner, you will receive $25,000, have your work published in the prestigious journal *Science* and be invited to visit Eppendorf in Hamburg, Germany.

Get recognized!
Deadline for entries:
June 15, 2007

www.eppendorf.com/prize
www.eppendorfscienceprize.org

$25,000 Prize

"I feel incredibly honored to receive this prestigious prize."

2006 Winner
Doris Tsao, Ph.D.
Institute for Brain Research
University of Bremen
Germany

eppendorf
& Science
PRIZE FOR
NEUROBIOLOGY

Pervasive Seismic Wave Reflectivity and Metasomatism of the Tonga Mantle Wedge

Yingcai Zheng,[1] Thorne Lay,[1]* Megan P. Flanagan,[2] Quentin Williams[1]

Subduction zones play critical roles in the recycling of oceanic lithosphere and the generation of continental crust. Seismic imaging can reveal structures associated with key dynamic processes occurring in the upper-mantle wedge above the sinking oceanic slab. Three-dimensional images of reflecting interfaces throughout the upper-mantle wedge above the subducting Tonga slab were obtained by migration of teleseismic recordings of underside *P*- and *S*-wave reflections. Laterally continuous weak reflectors with tens of kilometers of topography were detected at depths near 90, 125, 200, 250, 300, 330, 390, 410, and 450 kilometers. *P*- and *S*-wave impedances decreased at the 330-kilometer and 450-kilometer reflectors, and *S*-wave impedance decreased near 200 kilometers in the vicinity of the slab and near 390 kilometers, just above the global 410-kilometer increase. The pervasive seismic reflectivity results from phase transitions and compositional zonation associated with extensive metasomatism involving slab-derived fluids rising through the wedge.

Dipping oceanic lithosphere sinks at subduction zones in a fundamental process of plate tectonics. The overlying mantle wedge becomes enriched in volatiles released from the descending slab, undergoes localized partial melting and ascent of magmas to produce island or continental arcs, and experiences both slab-parallel and slab-perpendicular shear flows, often with back-arc spreading due to the seaward migration of the trench (*1*). Characterizing the structure and processes located in the mantle wedge is essential for understanding the formation of continental crust, evolution of back-arc basins, and volatile circulation in the mantle (*1*, *2*).

For the past 40 million years, the Pacific plate has been sinking at the Tonga subduction zone, the northern portion of which has the highest known rate of interplate convergence due to a combination of fast Pacific plate motion and rapid back-arc spreading of the Lau Basin (*3*). The number of intermediate- and deep-focus earthquakes in the Tonga slab is higher than in other subduction zones, and the seismicity reveals slab buckling and contortions caused by resistance to sinking near the global 660-km-deep seismic discontinuity, accentuated by interactions with lower-mantle flow patterns (*4*). Seismicity also occurs outside of the Tonga slab at depths below 500 km, in what appear to be remnant slab pieces from earlier subduction zones with different geometries (*5*), resulting in a broad horizontal distribution of deep-focus earthquakes.

Investigations of the structure of the mantle wedge above the Tonga slab have mainly used sparse seismic instrument deployments along the island arc and across the Lau Basin to image volumetric *P*- and *S*-wave velocity variations (*6*, *7*), *P*-wave attenuation (*8*), upper-mantle *S*-wave velocity discontinuities inferred from converted wave analyses (*9*, *10*), and *S*-wave splitting patterns (*11*). The data coverage is limited, resolving structure only along a couple of two-dimensional (2D) profiles parallel and perpendicular to the arc. The mantle wedge appears to be structurally complex (requiring a 3D characterization) but, as is true for other island-arc regions, it is prohibitively expensive to deploy large numbers of portable seismic stations above the wedge. We developed a 3D model of *P*- and *S*-wave reflecting interfaces throughout the Tonga mantle wedge using signals from deep Tonga slab earthquakes recorded at teleseismic global seismic stations. The startling extent of seismic reflectivity that we discovered allowed us to place constraints on petrological and dynamical phenomena in the wedge.

Seismic data analysis. Seismic wave investigations tend to focus on either the "smooth" components of internal Earth structure (such as volumetric velocity heterogeneity), which are best resolved by seismic tomography, or the "rough" components (involving strong gradients or discontinuities in material properties), which are best resolved by the stacking of reflected or converted arrivals. Most mantle-wedge studies have addressed smooth components of the structure, revealing broad patterns associated with thermal heterogeneity in the slab and wedge (*12*), but some have resolved the reflectivity of limited locations or sections of mantle wedges (*9*, *10*, *13*, *14*). One strategy for detecting reflecting structures in the wedge involves the analysis of initially up-going energy from deep-focus events that reflects downward from the underside of mantle discontinuities to eventually be observed at teleseismic distances (Fig. 1). This geometry provides high lateral spatial resolution of structure near the source. This strategy has previously been applied to individual events (*15*–*18*), but we exploited the abundant, widespread deep seismicity beneath the Tonga mantle wedge and the global distribution of broadband seismographic stations operated by the Federation of Digital Seismic Networks, regional networks, and EarthScope Transportable Array to generalize it into a multiple-event true-amplitude 3D wavefield migration, stacking signals to determine reflector positions at depth. Essentially, we turned standard reflection imaging upside down, using deep sources and distant observations to image a gridded representation of the seismic reflectivity in the mantle wedge between the source depths and Earth's surface above them.

Basic processing steps (*19*) involved (i) deconvolution of the instrument responses; (ii) deconvolution of the stacked down-going *P*- or horizontally polarized *S*-wave (*SH*) displacement source wavelet from the waveform interval precursory to and including the up-going depth-phase surface reflections (*pP* and *sSH*, where *p* is the up-going *P* wave from the earthquake to the reflector and *s* is the up-going *S*-wave); and then (iii) convolution with Ricker wavelets that had central frequencies of 0.06 Hz (*P*) and 0.05 Hz (*SH*). Each signal was normalized by the strength of the reference *P* or *S* phase, reflected from Earth's surface above the source (*pP* or *sSH*) to eliminate variations in source strength. Corrections were made for path sampling, geometric spreading from the source to the reflector, and radiation-pattern variations between the path to the reflector and the reference phase. We constrained the illuminated region to be in the vicinity of the geometrical ray path to avoid large radiation-pattern corrections; this intrinsically favors the imaging of near-horizontal structures. The normalization of the images by illumination factors and the summing of local dip-angle domain images achieved stable amplitude-balanced migrations (*19*).

The imaging domain extended from 15°S to 25°S, 175°E to 185°E, and from the surface to a depth of 500 km, discretized in 0.1° latitude and longitude increments and 5-km depth increments. About 2300 vertical-component teleseismic *P*-wave seismograms from 85 deep (>400 km) earthquakes with magnitudes larger than 5.0 that occurred between 1988 and 2006 were used, with any signals having weak *pP* arrivals being excluded. Stations at epicentral ranges from 40°

[1]Department of Earth and Planetary Sciences, University of California, Santa Cruz, CA 95064, USA. [2]Energy and Environment Directorate, Institute of Geophysics and Planetary Physics (IGPP), Lawrence Livermore National Laboratory (LLNL), Livermore, CA 94551, USA.

*To whom correspondence should be addressed. E-mail: thorne@pmc.ucsc.edu

to 140° were used. About 3100 *SH*-wave seismograms from 99 deep earthquakes were used, excluding any signals with weak *sSH* arrivals.

The image domain above a given source is an expanding cone, with overlapping paths from multiple events providing the redundant sampling needed for stable migration (Fig. 2 and fig. S1). The distribution of teleseismic stations relative to the source region is non-uniform, with concentrations at azimuths to North America and to Eurasia. Thus, the imaging domain was not uniformly sampled, but the illumination-factor normalization balanced the migration images proportionately, although we applied a threshold so that regions of very limited path coverage were not overly enhanced.

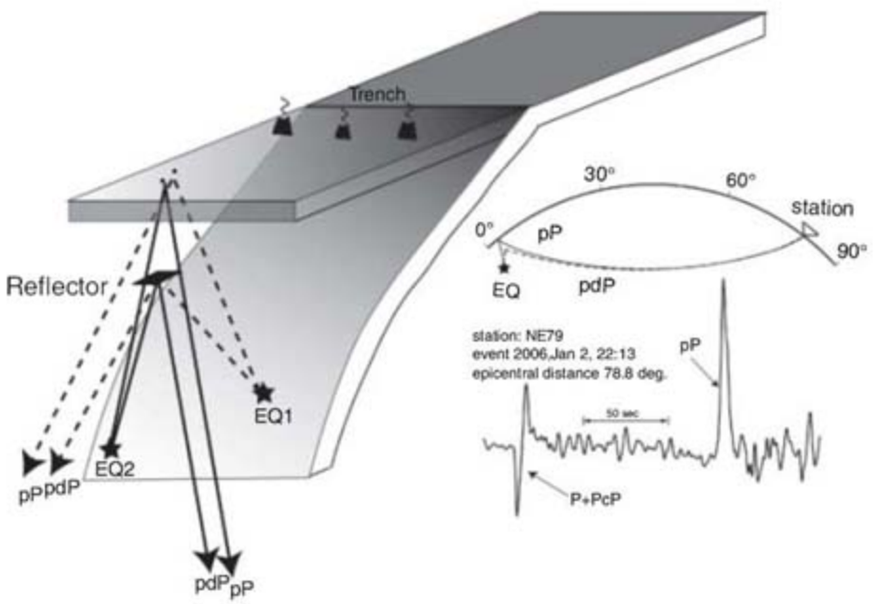

Fig. 1. Schematic of the Tonga mantle wedge imaging geometry. Deep-focus earthquakes within the subducted Pacific plate in the Tonga subduction zone radiate up-going energy that reflects from the underside of Earth's surface (*pP*) or the underside of velocity contrasts at depth *d* above the sources (p_dP) and then travels to teleseismic distances. The p_dP arrivals are precursors to the surface reflections. The inset shows ray paths for p_dP and *pP* to a teleseismic distance of 80°. Data from stations in the range from 40° to 140° were used for imaging the wedge. An example of a vertical-component seismogram is shown on the lower right, with energy between *P* and *pP* mainly caused by underside reflections, which arrive as precursors to *pP*. EQ, earthquake; *PcP*, down-going *P* wave that reflected from the core-mantle boundary.

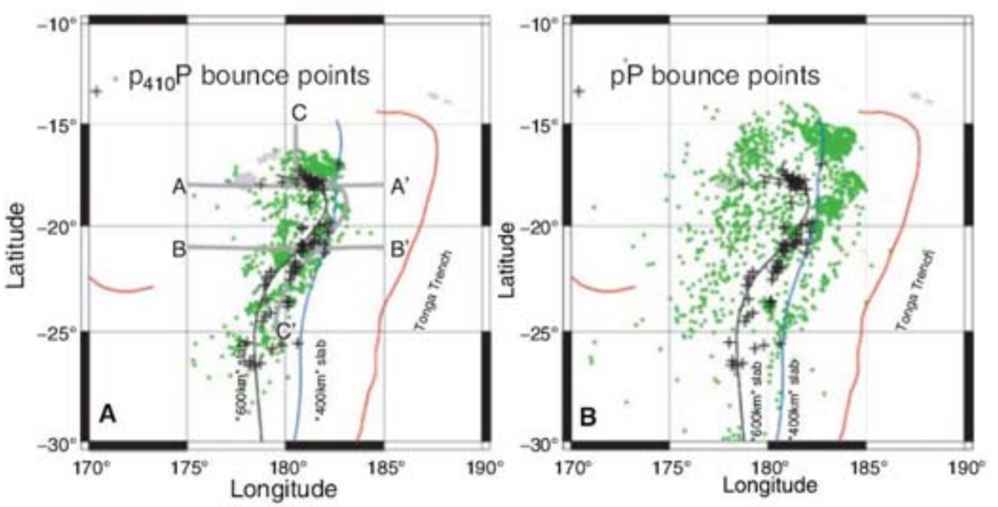

Fig. 2. Map showing earthquake locations (black crosses) and underside geometrical reflection points (green dots) (**A**) at 410 km, $p_{410}P$ and (**B**) at the free surface, *pP*. The positions of the Tonga and New Hebrides trenches are shown in red. The 400-km and 600-km depth contours for the top of the Tonga slab are indicated by the labeled blue and gray lines, respectively. The image volume expands upward toward the surface, with the *pP* surface-reflection points defining the maximum lateral extent of coverage. The locations of the vertical cross sections shown in Figs. 3 and 4 are indicated in (A).

Source depths were taken from a catalog of relocated hypocenters that includes depth phases (*20*) or, for events in 2006, from moment tensor inversions. Random perturbations of the source depths by up to 20 km did not have an important effect on the final migration images. The reference velocity model that we used for the inversions was the 1D model from the International Association of Seismology and Physics of the Earth's Interior (IASP91) (*21*). Minor distortions of the reflectors could occur because of neglect of the 3D volumetric velocity heterogeneity, but no high-resolution *P*- and *S*-wave tomographic models spanning the volume of our image are available for use in the migrations. This led us to emphasize frequencies below 0.1 Hz, so that travel-time decorrelation was not a problem (fig. S2). This bandwidth limited the resolution of the sharpness of the reflectors, but it also ensured that coherent signals stacked to give meaningful images (figs. S3 and S4). The use of multiple events with different focal mechanisms reduces down-going conversions and suppresses receiver-side effects to a great extent.

Confidence bounds on the images were established by performing 200 bootstrap iterations, retaining the same event distribution and total number of traces, while re-sampling the seismogram population. The final images shown are the averaged models, with the color hues saturated for highly resolved (97% confidence) features stronger than 3 SD above background and fading to white for poorly resolved features <1 SD above background (fig. S5).

***P* and *SH* reflectivity.** The migration yielded 3D reflectivity structures with associated variance estimates that are difficult to display in their entirety, so several 2D cross-sectional images are shown (Fig. 3 shows sections mainly along the trend of the Tonga slab; Fig. 4 shows east-west sections through the most densely sampled portions of the image volume, as depicted in Fig. 2). These images convey the primary aspects of the 3D structure (additional cross sections are presented in figs. S6 and S8 to S10). The color scale in Figs. 3 and 4 indicates the strength and sign of the reflected amplitude at each position, relative to the surface reflection, with color saturation decreasing proportional to the number of standard deviations above the noise level. Weak features that are likely to be artifacts are suppressed by this weighting (fig. S5). Because the reference phases were aligned to peak at the free surface, there is a (very saturated) blue stripe right at the surface, underlain by a broader red band that is an artifact caused by the side lobe of the Ricker wavelet. This negative side lobe has an amplitude that is ~40% of that of the positive surface-reflection peak, obscuring any reflectivity above 70 km, such as underside reflections from the crust-mantle boundary. The higher velocity of *P* waves causes the side lobe to broaden more in the *P* images than in the *SH* images. Weak side lobes are also ex-

pected to be present above and below strong arrivals at greater depths.

The reflectivity in the image volume is dominated by quasi-horizontal reflecting surfaces (steeply dipping interfaces, such as the upper boundary of the slab, could not be imaged because of a lack of stations at small epicentral distances), with strong blue features corresponding to *P*- or *SH*-impedance increases with increasing depth and strong red features corresponding to *P*- or *SH*-impedance decreases with increasing depth. Lateral disruptions of the reflectors at large depths occur in poorly sampled regions, underlain by few or no deep earthquakes, but spatial coverage expands upward from the deep sources, so that any lateral continuity is best resolved at shallower depths.

The immediate dominant attribute of the images is that there is extensive *P* and *SH* reflectivity in the Tonga mantle wedge, with extensive lateral continuity. The overall correlation coefficient between all of the *P* and *SH* images is low (with an absolute value of <0.13), but variable illumination and resolution of the structures must be considered. Some features correlate well, whereas others have the opposite sign or no correlation. Specifically, the *P*- and *SH*-wave images consistently show positive reflectors near depths from 75 to 100 km (we refer to this as the "90-km" feature), 300 km, and 410 km. Negative *P* and *SH* reflectors are seen near 330 and 450 km. In the eastern part of the wedge, a *P* reflector near 125 km is negative, but an *SH* reflector is positive. In addition, there is a positive *P* reflector near 200 km, accompanied by a weak positive *SH* reflector far away from the slab and a strong negative *SH* reflector near the slab. There is a patchy positive *P* reflector near 250 km with little *SH* reflectivity, and there is a negative *SH* reflector near 390 km with little *P* reflectivity. For both *P* and *SH* waves, the 410-km reflector becomes more shallow by tens of kilometers in the vicinity of the subducting slab (Fig. 4 and fig. S6). Other boundaries appear to have variable topography and lateral disruptions. In all cases, the apparent depths and apparent topography are probably biased by the use of a laterally homogeneous 1D background model for the migrations. Some other intermittent features are seen in the images, but we believe that our data set robustly resolves only the structures noted above.

Some of the reflectivity features in the Tonga wedge correspond to structures detected in other regions. The strong positive *SH* reflections and weak positive *P* reflections from near 90 km may represent the Hales discontinuity (*22*, *23*). The positive *P* reflector near 200 km may correspond to a feature commonly found under continental regions

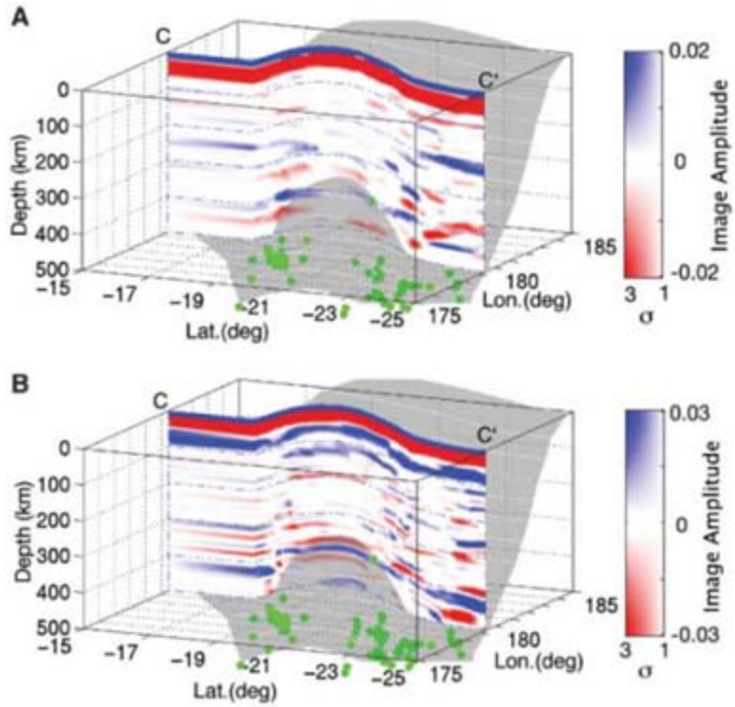

Fig. 3. (**A**) *P*-wave and (**B**) *SH*-wave profiles along vertical section C to C′ (Fig. 2) through the migration volumes. The period of the Ricker wavelet applied to the data is 16 s for *P* and 20 s for *SH*. Blue indicates positive impedance contrasts with increasing depth, whereas red indicates negative impedance contrasts with increasing depth. The color hues are saturated for features >3 SD (3σ) above the background level and fade to white for features <1 SD above the background. The strong blue and red stripes near the surface are the images of the *pP* and *sSH* surface reflections. The upper surface of the subducting Pacific plate is indicated by the gray facade. The deep-focus earthquake hypocenters are shown by green dots. Lat, latitude; Lon, longitude; deg, degrees.

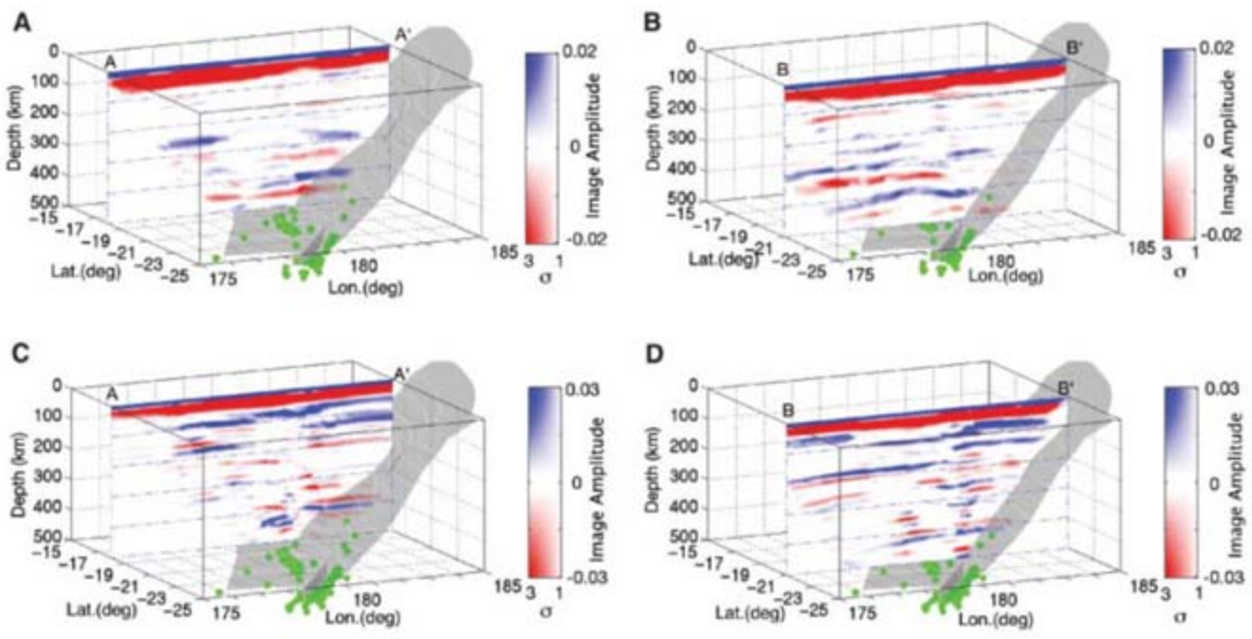

Fig. 4. Vertical west-east profiles in the (**A** and **B**) *P*-wave migration volume and (**C** and **D**) the *SH*-wave migration volume along profiles A to A′ (Fig. 2) at 18°S [(A) and (C)] and B to B′ at 21°S [(B) and (D)]. The period of the Ricker wavelet applied to the data is 16 s for *P* and 20 s for *SH*. Color scales correspond to those in Fig. 3. The strong blue and red stripes near the surface are the images of the *pP* and *sSH* surface reflections. The upper surface of the subducting Pacific plate is indicated by the gray facade. The deep-focus earthquake hypocenters are shown by green dots. The intermittence in the reflectors may be due to non-uniform ray path sampling. In many instances, the reflectors extend to the westward edge of our field of illumination.

(*22*, *24*, *25*) but also seen in back-arc (*23*) and oceanic (*26*) regions. The velocity increase near 300 km observed near 21°S (profile B to B′ in Fig. 4) has been seen in some back-arc and oceanic regions (*23*, *27*), and a weak increase near this depth has been reported along the Tonga arc (*22*) and in a 2D profile across our image volume near 18°S latitude (*10*). The sharp drop in velocity just above the 410-km increase that we find in *SH* images has been detected under continents (*28*, *29*). The 410-km increase is observed globally and regionally (*17*, *22*, *30*), and we consistently observe this in regions where the deep-focus events are concentrated and the up-going phases sample this depth range well.

Thermal and petrological interpretations. The notion of a simple homogeneous upper-mantle corner-flow regime dominated by temperature variations relative to the slab, as typically invoked in textbook cartoons of mantle-wedge processes, is clearly inadequate. The rough structure in the Tonga mantle wedge requires multiple reflecting contrasts in material properties in the wedge that need dynamical and petrological explanations. The bands of reflectivity in our images are not artifacts of wavelet side lobes or other processing effects, but they emerge from the extensive stacking of signals from different source depths and locations. Therefore, we believe they represent true structures, albeit ones that are possibly unique to this back-arc environment. Although corner flow and upwellings under the arc and back-arc basin must involve thermal heterogeneity, this reflectivity requires processes that sharpen the gradients in structure enough to reflect seismic waves, and this suggests petrological effects involving compositional differences, phase changes, partial melt, or anisotropic fabrics.

Standard Earth models predict relatively little upper-mantle reflectivity between 50 and 500 km: A velocity decrease is sometimes observed at the top of a low-velocity zone (the so-called Gutenberg discontinuity found near 65 km depth under oceanic regions), a 220-km velocity increase is primarily associated with continental regions, and the 410-km increase is typically interpreted as the olivine-to-wadsleyite (β-phase) transformation in $(Mg,Fe)_2SiO_4$. Relatively simple upper-mantle structures of this type are at odds with the observation of additional discontinuities in many regions (*22*, *23*, *31*).

The geochemical characteristics of the Lau Basin are notably complex and provide possible insights into the origin of some of the seismic layering in this region. In particular, both sediment-derived melts (*32*) and pervasive slab-derived fluids appear to have altered this region (*33*). When coupled with the observation that hydrous silica-rich melts may be critically important in the subarc mantle (*34*), the possible phase transitions and compositional zonation that might occur within a heavily metasomatized mantle emerge as potential explanations for the seismically layered Tonga mantle wedge. With the rapid eastward rollback of the trench in this region and the exposure of this region to subduction from the former Vitiaz slab (*5*), pervasive metasomatism is expected throughout the entire region of our study. Metasomatically associated mineralogic variations and transitions are thus consistent with the extended lateral continuity of the velocity contrasts we observed (Fig. 4). The spatial distribution of mineralogic heterogeneity associated with metasomatic alteration in the wedge is likely to be complex: Silica enrichment can occur through reactions between ascending liquids and ambient mantle (*35*), residue from solidified melts could be advected downward by corner flow, and lenses of mineralogic heterogeneities could be generated (*36*). In this context, mineralogic components that can produce detectable seismic contrasts (even in small abundance) include albite and silica, each of which undergoes phase transitions with large changes in elastic properties. The former is the dominant component of the trondhjemitic magmas that are likely to be derived from the slab (*34*). If these magmas react with the wedge, they can generate sodic amphibole and highly Mg-rich pyroxene; if they are spatially localized, they can give rise to veins of sodic metasomatic minerals. At ~2.5 GPa and 1000°C, albite decomposes to jadeite and quartz (*37*), with an increase in velocity at the transitions of ~23 and ~29% in *P*- and *S*-wave velocity, respectively (*38*). Accordingly, if even 5% by volume of sodic feldspar is present, seismic velocity increases of ~2% in *P*-wave velocity and ~3% in *S*-wave velocity should occur near 80 km depth (calculated using a Reuss average and assuming equal temperature dependences of the elasticity of each phase).

The key point is that modest quantities of minerals with phase transitions associated with major changes in elasticity can produce weak but resolvable seismic discontinuities, and a heavily altered mantle wedge is certainly mineralogically complex. Free silica could be generated in and subsequently advected throughout the wedge by basaltic liquid emplaced at depth and crystallizing as eclogite, by silica veining associated with aqueous fluids, or by crystallization of trapped silica-rich magmas (such as trondhjemites) at depth. Not only can free silica generate a discontinuity near 90 km depth associated with the quartz-coesite transition, but several percent of silica can generate *P*- and *S*-impedance increases of a few percent near 300 km depth, as a result of the coesite-stishovite phase transition (*27*). Another type of mechanism, the reaction of forsterite and periclase to anhydrous phase B (which involves the depletion of silica), may be an alternative explanation for discontinuities in the 275- to 300-km depth range (*39*). The presence of SiO_2 would decrease the V_p/V_s ratio (where V_p is *P*-wave velocity and V_s is *S*-wave velocity), so a detailed V_p/V_s tomographic map might help to distinguish between these explanations. A recent tomographic study (*7*) showed large decreases (~−0.1) in the V_p/V_s ratio in the depth range of 250 to 350 km beneath the Lau spreading center. This could indicate that free SiO_2 is indeed present.

The positive velocity contrast near 200 km depth may similarly be associated with the interaction of slab-derived siliceous melts with the mantle wedge: Such melts may equilibrate with normal mantle to form Mg-rich orthopyroxene (*34*–*36*), a phase known to undergo a transition near this depth to a high-pressure clinopyroxene structure. In this instance, an ~20% abundance of orthopyroxene would probably be required to generate a velocity contrast of 1 to 2% (*40*). However, abundances of orthopyroxene of near 40% have been observed in metasomatized xenoliths from the mantle wedge underlying the Kamchatka arc (*35*). The lateral variation in the sign of *S* reflectivity near this depth might require a flow-induced change in the anisotropic fabric, possibly a transition from horizontal inflow to slab-parallel downwelling.

The velocity decrease near 330 km depth is near the final depth at which water is anticipated to be released from the basaltic crust, as defined by the high-pressure stability limit of phengite (*41*). This decrease may accordingly define the lower limit of metasomatism and melting (and thus silica enrichment and veining and basalt liquid generation) within the mantle wedge. Stishovite, the stable form of silica at these depths, is ~30% faster than olivine in *S*-wave velocity and almost 40% faster in *P*-wave velocity: A lack of this phase below this depth (and a few percent above it) could generate this decrease in velocity. Although *P*- and *S*-velocities are positively correlated for some features such as the 90-km and 410-km reflectors, the possible range of causes for the structures that we observed does not dictate that they need to be strongly correlated overall. As data accumulate, improved resolution of the reflectivity will be possible.

If mafic melts do become negatively buoyant within the deep upper mantle (*42*), then, depending on their precise chemistry, some melts could descend to above the 410-km-deep olivine-to-wadsleyite transition and produce a thin melt layer, manifested by a sharp *SH*-velocity reduction near 390 km. The observed velocity reduction near 450 km is probably influenced by side lobes of the strong 410-km reflection, but it appears to be too strong to be completely attributed to these lobes. No obvious petrological complexity is anticipated at this depth, but this region may be strongly perturbed by the relic Vitiaz slab remnant, part of which overlies the Tonga slab.

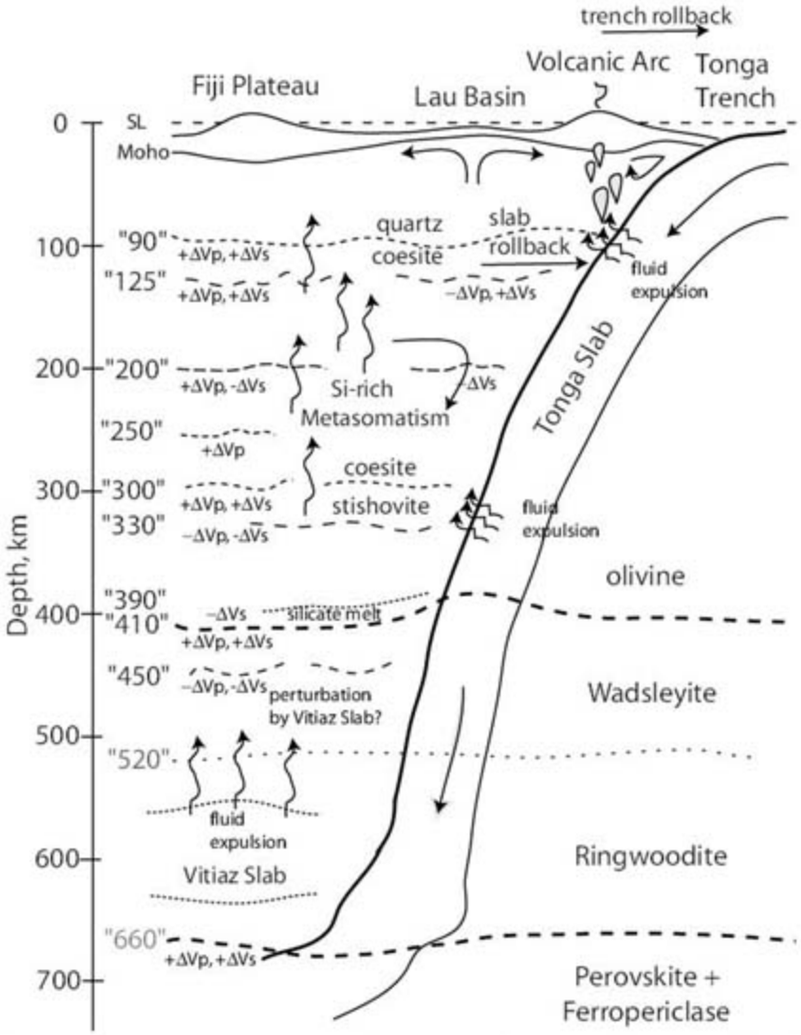

Fig. 5. Schematic cartoon of the Tonga mantle wedge environment above the subducting Tonga slab, highlighting the reflectivity detected in the *P* and *SH* migrations in Figs. 3 and 4. The overall concept is that extensive fluid expulsion has permeated the wedge environment with Si-rich melts and fluids. Fluid expulsion from the slab and possibly from relic pieces of the Vitiaz slab is concentrated at depths near 100 and 325 km. Phase changes in the Si contribute to the reflectivity near 90 and 300 km. The accumulation of silicate melt in a thin layer above the 410-km reflector may have origins in fluid accumulation, and partial melting in the transition zone associated with the perturbed region above the Vitiaz slab may cause reflectivity near 450 km. SL, sea level; ΔV_p, *P*-wave velocity contrast; ΔV_s, *S*-wave velocity contrast.

Fluid expulsion from the slab remnant could possibly lower the velocities or even cause partial melting.

Conclusions. Seismic reflectivity in the mantle wedge between 50 and 500 km was observed to be widespread, and it inspired the creation of a model of an extensively metasomatized region permeated by fluids from the subducted slab (Fig. 5). Given that the wedge is expected to have a complex corner flow, including slab-parallel transport associated with the fan-shaped back-arc spreading of the Lau Basin and slab and trench roll-back, we think it is unlikely that the reflectivity involves strong compositional stratification. Because phase changes of minor components, such as numerous SiO_2-rich veins, can have strong effects on seismic wave velocities, we believe that fluids (and their residues) play a paramount role in both partial melting and the development of the chemical complexity and silica enrichment of the wedge. Shear flows may accentuate the reflectivity by the development of gradients in anisotropic properties. Progress in understanding this very complex environment will require simultaneous consideration of the rough and smooth properties of the medium and not just refined tomographic images.

References and Notes

1. B. R. Hacker, G. A. Abers, S. M. Peacock, *J. Geophys. Res.* **108**, 2029 (2003).
2. K. A. Kelly *et al.*, *J. Geophys. Res.* **111**, B09208 (2006).
3. M. Bevis *et al.*, *Nature* **374**, 249 (1995).
4. M. Gurnis, J. Ritsema, H.-J. van Heijst, S. Zhong, *Geophys. Res. Lett.* **27**, 2373 (2000).
5. W.-P. Chen, M. R. Brudzinski, *Science* **292**, 2475 (2001).
6. D. Zhao *et al.*, *Science* **278**, 254 (1997).
7. J. A. Conder, D. A. Wiens, *Geochem. Geophys. Geosyst.* **7**, Q03018 (2006).
8. E. G. Roth, D. A. Wiens, L. Dorman, J. Hildebrand, S. C. Webb, *J. Geophys. Res.* **104**, 4795 (1999).
9. R. Tibi, D. A. Wiens, *J. Geophys. Res.* **110**, B06313 (2005).
10. H. J. Gilbert *et al.*, *Geophys. Res. Lett.* **28**, 1855 (2001).
11. G. P. Smith *et al.*, *Science* **292**, 713 (2001).
12. R. van der Hilst, *Nature* **374**, 154 (1995).
13. X. Li, S. V. Sobolev, R. Kind, X. Yuan, C. Estabrook, *Earth Planet. Sci. Lett.* **183**, 527 (2000).
14. L. Chen, L. Wen, T. Zheng, *J. Geophys. Res.* **110**, B11310 (2005).
15. J. E. Vidale, H. M. Benz, *Nature* **356**, 678 (1992).
16. Z. Zhang, T. Lay, *J. Geophys. Res.* **98**, 4389 (1993).
17. M. P. Flanagan, P. M. Shearer, *J. Geophys. Res.* **103**, 21165 (1998).
18. Y. Zheng, T. Lay, *J. Geophys. Res.* **111**, B01305 (2006).
19. Additional details of the processing steps are available as supporting material on *Science* Online.
20. E. R. Engdahl, R. D. van der Hilst, R. P. Buland, *J. Geophys. Res.* **88**, 3247 (1998).
21. B. L. N. Kennett, E. R. Engdahl, *Geophys. J. Int.* **105**, 429 (1991).
22. J. Revenaugh, T. H. Jordan, *J. Geophys. Res.* **96**, 19781 (1991).
23. A. Deuss, J. H. Woodhouse, *Geophys. Res. Lett.* **29**, 1249 (2002).
24. J. B. Gaherty, T. H. Jordan, *Science* **268**, 1468 (1995).
25. P. M. Shearer, *Geophys. J. Int.* **115**, 878 (1993).
26. S. Rost, M. Weber, *Geophys. J. Int.* **147**, 12 (2001).
27. Q. Williams, J. Revenaugh, *Geology* **33**, 1 (2005).
28. J. Revenaugh, S. A. Sipkin, *Nature* **369**, 474 (1994).
29. T.-R. A. Song, D. V. Helmberger, S. P. Grand, *Nature* **427**, 530 (2004).
30. E. G. Roth, D. A. Wiens, *Geophys. Res. Lett.* **26**, 1223 (1999).
31. D. L. Anderson, *Tectonophysics* **416**, 7 (2006).
32. S. Turner, C. Hawkesworth, *Nature* **389**, 568 (1997).
33. A. J. R. Kent, D. W. Peate, S. Newman, E. M. Stolper, J. A. Pearce, *Earth Planet. Sci. Lett.* **202**, 361 (2002).
34. G. Prouteau, B. Scaillet, M. Pichavant, R. Maury, *Nature* **410**, 197 (2001).
35. S. Arai, S. Ishimaru, V. M. Okrugin, *Isl. Arc* **12**, 233 (2003).
36. A. Zanetti, M. Mazzucchelli, G. Rivalenti, R. Vannucci, *Contrib. Mineral. Petrol.* **134**, 107 (1999).
37. A. L. Boettcher, P. J. Wyllie, *Contrib. Mineral. Petrol.* **17**, 224 (1968).
38. J. D. Bass, in *A Handbook of Physical Constants*, vol. 2, T. J. Ahrens, Ed. (American Geophysical Union, Washington, DC, 1995), pp. 45–63.
39. J. Ganguly, D. J. Frost, *J. Geophys. Res.* **111**, B06203 (2006).
40. J. Kung *et al.*, *Phys. Earth Planet. Inter.* **147**, 27 (2004).
41. M. W. Schmidt, S. Poli, *Earth Planet. Sci. Lett.* **163**, 361 (1998).
42. A. Suzuki, E. Ohtani, *Phys. Chem. Miner.* **30**, 449 (2003).

43. We thank D. L. Anderson for helpful discussions, P. Shearer and anonymous reviewers for helpful suggestions, and D. Wiens for kindly providing a copy of his 3D tomographic model. This is contribution University Collaborative Research Program grant UCRL-JRNL-229379, supported in part by IGPP-LLNL mini-grant 05-GS-016 and NSF under grants EAR-0125595, EAR-0310342, and EAR-0453884. Seismic data were obtained from the Incorporated Research Institutions for Seismology Data Management Center.

Supporting Online Material

www.sciencemag.org/cgi/content/full/1138074/DC1
Materials and Methods
Figs. S1 to S10

28 November 2006; accepted 27 March 2007
Published online 12 April 2007;
10.1126/science.1138074
Include this information when citing this paper.

Regulation of B Versus T Lymphoid Lineage Fate Decision by the Proto-Oncogene LRF

Takahiro Maeda,[1]* Taha Merghoub,[1] Robin M. Hobbs,[1] Lin Dong,[1] Manami Maeda,[1]* Johannes Zakrzewski,[2] Marcel R.M. van den Brink,[2] Arthur Zelent,[4] Hirokazu Shigematsu,[5] Koichi Akashi,[5] Julie Teruya-Feldstein,[3] Giorgio Cattoretti,[6]† Pier Paolo Pandolfi[1,3]‡

Hematopoietic stem cells in the bone marrow give rise to lymphoid progenitors, which subsequently differentiate into B and T lymphocytes. Here we show that the proto-oncogene *LRF* plays an essential role in the B versus T lymphoid cell-fate decision. We demonstrate that *LRF* is key for instructing early lymphoid progenitors in mice to develop into B lineage cells by repressing T cell–instructive signals produced by the cell-fate signal protein, Notch. We propose a new model for lymphoid lineage commitment, in which LRF acts as a master regulator of the cell's determination of B versus T lineage.

All hematopoietic cells are generated from a small subset of pluripotent stem cells (HSCs) via lineage-restricted progenitors. In adult mice, HSCs reside in the bone marrow (BM) and give rise to lymphoid-restricted progenitors (*1*), which subsequently develop into B and T lymphocytes in the BM and thymus, respectively. This developmental process is coordinated by the expression of distinct sets of genes at specific differentiation stages. Although some of the transcriptional regulators that play key roles in early stages of lymphocyte development are known (*2*, *3*), the precise molecular mechanisms by which lymphoid-restricted progenitors are instructed toward B or T cell fates are still undefined.

The proto-oncogene *LRF* (*4*), encoded by the *Zbtb7a* gene, [formerly known as *Pokemon* (*5*) and also described as *FBI-1* (*6*) and *OCZF* (*7*)] is a transcriptional repressor that belongs to the POK (POZ/BTB and Krüppel) protein family. Promyelocytic leukemia zinc finger (PLZF) and B cell lymphoma 6 (BCL6), two members of the POK family, are involved in chromosomal translocations associated with acute promyelocytic leukemia (APL) and non-Hodgkin's lymphoma (NHL), respectively (*8*, *9*). In a similar manner, we recently reported that *LRF* plays a pivotal proto-oncogenic role and is highly expressed in human NHL tissues (*5*). Emerging experimental evidence indicates that the POK family is indispensable for normal hematopoiesis and immune system developments (*9*–*12*). *BCL6* has been shown to be essential for germinal center (GC) formation and for T helper type 2 (T_H2) inflammatory responses (*9*). More recently, two independent groups reported that a close homolog of *LRF* (*Th-POK*, also known as *cKrox* or *Zbtb7b*) is a master regulator of $CD4^+/CD8^+$ (CD4/8) T cell lineage specification (*11*, *12*).

Given that LRF is broadly expressed in multiple hematopoietic lineages (fig. S2A), especially in the GC B cells (*5*), forms complexes with BCL6 (*4*), and is highly expressed in human NHL tissues, we hypothesized that this gene could play a key role in B cell development. We therefore investigated both fetal and adult lymphopoiesis using *LRF* gene deletion in mice.

B cell development. Deletion of the *Zbtb7a* gene in mouse was carried out with a conventional gene knockout approach (fig. S1, A and B). Although we did not observe a gross defect in the heterozygous mutant, homozygous deletion of the *Zbtb7a* gene ($Zbtb7a^{-/-}$) resulted in embryonic lethality around 16.5 days post coitum (DPC) because of severe anemia. Examination of B lymphopoiesis in 14.5 DPC fetal livers (FLs) from $Zbtb7a^{-/-}$ mice revealed a reduction in the total number of $CD19^+B220^+$ B cells (Fig. 1A). This was mainly due to reduction of B cells after the pro-B stage of differentiation. Absolute numbers of the earliest B cell precursors ($Lin^-AA4.1^+CD19^-B220^+$) were comparable to those of wild-type (WT) littermate controls, whereas total numbers of $Lin^-AA4.1^+CD19^+B220^+$ and $Lin^-AA4.1^-CD19^+B220^+$ B cells were markedly decreased in $Zbtb7a^{-/-}$ FLs (Fig. 1A, right). Hematopoietic stem cell (HSC) and common lymphoid progenitor (CLP) populations were intact in $Zbtb7a^{-/-}$ FLs (fig. S2B).

Pro-B cells can be propagated in vitro on OP9 stromal cell layers in the presence of interleukin 7 (IL-7) and Flt3 ligand (*13*). Substantial numbers of pro-B cells could be propagated from $Zbtb7a^{+/+}$ fetal liver HSCs (FL-HSCs), but $Zbtb7a^{-/-}$ pro-B cells were barely detectable (Fig. 1B), which indicated a cell-autonomous defect in early B cell development. In contrast, $Zbtb7a^{-/-}$ FL-HSCs retained their capacity for T cell development with $Zbtb7a^{-/-}$ FL-HSCs successfully giving rise to T cells in vitro, after culture on OP9-DL1 stromal cells overexpressing the Notch ligand Delta-like 1 (*14*) (fig. S2C). To further investigate the defect in early B cell development in $Zbtb7a^{-/-}$ FLs, we performed BM competitive repopulation assays (*15*). Thus, $Zbtb7a^{+/+}$ and $Zbtb7a^{-/-}$ FL cells were transplanted separately into lethally irradiated recipient mice along with WT BM cells from a congenic strain expressing the CD45.1 antigen (fig. S3A, left). In these experiments, $Zbtb7a^{+/+}$ FL cells successfully gave rise to peripheral blood (PB) B cells in the recipients; however, $Zbtb7a^{-/-}$ FL–derived B cells were virtually undetectable (fig. S3A, right).

The role of LRF in adult lymphopoiesis was next explored by using conditional deletion of the *Zbtb7a* gene (fig. S1, C and D). *Mx1-Cre* transgenic mice were used, in which *Cre* recombinase is induced in HSCs by administering polyinosinic-polycytidylic acid (pIpC) (*16*). A series of double-mutant mice were treated with pIpC at 3 weeks of age as previously described (Fig. 1C, left) (*16*), and peripheral blood was analyzed at 2-week intervals. After pIpC treatment, a significant decline of white blood cell (WBC) counts in the $Zbtb7a^{Flox/Flox\ Mx1cre+}$ mice was observed (Fig. 1C), primarily due to a considerable reduction in circulating $B220^+$ B cells, whereas T cell numbers remained similar to those of controls (Fig. 1C).

Like the defect seen in $Zbtb7a^{-/-}$ mice (Fig. 1A), B cell development in the BM of $Zbtb7a^{Flox/-\ Mx1cre+}$ mice was severely impaired (Fig. 1D). Thus, pro-B, pre-B, and immunoglobulin IgM^+ B cells were drastically reduced, whereas absolute numbers of the prepro-B cells (fig. S3B) (*17*) were increased in the pIpC-treated $Zbtb7a^{Flox/-\ Mx1cre+}$ BM (Fig. 1, D and E). Of note, *LRF* mRNA expression in the pIpC-treated $Zbtb7a^{Flox/-\ Mx1cre+}$ prepro-B cells was essentially undetectable, as revealed by quantitative real-time fluorescence polymerase chain reaction assays (QPCR) (fig. S3C).

[1]Cancer Biology and Genetics Program, Memorial Sloan-Kettering Cancer Center, 1275 York Avenue, New York, NY 10021, USA. [2]Department of Medicine and Immunology Program, Memorial Sloan-Kettering Cancer Center, 1275 York Avenue, New York, NY 10021, USA. [3]Department of Pathology, Memorial Sloan-Kettering Cancer Center, 1275 York Avenue, New York, NY 10021, USA. [4]Leukemia Research Fund Center at the Institute of Cancer Research, Chester Beatty Laboratories, Fulham Road, London SW3 6JB, London, UK. [5]Department of Cancer Immunology and AIDS, Dana-Farber Cancer Institute, Smith Building 770A, 1 Jimmy Fund Way, Boston, MA 02115, USA [6]Institute for Cancer Genetics, Columbia University, New York, NY 10032 USA.

*Present address: Department of Hematopoietic Stem Cell and Leukemia Research, City of Hope National Medical Center, 1500 East Duarte Road, Duarte, CA 91010, USA.
†Present address: Department of Pathology, Università degli Studi Milano-Bicocca and Azienda Ospedaliera San Gerardo, Via Pergolesi 33, 20052 Monza (MI), Italy.
‡To whom correspondence should be addressed. E-mail: p-pandolfi@ski.mskcc.org

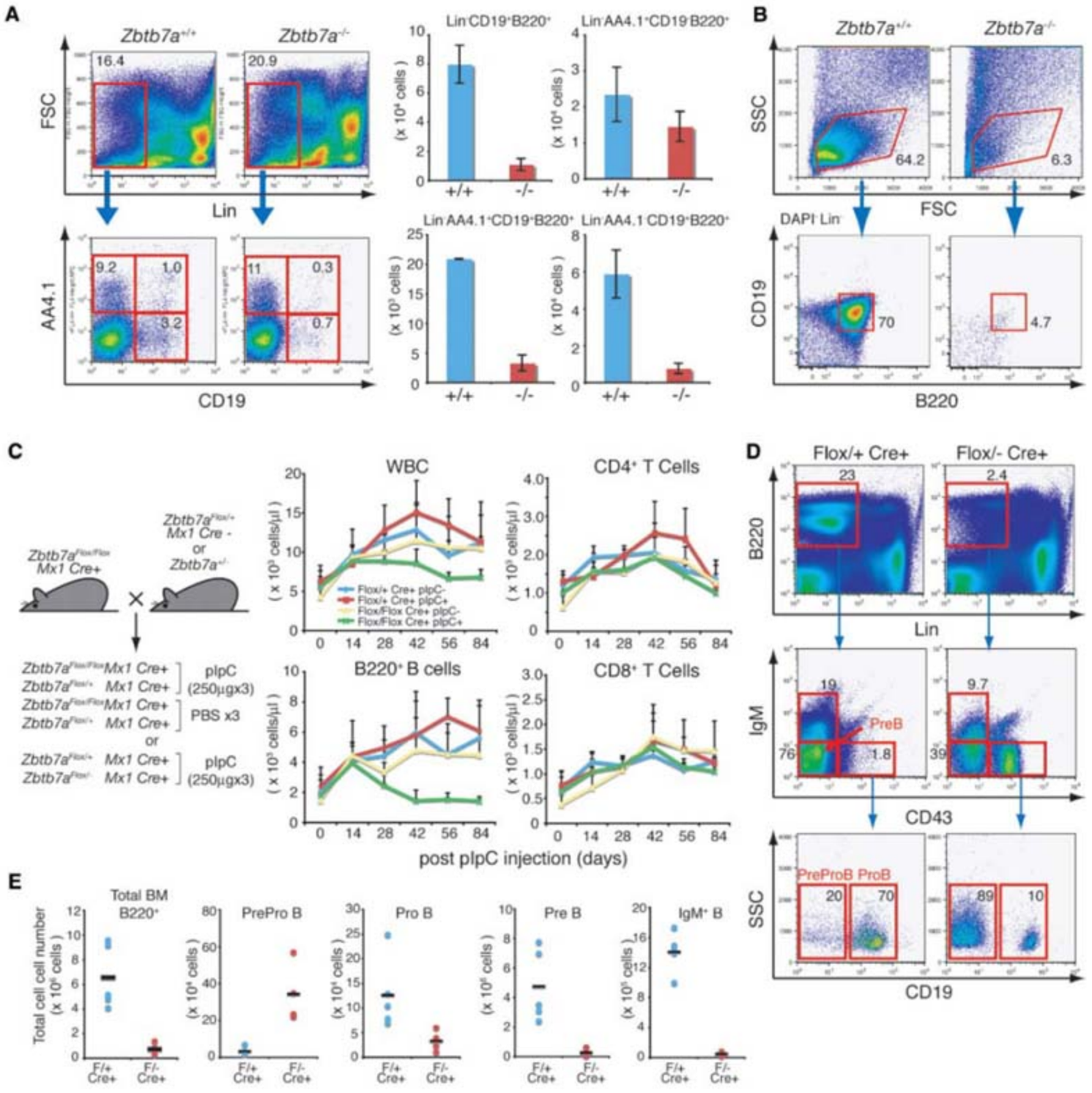

Fig. 1. LRF is indispensable for both fetal and adult B lymphopoiesis. (**A**) On 14.5 DPC, FL cells were stained with fluorochrome-conjugated antibodies against B220, CD19, AA4.1, and lineage markers. (Left) Representative profiles made by fluorescence-activated cell sorting (FACS) of the *Zbtb7a*$^{+/+}$ and *Zbtb7a*$^{-/-}$ FL cells. Total numbers of FL mononuclear cells were counted, and absolute number of B cells in each developmental stage was calculated. Average cell numbers of three independent embryos for each genotype are presented (±SD). (**B**) The 14.5 DPC FL-HSCs ($Lin^{-}Sca1^{+}c\text{-}Kit^{+}$) were cultured on OP9 stromal cell layers in the presence of IL-7 and Flt3 ligand. After 10 days of culture, cells were isolated and analyzed by FACS. (**C**) (Left) Schematic representations of mouse breeding strategy for conditional *LRF* knockout experiments. (Right) Follow-up of the PB counts after pIpC (or phosphate-buffered saline) injections over time. Four groups of mice were examined according to genotype and treatment. WBC counts in the PB were measured by a hematology analyzer, and total numbers of B and T cells were subsequently calculated based on the percent positive cells having B220 and CD4/8 expression, respectively. The average cell count of five animals was plotted on each time point with error bars (±SD). (**D**) BM cells were stained with fluorochrome-conjugated antibodies against B220, CD19, IgM, CD43, and lineage markers (*21*) 1 month after the last pIpC injection. Representative FACS profiles for each genotype are shown. (**E**) Absolute cell number of each population was calculated according to FACS profiles. Black horizontal bars represent mean cell counts among five animals.

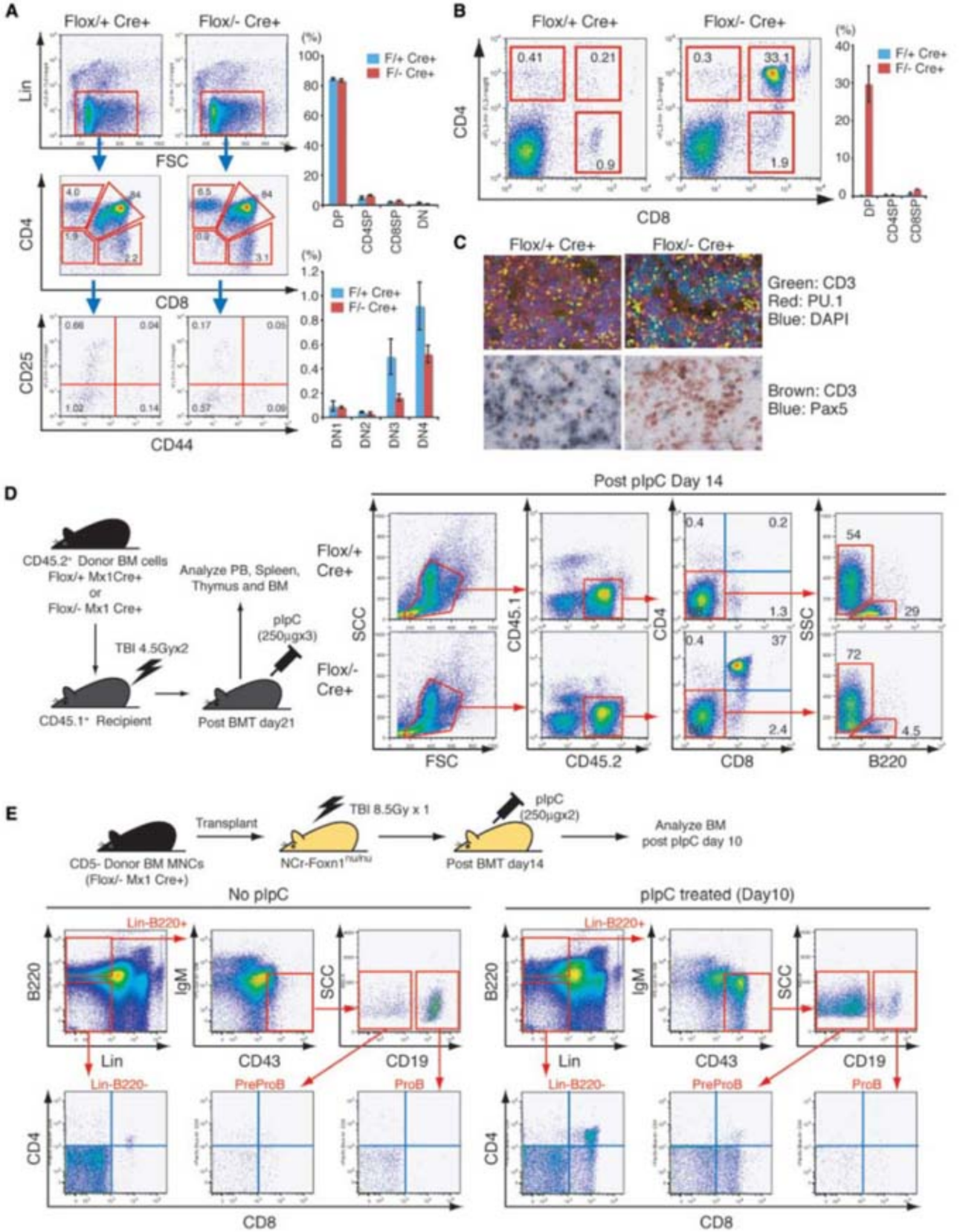

Fig. 2. Extrathymic DP T cell development in the BM after *LRF* loss. (**A**) Thymic T cells were analyzed 1 month after pIpC injection. (Left) Representative FACS profiles for each genotype. (Right) Proportions of CD4/8 DN, CD4/8 DP, CD4 single-positive (CD4SP) and CD8 single-positive (CD8SP) populations were examined, and the DN fraction was further stratified according to CD44 and CD25 expression. Three mice were analyzed for each genotype. (**B**) BMMNCs were analyzed for CD4/8 expression 1 month after pIpC treatment. (Left) Representative FACS profiles for each genotype. (Right) Average percentage positive of three mice for each genotype is demonstrated (±SD). (**C**) (Top) Immunofluorescent analysis of CD3 and PU.1 expression in BM sections. (Bottom) Immunohistochemical analysis of T cell and B cell markers (CD3 and Pax5, respectively) in BM sections 1 month after pIpC treatment. (**D**) Either $Zbtb7a^{Flox/+\ Mx1cre+}$ or $Zbtb7a^{Flox/-\ Mx1cre+}$ donor BMMNCs ($CD45.2^+$) were transplanted into lethally irradiated recipient mice ($CD45.1^+$). After engraftment, recipient mice were treated with pIpC. Recipients' BMMNCs were then collected and analyzed 2 weeks after the last pIpC administration. Representative FACS profiles are presented. (**E**) $Zbtb7a^{Flox/-\ Mx1cre+}$ donor BMMNCs ($CD45.2^+$) were transplanted into lethally irradiated recipient nude mice. Two weeks after transplantation, mice were treated with either pIpC or phosphate-buffered saline. Recipients' BMMNCs were harvested and subsequently analyzed 10 days after the last pIpC administration. Representative BM FACS profiles are presented.

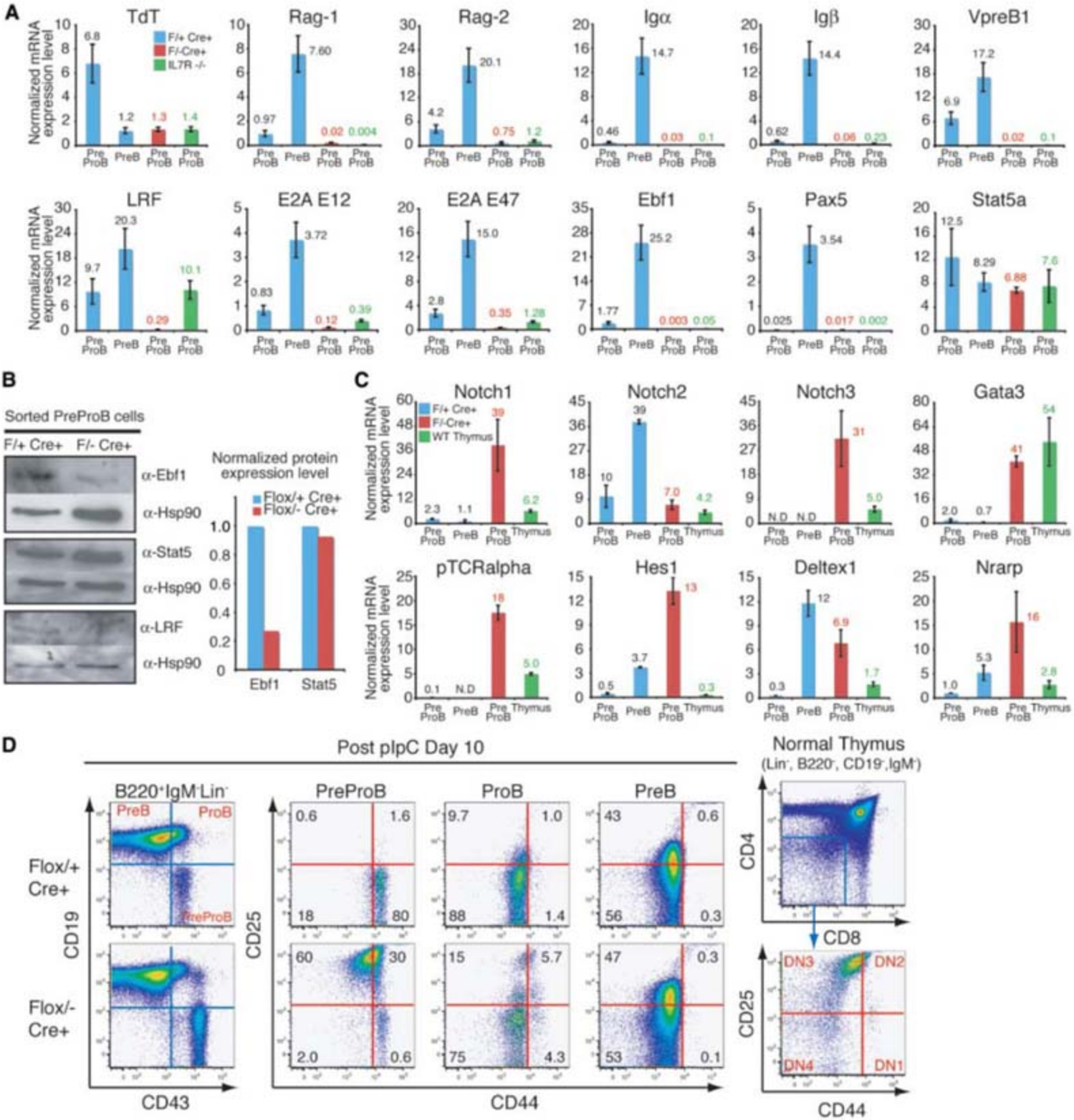

Fig. 3. pIpC-treated *Zbtb7a*$^{Flox/-\ Mx1cre+}$ prepro-B cells are defective in early B cell development and demonstrate a DN T cell signature. (**A**) QPCR analysis of the genes encoding pre-BCR components, TdT, the Rag recombinases, and the critical transcription factors in early B cell development. mRNA expression levels were normalized to hypoxanthine-guanine phosphoribosyl transferase (Hprt) mRNA amount and are represented by bar graphs. Each sample was analyzed in duplicate, and error bars indicate ±SD. BMMNCs were collected and flow-sorted 1 month after the last pIpC injection. (**B**) Western blot analysis for Ebf1 and Stat5 protein in the pIpC-treated prepro-B cells. Bar graph represents normalized protein expression level over corresponding heat shock protein Hsp90 protein level. (**C**) QPCR analysis of *Notch* and *Notch* target genes in the prepro-B cells. QPCR was performed as described in (A). (**D**) CD25 and CD44 expression in prepro-B cells was examined 10 days after the last pIpC injection. FACS profiles of normal thymic DN T cell populations are also presented. (**E**) Schematic representation of lymphoid lineage development in *LRF* conditional knockout mutants.

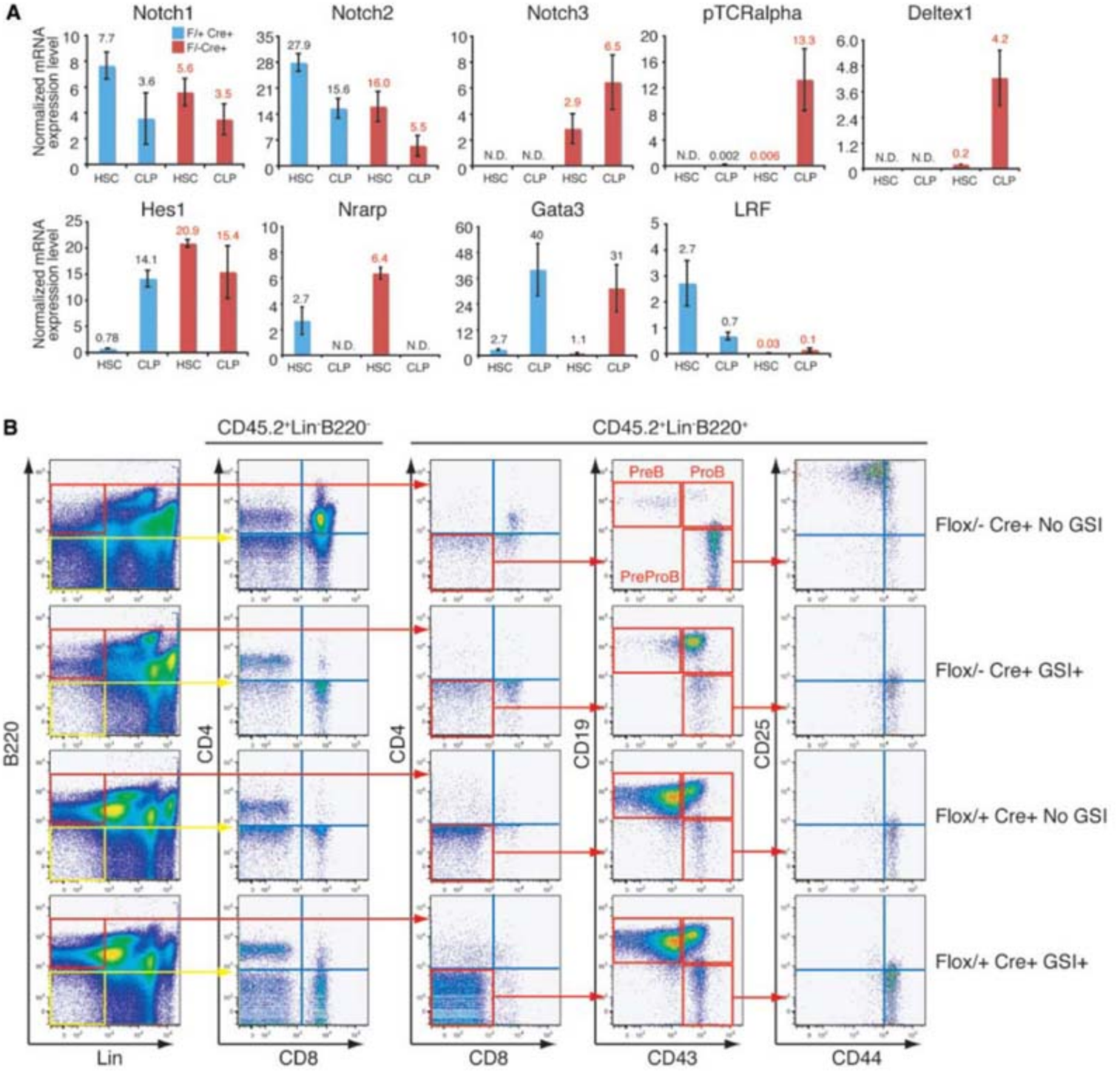

Fig. 4. LRF opposes Notch pathways at the HSC and CLP stage. (**A**) BM HSCs and CLPs were flow-sorted from pIpC-treated animals 1 month after the last pIpC injection. QPCR analyses were performed as described in Fig. 3A. (**B**) In vivo GSI treatment rescued aberrant lymphoid development in *LRF* conditional KO mice. Either $Zbtb7d^{Flox/+\ Mx1cre+}$ or $Zbtb7d^{Flox/-\ Mx1cre+}$ BMMNCs ($CD45.2^+$) were transplanted into lethally irradiated recipient mice (CD45.1) as described in Fig. 2D. Mice were subsequently treated with pIpC. Either GSI or vehicle alone (as a control) was orally administered as described in (*15*). Recipients' BMMNCs were collected and analyzed 3 weeks after the last pIpC administration. (**C**) RNA was extracted from flow-sorted pro-B cells, and QPCR analysis was subsequently performed as described in Fig. 3A.

Furthermore, proportions of the HSCs and CLPs were not grossly affected in the pIpC-treated $Zbtb7a^{Flox/-\ Mx1cre+}$ mice (fig. S3D), although absolute numbers of their HSCs and CLPs were slightly increased as compared with control mice (fig. S3E).

Extrathymic T cell development. Both T and B cells share their origins with a CLP (*1*). However, we did not observe a gross defect in the T cell compartment in pIpC-treated $Zbtb7a^{Flox/-\ Mx1cre+}$ thymus (Fig. 2A). Although a slight decrease was observed in double-negative 3 ($CD4^-CD8^-CD44^-CD25^+$ or DN3) and $CD4^-CD8^-CD44^-CD25^-$ (DN4) thymocyte populations, the proportions of CD4 single-positive (CD4-SP), CD8-SP, and CD4/8 double-positive (DP) T cells were comparable to those of control mice (Fig. 2A). Unexpectedly however, an accumulation of extrathymic DP T cells in the BM of pIpC-treated $Zbtb7a^{Flox/-\ Mx1cre+}$ mice was detected (Fig. 2B) that made up nearly 30% of the BM mononuclear cells (BMMNCs) 1 month after pIpC treatment (Fig. 2B). Immunohistochemical and/or fluorescent analyses further demonstrated that $CD3^{dim}$ DP T cells accumulated in the BM of $Zbtb7a^{Flox/-\ Mx1cre+}$ mice (Fig. 2C). These extrathymic BM DP T cells were polyclonal in origin, as revealed by Dβ1-to-Jβ1 rearrangement status of the T cell receptor β locus (fig. S4A). Moreover, quantitative measurement of gene dosage indicated that the *Zbtb7a* gene was almost undetectable in both thymic and BM DP T cells in the pIpC-treated $Zbtb7a^{Flox/-\ Mx1cre+}$ mice (fig. S4, B and C). Notably, extrathymic T cell development appeared to be limited to the BM, as these cells were not observed in spleen or Peyer's patches (fig. S4, D and E).

To investigate whether the extrathymic DP T cell accumulation seen when the *LRF* gene was deleted was caused by defects in a cell intrinsic mechanism, *LRF* inactivation was induced in BM-reconstituted recipient mice. Thus, $Zbtb7a^{Flox/+\ Mx1cre+}$ or $Zbtb7a^{Flox/-\ Mx1cre+}$ BMMNCs were transplanted into lethally irradiated recipient mice. After engraftment, recipient mice were treated with pIpC to induce Cre expression (Fig. 2D, left). In $Zbtb7a^{Flox/-\ Mx1cre+}$ reconstituted mice, an accumulation of donor-derived ($CD45.2^+$) DP T cells was seen in the BM with a significant reduction of B cells both in BM and PB in a cell-autonomous manner (Fig. 2D and fig. S4F). To determine whether extrathymic BM DP-T cell development was thymus-independent, $Zbtb7a^{Flox/-\ Mx1cre+}$ BMMNCs were transferred into lethally irradiated athymic nude mice, and the *LRF* gene was subsequently inactivated after engraftment by pIpC administration. DP T cell accumulation was observed in the BM 10 days after the last pIpC administration (Fig. 2E), indicating that in the absence of LRF, lymphoid progenitors in the BM gave rise to BM DP T cells in a thymus-independent fashion.

Aberrant lymphocyte commitment. To explore whether the early B cell developmental program takes place correctly in pIpC-treated $Zbtb7a^{Flox/-\ Mx1cre+}$ prepro-B cells, the expression of the genes encoding pre-BCR components, terminal deoxynucleotidyl transferase (TdT), and Rag recombinases was examined. In these experiments, mRNA levels of pre-BCR components (Igα, Igβ, and Vpre-B1), Rag recombinases (Rag-1, Rag-2) and TdT in $Zbtb7a^{Flox/-\ Mx1cre+}$ mice were markedly reduced compared with those of control mice (Fig. 3A).

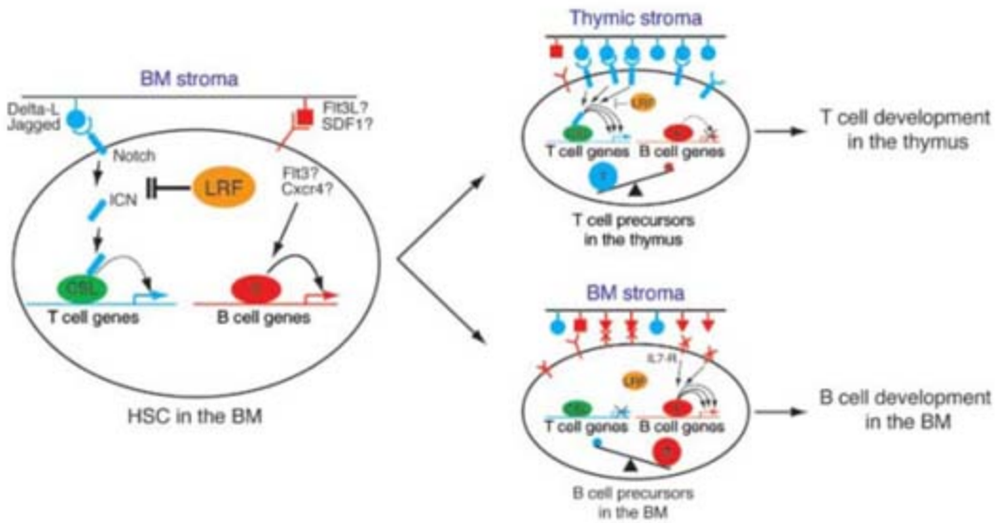

Fig. 5. Proposed model for the role of LRF in determining B versus T lineage fate. (**Left**) In BM, where stromal cells express moderate levels of Notch ligands, LRF expression in HSCs and lymphoid progenitors functions to repress T cell–instructive signals produced by Notch. ICN, intracellular domain of Notch; CSL, CBF-1 (RBP-Jκ, Jκ recombining binding protein)–Suppressor of Hairless–Lag1 (Notch effector). (**Right**) However, once progenitors home in on the thymus, where Notch ligands are more abundantly expressed, this repressive role of LRF on Notch function is overruled (top), which allows efficient production of T cell precursors.

Early B cell development is governed by a small set of cytokines and transcription factors. Both PU.1 and Ikaros are essential for the maintenance of HSCs and CLPs (*18*, *19*); Flt3 ligand is required for the generation of CLPs but not HSCs (*20*). Both IL-7 and its receptor (IL-7R) are indispensable for prepro-B to pro-B transition (*21*) and transcription factors Bcl11a, E2A, Stat5, and Ebf1 also play critical roles at this developmental stage (*3*) (fig. S5A). pIpC-treated $Zbtb7a^{Flox/-\ Mx1cre+}$ prepro-B cells showed a significant down-regulation of E2A, Ebf1, and Pax5 mRNA (Fig. 3A). Similarly, small amounts of Ebf1 protein were detected in pIpC-treated $Zbtb7a^{Flox/-\ Mx1cre+}$ prepro-B cells, whereas Stat5 protein was abundant (Fig. 3B). Because the enforced expression of Ebf1 is able to rescue B cell developmental defects in $PU.1^{-/-}$, $IL\text{-}7R^{-/-}$, and $E2A^{-/-}$ mice (*3*), we examined whether the overexpression of Ebf1 in $Zbtb7a^{-/-}$ FL-HSCs might have a similar effect. Positive control LRF-transduced $Zbtb7a^{-/-}$ FL cells successfully gave rise to splenic B cells in recipient mice (fig. S5B). However, neither GFP– vector nor Ebf1-transduced FL cells were able to rescue the $Zbtb7a^{-/-}$ B cell phenotype (fig. S5B).

Given that pIpC-treated $Zbtb7a^{Flox/-\ Mx1cre+}$ prepro-B cells were unable to progress further in the B cell developmental program, we speculated that they might have become aberrantly committed to the T cell lineage, thus generating the extrathymic DP T cells found in the BM. To test this, we examined mRNA expression levels of T cell–specific target genes in the pIpC-treated $Zbtb7a^{Flox/-\ Mx1cre+}$ prepro-B cells. In these analyses, mRNA levels of Notch1, Notch3, but not Notch2, and their downstream target genes were profoundly elevated in the pIpC-treated $Zbtb7a^{Flox/-\ Mx1cre+}$ prepro-B cells (Fig. 3C). Despite expressing the cell surface B cell marker B220 (Fig. 1D), pIpC-treated $Zbtb7a^{Flox/-\ Mx1cre+}$ prepro-B cells appeared aberrantly committed to the T cell rather than B cell lineage. To determine whether the pIpC-treated $Zbtb7a^{Flox/-\ Mx1cre+}$ prepro-B cells could differentiate into more mature stages of T cell development, sorted prepro-B cells were cultured on OP9 stromal cell layers. After coculture with control OP9-GFP cells, the pIpC-treated $Zbtb7a^{Flox/+Mx1cre+}$ prepro-B cells, in which one allele of *LRF* remained intact, efficiently differentiated into pro-B cells, while the pIpC-treated $Zbtb7a^{Flox/-\ Mx1cre+}$ prepro-B cells did not give rise to pro-B cells (fig. S6A, left). In the case of cells expressing the Delta notch ligand (OP9-DL1), however, control prepro-B cells still differentiated into pro-B cells, even though activation of the Notch pathway drives T cell development (fig. S6A). This is likely because normal prepro-B cells express very low levels of the Notch1 receptor and thus cannot respond to the DL1 signal (see Fig. 3C for Notch1 mRNA). On the

contrary, the pIpC-treated *Zbtb7a*$^{Flox/-\ Mx1cre+}$ prepro-B cells immediately lost B220 expression on the cell surface and effectively differentiated to CD4/8 DP T cells (fig. S6A, right). In agreement with these findings, *Zbtb7a*$^{Flox/-\ Mx1cre+}$ prepro-B cells were mostly positive for CD25 and negative for the CD44 surface markers, which is reminiscent of normal thymic DN3 T cells (Fig. 3D). Taken together, these data indicate that in the absence of LRF, lymphoid progenitors give rise to aberrant B220-positive DN T–like cells, which subsequently differentiate to DP T cells in the BM at the expense of normal B cell development (Fig. 3E).

Notch repression by LRF. Notch signaling is critical for T cell development and the perturbation of this pathway can result in cellular transformation (*22*). Furthermore, Notch is obligatory for correct fate determination toward B or T lineage in the lymphoid progenitors (*2*) and was recently reported as the most commonly mutated gene in human T cell acute lymphoblastic leukemia (T-ALL) (*23*). *Notch1* deletion in mouse HSCs results in a marked reduction in thymic T cells and simultaneous B cell development in the thymus (*24*). Conversely, constitutive activation of Notch1 pathways in HSCs and/or CLPs results in blocking of B cell development and a profound expansion of extrathymic DP T cells in the BM. Although these mice eventually develop T cell leukemia in the BM (*22*), thymic T cell development is not impaired, for the most part (*22*). Given that the phenotype of *LRF* conditional knockout mice is seen in mice overexpressing the intracellular domain of *Notch1* that leads to constitutive Notch pathway activation (*22*), we hypothesized that LRF might oppose Notch1 function at HSC and/or CLP stage. To test this directly, we examined expression of *Notch* genes and their targets in HSCs and CLPs. After pIpC treatment, *LRF* mRNA was efficiently eliminated both in HSCs and CLPs (Fig. 4A) and was followed by the up-regulation of all *Notch* target genes in the pIpC-treated *Zbtb7a*$^{Flox/-\ Mx1cre+}$ HSCs and CLPs (Fig. 4A). Corresponding *Notch1* mRNA levels were comparable to those of control mice (Fig. 4A). This "Notch signature" was evident mainly at the HSC and CLP stages, as relatively low levels of *Notch* target genes were detected in myeloid or erythroid progenitor compartments (fig. S6B). To further elucidate whether the aberrant T cell commitment in the absence of LRF was Notch-dependent, *LRF* conditional KO mice were treated with a gamma secretase inhibitor (GSI). GSIs are potent inhibitor of Notch signaling that act by preventing the cleavage and release of the intracellular moiety of the Notch receptor (*25*). Strikingly, this almost completely rescued abnormal B or T cell commitment seen in *LRF* conditional KO mice (Fig. 4B). After GSI treatment, neither the DP T cells nor aberrant DN T–like prepro-B cells were observed (Fig. 4B). Furthermore, *Zbtb7a*$^{Flox/-\ Mx1cre+}$ prepro-B cells could give rise to pro-B cells after GSI treatment (Fig. 4B). It was noteworthy that, in these pro-B cells, expression of VpreB1, a component of the pre-BCR, resumed after GSI treatment, whereas *LRF* mRNA became barely detectable, which confirmed that gene targeting was correct (Fig. 4C).

Discussion. Our findings allow us to reach two conclusions. First, we identify *LRF* as a master regulator in determination of B versus T lymphoid fate, with loss of *LRF* in HSCs and CLPs, resulting in an absence of B cell development and spontaneous extrathymic DP T cell development in the BM. Second, we demonstrate that loss of *LRF* results in aberrant activation of the Notch pathway, with *Notch* target genes becoming strongly up-regulated in HSCs and CLPs. Taken together, we propose a working model for B versus T cell lineage fate determination, in which LRF plays a pivotal role as a negative regulator of T lineage commitment by opposing Notch function (Fig. 5). In normal HSCs, LRF opposes Notch function. LRF blocks basal Notch signaling triggered from BM stromal cells, which express moderate level of Notch ligands (*26*). BM stromal cells also express molecules that support B cell commitment and development, such as Flt3 and SDF1 (*27*). Therefore, HSCs and lymphoid progenitors in the BM are committed to the B cell lineage by default and differentiate into B cells in the presence of signals, such as IL-7 (*21*). After homing to the developing thymus, in which Notch ligands are abundantly expressed (*26*), HSCs and/or lymphoid progenitors efficiently give rise to thymic T cells, because, at this point, Notch signaling would overrule the repressive role of LRF on Notch function. However, in the absence of LRF, the low levels of Notch ligands expressed by the BM stroma would now be sufficient to activate *Notch* target genes normally repressed by LRF in HSCs and CLPs, thus aberrantly specifying T cell fate (Fig. 5). In support of this working model, exogenous expression of LRF in HSCs was seen to result in inefficient DN T cell production, as compared with mock-infected HSCs in an OP9-DL1 culture system (fig. S6C).

Our data provide strong evidence that LRF can oppose the Notch signaling pathway. Given that GSI treatment, which blocks the Notch pathway upstream, was sufficient to cause resumption of normal B versus T cell commitment in mutant HSC and CLPs, *LRF* likely targets upstream components of the pathway rather than repressing downstream *Notch* target genes. As we observed high *LRF* expression in NHL patients (*5*) and Notch signaling is known to play a tumor suppressive role in human B cell malignancies (*28*), it is tempting to speculate that *LRF* can also exert its oncogenic activity by opposing Notch function in the B cell compartment. In addition, given that LRF is widely expressed in the organism and Notch has described roles in regulating the development and differentiation of multiple tissues, the extent of LRF's repressive role on Notch-dependent processes remains to be seen.

References and Notes

1. M. Kondo, I. L. Weissman, K. Akashi, *Cell* **91**, 661 (1997).
2. I. Maillard, T. Fang, W. S. Pear, *Annu. Rev. Immunol.* **23**, 945 (2005).
3. K. L. Medina, H. Singh, *Curr. Opin. Hematol.* **12**, 203 (2005).
4. J. M. Davies *et al.*, *Oncogene* **18**, 365 (1999).
5. T. Maeda *et al.*, *Nature* **433**, 278 (2005).
6. F. Pessler, P. S. Pendergrast, N. Hernandez, *Mol. Cell. Biol.* **17**, 3786 (1997).
7. A. Kukita *et al.*, *Blood* **94**, 1987 (1999).
8. Z. Chen *et al.*, *EMBO J.* **12**, 1161 (1993).
9. B. H. Ye *et al.*, *Nat. Genet.* **16**, 161 (1997).
10. F. Piazza, J. A. Costoya, T. Merghoub, R. M. Hobbs, P. P. Pandolfi, *Mol. Cell. Biol.* **24**, 10456 (2004).
11. G. Sun *et al.*, *Nat. Immunol.* **6**, 373 (2005).
12. X. He *et al.*, *Nature* **433**, 826 (2005).
13. P. Vieira, A. Cumano, *Methods Mol. Biol.* **271**, 67 (2004).
14. T. M. Schmitt, J. C. Zúñiga-Pflücker, *Immunity* **17**, 749 (2002).
15. Materials and methods are available as supporting material on *Science* Online.
16. R. Kuhn, F. Schwenk, M. Aguet, K. Rajewsky, *Science* **269**, 1427 (1995).
17. R. R. Hardy, C. E. Carmack, S. A. Shinton, J. D. Kemp, K. Hayakawa, *J. Exp. Med.* **173**, 1213 (1991).
18. H. Iwasaki *et al.*, *Blood* **106**, 1590 (2005).
19. D. Allman *et al.*, *Nat. Immunol.* **4**, 168 (2003).
20. E. Sitnicka *et al.*, *Immunity* **17**, 463 (2002).
21. K. Kikuchi, A. Y. Lai, C. L. Hsu, M. Kondo, *J. Exp. Med.* **201**, 1197 (2005).
22. J. C. Pui *et al.*, *Immunity* **11**, 299 (1999).
23. A. P. Weng *et al.*, *Science* **306**, 269 (2004).
24. F. Radtke *et al.*, *Immunity* **10**, 547 (1999).
25. H. D. Lewis *et al.*, *Chem. Biol.* **14**, 209 (2007).
26. B. C. Harman, E. J. Jenkinson, G. Anderson, *Semin. Immunol.* **15**, 91 (2003).
27. T. Nagasawa, *Nat. Rev. Immunol.* **6**, 107 (2006).
28. P. A. Zweidler-McKay *et al.*, *Blood* **106**, 3898 (2005).

29. We would like to thank G. Draetta, P. Strack, and V. Richon for providing us with GSI, MRK-003. We are grateful to J. C. Zúñiga-Pflücker for OP9-GFP and OP9-DL1 cells. We thank J.-H. Dong and other Memorial Sloan-Kettering Cancer Center (MSKCC) transgenic core facility members for help and advice on the generation of *Zbtb7a* mutant mice; Y. Igarashi-Alexander for assistance with transplantation experiment; J. Hendrikx and other MSKCC flow cytometry core facility members for assistance with FACS analysis and cell sorting; D. Robbiani and A. Gazumyan for advice and helpful discussion; C. Gurrieri, J. Costoya, F. Piazza, L. Khandker, I. Guernah, L. DiSantis, and other P.P.P. lab members for assistance and helpful discussion. This work is supported in part by the National Cancer Institute (NIH) grant CA-102142 to P.P.P.

Supporting Online Material

www.sciencemag.org/cgi/content/full/316/5826/860/DC1
Materials and Methods
Figs. S1 to S6
References

6 February 2007; accepted 27 March 2007
10.1126/science.1140881

Pairing Without Superfluidity: The Ground State of an Imbalanced Fermi Mixture

C. H. Schunck,* Y. Shin, A. Schirotzek, M. W. Zwierlein,† W. Ketterle

We used radio-frequency spectroscopy to study pairing in the normal and superfluid phases of a strongly interacting Fermi gas with imbalanced spin populations. At high spin imbalances, the system does not become superfluid even at zero temperature. In this normal phase, full pairing of the minority atoms was observed. Hence, mismatched Fermi surfaces do not prevent pairing but can quench the superfluid state, thus realizing a system of fermion pairs that do not condense even at the lowest temperature.

Fermionic superfluidity has many manifestations in nature; it occurs in such diverse systems as superconducting materials, liquid ^{3}He, neutron stars, and ultracold quantum gases. At its heart lies the formation of fermion pairs. Although the Pauli principle forbids identical fermions to occupy the same quantum state, pairs of fermions can condense and thus become superfluid. Superconductivity, the flow of electrical current without resistance, is a manifestation of fermionic superfluidity in a condensed-matter system. Superconductors are characterized by a temperature T^* where electrons start to pair and a critical temperature T_c for the onset of superconductivity. In conventional superconductors, understood within the framework of Bardeen-Cooper-Schrieffer (BCS) theory, fermion pairs form and condense simultaneously (i.e., $T^* = T_c$). In high-temperature superconductors, strongly correlated electrons exist in the normal phase, that is, $T^* > T_c$. The interactions that mediate pairing and ultimately lead to superconductivity in these complex systems are still subject to debate (*1*). Another strongly interacting but comparatively simple fermion system is an ultracold gas of neutral fermionic atoms. High-temperature superfluidity was recently observed in these gases (*2*), opening a new approach to explore the highly correlated normal phase of strongly interacting fermions and its relation to the onset of superfluidity.

Ultracold atomic Fermi mixtures of two spin states close to a Feshbach resonance constitute a highly controllable model system for strongly interacting fermions. By resonantly changing the interaction strength between the fermionic atoms, the crossover from BCS superfluidity of loosely bound pairs to Bose-Einstein condensation (BEC) of tightly bound molecules can be explored. BEC-BCS crossover theory at finite temperature contains pairing in the normal phase below a temperature $T^* > T_c$ (*1*, *3*–*5*). Evidence for pairing above T_c in ultracold Fermi gases was found in (*6*, *7*) via radio-frequency (rf) spectroscopy. Here, we use rf spectroscopy to study primarily the normal state of an imbalanced spin mixture. An imbalance in the spin populations of the two-state Fermi system leads to a qualitative change of the phase diagram: Above a certain interaction-dependent population imbalance, the transition to the superfluid state is suppressed even at zero temperature. This is known as the Chandrasekhar-Clogston (CC) or Pauli paramagnetic limit of superfluidity (*8*, *9*). In several works, the CC limit is assumed to imply pair dissociation and is referred to as "Pauli pair breaking" (*10*–*12*), that is, T^* and T_c are assumed to vanish simultaneously. The CC limit has been observed and characterized in ultracold atomic gases (*13*).

We report on the observation of a gap in a single-particle excitation spectrum (representing a spin response function) of a highly imbalanced sample. This implies that the system is in a correlated state and that the minority component is paired. Pairing of fermions is thus not necessarily a precursor to superfluidity: T^* is finite even when T_c vanishes. The CC limit of superfluidity, at least for strong interactions, is not associated with breaking of fermion pairs but only with the quenching of the superfluid state. Another and probably very different system with finite T^* and vanishing T_c has been discussed in strongly underdoped cuprates (*1*).

The rf spectra presented in this work were also correlated with an indirect signature for superfluidity by determining pair condensate fractions (*14*, *15*). We conclude that rf spectra cannot distinguish, at present experimental resolution, between normal and superfluid states.

In our experiment, a strongly interacting, imbalanced spin mixture of ^{6}Li fermions in the two lowest hyperfine states, labeled $|1\rangle$ and $|2\rangle$ (corresponding to the $|F = 1/2, m_F = 1/2\rangle$ and $|F = 1/2, m_F = -1/2\rangle$ states at low magnetic field) was created in an optical dipole trap at 833 G, the center of the $|1\rangle$-$|2\rangle$ Feshbach resonance [see (*15*, *16*) for details]. On resonance, all interactions in the $|1\rangle$-$|2\rangle$ mixture are universal, as the Fermi energy E_F and the inverse Fermi wavenumber $1/k_F$ are the only relevant energy and length scales. The imbalance δ of the mixture was controlled as reported in (*13*, *17*), where $\delta = (N_1 - N_2)/(N_1 + N_2)$ and N_1 and N_2 are the atom numbers in states $|1\rangle$ and $|2\rangle$, respectively. Here, E_F, k_F, and the Fermi temperature T_F are given for a noninteracting Fermi gas with the same atom number as the majority component. To access a broader range of temperatures, we used two optical traps with different waists, characterized by the axial and radial trapping frequencies ω_a and ω_r (as given in the figure captions of the rf spectra).

The interactions were spectroscopically probed in a three-level system (*18*). A 2-ms rf pulse resonant with the transition from state $|2\rangle$ (the minority component) to a third state, labeled $|3\rangle$ ($|F = 3/2, m_F = -3/2\rangle$ at low field) was applied. Immediately after the rf pulse, the optical trap was switched off and the cloud was allowed to expand for absorption imaging. Two absorption images of atoms in states $|2\rangle$ and $|1\rangle$ were taken successively, and the atom number fraction $N_2/(N_1 + N_2)$ was obtained as a function of the applied rf. The rf spectra at the highest imbalances were taken with a population transfer smaller than 3% of the total number of atoms. The data points in all spectra are the average of three

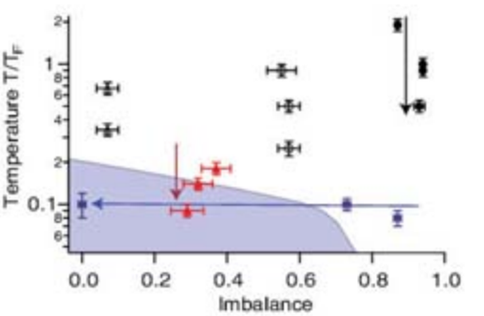

Fig. 1. The temperature-imbalance diagram shows where the rf spectra presented in Fig. 2 (black circles), Fig. 4, A to C (blue diamonds), and Fig. 4, D to F (red triangles) were taken. All spectra were obtained on resonance at 833 G. The arrows indicate the order in which the spectra are displayed in the figures. The shaded region indicates the superfluid phase. The spectra corresponding to the open circles and triangles are similar to the spectra of Fig. 2, A to C, and are shown in (*19*). Except for the data close to zero imbalance, for which the interacting temperature T' is given, temperatures have been determined from the noninteracting wings of the majority cloud (*25*).

Department of Physics, MIT-Harvard Center for Ultracold Atoms, and Research Laboratory of Electronics, Massachusetts Institute of Technology, Cambridge, MA 02139, USA.

*To whom correspondence should be addressed. E-mail: chs@mit.edu

†Present address: Institut für Physik, AG Quantum, Staudinger Weg 7, 55128 Mainz, Germany.

independent measurements. Temperature was adjusted by evaporation to different depths of the optical trap, followed by recompression. Spectra presented as a data set were taken with the same final trap depth. Figure 1 provides an overview of the imbalances and temperatures at which the rf spectra were obtained. Specific details are given in the figure captions and in (*19*). All radio frequencies were referenced to the $|2\rangle$-$|3\rangle$ resonance recorded in the absence of atoms in state $|1\rangle$.

The rf spectroscopy measures a single-particle spin excitation spectrum for the minority component of the mixture (*20*–*23*). To understand the expected rf spectra, one can use a simplified description of the gas as a mixture of free atoms and molecule-like pairs, which is strictly valid only in the BEC limit. Transferring an unbound atom from state $|2\rangle$ into state $|3\rangle$ requires an energy ΔE_{23}. As the $|1\rangle$-$|3\rangle$ mixture is also strongly interacting because of a $|1\rangle$-$|3\rangle$ Feshbach resonance located at 690 G (*18*), we first assume, as in (*6*, *7*), that mean-field shifts (i.e., shifts corresponding to Hartree terms) are absent in the rf spectrum. Then ΔE_{23} and the width of the atomic $|2\rangle$-$|3\rangle$ transition are independent of the density of atoms in state $|1\rangle$. However, if an atom in state $|2\rangle$ is paired with an atom in state $|1\rangle$, the rf photon must provide the binding energy E_B required to break the pair in addition to ΔE_{23}. Therefore, if pairing is present in the system, a second peak emerges in the minority rf spectrum that is separated from the atomic line and associated with pairing (*6*, *7*). In a Fermi cloud, pairing is strong only near the Fermi surface. Because the rf photons can excite atoms in the whole Fermi sea, the observed spectral gap $\Delta\nu$ may have to be interpreted as a pair-binding energy averaged over the Fermi sea. Indeed, in the BCS limit one has $h\Delta\nu \propto \Delta^2/E_F$, where h is Planck's constant and Δ is the BCS pairing gap (*23*). Under these working assumptions, we interpret the emergence of a gap in the spectrum as a pairing effect.

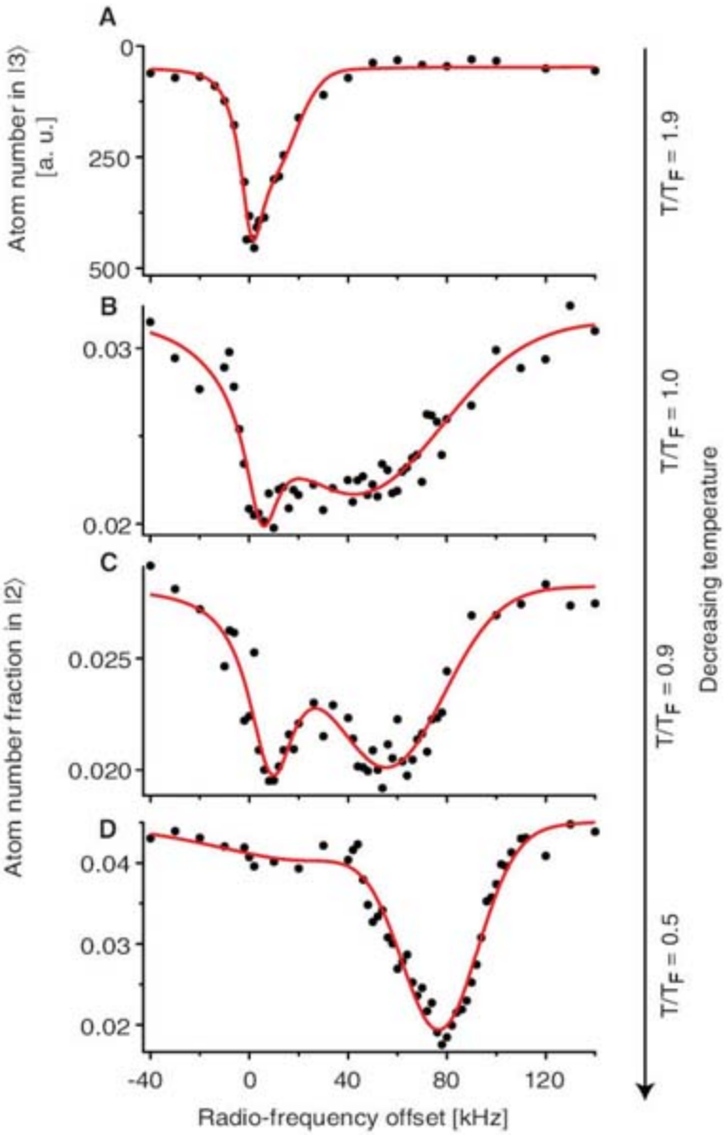

Fig. 2. Radio-frequency spectroscopy of the minority component in an imbalanced ($\delta \sim 0.9$), strongly interacting mixture of fermionic atoms above the CC limit of superfluidity. As the temperature is lowered, full pairing develops in the absence of superfluidity. (**A**) An asymmetric and broad peak centered at the position of the atomic line is observed. The asymmetry and the large width might be caused by the presence of pairing correlations already at T/T_F = 1.9. For this spectrum only, heating was applied and the atom number in state $|3\rangle$ was recorded (*19*). (**B** and **C**) The pairing peak emerges. (**D**) At T/T_F = 0.5, the pairing peak remains and the minority atoms are almost fully paired (see also Fig. 4A). As a guide to the eye, a double-peak line consisting of a Lorentzian fit to the atomic peak and a Gaussian fit to the pairing peak is included. Spectra were taken for the following parameters (see also the solid black circles in Fig. 1): (A) δ = 0.87, $E_F = h \times 260$ kHz, T/T_F = 1.9; (B) δ = 0.94, $E_F = h \times 360$ kHz, T/T_F = 1.0; (C) δ = 0.94, $E_F = h \times 360$ kHz, T/T_F = 0.9; (D) δ = 0.93, $E_F = h \times 340$ kHz, T/T_F = 0.5. The trapping frequencies were $\omega_r = 2\pi \times 3.5$ kHz and $\omega_a = 2\pi \times 77$ Hz.

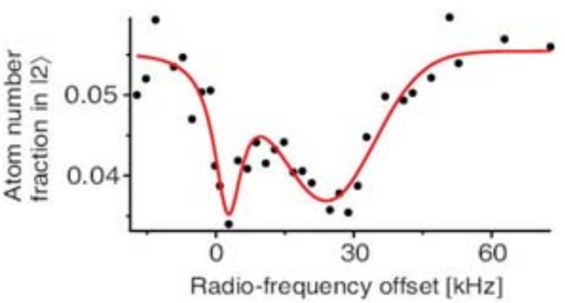

Fig. 3. Radio-frequency spectrum of the minority component obtained at a magnetic field of 937 G ($1/k_F a_{12} = -0.18$) and imbalance δ = 0.88, demonstrating strong pairing above the CC limit on the BCS side of the Feshbach resonance (a_{12} is the s-wave scattering length in the $|1\rangle$-$|2\rangle$ mixture). The rf spectrum was taken for the parameters $E_F = h \times 280$ kHz and T/T_F = 0.3. The trapping frequencies were $\omega_r = 2\pi \times 2.9$ kHz and $\omega_a = 2\pi \times 64$ Hz.

The presence of pairing in the normal phase has been observed in the rf spectra for a highly imbalanced mixture, with $\delta \sim 0.9$, on resonance at 833 G (Fig. 2) and on the BCS side at 937 G (Fig. 3). At high temperature, only the atomic peak was present, and as the temperature was lowered, a second peak—the pairing peak—emerged and separated from the atomic peak. At sufficiently low temperatures, essentially only the pairing peak remained. This behavior is qualitatively similar to what has been observed in an equal mixture (*6*). The spectral gap $\Delta\nu$ (i.e., the shift of the pairing peak relative to the atomic line) increases as the temperature is lowered. At the lowest temperature of $0.08T/T_F$ (Fig. 4A), we measured a shift of $0.38E_F$.

All the spectra in Figs. 2 and 3 were obtained at high imbalances above the CC limit of superfluidity. Here the system cannot undergo a phase transition to the superfluid state even at zero temperature. For a trapped gas on resonance the CC limit is reached at a critical imbalance of $\delta_{c,exp} = 0.74 \pm 0.05$ (*13*, *17*), in agreement with a calculated value of $\delta_{c,theory} = 0.77$ (*24*). On the BCS side of the Feshbach resonance, at an interaction strength of $1/k_F a_{12} = -0.18$, the critical imbalance is $\delta_{c,exp} = 0.6 \pm 0.1$, as previously measured around this interaction strength (*13*).

Because we observed full pairing in the normal phase of the strongly interacting gas, one might not expect the rf spectra to reveal the onset of superfluidity. We recorded rf spectra covering the phase transition from the normal to the superfluid state by varying imbalance (Fig. 4, A to C) as well as temperature (Fig. 4, D to F). In both cases, no signature of the phase transition was resolved, although both the emergence of fermion pair condensates and sudden changes in the density profiles (*13*, *17*) showed the phase transition. In our previous work (*2*, *13*), these indirect indicators of superfluidity were cor-

related with the presence of quantized vortices (i.e., superfluid flow).

Figure 4, A to C, illustrates that working with high imbalances has the advantage of reducing line-broadening effects that arise from averaging over the inhomogeneous density distribution of the sample. The narrowest line was observed at the highest imbalance (Fig. 4A), where the minority is considerably smaller than the majority cloud. The homogeneous linewidth should reflect the wave function of a single fermion pair. The observed narrow linewidth indicates localization in momentum space well below the Fermi momentum k_F, and hence a pair size on the order of the interparticle spacing.

We now examine the assumptions underlying our interpretation of the peaks in the rf spectra. In particular, we address the question of whether our observations can distinguish between pairing correlations and mean-field effects. Indeed, mean-field–like shifts were observed, for example, in the rf spectrum of Fig. 2C where the atomic line shows a shift of $0.03E_F$ to higher energy. Although the $|1\rangle$-$|3\rangle$ interactions are in the unitary regime for a typical value of $k_F a_{13} \approx -3.3$ (varying, for example, from –3 to –3.6 across the minority cloud in Fig. 2C), they may not have fully converged to their value at unitarity and thus may have caused the observed shifts (a_{13} is the s-wave scattering length in the $|1\rangle$-$|3\rangle$ mixture). However, all shifts of the atomic line are small relative to the size of the spectral gap of up to $0.38E_F$ and are only seen in the presence of the pairing peak (fig. S3 displays all observed shifts of atomic and pairing peaks versus temperature). Although the shifts of the atomic line are small at all temperatures, the shifts associated with the pairing peak start rising below $T/T_F \sim 1$, accompanied by a decrease in the weight of the atomic line. In the intermediate temperature range, where the rf spectra show a double-peak structure, the pairing peak should originate primarily from the higher-density region in the center of the cloud, and the atomic peak should originate from the low-density wings. Therefore, if one were to normalize the data according to the local density of majority atoms, the data points for the atom peaks would shift up in T/T_F by a factor of between 1.5 and 5, the smaller factor reflecting the cases of large imbalance, where the minority cloud is considerably smaller than the majority cloud. As a result, near $T/T_{F(local)} = 0.5$, we have observed both atomic peaks and pairing peaks, which is an indication for the local coexistence of unpaired and paired minority atoms. However, in this possible coexistence region, either the peak separation is small or one peak has very small weight. Therefore, more work is needed to study the possibility of coexistence. An alternative interpretation assumes single local peaks and a sudden onset of peak shifts below $T/T_F \sim 1$. This appears to be incompatible with a local mean-field approximation as well: The mean field in the unitarity limit should saturate when T approaches T_F and not vary strongly for $T < T_F$, because the relative momentum of two particles in this regime is dominated by the Fermi momentum and not by the thermal

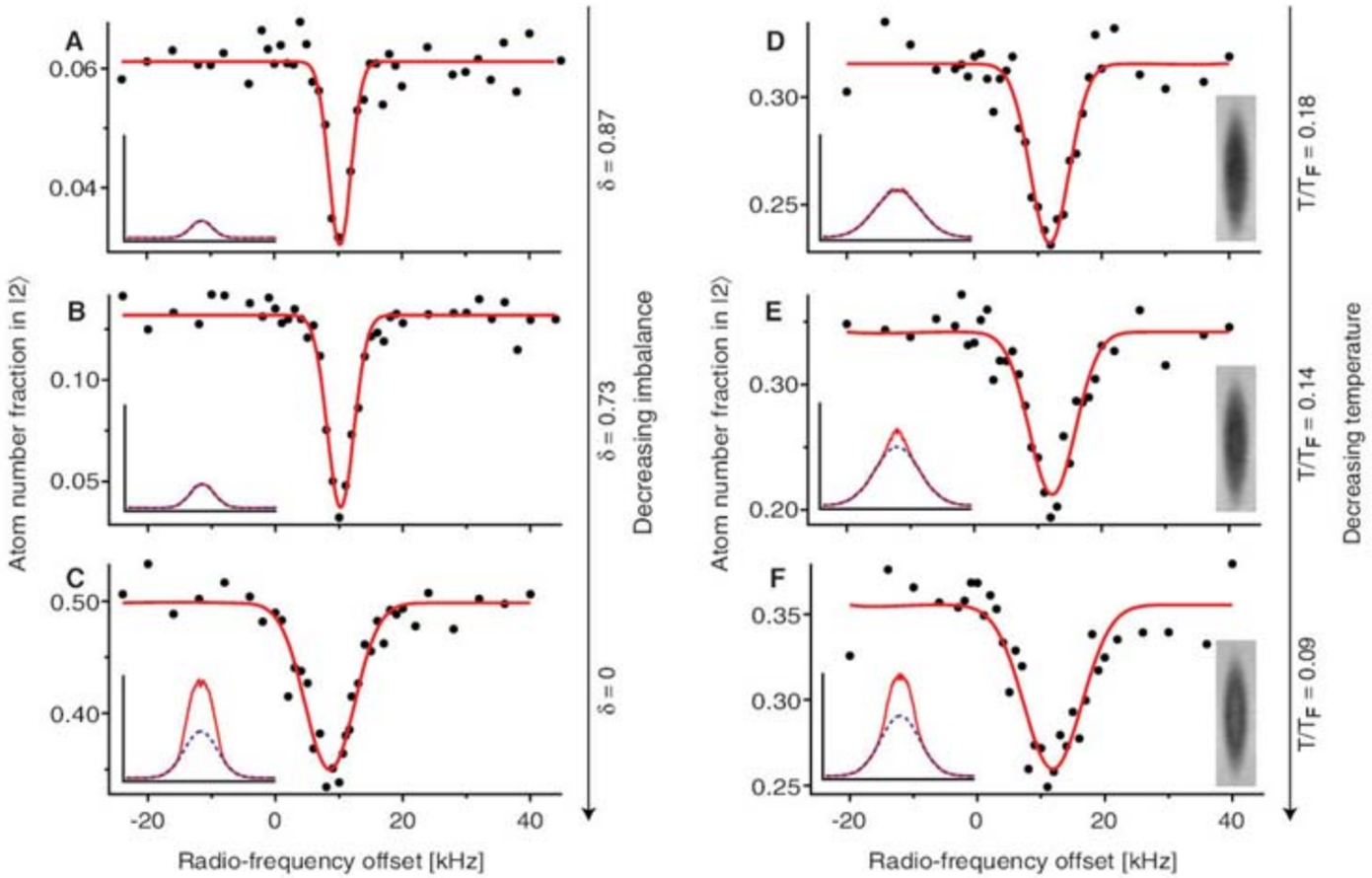

Fig. 4. Radio-frequency spectra of the minority component obtained while crossing the phase transition by reducing imbalance (**A** to **C**) and temperature (**D** to **F**). The rf spectra do not reveal the phase transition. The onset of superfluidity is indirectly observed by fermion pair condensation. The condensate fractions are zero in (A) and (B) and 35 ± 2% in (C). The onset of superfluidity as a function of temperature occurs between (D) and (F), with condensate fractions of 0% in (D), 3 ± 2% in (E), and 17 ± 3% in (F). The insets in (A) to (F) show the column density profile (red) of the minority cloud after a rapid magnetic field ramp to the BEC side and further expansion (*19*); the blue dashed line is a Gaussian fit to the thermal background. The additional insets in (D) to (F) show phase-contrast images for a trapped cloud, obtained at imbalances of the opposite sign. Spectra were taken for the following parameters in (A) to (C) (see also the blue diamonds in Fig. 1): (A) $\delta = 0.87$, $E_F = h \times 27$ kHz, $T/T_F = 0.08$; (B) $\delta = 0.73$, $E_F = h \times 27$ kHz, $T/T_F = 0.10$; (C) $\delta = 0.00$, $E_F = h \times 23$ kHz, $T/T_F = 0.10$. The trapping frequencies were $\omega_r = 2\pi \times 143$ Hz and $\omega_a = 2\pi \times 23$ Hz. For the spectrum in (C) we quote the temperature T' obtained from a fit to the interacting Fermi gas (*19*). Spectra were taken for the following parameters in (D) to (F) (see also the solid red triangles in Fig. 1): (D) $\delta = 0.37$, $E_F = h \times 38$ kHz, $T/T_F = 0.18$; (E) $\delta = 0.32$, $E_F = h \times 38$ kHz, $T/T_F = 0.14$; (F) $\delta = 0.29$, $E_F = h \times 35$ kHz, $T/T_F = 0.09$. The trapping frequencies were $\omega_r = 2\pi \times 192$ Hz and $\omega_a = 2\pi \times 23$ Hz.

momentum. Furthermore, a sudden onset of interactions would likely affect the density distribution of the minority atoms. However, the minority clouds observed in expansion are well fit by a single Thomas-Fermi profile (*25*).

The BEC-side picture of a mixture of single atoms and molecules seems to extend into the resonance region, in the sense that fermion pairs form high above the superfluid transition temperature and possibly coexist locally with unpaired atoms. However, the fermion pairs on resonance behave differently from "real" molecules: Their binding energy increases with lower temperature and higher atomic density. Most important, fermion pairs above the CC limit do not condense at low temperature as bosonic molecules would do at any imbalance. Although some extensions of BCS mean-field theories to the imbalanced case do not predict pairing at imbalances δ above the CC limit (*26*), a survival of Cooper pairs "far from the transition region" has been predicted (*27*) for a superconducting system that is driven into the normal, paramagnetic phase by Zeeman splitting.

The observed spectral gaps appear to be insensitive to the density of the minority atoms (Fig. 4, A to C). At very high imbalances, one should indeed approach the limit of one minority atom immersed in a fully polarized Fermi sea. In (*24*, *28*, *29*) the ground-state energy for this scenario has been calculated to be about $-0.6E_F$, for example, by using a modified Cooper-pair wave function ansatz (*28*). These calculations do not provide an excitation spectrum and do not distinguish between pairing (correlation) energies and mean-field (Hartree) terms. Therefore, the theoretical result cannot be directly compared to our spectroscopic measurement of $h\Delta\nu = -0.38E_F$ at $T/T_F = 0.08$.

Whether superfluidity can occur for large imbalances and low atom numbers in highly elongated geometries remains a subject of debate (*30*). In light of our findings, it may be important to clearly distinguish between the effects of pairing and of superfluidity. It has also been suggested that the presence of an atomic peak next to the pairing peak in the minority cloud at zero temperature and high imbalance could provide evidence for exotic forms of superfluidity, such as the Fulde-Ferrel-Larkin-Ovchinnikov state (*31*). However, for the parameters studied here, the atomic peak is seen to disappear as the temperature is reduced (Figs. 2 and 4A).

Working with imbalanced Fermi gases, we were able to study and characterize pairing in a situation where no superfluidity occurs even at zero temperature. The spectral gap $\Delta\nu$ appears to be only weakly dependent on the imbalance. This finding suggests that near unitarity, certain pairing correlations in the superfluid state are similar to those in a dilute cloud of minority atoms immersed into the Fermi sea of the majority. Moreover, it implies that the energetics that drive the normal-to-superfluid phase transition involve more than the observed pairing energy. Further studies of the strongly correlated normal state might yield new insights into the microscopic physics of the superfluid state.

References and Notes

1. P. A. Lee, N. Nagaosa, X.-G. Wen, *Rev. Mod. Phys.* **78**, 17 (2006).
2. M. W. Zwierlein, J. R. Abo-Shaeer, A. Schirotzek, C. H. Schunck, W. Ketterle, *Nature* **435**, 1047 (2005).
3. N. Trivedi, M. Randeria, *Phys. Rev. Lett.* **75**, 312 (1995).
4. A. Perali, P. Pieri, G. C. Strinati, C. Castellani, *Phys. Rev. B* **66**, 024510 (2002).
5. Q. Chen, J. Stajic, S. Tan, K. Levin, *Phys. Rep.* **412**, 1 (2005).
6. C. Chin *et al.*, *Science* **305**, 1128 (2004); published online 22 July 2004 (10.1126/science.1100818).
7. J. Kinnunen, M. Rodríguez, P. Törmä, *Science* **305**, 1131 (2004); published online 22 July 2004 (10.1126/science.1100782).
8. B. S. Chandrasekhar, *Appl. Phys. Lett.* **1**, 7 (1962).
9. A. M. Clogston, *Phys. Rev. Lett.* **9**, 266 (1962).
10. K. Capelle, *Phys. Rev. B* **65**, 100515 (2002).
11. M. Maška, *Phys. Rev. B* **66**, 054533 (2002).
12. K. Kumagai *et al.*, *Phys. Rev. Lett.* **97**, 227002 (2006).
13. M. W. Zwierlein, A. Schirotzek, C. H. Schunck, W. Ketterle, *Science* **311**, 492 (2006); published online 21 December 2005 (10.1126/science.1122318).
14. C. A. Regal, M. Greiner, D. S. Jin, *Phys. Rev. Lett.* **92**, 040403 (2004).
15. M. W. Zwierlein *et al.*, *Phys. Rev. Lett.* **92**, 120403 (2004).
16. Z. Hadzibabic *et al.*, *Phys. Rev. Lett.* **91**, 160401 (2003).
17. Y. Shin, M. W. Zwierlein, C. H. Schunck, A. Schirotzek, W. Ketterle, *Phys. Rev. Lett.* **97**, 030401 (2006).
18. S. Gupta *et al.*, *Science* **300**, 1723 (2003); published online 8 May 2003 (10.1126/science.1085335).
19. See supporting material on *Science* Online.
20. J. Kinnunen, M. Rodríguez, P. Törmä, *Phys. Rev. Lett.* **92**, 230403 (2004).
21. Y. Ohashi, A. Griffin, *Phys. Rev. A* **72**, 063606 (2005).
22. Y. He, Q. Chen, K. Levin, *Phys. Rev. A* **72**, 011602 (2005).
23. Z. Yu, G. Baym, *Phys. Rev. A* **73**, 063601 (2006).
24. C. Lobo, A. Recati, S. Giorgini, S. Stringari, *Phys. Rev. Lett.* **97**, 200403 (2006).
25. M. W. Zwierlein, C. H. Schunck, A. Schirotzek, W. Ketterle, *Nature* **442**, 54 (2006).
26. C. Chien, Q. Chen, Y. He, K. Levin, *Phys. Rev. Lett.* **98**, 110404 (2007).
27. I. L. Aleiner, B. L. Altshuler, *Phys. Rev. Lett.* **79**, 4242 (1997).
28. F. Chevy, *Phys. Rev. A* **74**, 063628 (2006).
29. A. Bulgac, M. M. Forbes, *Phys. Rev. A* **75**, 031605(R) (2007).
30. G. B. Partridge *et al.*, *Phys. Rev. Lett.* **97**, 190407 (2006).
31. J. Kinnunen, L. M. Jensen, P. Törmä, *Phys. Rev. Lett.* **96**, 110403 (2006).

32. We thank W. Zwerger, P. Lee, K. Levin, and Q. Chen for stimulating discussions and D. Miller for critical reading of the manuscript. Supported by NSF and the Office of Naval Research.

Supporting Online Material

www.sciencemag.org/cgi/content/full/316/5826/867/DC1
Materials and Methods
Figs. S1 to S3
References

2 February 2007; accepted 29 March 2007
10.1126/science.1140749

The Process of Tholin Formation in Titan's Upper Atmosphere

J. H. Waite Jr.,[1]* D. T. Young,[1] T. E. Cravens,[2] A. J. Coates,[3] F. J. Crary,[1] B. Magee,[1]* J. Westlake[4]

Titan's lower atmosphere has long been known to harbor organic aerosols (tholins) presumed to have been formed from simple molecules, such as methane and nitrogen (CH_4 and N_2). Up to now, it has been assumed that tholins were formed at altitudes of several hundred kilometers by processes as yet unobserved. Using measurements from a combination of mass/charge and energy/charge spectrometers on the Cassini spacecraft, we have obtained evidence for tholin formation at high altitudes (~1000 kilometers) in Titan's atmosphere. The observed chemical mix strongly implies a series of chemical reactions and physical processes that lead from simple molecules (CH_4 and N_2) to larger, more complex molecules (80 to 350 daltons) to negatively charged massive molecules (~8000 daltons), which we identify as tholins. That the process involves massive negatively charged molecules and aerosols is completely unexpected.

Methane and nitrogen in Titan's atmosphere are supplied with free energy from solar ultraviolet (UV) radiation and energetic particles in Saturn's magnetosphere. These circumstances make Titan, a prolific source of complex organic compounds, unparalleled in the solar system. Hydrocarbon chemistry is further enhanced by the escape of hydrogen from the exosphere, which accelerates the conversion of methane to unsaturated hydrocarbon-nitrile species by circumventing the buildup of molecular hydrogen, thus promoting unsaturated hydrocarbon formation (*1*, *2*). Sagan and Khare (*3*) have suggested that the penultimate result of the formation of these large compounds is the generation of hydrocarbon-nitrile aerosols (tholins) thought to populate haze layers in Titan's stratosphere (*4*, *5*). Similar organic chemistry occurs during soot formation in Earth's troposphere (*6*–*8*) and may have taken place in the

[1]Space Science and Engineering Division, Southwest Research Institute (SWRI), 6220 Culebra Road, San Antonio, TX 78238, USA. [2]Department of Physics and Astronomy, University of Kansas, Lawrence, KS 66045, USA. [3]Department of Space and Climate Physics, Mullard Space Science Laboratory, University College London, Holmbury St. Mary, Dorking RH5 6NT, UK. [4]Department of Physics and Astronomy, University of Texas, San Antonio, TX 78249, USA.
*To whom correspondence should be addressed. E-mail: hwaite@swri.edu (J.H.W.); bmagee@swri.edu (B.M.)

Table 1. INMS observed neutral mole fractions at closest approach. Mole fractions are found from inbound observations within 15 km of closest approach to maximize signal and reduce contamination. Uncertainties are shown in parentheses. H_2 values for all flybys [4.05×10^{-3} (3.00×10^{-5})] have been adopted from analysis of the first Cassini encounter with Titan (TA). Temperature values are obtained from the scale height of N_2 measured within 100 km of closest approach. SZA, solar zenith angle.

	T16	T17	T18	T19	T20	T21	T23
Total density (cm^{-3})	1.78×10^{10} (5.33×10^{6})	5.39×10^{9} (3.04×10^{6})	1.06×10^{10} (4.18×10^{6})	7.10×10^{9} (3.45×10^{6})	3.28×10^{9} (3.33×10^{6})	7.23×10^{9} (3.46×10^{6})	7.66×10^{9} (3.49×10^{6})
N_2	0.975 (3.52×10^{-4})	0.965 (9.64×10^{-3})	0.971 (4.56×10^{-4})	0.968 (5.47×10^{-4})	0.968 (1.13×10^{-3})	0.971 (5.37×10^{-4})	0.975 (5.36×10^{-4})
CH_4	0.0127 (3.18×10^{-5})	0.0241 (7.69×10^{-5})	0.0155 (4.59×10^{-5})	0.0213 (6.46×10^{-5})	0.0193 (1.27×10^{-4})	0.0184 (5.89×10^{-5})	0.0137 (5.03×10^{-5})
C_2H_2	2.05×10^{-4} (3.07×10^{-6})	2.60×10^{-4} (6.04×10^{-6})	2.52×10^{-4} (4.43×10^{-6})	2.03×10^{-4} (4.77×10^{-6})	2.51×10^{-4} (1.10×10^{-5})	2.04×10^{-4} (4.69×10^{-6})	2.24×10^{-4} (4.89×10^{-6})
C_2H_4	6.80×10^{-4} (6.02×10^{-6})	1.01×10^{-3} (1.28×10^{-5})	7.15×10^{-4} (8.04×10^{-6})	9.93×10^{-4} (1.14×10^{-5})	7.69×10^{-4} (2.06×10^{-5})	7.33×10^{-4} (9.58×10^{-6})	8.31×10^{-4} (1.02×10^{-5})
C_2H_6	1.66×10^{-5} (8.52×10^{-7})	1.06×10^{-5} (1.19×10^{-6})	2.04×10^{-5} (1.23×10^{-6})	9.68×10^{-6} (1.02×10^{-6})	1.26×10^{-5} (2.39×10^{-6})	8.74×10^{-6} (9.47×10^{-7})	1.17×10^{-5} (1.09×10^{-6})
C_3H_4	1.21×10^{-5} (6.81×10^{-7})	9.61×10^{-6} (1.06×10^{-6})	1.09×10^{-5} (8.39×10^{-7})	1.08×10^{-5} (1.01×10^{-6})	7.23×10^{-6} (1.69×10^{-6})	7.26×10^{-6} (8.06×10^{-7})	1.21×10^{-5} (1.04×10^{-6})
C_4H_2	4.58×10^{-6} (3.97×10^{-7})	3.95×10^{-6} (6.44×10^{-7})	5.05×10^{-6} (5.43×10^{-7})	5.81×10^{-6} (6.99×10^{-7})	3.96×10^{-6} (1.19×10^{-6})	2.33×10^{-6} (4.34×10^{-7})	5.86×10^{-6} (6.85×10^{-7})
C_2N_2	3.51×10^{-6} (5.43×10^{-7})	4.53×10^{-6} (1.08×10^{-6})	3.30×10^{-6} (6.86×10^{-7})	5.81×10^{-6} (1.09×10^{-6})	4.16×10^{-6} (1.91×10^{-6})	2.43×10^{-6} (6.92×10^{-7})	5.16×10^{-6} (1.01×10^{-6})
C_6H_6	4.39×10^{-6} (3.21×10^{-7})	1.35×10^{-6} (3.11×10^{-7})	3.30×10^{-6} (3.62×10^{-7})	2.42×10^{-6} (3.72×10^{-7})	1.55×10^{-6} (6.14×10^{-7})	1.07×10^{-6} (2.42×10^{-7})	5.07×10^{-6} (5.25×10^{-7})
C_3H_6	4.00×10^{-6} (4.29×10^{-7})	1.83×10^{-6} (5.07×10^{-7})	2.72×10^{-6} (4.61×10^{-7})	2.03×10^{-6} (4.78×10^{-7})	1.55×10^{-6} (8.61×10^{-7})	1.75×10^{-6} (4.53×10^{-7})	3.02×10^{-6} (5.69×10^{-7})
Altitude (km)	950	1000	960	980	1030	1000	1000
Latitude	85°	23°	71°	61°	7.5°	44°	31°
SZA	105°	45°	90°	81°	25°	124°	53°
T (K)	128 ± 5	116 ± 16	132 ± 8	133 ± 7	200 ± 13	142 ± 8	168 ± 10

early Earth's atmosphere before the buildup of oxygen 2.2×10^9 years ago (*9*).

During the Cassini spacecraft's first encounters with Titan, the Ion Neutral Mass Spectrometer (INMS) revealed an atmosphere dominated by N_2 and CH_4, accompanied by a rich mixture of hydrocarbon-nitrile compounds with masses up to 100 daltons (*10*), which was the upper detectable limit of the mass range of the INMS. Of particular importance for the development of complex chemistry in the upper atmosphere was the tentative identification of benzene (C_6H_6), which is a critical component in the formation of polycyclic aromatic hydrocarbon (PAH) compounds. In this paper, we report on quantitative observations of hydrocarbon-nitrile compounds in Titan's upper atmosphere (950 to 1150 km) by the INMS, together with evidence from the Cassini Plasma Spectrometer (CAPS) (*11*) of heavy positively charged (100 to 350 daltons) and negatively charged (20 to 8000 daltons) ions (*12*). The presence of negative ions in particular was a complete surprise, and we argue that they play an important role in tholin formation. These data were obtained during six recent Titan encounters (Tables 1 and 2), indicating that the chemical processes are a persistent phenomenon.

The low altitude (950 km) and high latitude (>70°) of the closest Cassini encounter with Titan (T16) allowed accurate determination of benzene density and mixing ratios over an altitude range of 130 km. Assuming local thermodynamic equilibrium with the major species (N_2), the fits to data (Fig. 1) give a scale height of ~15 km, which is consistent with a species with a molecular mass of 78 atomic mass units acting under molecular diffusion. This finding indicates that molecular diffusion, rather than turbulent atmospheric mixing, is the dominant transport process and that transport time scales are

Table 2. INMS observed ion densities (ions/cm^3) at closest approach. Ion data are not available for T20 because the ram-directed flow of ions during the encounter was outside the INMS field of view. LST, local solar time.

	T16	T17	T18	T19	T21	T23
CH_5^+	8.47×10^3 (1.03×10^4)	25.9 (0.977)	4.68 (0.600)	3.95×10^4 (9.93×10^3)	0.422 (0.272)	2.85×10^4 (4.88×10^4)
$C_2H_5^+$	2.83×10^4 (3.59×10^4)	153.0 (22.2)	13.75 (2.44)	2.18×10^5 (6.53×10^4)	1.09 (0.450)	1.35×10^5 (2.31×10^5)
$HCNH^+$	1.28×10^5 (1.62×10^5)	767 (85.8)	66.4 (10.4)	1.28×10^6 (3.01×10^5)	5.66 (3.24)	5.42×10^5 (9.28×10^5)
$C_3H_3^+$	1.12×10^5 (1.57×10^5)	113 (24.7)	71.7 (9.92)	7.51×10^5 (4.01×10^5)	41.9 (29.47)	2.41×10^5 (4.20×10^5)
$C_4H_3^+$	9.98×10^3 (1.73×10^4)	19.8 (9.95)	6.39 (0.903)	5.53×10^4 (5.55×10^4)	0.766 (0.216)	1.06×10^4 (1.99×10^4)
$C_4H_5^+$	9.05×10^3 (1.56×10^4)	14.8 (9.17)	7.26 (1.12)	3.52×10^4 (3.86×10^4)	1.09 (0.223)	1.15×10^4 (2.13×10^4)
$C_6H_5^+$	834 (2.10×10^3)	2.60 (2.70)	5.14 (0.763)	3.06×10^3 (4.98×10^3)	0.900 (0.755)	1.64×10^3 (3.88×10^3)
$C_6H_7^+$	1.04×10^3 (2.55×10^3)	3.80 (4.26)	5.83 (0.868)	3.61×10^3 (6.42×10^3)	0.504 (0.394)	2.22×10^4 (5.22×10^3)
$C_7H_7^+$	2.05×10^3 (3.40×10^3)	6.82 (8.33)	17.1 (2.30)	5.55×10^3 (9.33×10^3)	2.20 (1.96)	3.25×10^3 (7.40×10^3)
Altitude (km)	950	1000	960	980	1000	1000
LST	17.4	10.5	4.8	2.3	20.4	14.1

more rapid than chemical-loss time scales. Data taken during subsequent flybys have confirmed the presence of benzene at a mole fraction of ~1 to 5 parts per million (Table 1) and the dominance of transport in determining the altitude variation. INMS-derived ion and neutral spectra from 1 to 100 daltons (Fig. 2) illustrate the ion-neutral chemistry correspondence for compounds, starting with C1 compounds and continuing through benzene and toluene. In the case of benzene, a chemical equilibrium exists between it and the benzene cation $C_6H_7^+$. Other combinations of ion and neutral species seen in the spectra suggest the complexity of the chemical processes at work.

In addition to INMS data, the CAPS Ion Beam Spectrometer (IBS) (*11*) (Fig. 3A) found complex hydrocarbon-nitrile species at much higher molecular masses (~350 daltons) than can be measured by the INMS. However, whereas the INMS is a quadrupole mass spectrometer (*10*), the CAPS IBS is an electrostatic analyzer that makes use of the high Mach number (14 for a mass of 100 daltons) of cold ionospheric ions rammed into the instrument to infer mass/charge spectra from measured ion energy/charge and knowledge of the spacecraft's electrical potential in Titan's atmosphere. The IBS was not designed specifically for this task, and so its effective mass resolution at Titan is limited to a mass resolution ($M/\Delta M$, where M is the mass in daltons and ΔM is the mass resolution in daltons) of ~8 versus 100 for the INMS. However, IBS resolution is sufficient to separate families of mass peaks. This functionality is evident in the spectrum shown (Fig. 3A), where the unresolved mass groupings <100 amu correspond to families of peaks in the INMS spectra (Fig. 2). Of particular interest are several prominent peaks at ~130, ~170, and ~335 daltons. These we identify as naphthalene, anthracene derivatives, and an anthracene dimer.

The IBS analysis method can be applied to energy spectra (Fig. 3B) obtained from the CAPS Electron Spectrometer (ELS) (*11*, *12*) to infer the existence of heavy negative ions. Although designed to detect electrons, the ELS can also detect negatively charged ions. Analysis of the three-dimensional velocity distribution of the ions shows that, although extending to ~2 keV due to their kinetic energy in the moving spacecraft reference frame (6 km/s), the ions are very cold (~0.1 eV) and hence highly supersonic. Taking the energy spectra as proxies for mass spectra (Fig. 3B), we can identify peaks at ~15, ~35, and ~100 daltons and a broad range of masses between 100 and ~8000 daltons, with a peak at ~1500 daltons. Thus, both IBS and ELS data clearly show the presence of heavy molecules well above the mass range of the INMS, implying a complex organic chemistry that has neither been observed nor considered before.

The existence of large negative ions is an indication of complex carbon-nitrogen precursors (PAHs and assorted nitriles) that may lead to the production of tholins. Our analysis suggests that the organic compounds seen by the INMS and IBS are formed through ion-neutral chemical processes, which then give rise to the complex hydrocarbon-nitrile negative ions found by the ELS.

Earlier modeling efforts [for information on the initial model and revised ion-neutral chemistry added, see (*13*) and (*14*), respectively; for original references for benzene production, see (*6*–*8*)] showed that benzene can be produced by ion-neutral chemistry involving small molecules at altitudes near 1000 km in Titan's upper atmosphere and through three body–association reactions of carbon radicals near 750 km. INMS measurements (Fig. 2 and Tables 1 and 2) provide a direct means of evaluating high-altitude production pathways (Table 3). Although dissociation of methane and nitrogen is key to initiating the production of simple organic units (such as acetylene, ethylene, ethane, and hydrogen cyanide), ion-neutral chemistry must play a central role in linking these organic units together to form more complex organics, starting with benzene.

By untangling the complex hydrocarbon-nitrile mixture (*15*, *16*) that the INMS observes, we can estimate the chemical formation process for benzene using chemical schemes (Table 3) developed to understand the formation of soot on Earth (*6*–*8*, *13*, *14*) and PAHs in interstellar clouds (*17*). In the low-pressure regime found at ~1000 km, the ion-neutral formation pathway involving $C_4H_3^+$ and $C_4H_5^+$ is over five orders of magnitude faster than neutral reaction pathways acting through photochemical or energetic particle production of radical hydrocarbon species, such as C_2H. However, the photodissociation rate of benzene is large (>10^{-5} s^{-1}) and, when combined with the estimated ion-neutral production rate of 1×10^{-2} cm^{-3} s^{-1}, leads to the underestimation of the benzene concentration by about an order of magnitude. Potential solutions to this dilemma include (i) an unidentified benzene source at the altitude of observation, (ii) a stabilization or regeneration process that mitigates the photodissociation of benzene, or (iii) some combination of the two.

In addition to the measured benzene density profile (Fig. 1), independent evidence (*18*) indicates that the level at which molecular diffusion dominates turbulent mixing is over two scale heights below 1000 km. We calculate a transport lifetime based on the molecular diffusion coefficient (*14*) of 5×10^5 s, which is to be compared with the chemical loss lifetime of 1×10^5 s. Thus, the photodissociation pathway cannot be representative of the chemical lifetime. An alternative involves rapid regeneration of benzene after dissociation to the C_6H_5 or C_6H_4 radicals. Most of the obvious reactive pathways involving reactions with H_2, CH_4, C_2H_2, C_2H_4, or C_2H_6 have activation energies (*19*, *20*) that render these reactions ineffective in the low temperature (120 to 130 K) of Titan's atmosphere (near 1000 km) in high northern latitudes, whereas pathways that involve growth to more complex organics proceed with lower activation energies and therefore more rapid reaction rates. Therefore, we conclude that the

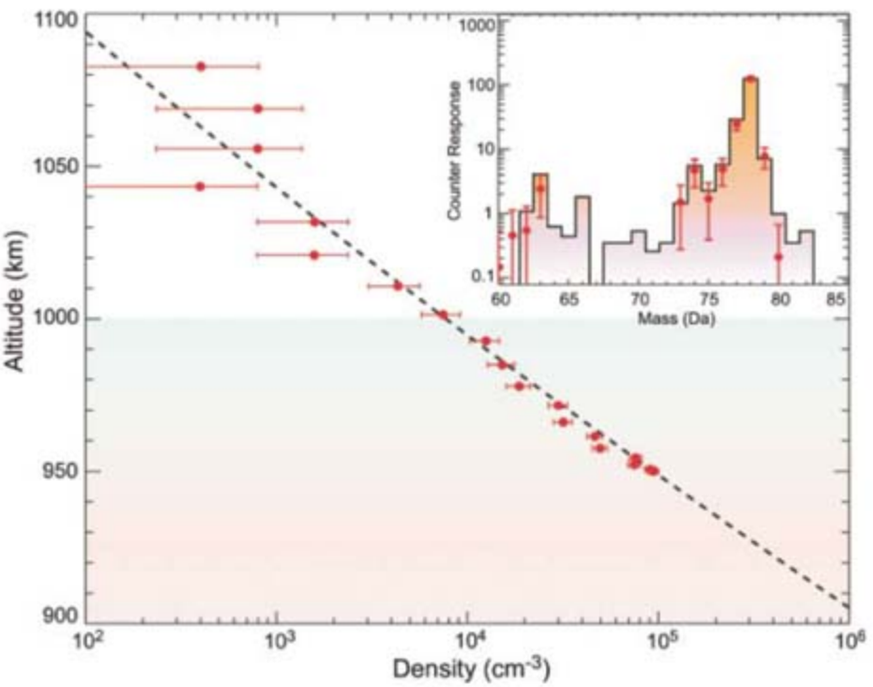

Fig. 1. INMS measurements of the altitude distribution of benzene during the T16 Titan encounter. Error bars indicate statistical uncertainty in counting rates. The dashed line is an exponential fit to the data, indicating the molecular diffusive scale height of a molecule the mass of benzene in Titan's atmosphere. Data below 1000 km (blue region) were averaged to produce the mass spectrum shown in the inset. (**Inset**) Fits to the benzene mass spectrum with the use of recent INMS calibration values are shown, along with estimated uncertainty (error bars).

ultimate fate of benzene dissociation is the production of higher-order PAHs and that diffusive mixing inferred from the observed altitude distribution requires a loss rate through photodissociation that is an order of magnitude slower than present measurements and theories suggest [for rates used, see (*21*); see also (*22*) and, for dissociation products, (*23*–*25*)]. Indeed, this is consistent with the measured benzene concentration based on our present inferences of chemical production rates. Model calculations (*14*) suggest that production at smaller solar-illumination angles rises at a rate that compensates for increased losses from photodissociation, and therefore the benzene concentration may remain the same in the illuminated upper atmosphere (T17 in Tables 1 and 2). Our present observations thus leave open the questions of missing benzene production mechanisms and stabilization of the "hot" benzene formed through photodissociation.

Our data show that the key chemical role of benzene-PAH formation begins at high altitudes. CAPS IBS measurements (Fig. 3A) allow us to tentatively infer the existence of higher-order PAH ions associated with higher-order PAHs, such as naphthalene (~130 daltons) and anthracene (~170 daltons). Furthermore, comparison of measured densities with the saturation vapor pressure (*26*) shows that benzene and hydrogen cyanide are near saturation vapor pressure and that diacetylene, naphthalene, and anthracene are highly supersaturated at 125 K (Table 1). This comparison is reinforced by the tentative identification of ions associated with the anthracene dimer near 340 daltons as measured by the IBS. The decreasing density of the intervening species between 170 and 340 daltons suggests a competition between chemistry and physical condensation processes. Dimer formation is the first step in condensation in the free molecular flow regime, where bimolecular reactions dominate the condensation formation process (*27*) and competing condensation and chemical kinetics are a hallmark of existing soot formation models (*6*–*8*). From the measured ion densities, we infer the relative rate of condensation to be one-tenth that of chemical processes. We also estimate a production rate (>1×10^{-16} g cm^{-2} s^{-1}) for formation of more complex PAH-nitrile compounds from benzene.

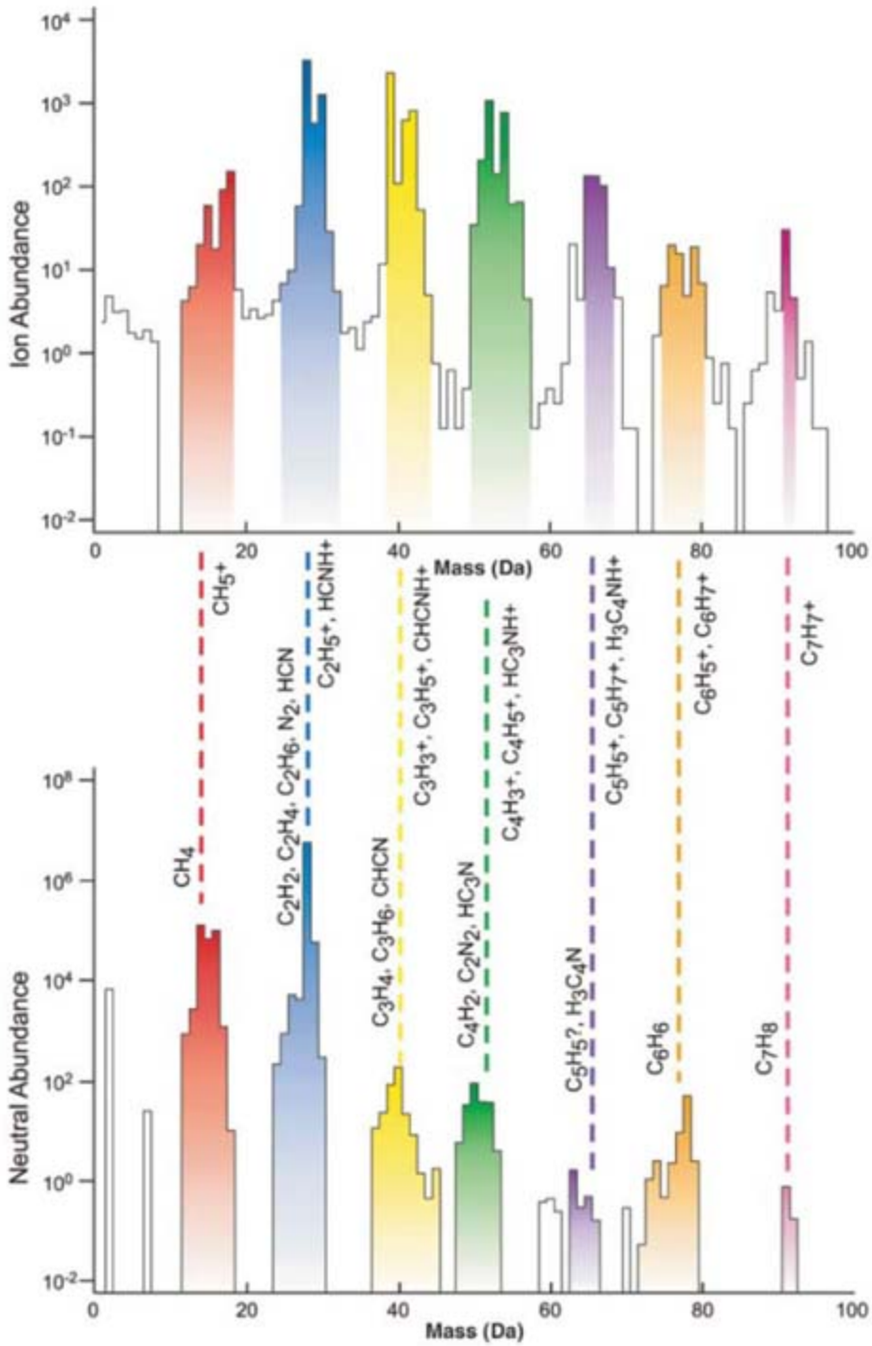

Fig. 2. Correspondence of ion (**upper**) and neutral (**lower**) mass spectra measured by INMS during T19 between 950 and 1000 km. Benzene molecules and their ion counterpart can be identified at 78 and 79 daltons in the spectra. High-pressure background in the ion source has been subtracted from the neutral spectrum.

The final step in the tholin formation process is aggregation of higher-order PAH-nitrile compounds that lead to negative ions. Negative ion formation is expected as a result of the tendency of complex PAHs and cyanoaromatics (*28*, *29*) to have electron affinities that range between 2 and 5 eV. Our observations of ions with mass/charge (amu per atomic charge e) between 1000 and 8000 daltons (Fig. 4) suggest that this is indeed occurring. Under the conditions at ~1000 km (T_e = ~125 K and n_e = ~10^9 m^{-3}, where T_e is electron temperature and n_e is electron density), small dust grains immersed in a plasma will charge negatively to a potential (*30*) $\varphi \sim -2.5$ kT/e ~ −0.027 V with a charge $Q = 4\pi\varepsilon_0 a \varphi \exp(-a/\lambda_D)$, where ε_0 is the permittivity of free space, a is the particle radius, and λ_D is Debye length. If we assume the ions are singularly charged with a density of 1×10^{-3} kg m^{-3}, then the particle radius lies between 75 and 150 nm. Because we cannot measure charge independently, the ion mass may actually be much larger. A particle with mass/charge of 8000 daltons, an assumed density of 1×10^{-3} kg m^{-3}, and Q = 5e has a mass of 40,000 amu and a radius of 260 nm. These particles are clearly the size of aerosols that, because of the chemical processes taking place around them, we identify as tholins. Particles of this size are gravitationally bound to Titan and will tend to sink into the lower atmosphere, where they are indeed found (*3*, *4*). The interactions of these charged tholins with ambipolar (*31*) and induced corotational (*31*) electric fields remain to be investigated. Depending on the influence of the electric fields, the charged tholins may descend into the stratosphere or escape Titan's atmosphere altogether.

Other instrumentation aboard the Cassini spacecraft is providing corroborating evidence of high-altitude aerosols. The Cassini Ultraviolet Spectrometer (UVIS) has recently observed aero-

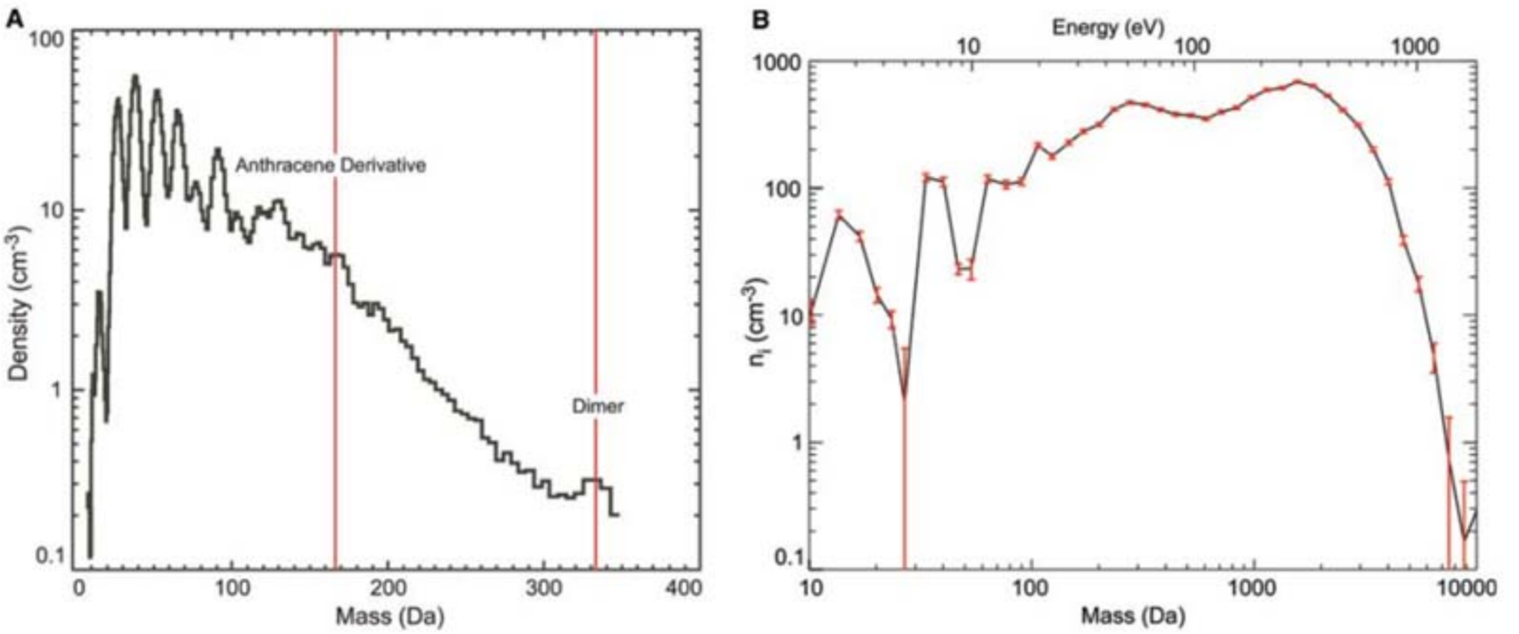

Fig. 3. (**A**) Positive ion spectrum from 1 to 350 daltons inferred from energy/charge measurements made by the CAPS IBS near 1000 km during the T18 encounter. There is a change in slope of the ion abundance near 170 daltons and a change in the appearance of peaks near 170 and 340 daltons. These appear to be an indication of the onset of condensation of the complex carbon-nitrogen aromatics. (**B**) Negative ion (n_i) spectrum from 10 to 10,000 daltons inferred from energy/charge measurements made by the CAPS ELS near 1000 km during the T16 encounter. Error bars indicate uncertainty in the number density.

Table 3. The primary ion and neutral chemical reactions in Titan's atmosphere at ~1000 km (*37*–*40*). *k*, chemical rate coefficient; *hυ*, photonic energy; -, not measured. The asterisk indicates that the reaction occurs at 125 K.

Formation of	Relevant reaction(s)	*k* ($cm^3\ s^{-1}$)
$C_4H_3^+$	$C_4H_2 + C_2H_5^+$, $HCNH^+$, $CH_5^+ \rightarrow C_4H_3^+ +$ products	-
$C_4H_5^+$	$C_2H_2 + C_2H_5^+ \rightarrow C_4H_5^+ + H_2$	-
$C_6H_7^+$	1. $C_4H_5^+ + C_2H_4 \rightarrow C_6H_7^+ + H_2$	7.3×10^{-11}
	2. $C_4H_3^+ + C_2H_4 \rightarrow C_6H_5^+ + H_2$	1.2×10^{-10}
	(followed by) $C_6H_5^+ + H_2 \rightarrow C_6H_7^+ + h\upsilon$	3.0×10^{-11}
	(or) $C_6H_5^+ + C_2H_4 \rightarrow C_6H_7^+ + C_2H_2$	1.7×10^{-11}
	(which competes with) $C_6H_5^+ + CH_4 \rightarrow C_7H_7^+ + H_2$	7.5×10^{-11}
	(which recombines to form benzene) $C_6H_7^+ + e \rightarrow C_6H_6 + H$	1.5×10^{-6}*

sols at an altitude of 1000 km (*32*). They suggest that Mie scattering from particles with radii of 12.5 nm with number densities of ~50 cm^{-3} provides an adequate explanation of the data. The size that UVIS infers for the aerosols is to be compared to the mass/charge group detected at 8000 daltons by the CAPS ELS. Each of these particles is interpreted as having a mass of 40,000 amu, a density of 1×10^{-3} kg m^{-3}, and a size of 260 nm. However, the CAPS-inferred densities are lower than those acquired by the UVIS, albeit at a very different time and place.

Benzene and higher-order PAH production at high altitudes is indicative of additional complex chemistry involved in the growth of tholins at lower, stratospheric altitudes. Evidence identifying the existence of benzene in the troposphere (*33*) and stratosphere (*4*) also suggests that benzene plays a major role in the growth of tholins throughout the atmosphere. Benzene has been observed to vary with latitude in the stratosphere, with mixing ratios of 5×10^{-10} in the south and a maximum of 3×10^{-9} in the north at 75°N (*4*). Low temperatures (120 to 130 K) measured at high northern latitudes in the upper atmosphere near 1000 km result in near saturation pressures for benzene and hydrogen cyanide and highly supersaturated conditions for diacetylene, naphthalene, and anthracene (*26*). This promotes rapid tholin growth through heterogeneous condensation (*27*) and internal particulate chemistry (*6*–*8*, *17*, *27*) and leads to a transfer of benzene and other organics from the gas phase to the surface of the tholins. The loss of benzene and other compounds through condensation onto the nascent tholin may account for the observation that benzene mixing ratios observed in the thermosphere are more than four orders of magnitude larger than those in the stratosphere.

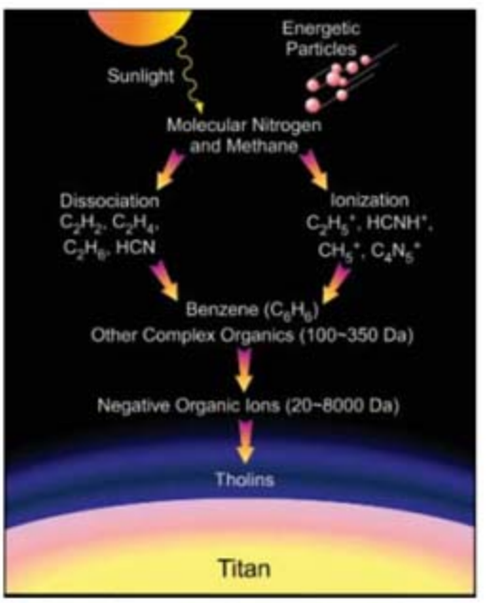

Fig. 4. Cartoon showing the chemical process leading up to the formation of tholins in Titan's upper atmosphere. The process begins with free energy from solar UV radiation and energetic particles impinging on Titan's atmosphere. The most abundant constituents (CH_4 and N_2) combine through a number of reaction pathways to form larger organic and nitrile compounds (100 to 350 daltons) that eventually lead to the formation of negatively charged tholin aerosols (20 to 8000 daltons) observed at ~1000 km.

We have presented data from three Cassini particle spectrometers that indicate that a complex ion-neutral chemistry in Titan's atmosphere near 1000 km plays a major role in the formation

of progressively more complex hydrocarbon molecules, from benzene to PAHs and ultimately to aerosol particles with ~260-nm radii. The existence of ~40,000-amu aerosols, formed by the growth of complex organic compounds in the upper atmosphere, appears to answer the long-unresolved question of the origin of tholin precursors found at Titan. The chain of molecular growth that we have identified in this study is similar to that first identified in the Miller-Urey experiments (*3*). We suspect that the ultimate destination of these large organic molecules and aerosols lies in the organic haze layers in Titan's stratosphere (*3*, *4*). However, depending on the dynamic effects of atmospheric and induced corotational electric fields on these particles, they might also escape Titan's atmosphere to become the source of PAHs observed to collect on the surfaces of Saturn's icy moons (*34*, *35*).

References and Notes

1. R. V. Yelle *et al.*, *Icarus* **72**, 468 (2006).
2. Y. L. Yung, M. Allen, J. P. Pinto, *Astrophys. J. Suppl. Ser.* **55**, 465 (1984).
3. C. Sagan, B. N. Khare, *Nature* **277**, 102 (1979).
4. C. P. McKay *et al.*, *Planet. Space Sci.* **49**, 79 (2001).
5. A. Coustenis *et al.*, *Icarus*, in press; available online at http://dx.doi.org/10.1016/j.icarus.2006.12.022.
6. H. Richter, J. B. Howard, *Prog. Energy Combust. Sci.* **26**, 565 (2000).
7. H. F. Calcote, D. G. Keil, *Pure Appl. Chem.* **62**, 815 (1990).
8. M. Frenklach, *Phys. Chem. Chem. Phys.* **4**, 2028 (2002).
9. A. A. Pavlov, M. T. Hurtgen, J. F. Kasting, M. A. Arthur, *Geology* **31**, 87 (2003).
10. J. H. Waite Jr. *et al.*, *Science* **308**, 982 (2005).
11. D. T. Young *et al.*, *Space Sci. Rev.* **114**, 1 (2004).
12. A. J. Coates *et al.*, *Eos Trans. Am. Geophys. Union* **87** (fall meeting suppl.), 52, abstract P21B-06 (2006).
13. E. H. Wilson, S. K. Atreya, A. Coustenis, *J. Geophys. Res. (Planets)* **108**, 5014 (2003).
14. V. De La Haye, thesis, University of Michigan, Ann Arbor, MI (2005).
15. T. E. Cravens *et al.*, *Geophys. Res. Lett.* **32**, L12108 (2005).
16. V. Vuitton, R. V. Yelle, V. G. Anicich, *Astrophys. J.* **647**, L175 (2006).
17. D. K. Bohme, *Chem. Rev.* **92**, 1487 (1992).
18. All minor neutral constituents (with the exception of methane) show molecular diffusive scale heights at our lowest altitude on T16, most notably the inert species ^{40}Ar. We can use the mixing ratio of ^{40}Ar measured in the lower atmosphere by the Huygens Gas Chromatograph Mass Spectrometer [4.32×10^{-5} (*33*)] and the ^{40}Ar mixing ratio measured by the INMS on T16 at 975 km of $1.46 \times 10^{-5} \pm 0.14 \times 10^{-5}$ to infer that the homopause or turbulent mixing boundary lies ~110 km below our observation point (865 ± 25 km), where the altitude uncertainty represents uncertainties in the atmospheric temperature profile and the mixing ratio of ^{40}Ar. The lack of compliance of methane with a molecular diffusive scale height has been suggested as due to outflow (*1*, *2*).
19. National Institute of Standards and Technology (NIST) Chemical Kinetics Database (www.kinetics.nist.gov/kinetics/index.jsp).
20. I. V. Tokmakov *et al.*, *J. Phys. Chem. A* **103**, 3636 (1999).
21. J. Crovisier, *J. Geophys. Res.* **99**, 3777 (1994).
22. J. I. Moses *et al.*, *J. Geophys. Res.* **110**, e08001 (2005).
23. A. Yokoyama *et al.*, *J. Chem. Phys.* **92**, 4222 (1990).
24. K. Shindo, S. Lipsky, *J. Chem. Phys.* **45**, 2292 (1966).
25. N. Nakashima, Y. Keitaro, *J. Chem. Phys.* **79**, 2727 (1983).
26. We calculated vapor pressure (P) values using the Antoine equation [$\log P = A - B/(T + C)$] and the parameters A, B, and C using experimental data in a specific temperature (T) range. The extrapolation of these data by means of the Antoine equation to lower temperatures has been verified with the use of benzene and methane data. We performed a verification by producing a test case where the Antoine equation fit was produced using only the high-temperature values, which we then compared with the experimental low-temperature data. Our test case shows a maximum uncertainty of one decade at the extreme low temperatures (less than 100 K) and, at 130 K, the extrapolated data differ by a factor of five. The parameters A, B, and C are obtained from (*36*).
27. A. J. Friedson, A.-S. Wong, Y. L. Yung, *Icarus* **158**, 389 (2002).
28. T. Moustefaoui *et al.*, *Faraday Discuss. Chem. Soc.* **109**, 71 (1998).
29. X. Zhang *et al.*, *Chem. Commun.* **2006**, 758 (2006).
30. C. K. Goetz, *Rev. Geophys.* **27**, 271 (1989).
31. M. G. Kivelson, C. T. Russell, Eds. *Introduction to Space Physics* (Cambridge Univ. Press, Cambridge, 1995).
32. M.-C. Liang, Y. L. Yung, D. E. Shemansky, paper presented at the 38th Annual Meeting of the Division of Planetary Sciences, American Astronomical Society, Pasadena, CA, 8 to 13 October 2006.
33. H. B. Niemann *et al.*, *Nature* **438**, 779 (2005).
34. D. P. Cruikshank *et al.*, *Icarus*, in press.
35. R. N. Clark *et al.*, *EOS Trans. Am. Geophys. Union*, **87** (fall meeting suppl.), abstract P32A-03 (2006).
36. P. J. Linstrom, W. G. Mallard, Eds. *The National Institute of Standards and Technology Chemistry WebBook* (NIST Standard Reference Database Number 69, June 2005 release); (http://webbook.nist.gov/chemistry/).
37. J. L. McLain, V. Poterya, C. D. Molek, L. M. Babcock, N. G. Adams, *J. Phys. Chem. A* **108**, 6704 (2004).
38. V. G. Anicich, "An index of the literature for bi-molecular gas-phase-cation-molecule reaction kinetics" (NASA Jet Propulsion Laboratory, JPL Publication 03-19, Pasadena, CA, 2003).
39. V. G. Anicich, M. McEwan, *Planet. Space Sci.* **45**, 897 (1997).
40. V. G. Anicich, P. F. Wilson, M. J. McEwan, *J. Am. Soc. Mass Spectrom.* **17**, 544 (2006).

41. We thank NASA for its continuing support of operations and data analysis from the Cassini mission and A.J.C. thanks the Science and Technology Facilities Council for support of ELS. The INMS and CAPS teams acknowledge support from NASA and the Jet Propulsion Laboratory (SWRI subcontract numbers 1283095 and 1243218, respectively), as well as the support of their respective science and operations teams. J.H.W. acknowledges numerous helpful discussions with G. R. Gladstone, and A.J.C. acknowledges help with the data analysis from G. R. Lewis.

9 January 2007; accepted 26 March 2007
10.1126/science.1139727

The Orientation of the Local Interstellar Magnetic Field

M. Opher,[1]* E. C. Stone,[2] T. I. Gombosi[3]

The orientation of the local interstellar magnetic field introduces asymmetries in the heliosphere that affect the location of heliospheric radio emissions and the streaming direction of ions from the termination shock of the solar wind. We combined observations of radio emissions and energetic particle streaming with extensive three-dimensional magnetohydrodynamic computer simulations of magnetic field draping over the heliopause to show that the plane of the local interstellar field is ~60° to 90° from the galactic plane. This finding suggests that the field orientation in the Local Interstellar Cloud differs from that of a larger-scale interstellar magnetic field thought to parallel the galactic plane.

The heliosphere created by the supersonic solar wind is compressed by the motion of the Sun relative to the local interstellar medium, producing a comet-like shape with an extended tail. The solar wind abruptly slows, forming a termination shock as it approaches contact with the interstellar medium at the heliopause. Beyond the heliopause, the interstellar wind contains mainly hydrogen and helium, both as neutral atoms and as ions that carry the frozen-in interstellar magnetic field.

Recent Voyager observations of ions streaming from the termination shock (*1*, *2*) have led to the suggestion that north-south and east-west asymmetries of the heliosphere are induced by the interstellar magnetic field (*3*). However, the inferred field direction from the model of (*3*) was parallel to the hydrogen deflection plane (HDP) rather than the galactic plane (GAL). On the basis of the polarization of light from nearby stars, Frisch (*4*, *5*) suggested that the galactic magnetic field is parallel to the GAL. However, the direction of the galactic magnetic field is deduced from measurements averaged over a much larger distance (light-years). A direction parallel to the HDP was suggested by Lallement *et al.* (*6*) for the local interstellar field, on the basis of solar Lyman-α radiation that is resonantly backscattered by interstellar hydrogen atoms. The HDP is tilted from the ecliptic plane by 60° and differs from the GAL by 60°. We used Voyager 1 and 2 observations in conjunction with a magnetohydrodynamic model to discriminate between these two planes and to constrain the orientation of the local interstellar magnetic field.

[1]Department of Physics and Astronomy, George Mason University, 4400 University Drive, Fairfax, VA 22030, USA. [2]California Institute of Technology, Pasadena, CA 91125, USA. [3]Center for Space Environment Modeling, University of Michigan, Ann Arbor, MI 48109, USA.

*To whom correspondence should be addressed. E-mail: mopher@physics.gmu.edu

In the past 20 years, Voyager 1 (V1) and 2 (V2) have been detecting radio emissions in the outer heliosphere at frequencies from 2 to 3 kHz (*7*–*9*). The radio emissions were detected each solar cycle: first in 1983–1984 during solar cycle 21 (*7*), second in 1992–1994 during solar cycle 22 (*8*), and most recently during solar cycle 23 (*9*). The currently accepted scenario is that the radio emissions are generated when a strong interplanetary shock produced by a period of intense solar activity reaches the vicinity of the heliopause and moves into the interstellar plasma beyond (*9*, *10*). Radio direction-finding measurements from V1 and V2 have been used to determine the positions near the heliopause at which the radio emissions are generated (*11*) (Fig. 1). The sources lie along a line that passes near the nose of the heliosphere that roughly parallels the GAL. The GAL is 120° from the ecliptic plane (*12*). Because the galactic magnetic field is oriented nearly parallel to the GAL, Kurth and Gurnett (*11*) suggested that the local interstellar magnetic field (in the local neighborhood of the Sun) was also parallel to the GAL.

However, Gurnett *et al.* (*13*) recently pointed out that at Earth's bow shock and interplanetary shocks, the radio emission occurs where the magnetic field lines are tangential to the shock surface, and they suggested that heliospheric radio emissions occur where the local interstellar magnetic field is tangential to the surface of the shock that excites the plasma (or $\mathbf{B}\cdot\mathbf{n} = 0$, where $\mathbf{B}$ is the magnetic field and $\mathbf{n}$ is the shock normal). They concluded that the condition $\mathbf{B}\cdot\mathbf{n} = 0$, combined with the source location observed by the two Voyager spacecraft, implies that the local interstellar magnetic field is perpendicular to the GAL. This direction differs from the earlier suggestion (*9*) and is within 16° of the HDP.

The interstellar magnetic field is frozen into interstellar plasma that is deflected around the heliopause, causing the field to drape over the heliopause. As a result, the region where $\mathbf{B}\cdot\mathbf{n} = 0$ will depend on the shape of the heliopause, which is distorted by pressure of the local interstellar magnetic field. For intensities around a few microgauss, the ambient interstellar magnetic pressure is comparable to the gas pressure, with the magnetic pressure increasing in those regions where the interstellar flow decreases as it approaches the heliopause. We investigated how the proposed location of the radio sources (where $\mathbf{B}\cdot\mathbf{n} = 0$ on the surface of the heliopause) varies with the orientation and strength of the local interstellar magnetic field.

We considered several directions of the interstellar magnetic field—the HDP, the GAL, and the plane perpendicular to the radio source plane (*13*) (PPG)—with different inclination angles α (the angle between the interstellar magnetic field and interstellar wind velocity). In the model coordinate system, where β is the angle between the interstellar magnetic field and the solar equator, the HDP corresponds to $\beta = 60°$, the GAL to $\beta = 120°$, and the PPG to $\beta = 44°$ (*12*). Assuming a spherical interplanetary shock,

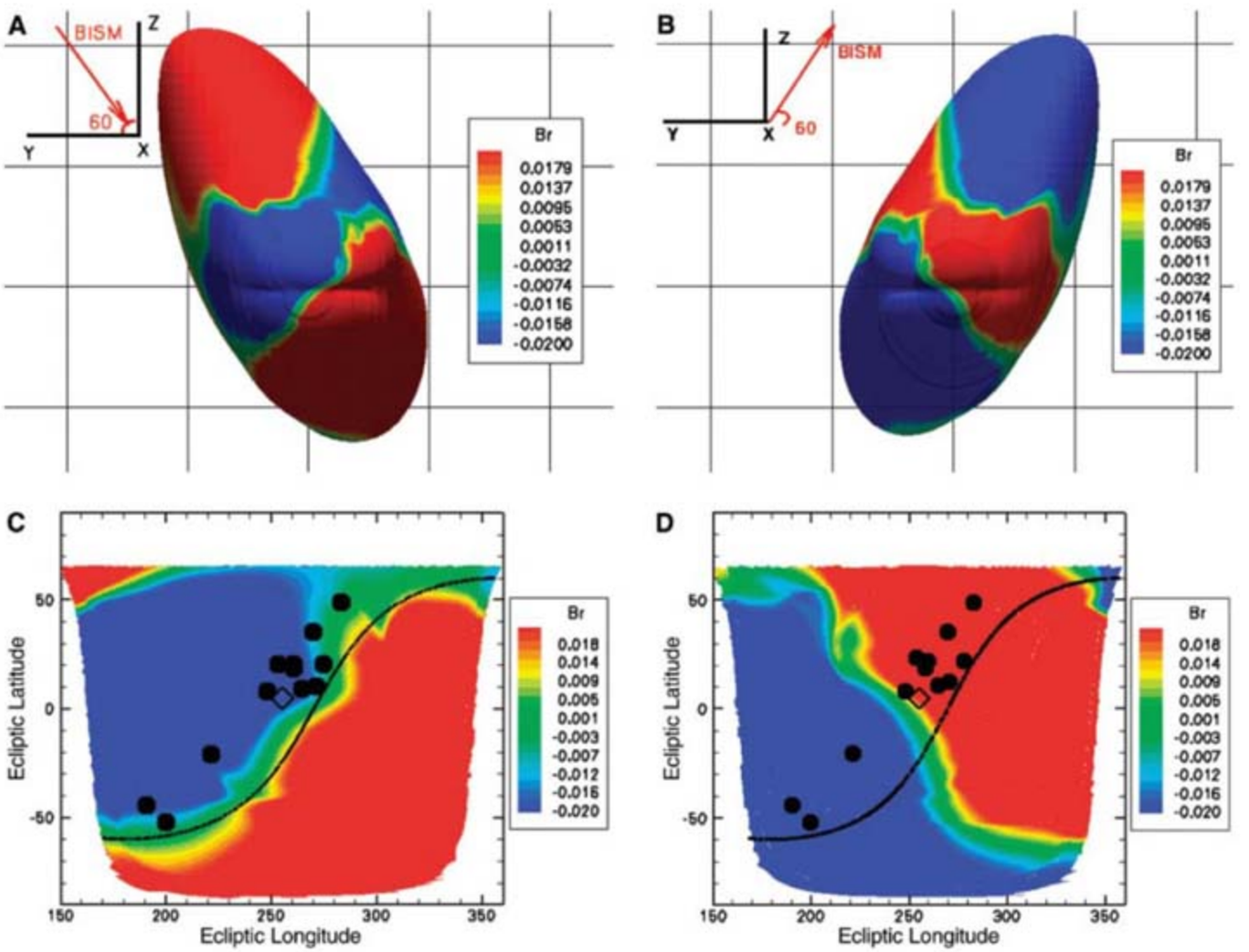

Fig. 1. (**A** and **B**) Radio source location as a function of the interstellar magnetic field (B_{ISM}) direction in (A) the HDP plane and (B) the GAL plane (with $\alpha = 45°$). The surface of the heliopause is shown from upwind with respect to the interstellar wind. The isocontours show the strength of the radial component of the interstellar magnetic field, B_r, on the heliopause. The green band is the location of the radio sources (at $B_r = 0$). The red arrows show the direction of B_{ISM}. (**C** and **D**) Same as (A) and (B) but converted to ecliptic coordinates for B_{ISM} in (C) the PPG (with $\alpha = 30°$) and (D) the GAL (with $\alpha = 45°$). The direction of the nose of the heliosphere (diamond) and the GAL (black line) are indicated for reference. The radio sources detected by V1 and V2 are shown as solid circles. Note that the colors are inverted from (C) to (D) because the interstellar magnetic direction was inverted from (A) to (B) (see red vectors in the insets).

the tangential field condition for the radio sources translates to $B_r = 0$, where B_r is the radial component of the interstellar magnetic field. For each modeled direction of the interstellar magnetic field, we compared the expected location of the radio sources ($B_r = 0$ at the heliopause) with the observed location of the radio sources detected by V1 and V2.

The model used here is the same as used by (*3*) [see (*12*)]. The interstellar magnetic field (B_{ISM}) magnitude is taken to be $B_{ISM} = 1.8$ μG [with the y component of B_{ISM} ($B_{ISM,y}$) < 0]. The coordinate system has the interstellar velocity direction in the $+x$ direction and the z axis as the solar rotation axis of the Sun, with y completing the right-handed coordinate system. In this coordinate system, V1 is at 29.1° latitude and 213.4° longitude and V2 is at –31.2° latitude and 178.4° longitude, which ignores the 7.25° tilt of the solar equator with respect to the ecliptic plane.

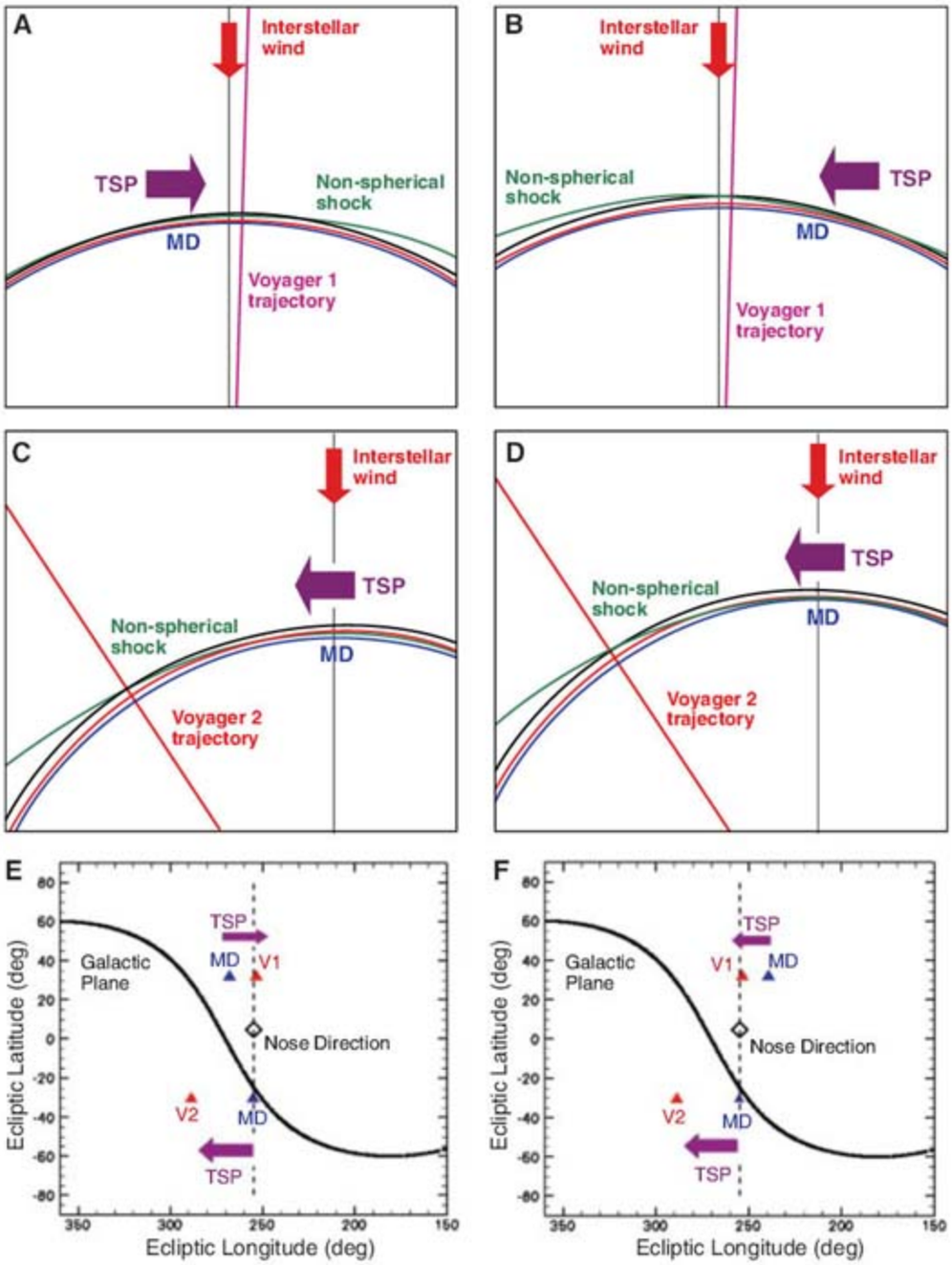

Fig. 2. (**A** and **B**) Streaming of TSPs from the MD point to V1 for the interstellar magnetic field in (A) the HDP (with $\alpha = 45°$) and (B) the GAL (with $\alpha = 45°$). The interplanetary magnetic field is carried radially outward by the solar wind, forming a spiral on a conical surface. The conical surfaces coinciding with the V1 trajectory are shown. V1 is first connected to the shock along the spiral magnetic field lines that contact the shock at the MD point. The solar magnetic field lines that intersect V1 are colored as follows: black, the 0 AU field line intersecting the shock where V1 crosses the shock; red and blue, magnetic field lines 2.0 AU and 3.0 AU upwind, respectively, from the 0 AU line; green, the nonspherical termination shock. The magenta arrow indicates the streaming direction of the TSPs from the shock along the field line to V1. (**C** and **D**) Similar plots for V2, showing field lines 3.0 AU (red) and 5.0 AU (blue) upwind of the 0 AU line. Note that in both views the solar magnetic field spirals clockwise with increasing distance outward. (**E** and **F**) Summary of the streaming of TSPs from the MD point back to V1 and V2. The nose direction (diamond) and the GAL are indicated.

Figure 1 indicates that the heliopause is strongly influenced by the interstellar magnetic field direction; the heliopause is asymmetric both north-south and east-west and has a plane of symmetry approximately parallel to the plane of the local interstellar magnetic field. As a result, the heliopause surfaces for HDP and GAL field orientations are almost mirror images of each other.

With B_{ISM} parallel to the GAL (with $\alpha = 45°$, Fig. 1D), the region where $B_r = 0$ is almost perpendicular to the GAL, which is inconsistent with the radio observations. With B_{ISM} in the PPG with $\alpha = 30°$ (Fig. 1C) produces the best agreement with the Voyager radio observations, as suggested by Gurnett *et al.* (*13*). The HDP orientation differs from that of PPG by only 16° and is also in general agreement, as suggested by the similarity of the regions with $B_r = 0$ in Fig. 1A (HDP) and Fig. 1C (PPG). The offset of ~15° between the observations and the region with $B_r = 0$ for the model in best agreement (Fig. 1C) indicates that the accuracy of the model is not adequate to distinguish between the PPG and HDP field orientations.

We also investigated the effects of changing the interstellar wind direction to 5° above the ecliptic plane [in the solar ecliptic coordinate system, the interstellar wind direction is 255° (longitude) and 5° (latitude)] and changing the intensity of B_{ISM} from 1.8 μG to 2.5 μG. For both cases, the change in the predicted location of radio sources was minor (*12*). As α increases from 15° to 60°, the $B_r = 0$ band moves counterclockwise, with the best agreement for $\alpha = 30°$ to 45° (*12*).

The second set of observational data that we used to constrain the orientation of the local interstellar magnetic field was the streaming ions from the termination shock. V1 crossed the termination shock at 94 AU in December 2004 and is now beyond 100 AU in the heliosheath (*1*, *2*, *14*). V2 is already detecting signs of the upcoming shock (*2*, *15*) and is expected to cross the termination shock within the next 1 to 2 years. In mid-2002, V1 began observing enhanced intensities of ions streaming from the shock (*16*, *17*). The beams of energetic termination shock particles (TSPs) were streaming outward along the solar spiral magnetic field. The strong upstream TSP beams were observed much of the time until V1 crossed the shock at 94 AU. The streaming along the magnetic field upstream of the shock source was expected to be inward along the spiral field if the termination shock were spherical. However, the observed flow was outward along the field, requiring a shock source located inward along the spiral field several AU closer to the Sun than is V1. With a nonspherical shock, V1 could be connected to the termination shock along magnetic field lines that crossed the termination shock and crossed back to the supersonic solar wind. This led to the suggestion that the upstream

beaming resulted from a blunt (*18*) or asymmetric shock (*2*). The asymmetric shock could result from an interstellar magnetic field inclined in a particular direction (*19*, *20*). In a recent report (*3*), we showed that an interstellar magnetic field in the HDP could distort the termination shock in a direction that explains the TSPs streaming outward at V1.

Figure 2 shows that for B_{ISM} parallel to the HDP, the longitude of the MD point (the minimum radial distance of the termination shock to the Sun) is greater than the longitude of V1, so the TSPs will stream outward along the spiral field. In the heliospheric southern hemisphere the longitude of V2 is greater than that of the MD point of the shock, so the TSPs will stream inward toward V2, as is observed. However, for B_{ISM} parallel to the GAL, the MD in the northern hemisphere shifts to a smaller longitude than V1, so that the TSPs would stream inward toward V1, opposite to what is observed.

In this calculation we did not include the neutral hydrogen atoms that interact with the ionized component by charge exchange. Although the inclusion of the neutral atoms will tend to symmetrize the solution and quantitatively affect the degree of asymmetry, the general character of the asymmetry is expected to remain the same, with the plane of symmetry of the distorted heliopause determined by the plane of the local interstellar magnetic field (*21*, *22*). Thus, it would be expected that different orientations of the local interstellar magnetic field would result in the same qualitative differences in the predicted radio source locations and streaming directions of upstream ions as described here. On the basis of those differences, and assuming that the source of radio emission is the region where the field draped on the heliopause is perpendicular to the radial direction, we find from Voyager observations that the plane of the local interstellar magnetic field is not parallel to the GAL but is 60° to 90° from that plane (rotated clockwise from a view from the Sun). This suggests that the field orientation in the Local Interstellar Cloud differs from that of a larger-scale interstellar magnetic field thought to parallel the GAL.

References and Notes

1. R. B. Decker *et al.*, *Science* **309**, 2020 (2005).
2. E. C. Stone *et al.*, *Science* **309**, 2017 (2005).
3. M. Opher, E. C. Stone, P. C. Liewer, *Astrophys. J.* **640**, L71 (2006).
4. P. C. Frisch, in *Physics of the Outer Heliosphere: Proceedings of the 1st COSPAR Colloquium* (Pergamon, Oxford, UK, 1990), pp. 19–28.
5. P. C. Frisch, *Space Sci. Rev.* **78**, 213 (1996).
6. R. Lallement *et al.*, *Science* **307**, 1447 (2005).
7. W. S. Kurth, D. A. Gurnett, F. L. Scarf, R. L. Poynter, *Nature* **312**, 27 (1984).
8. D. A. Gurnett, W. S. Kurth, S. C. Allendorf, R. L. Poynter, *Science* **262**, 199 (1993).
9. D. A. Gurnett, W. S. Kurth, E. C. Stone, *Geophys. Res. Lett.* **30**, 10.1029/2003GL018514 (2003).
10. D. A. Gurnett, W. S. Kurth, *Adv. Space Sci.* **16**, 279 (1995).
11. W. S. Kurth, D. A. Gurnett, *J. Geophys. Res.* **108**, 10.1029/2003JA009860 (2003).
12. See supporting material on *Science* Online.
13. D. A. Gurnett, W. S. Kurth, I. H. Cairns, J. Mitchell, *AIP Conf. Proc.* **858**, 129 (2006).
14. L. F. Burlaga *et al.*, *Science* **309**, 2027 (2005).
15. A. C. Cummings *et al.*, American Geophysical Union, Fall Meeting 2005, abstract SH51A-1184 (2005).
16. F. B. McDonald *et al.*, *Nature* **426**, 48 (2003).
17. S. M. Krimigis *et al.*, *Nature* **426**, 45 (2003).
18. J. R. Jokipii, J. Giacalone, J. Kota, *Astrophys. J.* **611**, L141 (2004).
19. R. Ratkiewicz *et al.*, *Astron. Astrophys.* **335**, 363 (1998).
20. N. V. Pogorelov, T. Matsuda, *J. Geophys. Res.* **103**, 237 (1998).
21. N. V. Pogorelov, G. P. Zank, *Astrophys. J.* **636**, L161 (2006).
22. V. Izmodenov, D. Alexashov, A. Myasnikov, *Astron. Astrophys.* **437**, L35 (2005).

23. We thank the staff at NASA Ames Research Center for the use of the Columbia supercomputer.

Supporting Online Material

www.sciencemag.org/cgi/content/full/316/5826/875/DC1
SOM Text
Figs. S1 to S4
References

3 January 2007; accepted 27 March 2007
10.1126/science.1139480

Ultralow Friction of Carbonate Faults Caused by Thermal Decomposition

Raehee Han,[1]* Toshihiko Shimamoto,[2]† Takehiro Hirose,[2]‡ Jin-Han Ree,[1] Jun-ichi Ando[3]

High-velocity weakening of faults may drive fault motion during large earthquakes. Experiments on simulated faults in Carrara marble at slip rates up to 1.3 meters per second demonstrate that thermal decomposition of calcite due to frictional heating induces pronounced fault weakening with steady-state friction coefficients as low as 0.06. Decomposition produces particles of tens of nanometers in size, and the ultralow friction appears to be associated with the flash heating on an ultrafine decomposition product. Thus, thermal decomposition may be an important process for the dynamic weakening of faults.

The strength of seismogenic faults, which is frictional resistance to fault slip during earthquakes, has been a major subject of debate in fault mechanics for 30 years (*1*, *2*). Although the stress–heat flow paradox for the San Andreas fault (no heat-flow anomaly, contrary to the prediction from in situ stress measurement and laboratory data of rock friction) favors extremely low fault strength (*3*, *4*), reasons for the weakness have been unclear. Recent work has shown that the dynamic weakening of faults during seismic slip can be caused by mechanisms such as frictional melting (*5*–*9*), thermal pressurization (*10*–*13*), and silica-gel formation (*14*, *15*). Fault gouge was also shown to exhibit pronounced slip weakening at high slip rates (*16*), presumably because of flash heating (*13*). Some analyses have predicted that slip-weakening distance, over which the initial peak friction drops to steady-state dynamic friction (*8*, *12*), and fracture energy (*13*, *16*) are of the same order as those parameters that are determined seismologically, narrowing the gap between laboratory studies of fault mechanics and seismology. Modeling the generation of large earthquakes is now becoming possible on the basis of the measured mechanical and transport properties of fault zones. Moreover, the dynamic weakening of faults may explain the lack of heat-flow anomaly after earthquake events along the San Andreas fault.

Thermal decomposition of rock-forming minerals at high ambient temperature and pressure can dramatically lower the strength of rocks because of the buildup of pore fluid pressure and the associated reduction of effective normal stress, provided that the sample is effectively undrained (*17*). Even at shallow crustal levels with low ambient temperature, thermal decomposition may occur at an elevated temperature because of coseismic frictional heating along fault zones. We demonstrated that a carbonate fault can lose frictional strength almost completely because of the thermal decomposition of calcite caused by frictional heating during high-velocity friction experiments on Carrara marble at seismic slip rates.

Forty-two friction experiments were conducted on precut bare surfaces of a pair of solid cylindrical specimens of Carrara marble (~99% calcite) at room temperature and room humidity. The experiments were carried out at normal stresses of 1.1 to 13.4 MPa and at equivalent slip rates of 0.03 to 1.30 m s^{-1}, with a rotary-shear, high-velocity friction apparatus at Kyoto University (*18*). The diameter and length of the specimen were 21.8 to 24.8 mm and about 20 mm, respectively (*19*). Because there is a slip-rate gradient across the fault due to cylindrical specimen geometry, we use the term "equivalent slip rate" ("slip rate" or "velocity" hereafter) (*7*, *18*, *19*).

[1]Department of Earth and Environmental Sciences, Korea University, Seoul 136-701, South Korea. [2]Division of Earth and Planetary Sciences, Graduate School of Science, Kyoto University, Kyoto 606-8502, Japan. [3]Department of Earth and Planetary Systems Science, Hiroshima University, Higashi-Hiroshima 739-8526, Japan.

*To whom correspondence should be addressed. E-mail: rhhan@korea.ac.kr

†Present address: Department of Earth and Planetary Systems Science, Hiroshima University, Higashi-Hiroshima 734-8526, Japan.

‡Present address: Instituto Nazionale di Geofisica e Vulcanologia, 00143 Rome, Italy.

At different slip rates (Fig. 1A), the friction coefficient of the specimens decreased nearly exponentially from peak friction, μ_p, to nearly steady-state friction, μ_{ss} (*20*), with increasing displacement. The slip-weakening distance ranged from a few to several meters. The μ_{ss} decreased markedly from ~0.6 to a range of 0.04 to 0.11 with an increase in slip rate (Fig. 1B). A linear friction law holds for both peak and steady-state friction, yielding μ_p of 0.60 ± 0.01 and μ_{ss} of 0.06 ± 0.01 (Fig. 1C). This μ_p value is more or less typical for marble (0.4 to 0.8) from conventional slow slip-rate (<1 mm s^{-1}) experiments (*21*). But μ_{ss} at a high slip rate (1.1 to 1.2 m s^{-1}) was extremely low. In contrast, μ_{ss} values remained high (0.46 to 0.63) at slow slip rates (0.03 to 0.08 m s^{-1}).

Microstructural observations and electron probe microanalysis of deformed specimens were conducted on thin sections normal to the fault and parallel to the slip direction. We started experiments with precut surfaces of Carrara marble, but gouge zones formed very quickly on both sides of the slip surface, which nearly coincides with the precut surface (Fig. 2A). Samples were collected from the slip surface for observations with a field-emission scanning electron microscope (FE-SEM) and a transmission electron microscope (TEM) and for x-ray diffraction (XRD) analyses. Those analyses revealed that the gouge zone forms at a very early stage of displacement (<2 m), when the outer and inner zones of gouge consist of calcite and lime (CaO) and/or hydrated lime [$Ca(OH)_2$], respectively. In the host rock adjacent to the fault gouge, fracturing of calcite grains occurred, and the size of calcite fragments decreased toward the slip surface to become calcite gouge. Calcite thermally decomposes into lime and CO_2 gas at about 720 to 900°C (*22*, *23*), and the lime can be transformed to hydrated lime by absorbing moisture when it is exposed to the atmosphere. Thus, thermal decomposition of calcite occurred from a very early stage of slip.

Many fractures were present over a wide decomposition zone between the decomposition fronts (DFs) (Fig. 2A); those fractures must have increased permeability. The decomposed zone consisted of grainlike aggregates ranging from about 100 to a few hundred nanometers in diameter (Fig. 2B), but each aggregate was composed of ultrafine grains that were several to a few tens of nanometers in size (Fig. 2C and fig. S3). Calcite decomposition was confirmed in specimens at fast slip rates (>0.4 m s^{-1}), but no evidence of decomposition was present in a specimen deformed at a slow slip rate of 0.08 m s^{-1} (run number HVR522; compare XRD curves in Fig. 2D). We did not recognize glass or amorphous material in any of the specimens (fig. S3).

To determine the timing of decomposition with respect to the slip-weakening behavior, we measured the emission of CO_2 released from a deforming sample by using two solid electrolyte-type CO_2 sensors (*19*). Sensor 1 (without a filter) was set very close to the fault (about 30 mm

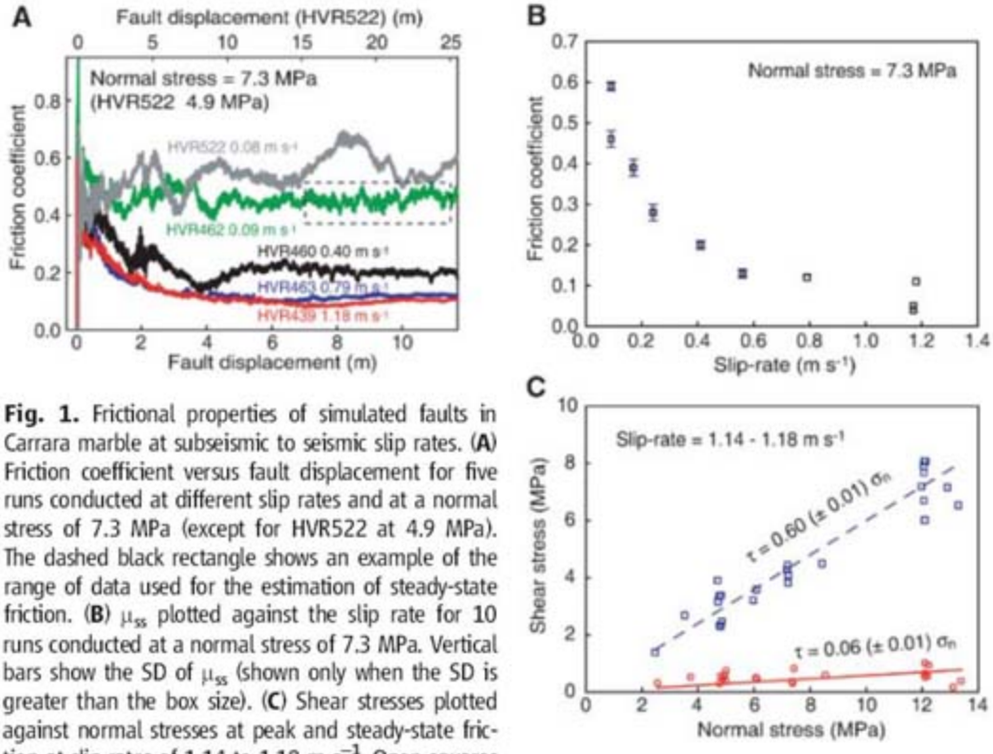

Fig. 1. Frictional properties of simulated faults in Carrara marble at subseismic to seismic slip rates. (**A**) Friction coefficient versus fault displacement for five runs conducted at different slip rates and at a normal stress of 7.3 MPa (except for HVR522 at 4.9 MPa). The dashed black rectangle shows an example of the range of data used for the estimation of steady-state friction. (**B**) μ_{ss} plotted against the slip rate for 10 runs conducted at a normal stress of 7.3 MPa. Vertical bars show the SD of μ_{ss} (shown only when the SD is greater than the box size). (**C**) Shear stresses plotted against normal stresses at peak and steady-state friction at slip rates of 1.14 to 1.18 m s^{-1}. Open squares and circles indicate initial peak friction and steady-state friction, respectively. The slopes of the lines give frictional coefficients at peak and steady-state friction. τ, shear stress; σ_n, normal stress.

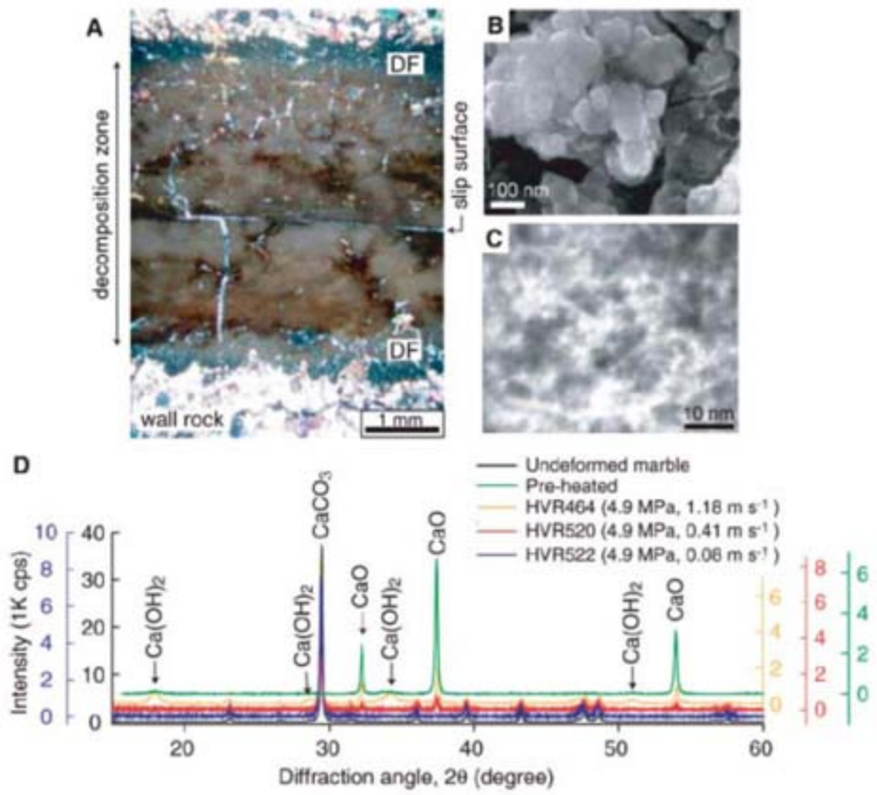

Fig. 2. Textures and decomposition products in fault zones. (**A**) A cross–polarized light photomicrograph of a thermally induced decomposition zone developed in Carrara marble, deformed at a slip rate of 1.30 m s^{-1} and at a normal stress of 4.6 MPa (HVR398, total slip = 125 m). DFs are between the wall rock and the decomposition zone. Slip was highly localized along the surface denoted by "slip surface." (**B** and **C**) SEM and TEM photomicrographs, respectively, illustrating microstructures of the lime (CaO) aggregates on the slip interface. (**D**) XRD spectra of an undeformed specimen, a preheated specimen, and specimens deformed at different conditions. Diffraction intensity is shown in 1000 × counts per second (cps) on all vertical axes.

away) to detect the onset of decomposition. It took about 0.9 to 1.0 s for this sensor to begin to detect CO_2. Sensor 2 (with a filter) had an initial response time of about 2 s and a 90% response time of ~90 s. This sensor was used to determine the total amount of CO_2 emission. At a high normal stress (12.2 MPa) and the largest slip rate (1.17 m s^{-1}), μ_p of about 0.6 dropped to μ_{ss} of about 0.04 (Fig. 3A). Sensor 2 showed a continuous increase toward a CO_2 concentration of about 29,000 parts per million. This concentration roughly agrees with the expected emission of CO_2 from the volume of decomposed calcite that was estimated on photomicrographs. The output from sensor 1 showed a reduction of CO_2 concentration after the end of a run because of dissipation of concentrated CO_2 near the fault (Fig. 3A). The first detectable output from sensor 1 was recognized at 1.0 s (Fig. 3B). The initial response time was 0.9 to 1.0 s for this sensor, so there must have been an emission of CO_2 almost immediately after the onset of slip (*24*). Another run at a lower slip rate (0.17 m s^{-1}) and at a normal stress of 9.8 MPa also indicated that the slip weakening was concurrent with the thermal decomposition of calcite (fig. S4).

Thus, a fault in Carrara marble clearly shows pronounced slip weakening at high slip rates while undergoing calcite decomposition along the slip surface. This means that a fault can become very weak as a result of frictional heating caused by its own motion. Such dynamic weakening should destabilize fault slip and foster the generation of large earthquakes (*13*). We next address the question of what causes such a pronounced weakening of a fault. One may consider that a buildup of pore pressure in a fault zone owing to the release of CO_2 gas is the most likely cause for fault weakening. To test this possibility, we conducted a critical experiment using preheated and decomposed specimens of Carrara marble (left in an oven at 900° to 904°C for 1.5 hours). We quantitatively confirmed complete decomposition by measuring weight loss after heating and by XRD analyses (Fig. 2D). The decomposed specimens could no longer emit CO_2 gas (*19*). The behavior is markedly similar between faults in Carrara marble and in decomposed specimens (Fig. 4). We have not measured the permeability of the decomposed zone in marble yet. But fractures in the decomposed zone in Fig. 2A suggest that the permeability of the decomposed zone is large enough for CO_2 to escape and to prevent the buildup of high pore fluid pressures. Enhanced permeability during the dehydration of serpentinite at elevated ambient temperature (not due to frictional heating) was also confirmed recently (*25*).

These results indicate that the weakening is attributed not to CO_2 pressure but to the low frictional strength of newly formed ultrafine lime grains. Among other possibilities, frictional melting can be immediately removed because calcite decomposition occurs before melting. Also, CaO melting would be unlikely because its melting temperature (~2572°C) is much higher than the temperatures recorded at the slip interface. Indeed, we did not detect any glass or amorphous materials in fault zones (fig. S3). Wrinkle-like pulses or normal separation of a fault along a bimaterial interface (*26*) is also unlikely because there is no material contrast across a fault in our experiments.

In view of the existing data, we considered that flash heating (*13*) at interfaces of ultrafine particles is critical for pronounced weakening of carbonate fault. The weakening by flash heating or transient local heating at asperity contacts has been proposed to occur via local melting at asperity contacts and/or by strength degradation of asperity contacts at submelting temperatures (*13*). The latter case is more likely for decomposed calcite because lime has a very high melting temperature. However, exact deformation mechanisms along sliding asperity or grain contacts still remain to be explored.

To demonstrate the importance of temperature rise during high-velocity sliding, we measured the temperature along the fault of the specimens (Fig. 3, C and D), using a radiation thermometer (*19*, *27*) during a run conducted at about the same sliding condition as that in HVR601. The thermometer measured an average temperature higher than 550°C over an area of 0.4 mm in diameter with a fast response time (<0.1 s). The measured temperature reached a maximum of 950°C at 30 s (high enough for calcite decomposition) after attaining about 650°C during the first 9 s (Fig. 3C). The local temperature at sliding asperities should be higher than the measured surface temperature even in the early stage (<9 s), in view of the CO_2 emission data (Fig. 3, A and B). The friction and thermal evolution in the final stages of the experiment are very interesting. After the specimen was disconnected from the motor, fault slip decelerated and stopped in about 3 s (Fig. 3, C and D). Friction increased at an accelerating rate as the temperature fell. The inverse relation between friction and temperature strongly suggests that the immediate strength recovery could be related to a rapid drop in temperature.

The simulated faults of Carrara marble exhibit lower friction than does the Nojima fault gouge, although their overall behaviors are similar (*16*). A possible reason for this difference is a very effective production of ultrafine grains that are tens of nanometers in diameter (Fig. 2C) by a

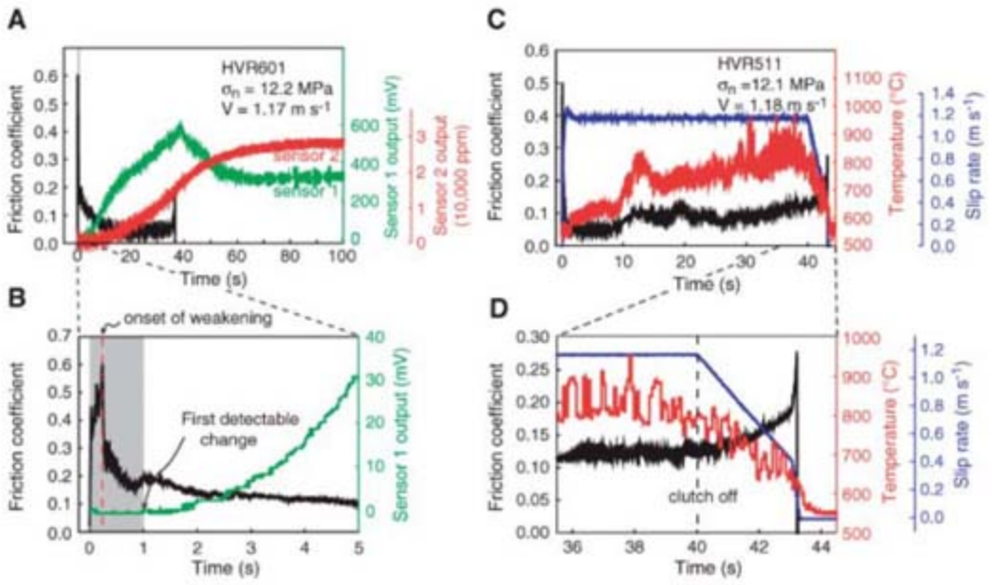

Fig. 3. Monitoring of CO_2 gas emission and temperature measurement. (**A**) Friction coefficient and outputs from two CO_2 sensors plotted against time. Sensor 1 (without a filter) is a quick-response sensor for detecting the onset of CO_2 emission, and sensor 2 (with a filter) is a slow-response sensor for monitoring the amount of emitted CO_2. *V*, slip rate. (**B**) Enlargement of (A) for the first 5 s of slip, with an output only from sensor 1 shown with mechanical data. The timing of peak friction and the first detectable change in output from sensor 1 are indicated by arrows. Vertical gray bars in both (A) and (B) indicate the response time of sensor 1 (about 1 s). (**C**) Friction coefficient (black), slip rate (blue), and temperature measured with a radiation thermometer (red) plotted against time in HVR511, which was conducted at about the same sliding condition (normal stress and slip rate of 12.1 MPa and 1.18 m s^{-1}, respectively) as that in HVR601. (**D**) Enlargement of the decreasing slip-rate phase of the experiment after turning off the magnetic clutch in (C).

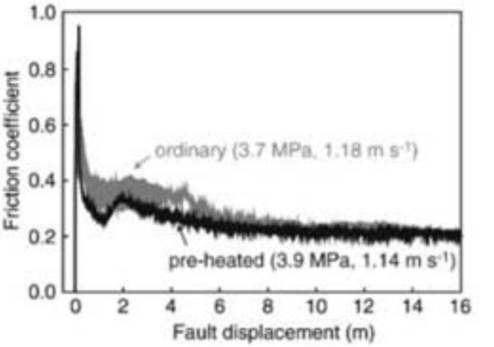

Fig. 4. Comparison of frictional behavior of a fault in Carrara marble (ordinary) and a fault in preheated and completely decomposed specimens of Carrara marble.

decomposition reaction (no time for grain growth during seismic-fault motion). The process may be similar to the cases of intermediate- to deep-focus earthquakes, for which the formation of ultrafine reaction products may play a decisive role in earthquake generation (*28*). Other gouge materials have to undergo grain comminution to form ultrafine grains, which requires extra work in fault zones, resulting in higher friction. For slip on faults in Carrara marble, understanding friction between nanometer-scale particles seems to be a key for delineating the exact mechanisms of the dynamic weakening of faults.

Our results have important implications for earthquake geology and fault mechanics. Marked decomposition weakening may be a widespread phenomenon, because fault gouges commonly contain sheet silicate minerals that decompose even at lower temperatures than that for calcite decomposition, although thermal decomposition of sheet silicates may be followed by frictional melting (*29*). Also, thermally induced decomposition may leave geological evidence (other than pseudotachylytes) of seismic-fault slip, contrary to geologists' opinion that faults do not preserve a record of seismic slip, except for the small percentage of faults containing pseudotachylyte (*30*). Indeed, we have shown that coseismic decomposition of siderite produces a stable mineral, magnetite (*31*). Thus, the clear demonstration of thermal decomposition during seismic slip opens up a new series of investigations in integrated fault and earthquake studies.

References and Notes

1. C. H. Scholz, *The Mechanics of Earthquakes and Faulting* (Cambridge Univ. Press, New York, ed. 2, 2002).
2. M. D. Zoback *et al.*, *Science* **238**, 1105 (1987).
3. J. N. Brune, T. L. Henyey, R. F. Roy, *J. Geophys. Res.* **74**, 3821 (1969).
4. A. H. Lachenbruch, J. H. Sass, *J. Geophys. Res.* **85**, 6185 (1980).
5. R. H. Sibson, *Geophys. J. R. Astron. Soc.* **43**, 775 (1975).
6. A. Tsutsumi, T. Shimamoto, *Geophys. Res. Lett.* **24**, 699 (1997).
7. T. Hirose, T. Shimamoto, *J. Geophys. Res.* **110**, B05202 (2005).
8. T. Hirose, T. Shimamoto, *Bull. Seismol. Soc. Am.* **95**, 1666 (2005).
9. G. Di Toro, T. Hirose, S. Nielsen, G. Pennacchioni, T. Shimamoto, *Science* **311**, 647 (2006).
10. R. H. Sibson, *Nat. Phys. Sci.* **243**, 66 (1973).
11. A. H. Lachenbruch, *J. Geophys. Res.* **85**, 6097 (1980).
12. C. A. J. Wibberley, T. Shimamoto, *Nature* **436**, 689 (2005).
13. J. R. Rice, *J. Geophys. Res.* **111**, B05311 (2006).
14. D. L. Goldsby, T. E. Tullis, *Geophys. Res. Lett.* **29**, 1844 (2002).
15. G. Di Toro, D. E. Goldsby, T. E. Tullis, *Nature* **427**, 436 (2004).
16. K. Mizoguchi, T. Hirose, T. Shimamoto, E. Fukuyama, *Geophys. Res. Lett.* **34**, L01308 (2007).
17. C. B. Raleigh, M. S. Paterson, *J. Geophys. Res.* **70**, 3965 (1965).
18. T. Shimamoto, A. Tsutsumi, *Struct. Geol.* **39**, 65 (1994) (in Japanese with English abstract).
19. Materials and methods are available as supporting material on *Science* Online.
20. μ_p is the ratio of the highest shear stress to normal stress before the onset of weakening, and μ_{ss} is the ratio of steady-state shear stress to normal stress.
21. M. S. Paterson, T.-f. Wong, *Experimental Rock Deformation—The Brittle Field* (Springer-Verlag, Berlin, ed. 2, 2005).
22. W. A. Deer, R. A. Howie, J. Zussman, *An Introduction to the Rock Forming Minerals* (Longman Scientific and Technical, Harlow, UK, ed. 2, 1992).
23. Z. D. Sharp, J. J. Papike, T. Durakiewicz, *Am. Mineral.* **88**, 87 (2003).
24. The calculated bulk temperature (~850°C) on the sliding surface after 0.2 s appears to be consistent with the immediate decomposition after the onset of slip (*19*).
25. E. Tenthorey, S. F. Cox, *Geology* **31**, 921 (2003).
26. D. J. Andrews, Y. Ben-Zion, *J. Geophys. Res.* **102**, 553 (1997).
27. A. Tsutsumi, T. Shimamoto, in *Contemporary Lithosphertic Motion in Seismic Geology: Proceedings of the 30th International Geological Congress*, Y. Hong, Ed. (VNU Science Press, Leiden, Netherlands, 1997), pp. 223–232.
28. H. W. Green II, C. Marone, in *Plastic Deformation of Minerals and Rock*, S. Karato, H.-R. Wenk, Eds. (Mineralogical Society of America, Washington, DC, 2002), pp. 181–199.
29. J.-H. Ree, R. Han, T. Shimamoto, J. Kim, *Eos* **87**, S33A (2006).
30. D. S. Cowan, *J. Struct. Geol.* **21**, 995 (1999).
31. R. Han, T. Shimamoto, T. Hirose, J.-H. Ree, J. Ando, *Eos* **87**, S33A (2006).

32. The observations of the experimental specimens were made with the use of TEM (JEOL JEM-2010) at the Natural Science Center for Basic Research and Development of Hiroshima University and FE-SEM (JEOL JSM-7000F) at Geodynamics Research Center of Ehime University. This work was supported by the Brain Korea 21 Project of the Ministry of Education, Korea Research Foundation grant C00435 (100699), the Grant-in-Aid for Scientific Research, Japan Society for Promotion of Science (16340129 and 18340159), and the Center of Excellence Program for the 21st Century of Kyoto University, "Active Geosphere Investigation."

Supporting Online Material

www.sciencemag.org/cgi/content/full/316/5826/878/DC1
Materials and Methods
Figs. S1 to S4
References

10 January 2007; accepted 26 March 2007
10.1126/science.1139763

GRACE Gravity Data Constrain Ancient Ice Geometries and Continental Dynamics over Laurentia

M. E. Tamisiea,[1]*† J. X. Mitrovica,[2] J. L. Davis[1]

The free-air gravity trend over Canada, derived from the Gravity Recovery and Climate Experiment (GRACE) satellite mission, robustly isolates the gravity signal associated with glacial isostatic adjustment (GIA) from the longer–time scale mantle convection process. This trend proves that the ancient Laurentian ice complex was composed of two large domes to the west and east of Hudson Bay, in accord with one of two classes of earlier reconstructions. Moreover, GIA models that reconcile the peak rates contribute ~25 to ~45% to the observed static gravity field, which represents an important boundary condition on the buoyancy of the continental tectosphere.

The similarity between the geometry of the free-air gravity anomaly (FAGA) over Laurentia (*1*) and the perimeter of the ancient ice complex that covered the region led to a long-held view that the perturbation largely reflected incomplete GIA in response to the ice age (*1*–*4*). In this case, the seismic high-velocity anomaly underlying the continent (*5*) would be interpreted as a neutrally buoyant, chemically distinct continental root, in accord with the tectosphere hypothesis (*6*). In contrast, forward analyses of GIA and/or mantle convection aimed at fitting the peak anomaly (*7*–*9*) have concluded that GIA is responsible for only ~10 to ~30% of the total signal. In this scenario, the seismic anomaly would be associated with active downwelling flow that drives a dynamic depression, and gravity low, on the overriding craton. Simons and Hager (*10*) have, on the basis of GIA modeling combined with an analysis of the spatio-spectral content of the Laurentian gravity field, proposed an intermediate scenario in which GIA and convection contribute roughly equally to the observed signal.

The characteristic time scale of GIA (a few thousand years) is orders of magnitude shorter than that of convective flow. Accordingly, Mitrovica and Peltier (*4*) suggested that consideration of the time rate of change of the gravity field would, when it became available, provide a robust method for isolating the GIA signal. The trend field would also provide finer spatial resolution of ice-sheet history than the static field. Observational constraints on gravity trends from land-based surveys in Hudson Bay exist (*11*, *12*), but these are too sparse to accurately constrain the regional (and peak) GIA signal. Recently, measurements obtained by the GRACE satellite mission (*13*) have reached sufficient time span to yield useful constraints on regional gravity trends. Our goal is to make use of the GRACE data to constrain the GIA signal and thus test the suite of published models for the dynamics of the Laurentian craton. We also use the GRACE-derived maps of gravity rates to address a century-long debate concerning the geometry of late Pleistocene ice cover over the region.

We use monthly Center for Space Research (CSR) RL01 GRACE solutions for the geoid,

[1]Harvard-Smithsonian Center for Astrophysics, 60 Garden Street, Mail Stop 42, Cambridge, MA 02143, USA. [2]Department of Physics, University of Toronto, 60 St. George Street, Toronto, ON M5S 1A7, Canada.

*Present address: Proudman Oceanographic Laboratory, 6 Brownlow Street, Liverpool L3 5DA, UK.
†To whom correspondence should be addressed. E-mail: mtamisiea@cfa.harvard.edu

spanning April 2002 to April 2006. Our analysis procedure (*14*) adopts a truncation at spherical harmonic degree and order (l and m, respectively) of 70, applies standard approaches to smoothing (Gaussian with a 500-km radius) and destriping the solutions to reduce satellite errors, and yields estimates for parameters governing the in- and out-of-phase annual, trend, and constant terms and their errors. We calculate the geoid height anomaly rates from each solution on a 1° by 1° grid. The result, over Laurentia, is shown in Fig. 1.

Previous applications of GRACE data have focused on rates associated with hydrological processes (*13*), and the standard approach in such cases is to convert the geoid height rates to changes in equivalent water thickness. With respect to the spherical harmonic expansion, each term is multiplied by $2l + 1$ (*15*), thus accentuating higher degree and order terms (and their associated error). The signal associated with GIA is largely due to the motion of mass within the Earth's crust and mantle, as opposed to variations of surface and groundwater mass. In this application, or indeed in studies of surface observations related to mantle convection, geoid rates are commonly converted to trends in the FAGA. In this case, a multiplicative factor of $l - 1$ is applied (*16*) to each term in the spherical harmonic expansion, which acts to shift power to shorter wavelengths. Smaller-scale features in the FAGA are therefore emphasized relative to those in the geoid.

Our GRACE-derived map of the FAGA trend over Laurentia (Fig. 2A and the associated error estimate in fig. S1A) unambiguously indicates that the ancient ice complex that once covered the region had a multidomal structure. Specifically, deglaciation centers are apparent in regions to the west (Keewatin) and east (northern Quebec) of Hudson Bay. The broad-scale geometry of the Laurentide Ice Sheet at the Last Glacial Maximum has been the source of long-standing debate [see (*17*) for a review of early work]. Before the mid-20th century, reconstructions of Laurentide ice cover generally included ice domes over Keewatin and northern Quebec, but this view was superseded by the monodomal model advocated by Flint (*18*) on the basis of an analysis of gravity data. Subsequent studies, in particular the detailed geomorphological analysis of Dyke and Prest (*19*), returned to the multidomal (i.e., ice domes over Keewatin, northern Quebec, and the Foxe Basin just south of Baffin Island) model, although the ICE-3G (*17*) and ICE-4G (*20*) global ice-sheet reconstructions, based on both geological and geophysical data, were once again characterized by a largely monodomal Laurentian complex. A recent revision to these global models, ICE-5G (*21*), motivated in part by crustal motion data in Yellowknife and ground-based gravity measurements along a transect including the west coast of Hudson Bay (*11*), involved a major ice dome over Keewatin and a smaller ice center in northern Quebec, in qualitative accord with the Dyke and Prest (*19*) reconstruction. Our results strongly support the multidomal Laurentide ice geometry advocated by Dyke and Prest (*19*) and allow us to reject the monodomal model.

GIA is not the only process contributing to the observed rate fields. Interannual variations in hydrology, mass loss from Greenland Ice Sheet and Alaskan glacier fields, and errors in the ocean model of Hudson Bay could all contribute to the observed signal. In an attempt to account for hydrology, we have calculated the rate over the same time period from the Global Land Data Assimilation System (GLDAS)/Noah hydrology data set (*14*, *22*). This correction is small in terms of the total signal observed in the region, but it slightly decreases the local maximum value of the observed FAGA rate west of Hudson Bay and moves the location of this peak rate farther north (Fig. 2B). In an attempt to reduce the contamination from mass loss of the ice fields, this paper focuses on comparisons of forward predictions of GIA with the observed FAGA in a region bounded by longitudes 110°W to 85°W and latitudes 50°N to 70°N (indicated by the area within the black line in Fig. 2B). Possible errors due to ocean variability in Hudson Bay are part of an ongoing study.

We adopt the following procedure to estimate the contribution of GIA to the static FAGA over Laurentia. First, we use standard numerical simulations of the GIA process to generate a model (or set of models) that provides a good fit to the rate map in Fig. 2B. We next use this model to predict the static FAGA and then compare this prediction to the GRACE-derived static field within the bounded region. In all cases, we apply the same smoothing, destriping, and harmonic truncation to the GIA model predictions that were used to analyze the GRACE observations (*14*).

Our GIA predictions are based on spherically symmetric, self-gravitating Maxwell viscoelastic Earth models with elastic structure given by the Preliminary Reference Earth Model (*23*). We assume an elastic lithosphere of 120-km thickness (the predictions are insensitive to reasonable variations in this choice) and a radial viscosity profile characterized by isoviscous upper and lower mantle (UM and LM) regions. The boundary between these regions is taken at 670-km depth, and the viscosities above and below this interface are free parameters denoted by ν_{UM} and ν_{LM}, respectively. We use the global ICE-5G ice history (*21*) and solve for a gravitationally self-consistent ocean load.

Figure 3 shows the reduced χ^2 misfit between predictions of the geoid and FAGA rate fields over Laurentia and the associated GRACE observations [Fig. 1 (with the hydrological signal removed) and Fig. 2B, respectively]. Good fits (*24*) to the data are generally obtained for models with ν_{LM} values between 2.5×10^{21} and 4×10^{21} Pa s and ν_{UM} values between 3×10^{20} and 1×10^{21} Pa s. A second set of models characterized by ν_{UM} above 6×10^{20} Pa s and

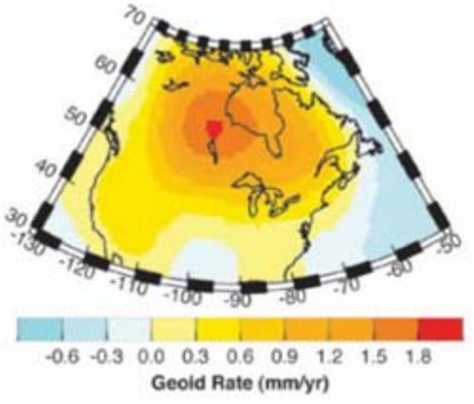

Fig. 1. Observed time rate of change of the geoid over Laurentia from CSR RL01 GRACE solutions from April 2002 to April 2006.

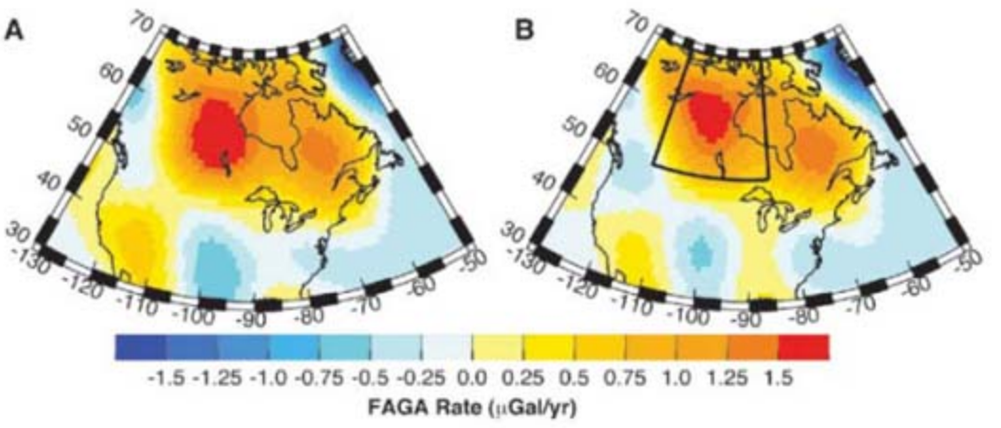

Fig. 2. (**A**) Rate of change of the FAGA from CSR RL01 GRACE solutions from April 2002 to April 2006. (**B**) Same as (A) but with an estimate of the hydrological contribution derived from the GLDAS/Noah data set (*22*) removed. The thick black line encloses the region used for the comparison of the forward GIA models with the observed fields. This region was chosen in order to limit contamination from ongoing ice mass variations in Greenland, Alaska, and British Columbia, as well as hydrological mass variations across the rest of the North American continent.

ν_{LM} greater than 3×10^{22} Pa s also yields relatively low χ^2 values. Two sets of solutions of this type are common in studies of present-day GIA observations. A weak lower mantle associated with the first class of models initially adjusts quickly and thus reaches close to equilibrium since the end of the deglaciation, whereas a stronger lower mantle (in the second class of models) adjusts slowly throughout the loading cycle. We can rule out the higher mantle viscosity models on the basis of independent analyses of postglacial decay times in the Hudson Bay region (*20*, *25*). The minimum reduced χ^2 misfit, for the FAGA rate (Fig. 3B) observation, is obtained by the model with $\nu_{UM} = 8 \times 10^{20}$ Pa s and $\nu_{LM} = 3 \times 10^{21}$ Pa s.

Next, we turn to the static FAGA field. In this case, our GRACE-derived (Fig. 4A) estimate is based on the CSR GGM02S solution (*26*). Note that this static field shows a single large anomaly with peak amplitude of −34 mGal (where 1 Gal = 10^{-2} m s^{-2}) centered over Hudson Bay and, as discussed above, a geometry that is less reflective of the morphology of the ancient ice complex that covered the region. Our next step is to predict the static FAGA field due to GIA with the use of the same Earth model that best fits the FAGA rate (*27*). Figure 4B shows the residual field generated by removing this GIA prediction from the observed static field (Fig. 4A). Classically, peak estimates of the GIA prediction and the static FAGA observation, which do not necessarily occur at the same location, have been compared to determine the relative contribution of GIA to the observed field. The application of this procedure indicates a GIA contribution of ~38% (or −13 mGal) to the observed peak.

As noted, a range of GIA models provides similar fits to the GRACE-derived rates (Fig. 3). Therefore, we repeated the above analysis for a large suite of models within this range and, in each case, we computed the GIA contribution to the static FAGA. In addition, we also considered the impact on this contribution (and on the preferred set of models) of errors in the hydrology model and variations in the parameters governing the GRACE data analysis [e.g., destriping and Gaussian smoothing (*14*)]. These tests mapped out a possible range in the GIA contribution to the static FAGA field of ~25 to ~45%. Thus, the continental root beneath Laurentia is contributing, via a convectively supported dynamic depression of the craton, to the FAGA field. This range is intermediate as compared to estimates by Simons and Hager (*10*), who argued for a 50% contribution from GIA, and other studies that have concluded that GIA is a minor contributor to the static field (*7*–*9*). In any case, although chemical heterogeneity in the continental root beneath Laurentia is compensating for thermal buoyancy, the cancellation implied by the tectosphere hypothesis is not supported by our analysis of the GRACE-derived gravity field.

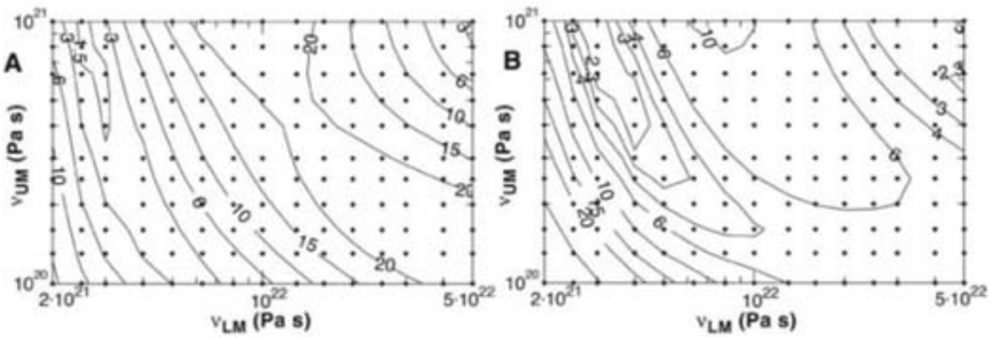

Fig. 3. (**A**) Reduced χ^2 residual between GIA predictions of the geoid rate and the observed field (Fig. 1) on a 1° by 1° grid within the region bounded by the thick black line in Fig. 2B. The GIA models are distinguished on the basis of the adopted ν_{UM} and ν_{LM} values, and the grid of dots indicates the set of models used to generate the contour lines. (**B**) Same as in (A) but for the FAGA rate field.

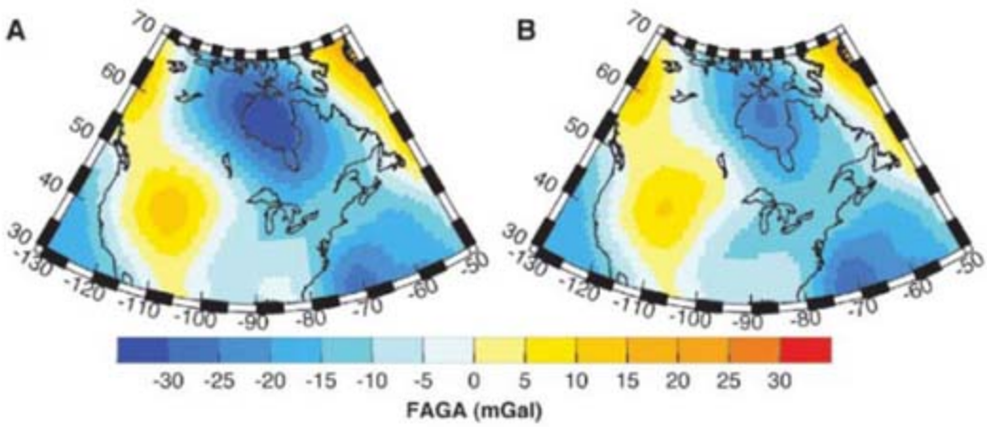

Fig. 4. (**A**) Static FAGA field over Laurentia derived from the CSR GGM02S GRACE solution (*26*). A destriping algorithm (*14*) was not applied to generate this field. (**B**) Same as (A) but with a "preferred" GIA prediction removed. The GIA prediction is based on an Earth model with a 120-km-thick lithosphere, a ν_{UM} value of 8×10^{20} Pa s, and a ν_{LM} value of 3×10^{21} Pa s.

References and Notes

1. R. I. Walcott, *Can. J. Earth Sci.* **7**, 716 (1970).
2. L. M. Cathles, *The Viscosity of the Earth's Mantle* (Princeton Univ. Press, Princeton, NJ, 1975).
3. P. Wu, W. R. Peltier, *Geophys. J. R. Astron. Soc.* **74**, 377 (1983).
4. J. X. Mitrovica, W. R. Peltier, *J. Geophys. Res.* **94**, 13651 (1989).
5. J. Ritsema, H. J. van Heijst, J. H. Woodhouse, *Science* **286**, 1925 (1999).
6. T. H. Jordan, *Rev. Geophys. Space Phys.* **13**, 1 (1975).
7. W. R. Peltier, A. M. Forte, J. X. Mitrovica, A. M. Dziewonski, *Geophys. Res. Lett.* **19**, 1555 (1992).
8. T. S. James, *Geophys. Res. Lett.* **19**, 861 (1992).
9. G. Pari, W. R. Peltier, *J. Geophys. Res.* **101**, 28105 (1996).
10. M. Simons, B. H. Hager, *Nature* **390**, 500 (1997).
11. A. Lambert *et al.*, *Geophys. Res. Lett.* **28**, 2109 (2001).
12. A. Lambert, N. Courtier, T. S. James, *J. Geodyn.* **41**, 307 (2006).
13. B. D. Tapley, S. Bettadpur, J. C. Ries, P. F. Thompson, M. M. Watkins, *Science* **305**, 503 (2004).
14. Materials and methods are available as supporting material on *Science* Online.
15. J. Wahr, M. Molenaar, F. Bryan, *J. Geophys. Res.* **103**, 30205 (1998).
16. G. D. Garland, *Introduction to Geophysics: Mantle, Core, and Crust* (Saunders, Philadelphia, ed. 2, 1979).
17. A. M. Tushingham, W. R. Peltier, *J. Geophys. Res.* **96**, 4497 (1991).
18. R. F. Flint, *Glacial Geology and the Pleistocene Epoch* (Wiley, New York, 1947).
19. A. S. Dyke, V. K. Prest, *Geogr. Phys. Quat.* **41**, 237 (1987).
20. W. R. Peltier, *Rev. Geophys.* **36**, 603 (1998).
21. W. R. Peltier, *Annu. Rev. Earth Planet. Sci.* **32**, 111 (2004).
22. M. Rodell *et al.*, *Bull. Am. Meteorol. Soc.* **85**, 381 (2004).
23. A. M. Dziewonski, D. L. Anderson, *Phys. Earth Planet. Inter.* **25**, 297 (1981).
24. If we assume that we can apply a standard *F* test to the data, then a reasonable 95% confidence limit for χ^2 would be 1.5 and 2.3 for Fig. 3, A and B, respectively. We have conservatively taken the degrees of freedom in the problem to be 10% of the total number of grid points.
25. J. X. Mitrovica, A. M. Forte, *J. Geophys. Res.* **102**, 2751 (1997).
26. B. Tapley *et al.*, *J. Geodesy* **79**, 467 (2005).
27. The number of glacial cycles used in the calculation will affect predictions of the static FAGA caused by GIA. Thus, we have included three complete glacial cycles before the last cycle specified by ICE-5G. The inclusion of these cycles will have little impact on the estimates of present-day rates.

28. This work was supported under the National Aeronautics and Space Administration (grant number NNG04GF09G), the Natural Sciences and Engineering Research Council of Canada, Geomatics for Informed Decisions, and the Canadian Institute for Advanced Research. We thank E. Hill, K. Latychev, S. Swenson, I. Velicogna, J. Wahr, and W. van der Wal for useful conversations and two anonymous reviewers for helpful suggestions for improving the manuscript.

Supporting Online Material

www.sciencemag.org/cgi/content/full/316/5826/881/DC1
Materials and Methods
Figs. S1 and S2
References

3 November 2006; accepted 28 March 2007
10.1126/science.1137157

The Role of Wheat Awns in the Seed Dispersal Unit

Rivka Elbaum,[1]* Liron Zaltzman,[1,2] Ingo Burgert,[1] Peter Fratzl[1]*

The dispersal unit of wild wheat bears two pronounced awns that balance the unit as it falls. We discovered that the awns are also able to propel the seeds on and into the ground. The arrangement of cellulose fibrils causes bending of the awns with changes in humidity. Silicified hairs that cover the awns allow propulsion of the unit only in the direction of the seeds. This suggests that the dead tissue is analogous to a motor. Fueled by the daily humidity cycle, the awns induce the motility required for seed dispersal

Awns and other appendages on the seed dispersal unit of plants aid in dispersing the seed to a germination site (*1*–*3*). Hairs, wings, and hooks influence the route of seeds from the mother plant to a surface by wind or animal dispersal [phase I dispersal (*4*)]. Hygroscopically active awns propel seeds on the ground through coiling and uncoiling (*5*, *6*) and, thus, mainly affect the movement of the seed after it reaches the resting surface [phase II dispersal (*4*)]. The nature of the soil affects the ability of the seeds to locate a safe site. Larger seed dispersal units are more easily buried in coarse particle soils, where the lumps are similar in size to the dispersal units. On finer-grained earth, they tend to move along the soil surface (*7*). Seeds bearing active awns are more abundant in structured soils, meaning soils that contain a stable system of pores and aggregates of different sizes, perhaps because the seeds are easily anchored. Unawned small seeds are prevalent in light sandy soils, where they are trapped, mainly by random movement of earth. Seeds equipped with passive awns are evenly abundant in both environments, with a preference for stable porous soils (*8*, *9*). These observations do not conform to the prediction made by Chambers *et al.* (*7*) that larger seed dispersal units will be trapped preferentially in soils of large particle size, which suggests that passive awns may interact with the soil by a mechanism yet unknown.

To find the specific features that may support this interaction, we studied awns of wild and domesticated tetraploid wheat lines [*Triticum turgidum* ssp. (*10*)]. Thin cross sections and oblique sections examined by scanning electron microscopy showed two photosynthetic zones surrounded by cells that provide mechanical support to the awn (Fig. 1). This design is common to passive awns of wheat and other crops (*11*). A silica layer is deposited on the external surface of the epidermis (*11*) (Fig. 2A), covering separated papillae and hair cells (fig. S1). This form of tiling creates a surface that is mechanically both hard and tough, to interact with the soil. The hairs are 0.1 to 0.2 mm long and point toward the tip of the awn. More hairs are found on the ridge surface, facing away from the dispersal unit axis (Fig. 1). Back-scattered electron images of the supporting tissue showed no evidence for structural or compositional differences between the cap and the narrower ridge. Nonetheless, scanning acoustic microscopy revealed a huge acoustic impedance contrast in the same sample, related to variations in stiffness (Fig. 2B). The impedance at the ridge was about 1/10th that at the cap. To support this finding, we measured the local effective Young's modulus at the cap and at the ridge using a nano-indentation probe. At the ridge, the reduced Young modulus was 10.0 ± 2.8 GPa (n = 16); however, the cap was much firmer, with a modulus of 20.5 ± 2.6 GPa (n = 7), corresponding to the upper range of spruce wood [7 to 23 GPa (*12*)]. Wheat stems were studied by a four-point bending test, with reported Young moduli values about half of those we obtained at the ridge [4.76 to 6.58 GPa (*13*)]. Nano-indentation measures the cell walls specifically and is insensitive to voids in the underlying tissue, so it is likely to yield higher values than macroscopic tests.

To understand the difference in stiffness between the cap and the ridge, we first checked whether lignin is more abundant in the cap. We rejected this hypothesis, as staining by astra-blue–safranin indicated an even distribution of lignin in the cross section (fig. S2). Next, we checked whether changes in the cellulose orientation contribute to the observed variation in stiffness (*14*). It is well known that in the secondary wall of wood cells, cellulose microfibrils are winding helically around the cell. The tilt angle of the fibrils with respect to the cell axis, usually called microfibril angle (MFA), determines the stiffness of the wood cell. Specifically, when the cellulose MFA in different wood types decreases from 50° to 5°, the corresponding stiffness is known to increase from 1 to 14 GPa (*12*, *15*). We used wide-angle x-ray scattering to measure the MFA in different regions of the awns (*10*). We found that the cellulose fibrils are very well aligned along the long axis of the awn in the cap, with a MFA close to zero (Fig. 2C). At the ridge, the fibrils were found to be randomly oriented (Fig. 2D), similarly to the parenchyma of the wheat stem (*16*). However, this structure characterizes only the lower part of the awn, close to the seed. At the upper part, the cellulose was found to be aligned both at the ridge and at the cap.

We suggest an active role to this structure in the seed dispersal unit. The two different cellulose arrangements expand differently at ambient humidity conditions, similar to the mechanism of seed explosion in the Acanthaceae capsule (*17*) and the opening of pine cone scales (*18*). Water molecules that adsorb to the long crystalline cellulose fibrils will not make

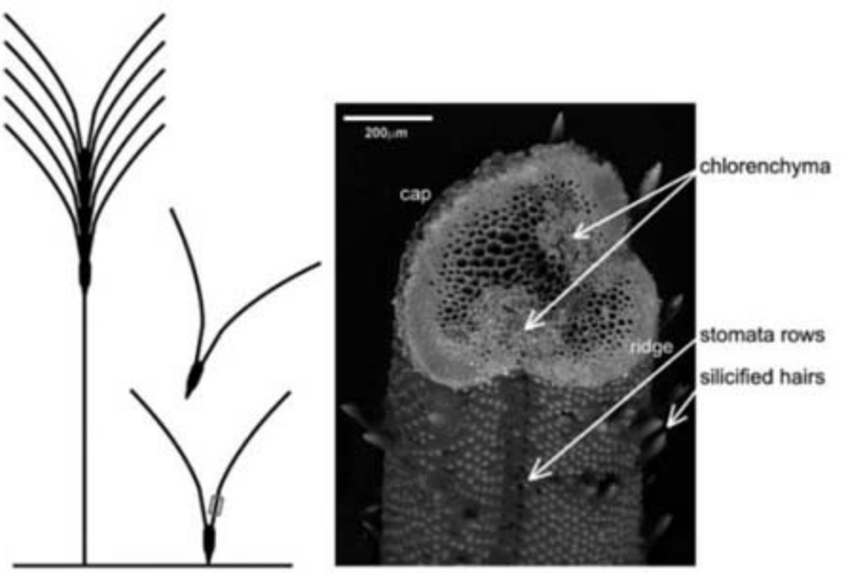

Fig. 1. (Left) Illustration of the wild wheat plant (*Triticum turgidum* ssp. *diccocoides*) and two dispersal units (not to scale). Each dispersal unit carries two pronounced awns that balance the dispersal unit as it falls. A scanning electron micrograph in the back scattering mode of a section through a wild wheat awn is shown on the right. The section is taken from the lower third of the awn and is oriented in a way similar to the rectangle drawn over the bottom dispersal unit. The different tissues are indicated by arrows. The cap and ridge are facing in the same direction along the awn.

[1]Biomaterials Department, Max Planck Institute of Colloids and Interfaces, Golm, Germany. [2]Biotechnology Department, Tel Hai Academic College, Upper Galilee, Israel.

*Correspondence should be addressed to elbaum@mpikg.mpg.de (R.E.) or to fratzl@mpikg.mpg.de (P.F.)

them longer but will cause a lateral expansion by swelling of the noncrystalline hemicelluloses between the crystallites. Thus, the awns will generally expand only laterally, except for the lower part of the ridge, where the fibrils are not aligned but are randomly oriented. This part will work like a muscle: expanding in length with humidity, pushing the awns together, and contracting with drying, pulling the awns apart. Such movement was observed long ago in awns of wild wheat (*T. turgidum* ssp. *diccocoides*), goat grasses (*Aegilops* ssp.), and *Bromus* ssp., but its importance for dispersal was not known (*19*).

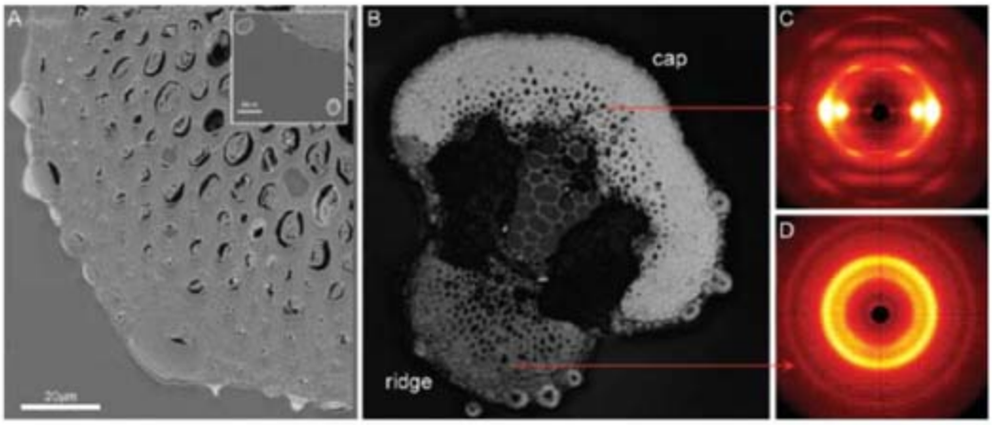

Fig. 2. Structural features of the lower part of the wheat awn. (**A**) Silica deposited at the epidermis, epidermal papillae, and hairs (inset) is detected on a polished sample by a scanning electron microscope in the back-scattered mode. Silica tiles stiffen the epidermis and protect the structure as it interacts with the soil. (**B**) The differential stiffness between the cap and the ridge is demonstrated by an acoustic impedance map (1 by 1 mm^2 field, brightness level is correlated to the relative impedance). Wide angle x-ray scattering patterns of the crystalline cellulose at the cap (**C**) and at the ridge (**D**) suggest that the difference in stiffness is created by different organization of the fibrils in the two regions.

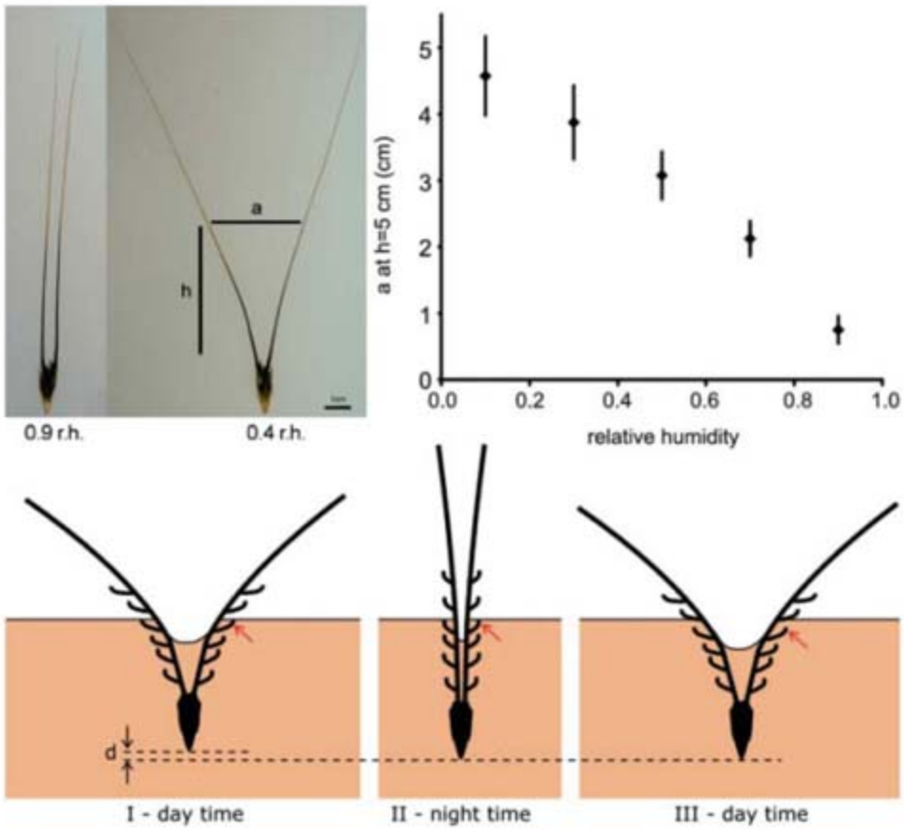

Fig. 3. The principle of the dispersal unit movement. (**Top**) The average distance (± SD) between the awns of four dispersal units is presented versus relative humidity (r.h.) of the surrounding air. (**Bottom**) One cycle in the humidity-driven movement of the awns. (I) shows the seeds and part of the awns immersed in soil. The red arrow indicates one of the silica hairs. (II) Because of increased humidity, the awns straighten. The silica hairs lock the awn and prevent an upward movement. As a consequence, the seed has to move downward by a distance *d*, indicated in (I), to account for the increased length projected onto the vertical. (III) After drying, the awns bend again, which shortens the length projected onto the vertical. Because the silica hairs are locked into place, the seed cannot move back upward, and the awns are drawn further down into the soil (see the silica hair marked by a red arrow). Hence, the net movement of the seed in one cycle corresponds to *d*.

To study the bending of the awns, we scanned the relative humidity of the air between 0.1 and 0.9 at 30°C and followed the change in the distance between the two awns on the same dispersal unit (Fig. 3 and movie S1). The awns bent at a point about 2 cm above the seed, corresponding to the location of the randomly oriented cellulose crystals. Above this position, no bending was observed, in agreement with the finding that the cellulose crystallites were aligned throughout the cross section. In principle, the elongation of the lower ridge relative to the cap may also induce twisting of the structure rather than bending, but we believe that the shape of the cross section with a wide cap, shaped like a half moon (Fig. 2B), may favor bending and creates a joint movement.

The movement is reversible; thus, the humidity cycle causes a periodic movement of the awns, which resembles the swimming stroke of frog legs. Most interestingly, there is a humidity cycle in the natural habitat of the wheat in the dry period after the seeds ripen; during the day, the air is dry, but at night, as the temperature goes down, humidity rises. This suggests that the awns may provide the motility required for seed dispersal, as was shown for the hygroscopically active awns (*1*).

To propel the seed on the soil surface, prominent friction forces must exist. This is most likely supplied by the silicified epidermal hairs that couple the unit to the soil in a ratchet manner. As the awns bend, the hairs slide on the soil particles, allowing movement only in the direction of the seed (Fig. 3). The rough soil lumps, which often contain silicates, are probably not able to burnish away the silicified protrusions even after several cycles of the awns' movement. In this way, the seed is pushed into the soil and, thus, is protected from predators, extreme dryness, and fires. With the first rains, the seed will have a better chance of germinating in a safe site. To show the ability of the seed dispersal unit to propel, we placed it horizontally on a felt cloth, which entangled the epidermal hairs. As we cycled the relative air humidity, the dispersal unit moved in the direction of the seed (movie S2). An identical design is preserved in awns of domesticated wheat, even though their function was lost during the domestication process, as the seeds do not disperse spontaneously. The short evolutionary time since domestication (about 10,000 years) probably allowed the complete loss of awns in several domesticated wheat lines, but not the alteration of the awn structure.

The wheat dispersal unit seems to be optimized to multiply the species in the environment

of the Fertile Crescent with long dry summers and short rainy winter seasons. As a self-pollinating annual that grows in dense stands, long-distance dispersal would not improve survival. The local surroundings of the mother plant should be sufficient to support the next generation as well. However, the place where the seed falls may be less ideal than a nearby location. It was shown that active awns are able to propel seeds on the ground for several centimeters (*6*). We suggest that the paired passive awns of wheat are also able to move the seed along the soil surface, as well as vertically, for burial. The movement, based on a unique arrangement of cellulose fibrils, is fueled by the daily changes in air humidity. The pointed epidermal hairs break the symmetry and allow the unit to move as a ratchet, promoting faster burial. This system increases the chances of the seed to germinate and to reach maturity and may increase the likelihood of a specific stand to proliferate.

The understanding of this seed dispersal mechanism may help in developing new concepts in weed control. The microscopic mechanism found to provide motility to the seed may also serve as a model in biomimetic materials research. Indeed, a hydration-dependent bending movement was recently reported in an artificial system consisting of nano–silicon columns embedded in a hydrogel film (*20*). From a mechanistic point of view, we have discovered a device for movement that is composed of passive elements. Locomotion is provided by a volume containing nonoriented cellulose crystallites that shortens on drying and pulls the awn like a muscle. The energy source for this active movement is the daily cycle of air humidity.

References and Notes

1. L. Van der Pijl, *Principles of Dispersal in Higher Plants* (Springer-Verlag, Berlin, ed. 3, 1982).
2. M. H. Peart, *J. Ecol.* **69**, 425 (1981).
3. J. L. Harper, P. H. Lovell, K. G. Moore, *Annu. Rev. Ecol. Syst.* **1**, 327 (1970).
4. J. C. Chambers, J. A. MacMahon, *Annu. Rev. Ecol. Syst.* **25**, 263 (1994).
5. M. H. Peart, *J. Ecol.* **67**, 843 (1979).
6. N. H. Stamp, *Am. J. Bot.* **76**, 555 (1989).
7. J. C. Chambers, J. A. MacMahon, J. H. Haefner, *Ecology* **72**, 1668 (1991).
8. M. H. Peart, *J. Ecol.* **72**, 437 (1984).
9. M. H. Peart, H. T. Clifford, *J. Ecol.* **75**, 569 (1987).
10. Materials and methods are available on *Science* Online.
11. F. J. Grundbacher, *Bot. Rev.* **29**, 366 (1963).
12. A. Reiterer, H. Lichtenegger, S. Tschegg, P. Fratzl, *Philos. Mag. A* **79**, 2173 (1999).
13. M. J. O'Dogherty, J. A. Huber, J. Dyson, C. J. Marshall, *J. Agric. Eng. Res.* **62**, 133 (1995).
14. I. D. Cave, *Wood Sci. Technol.* **3**, 40 (1969).
15. J. Keckes *et al.*, *Nat. Mater.* **2**, 810 (2003).
16. R. Liu, H. Yu, Y. Huang, *Cellulose* **12**, 25 (2005).
17. A. Witztum, K. Schulgasser, *J. Theor. Biol.* **176**, 531 (1995).
18. C. Dawson, J. F. V. Vincent, A. M. Rocca, *Nature* **390**, 668 (1997).
19. M. Zohary, *Beih. Bot. Zentbl. A.* **56**, 1 (1937).
20. A. Sidorenko, T. Krupenkin, A. Taylor, P. Fratzl, J. Aizenberg, *Science* **315**, 487 (2007).

21. We are grateful to M. Feldman for interesting comments and for providing the wheat seeds. Many thanks to S. Lev-Yadun for critical reading of the manuscript and to K. Kohl and D. Zerning for the help in growing the plants. R.E. thanks the Alexander von Humboldt Foundation for a fellowship.

Supporting Online Material

www.sciencemag.org/cgi/content/full/316/5826/884/DC1
Materials and Methods
Figs. S1 and S2
Table S1
References
Movies S1 and S2

18 January 2007; accepted 4 April 2007
10.1126/science.1140097

Positive Regulation of Itk PH Domain Function by Soluble IP_4

Yina H. Huang,[1] Juris A. Grasis,[2] Andrew T. Miller,[3] Ruo Xu,[4] Stephen Soonthornvacharin,[3] Amy H. Andreotti,[4] Constantine D. Tsoukas,[2] Michael P. Cooke,[3] Karsten Sauer[1]*

Pleckstrin homology (PH) domain–mediated protein recruitment to cellular membranes is of paramount importance for signal transduction. The recruitment of many PH domains is controlled through production and turnover of their membrane ligand, phosphatidylinositol 3,4,5-trisphosphate (PIP_3). We show that phosphorylation of the second messenger inositol 1,4,5-trisphosphate (IP_3) into inositol 1,3,4,5-tetrakisphosphate (IP_4) establishes another mode of PH domain regulation through a soluble ligand. At physiological concentrations, IP_4 promoted PH domain binding to PIP_3. In primary mouse $CD4^+CD8^+$ thymocytes, this was required for full activation of the protein tyrosine kinase Itk after T cell receptor engagement. Our data suggest that IP_4 establishes a feedback loop of phospholipase C–γ1 activation through Itk that is essential for T cell development.

Pleckstrin homology (PH) domains play a critical role in signaling by recruiting signal-transducing proteins to cellular membranes. For example, T cell receptor (TCR) signaling induces the recruitment of phospholipase C–γ1 (PLC-γ1) and the Tec family protein tyrosine kinases Itk and Tec via binding of their PH domains to the membrane lipid phosphatidylinositol 3,4,5-trisphosphate (PIP_3). This allows the Tec kinases to phosphorylate and activate PLC-γ1, which subsequently produces the second messengers inositol 1,4,5-trisphosphate (IP_3) and diacylglycerol (DAG) (*1*). Recruitment of PIP_3-binding PH domains is believed to be controlled by PIP_3 generation and turnover. Here, we show that IP_3 phosphorylation into inositol 1,3,4,5-tetrakisphosphate (IP_4) by IP_3 3-kinase B (ItpkB) generates a soluble PH domain ligand that regulates PH domain binding to PIP_3 in vivo. At physiological concentrations, IP_4 promotes Itk recruitment to PIP_3. In thymocytes, this is essential for full activation of Itk and its effector PLC-γ1. Thus, IP_4 acts as an important "third messenger" in vivo.

$ItpkB^{-/-}$ mice are severely immunocompromised and lack mature T cells because of a block of T cell development at the $CD4^+CD8^+$ double-positive (DP) stage in the thymus (*2*, *3*). At the DP stage, potentially useful thymocytes are positively selected to develop into mature CD4 or CD8 single-positive (SP) T cells. Potentially autoreactive or nonfunctional thymocytes are deleted (*1*). Positive selection is mediated by TCR engagement, resulting in PLC-γ1 activation. Its products IP_3 and DAG mobilize Ca^{2+} or activate the Ras-Erk pathway, respectively (*1*, *4*). Surprisingly, TCR-induced IP_3 accumulation and Ca^{2+} release were normal in $ItpkB^{-/-}$ thymocytes (*2*, *3*), but Erk activation was severely perturbed (*3*, *5*) (fig. S1A).

Normal proximal TCR signaling (fig. S1B) suggested a defect downstream of LAT (linker of activated T cells), an adapter protein that binds Itk and PLC-γ1 (*6*). To identify the most proximal defect causing perturbed Ras-Erk activation, we examined DAG production. TCR-induced DAG accumulation was strongly reduced in $ItpkB^{-/-}$ DP cells (Fig. 1A). Moreover, TCR-induced PLC-γ1 activation was strongly but incompletely reduced (Fig. 1B and fig. S1C). Thus, defective Erk activation in $ItpkB^{-/-}$ cells likely results from impaired DAG-dependent Ras activation. In support of this view, transgenic overexpression of the DAG effector RasGRP1 failed to rescue $ItpkB^{-/-}$ thymocyte development (fig. S1D), but treatment with the DAG analog phorbol 12-myristate 13-acetate (PMA) rescued Erk activation in $ItpkB^{-/-}$ cells (*3*). Furthermore, low-dose PMA rescued CD69 up-regulation on $ItpkB^{-/-}$ DP cells in vitro (Fig. 1C) and induced substantial development of mature, HSA^{low} SP thymocytes in $ItpkB^{-/-}$ neonatal thymic organ cultures (Fig. 1D). Thus, impaired DAG production due to reduced PLC-γ1 activation is a major component of the maturational defects in

[1]Department of Immunology, Scripps Research Institute, La Jolla, CA 92037, USA. [2]Department of Biology and Center for Microbial Studies, San Diego State University, San Diego, CA 92182, USA. [3]Genomics Institute of the Novartis Research Foundation (GNF), San Diego, CA 92121, USA. [4]Department of Biochemistry, Biophysics and Molecular Biology, Iowa State University, Ames, IA 50011, USA.

*To whom correspondence should be addressed. E-mail: ksauer@scripps.edu

ItpkB$^{-/-}$ thymocytes. These results reveal a specific requirement for DAG in thymocyte positive selection and suggest that ItpkB is required for DAG production by PLC-γ1.

We next addressed how ItpkB regulates PLC-γ1. The inability of catalytically inactive ItpkB to rescue T cell development from ItpkB$^{-/-}$ bone marrow (fig. S2) demonstrated that its catalytic activity is required. Normal IP_3 accumulation in ItpkB$^{-/-}$ thymocytes (*2*, *3*, *5*) (fig. S3) suggests that IP_4 is the key ItpkB effector. The PH domain of the close Itk relative Btk, a PLC-γ activator in B cells, binds IP_4 in vitro. Whether Itk can bind IP_4 is unclear (*5*, *7*–*9*). We found that wild-type but not PH domain–mutant Itk bound to PIP_3- or IP_4-coated beads in cell extracts (fig. S4A), which suggests that Itk could act as an IP_4 effector. Indeed, endogenous Itk bound to PIP_3- or IP_4-coated beads in thymocyte lysates (Fig. 2A). Stimulation with antibodies to CD3 and CD4 transiently increased Itk binding to both PIP_3- and IP_4-coated beads (Fig. 2A), which suggests that TCR stimulation could induce an Itk conformation with higher affinity for PIP_3 and IP_4. Secondary PIP_3 pull-downs from the supernatants of primary PIP_3 or IP_4 precipitations did not precipitate additional Itk (Fig. 2A). Thus, PIP_3 and IP_4 levels were not limiting, and IP_4-coated beads could quantitatively deplete the cellular Itk pool capable of binding PIP_3.

In contrast to wild-type cells, Itk interactions with PIP_3-coated beads were unaffected by TCR stimulation of ItpkB$^{-/-}$ DP cells (Fig. 2B). Thus, TCR-augmented Itk binding to PIP_3 depends on IP_4 production. PIP_3 is believed to be concentrated at sites of TCR engagement (*10*). Consistent with defective PIP_3 binding, beads coated with antibodies to CD3 and CD4 or to CD3 alone induced the translocation of green fluorescent protein (GFP)–tagged Itk to bead contact sites in controls, but not in ItpkB$^{-/-}$ DP thymocytes (Fig. 3, A and B). By contrast, LAT enrichment was indistinguishable (Fig. 3B). As in Jurkat cells (*11*), PH domain deletion abrogated Itk enrichment even in wild-type cells (Fig. 3C). Constitutive membrane localization through addition of a myristoylation motif restored recruitment even of PH domain–deficient Itk in wild-type and ItpkB$^{-/-}$ DP thymocytes (Fig. 3C). Thus, IP_4 is required for TCR-induced Itk recruitment.

Defective localization should prevent the assembly of Itk into adapter protein complexes containing LAT and the Itk substrate PLC-γ1 (*6*). Indeed, small amounts of Itk and LAT reciprocally coimmunoprecipitated from wild-type DP thymocytes, but not from ItpkB$^{-/-}$ cells (Fig. 3D). Moreover, Itk interactions with PLC-γ1 were strongly reduced, consistent with the decreased PLC-γ1 activity in ItpkB$^{-/-}$ cells (Fig. 1B and fig. S1C). By contrast, coprecipitation of LAT and PLC-γ1 was largely IP_4-independent (Fig. 3D). LAT binding is required for Itk activation (*6*). Consistent with impaired LAT binding, Itk activation was strongly reduced in ItpkB$^{-/-}$ DP cells stimulated with antibodies to CD3 and CD4 (Fig. 3E). Thus, IP_4 is required for Itk recruitment to LAT and Itk activation. Because IP_4 had no substantial effect on Itk kinase activity in vitro (fig. S4B), its role in Itk activation in T cells likely reflects its requirement for Itk membrane recruitment through PIP_3.

We therefore examined the effect of exogenous IP_4 on PIP_3 interactions with Itk. Surprisingly, we found that addition of IP_4 at physiological concentrations reported for TCR-stimulated T cells (*12*) augmented Itk binding to PIP_3 (Fig. 4, A and B). This augmentation occurred even with Itk PH domain fragments in cell extracts (Fig. 4, C and D) or in a purified in vitro system (Fig. 4E). Thus, IP_4 augments PIP_3 binding to the Itk PH domain alone, independent of other domains or of the activation state of Itk. At very high concentrations, IP_4 inhibited PIP_3 binding. Regioisomeric inositol 1,2,4,5-tetrakisphosphate

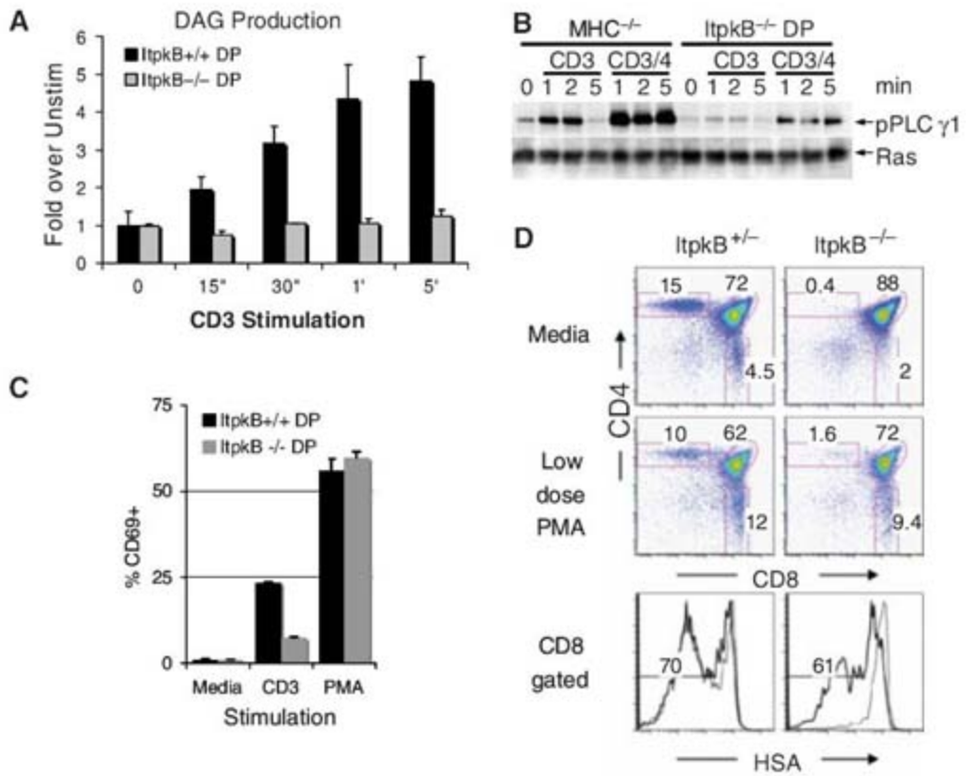

Fig. 1. Impaired DAG production and PLC-γ1 phosphorylation in ItpkB$^{-/-}$ thymocytes. (**A**) DAG content in ItpkB$^{+/+}$ or ItpkB$^{-/-}$ DP thymocytes stimulated with an antibody to CD3 is shown as relative change (±SEM) versus unstimulated samples at 15 s, 30 s, 1 min, and 5 min after stimulation. (**B**) Immunoblot analysis of PLC-γ1 activation, monitored via Tyr^{783} phosphorylation (*18*), in major histocompatibility complex–deficient (MHC$^{-/-}$) versus ItpkB$^{-/-}$ DP thymocytes. The blot was reprobed with an antibody to Ras as a loading control. Data are representative of three independent experiments. (**C**) ItpkB$^{+/+}$ or ItpkB$^{-/-}$ thymocytes cultured overnight with medium, with beads coated with antibody to CD3, or with PMA (1 ng/ml) were assessed for CD4, CD8, and CD69 surface expression by flow cytometry. Shown are percentages of CD69^{+} DP cells from four independent experiments (±SEM). (**D**) ItpkB$^{-/-}$ or ItpkB$^{+/-}$ neonatal thymic lobes were cultured with medium or PMA (0.1 ng/ml) for 4 to 5 days, followed by medium for 1 day, and analyzed. Top: TCRγδ^{-} gated CD4 and CD8 profiles. Bottom: Heat-stable antigen (CD24, HSA) expression on CD8 SP T cells. Data are representative of three independent experiments.

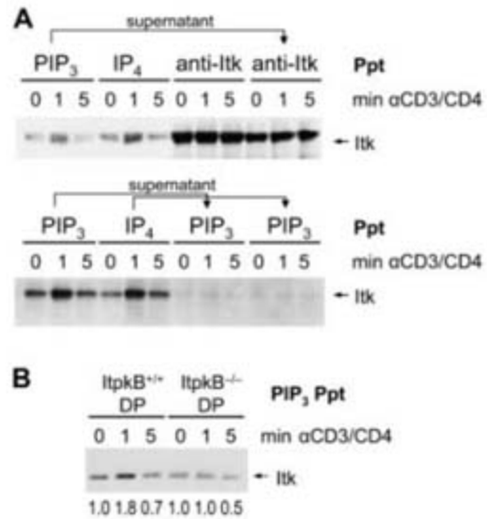

Fig. 2. TCR stimulation induces a transient, IP_4-dependent increase in Itk binding to PIP_3. (**A**) Lysates from wild-type DP cells unstimulated (0 min) or stimulated with antibodies to CD3 and CD4 (1 or 5 min) were precipitated with beads coated with PIP_3 or IP_4 or with antibody to Itk, followed by immunoblot analysis of Itk content. Where indicated, supernatants from primary precipitations were incubated with additional PIP_3-coated beads or antibody to Itk for secondary precipitation of unbound Itk. (**B**) Lysates from ItpkB$^{+/+}$ or ItpkB$^{-/-}$ DP thymocytes, either unstimulated or stimulated with antibodies to CD3 and CD4, were analyzed for Itk binding to PIP_3 as in (A). Quantification below lanes indicates relative change versus unstimulated controls.

or inositol 1,4,5,6-tetrakisphosphate had no effect on Itk binding to PIP_3 (Fig. 4, A and E). IP_4 augmentation is PIP_3-specific, as Itk binding to phosphatidylinositol 4,5-bisphosphate or phosphatidylinositol 3,4-bisphosphate (PIP_2) was unaffected (fig. S5, A and B).

The ability of IP_4 to promote PH domain binding to the cognate ligand PIP_3 is unexpected and striking. Several potential mechanisms could be envisioned (fig. S6). In one model, IP_4 binding induces a PH domain conformation with high affinity for both IP_4 and PIP_3. Excess PIP_3

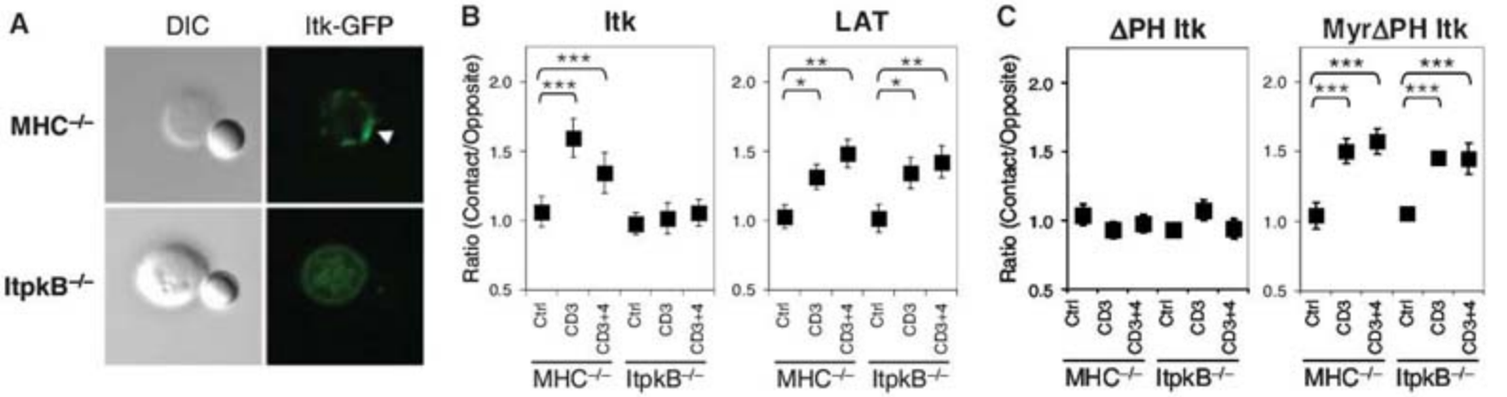

Fig. 3. IP_4 is required for Itk recruitment and activation. (**A** to **C**) $MHC^{-/-}$ or $ItpkB^{-/-}$ thymocytes nucleofected with wild-type (Itk), PH domain–deleted (ΔPH Itk), or myristoylated PH domain–deleted (MyrΔPH Itk) Itk-GFP or LAT-GFP fusion protein constructs were exposed to isotype control (Ctrl) beads or to beads coated with antibodies to CD3 and CD4 or to CD3 alone and analyzed by confocal microscopy. (A) Representative images of topologically comparable complexes [dichroic images, differential interference contrast (DIC)] reveal GFP-Itk accumulation at the bead-cell contact site for controls ($MHC^{-/-}$) but not for $ItpkB^{-/-}$ cells. (B) and (C) show mean localization indices (±SEM; n = 10 to 40). Statistical significance (Student's t test): $^*P < 0.044$, $^{**}P < 0.016$, $^{***}P < 0.0001$. Data are representative of three independent experiments. (**D**) Itk and LAT complex formation in $ItpkB^{+/+}$ or $ItpkB^{-/-}$ DP cells stimulated with antibodies to CD3 and CD4, as assessed by immunoblot analysis of Itk or LAT immunoprecipitates. LC, immunoglobulin light chain. (**E**) Itk immunoprecipitates from $ItpkB^{+/+}$ or $ItpkB^{-/-}$ DP thymocytes stimulated with antibodies to CD3 and CD4 were assessed for Itk phosphorylation by immunoblot with antibody to Btk phosphorylated at Tyr^{551} and to Itk phosphorylated at Tyr^{511} (pItk) or control antibody to Itk (Itk). Immunoblot analysis of ZAP-70 phosphorylation and LAT expression in whole-cell lysates (WCL) indicates robust activation (pZAP-70) and equal loading (LAT). Data are representative of three independent experiments.

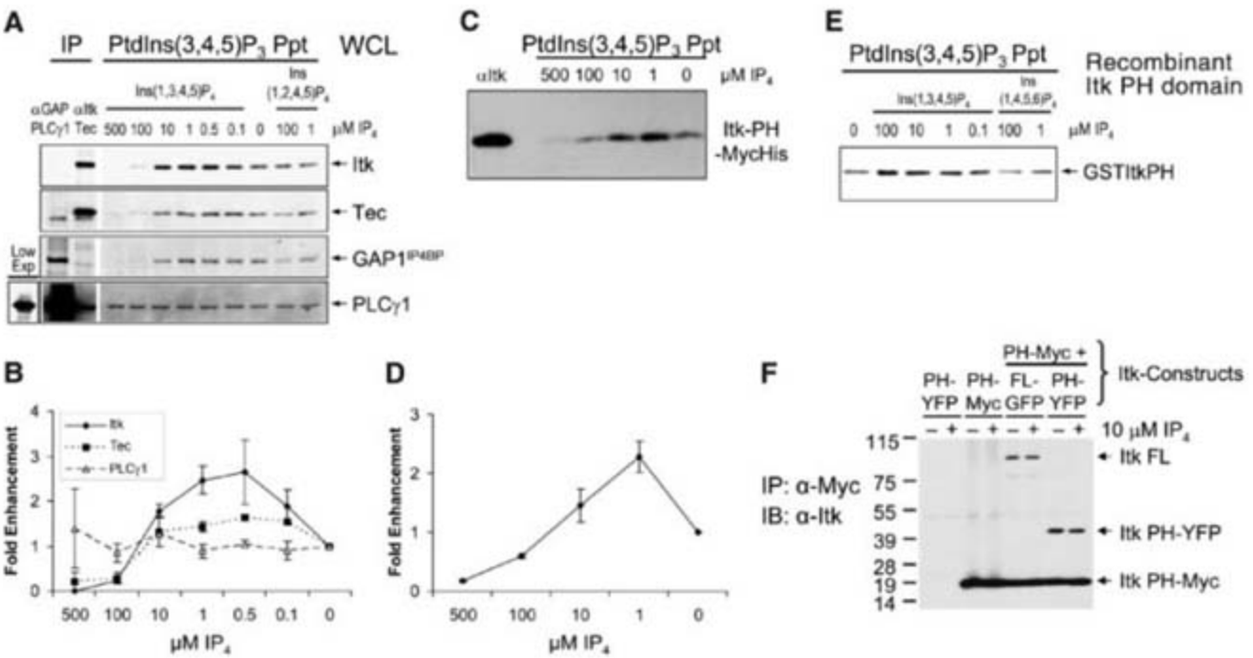

Fig. 4. IP_4 augments Itk PH domain binding to PIP_3. (**A**) Wild-type DP thymocyte lysates were incubated with PIP_3-coated beads with or without IP_4 or inositol 1,2,4,5-tetrakisphosphate [$Ins(1,2,4,5)P_4$], followed by immunoblot analysis of bound Itk, Tec, $GAP1^{IP4BP}$, or PLC-γ1. (**B**) Quantified data indicate relative change versus IP_4-free controls (±SEM). Data are representative of three independent experiments. (**C** and **D**) 293T cell lysates expressing Myc- and His-double-tagged Itk PH domain fragments were incubated with PIP_3-coated beads with or without IP_4 and analyzed as above. (D) Quantified data indicate average relative change ± range (n = 2). (**E**) Purified recombinant GST-Itk PH domain fusion protein was incubated with PIP_3-coated beads with or without IP_4 or inositol 1,4,5,6-tetrakisphosphate [$Ins(1,4,5,6)P_4$] and analyzed as in (A). (**F**) Immunoprecipitations with an antibody to Myc were conducted from lysates of 293T cells expressing Myc- and His-tagged (PH-Myc) or yellow fluorescent protein–tagged (PH-YFP) Itk PH domain fragments alone or together, or PH-Myc together with full-length Itk-GFP (FL-GFP) without or after addition of 10 μM IP_4, and were analyzed via SDS–polyacrylamide gel electrophoresis and immunoblot with an antibody to Itk.

at bead surfaces or sites of TCR ligation then displaces the bound IP_4 (fig. S6A). The ability of soluble PIP_3 to modulate Itk binding to PIP_3-coated beads with a dose response similar to that of IP_4 (fig. S5, C and D) is consistent with this "induced-fit model." An attractive alternative model is suggested by our finding that the Itk PH domain aggregates with other Itk PH domain fragments or full-length Itk in a manner unaffected by 10 μM IP_4 (Fig. 4F). IP_4 binding to one PH domain might induce conformational changes in the other subunits that increase their affinities for PIP_3 allosterically (fig. S6B). Future research will distinguish between these models and conclusively determine the precise mechanism by which IP_4 augments PH domain interactions with PIP_3.

Our results show that IP_4 acts as an essential mediator of Itk and PLC-γ1 activation and DAG production in DP thymocytes through Itk recruitment to sites of TCR engagement (fig. S7). This IP_4 function is essential for TCR signaling during thymocyte positive selection. Besides Itk, low-micromolar concentrations of IP_4 also augmented PIP_3 interactions of several other PH domain proteins, including Tec and $GAP1^{IP4BP}$ (*3*, *13*–*15*) (Fig. 4, A and B). In particular, IP_4 augmented PIP_3 binding of $GAP1^{IP4BP}$ PH domain fragments (fig. S5E). Dysregulation of several IP_4-regulated PH domain proteins could explain the phenotypic differences between $Itpkb^{-/-}$ (*2*, *3*) and $Itk^{-/-}$ mice (*6*). By contrast, PH domain–dependent PLC-γ1 binding to PIP_3-coated beads was unaffected by IP_4 (Fig. 4, A and B). Thus, positive or negative regulation of PIP_3 binding through soluble IP_4 may serve as a general mechanism that controls membrane recruitment of a group of PIP_3-binding proteins in a specific manner (Fig. 4 and fig. S5) (*16*). It will be interesting to determine whether defects in this mechanism of IP_4 action contribute to the impaired B cell development and function in $Itpkb^{-/-}$ mice, as reported in (*17*). PIP_3-binding proteins and IP_4 exist in all eukaryotes. Thus, IP_4 modulation of PH domain function likely has global implications.

References and Notes

1. T. K. Starr, S. C. Jameson, K. A. Hogquist, *Annu. Rev. Immunol.* **21**, 139 (2003).
2. V. Pouillon *et al.*, *Nat. Immunol.* **4**, 1136 (2003).
3. B. G. Wen *et al.*, *Proc. Natl. Acad. Sci. U.S.A.* **101**, 5604 (2004).
4. J. P. Roose, M. Mollenauer, V. A. Gupta, J. Stone, A. Weiss, *Mol. Cell. Biol.* **25**, 4426 (2005).
5. See supporting material on *Science* Online.
6. L. J. Berg, L. D. Finkelstein, J. A. Lucas, P. L. Schwartzberg, *Annu. Rev. Immunol.* **23**, 549 (2005).
7. M. Fukuda, T. Kojima, H. Kabayama, K. Mikoshiba, *J. Biol. Chem.* **271**, 30303 (1996).
8. T. Kojima, M. Fukuda, Y. Watanabe, F. Hamazato, K. Mikoshiba, *Biochem. Biophys. Res. Commun.* **236**, 333 (1997).
9. A. August, A. Sadra, B. Dupont, H. Hanafusa, *Proc. Natl. Acad. Sci. U.S.A.* **94**, 11227 (1997).
10. P. S. Costello, M. Gallagher, D. A. Cantrell, *Nat. Immunol.* **3**, 1082 (2002).
11. K. A. Ching, Y. Kawakami, T. Kawakami, C. D. Tsoukas, *J. Immunol.* **163**, 6006 (1999).
12. A. H. Guse, E. Greiner, F. Emmrich, K. Brand, *J. Biol. Chem.* **268**, 7129 (1993).
13. P. J. Cullen *et al.*, *Nature* **376**, 527 (1995).
14. M. Fukuda, K. Mikoshiba, *J. Biol. Chem.* **271**, 18838 (1996).
15. S. Yarwood, D. Bouyoucef-Cherchalli, P. J. Cullen, S. Kupzig, *Biochem. Soc. Trans.* **34**, 846 (2006).
16. R. Stricker, S. Adelt, G. Vogel, G. Reiser, *Eur. J. Biochem.* **265**, 815 (1999).
17. A. T. Miller *et al.*, *Nat. Immunol.* **8**, 514 (2007).
18. C. J. Serrano *et al.*, *J. Immunol.* **174**, 6233 (2005).

19. We thank J. Alberola-Ila, A. Altman, N. Gascoigne, T. Kawakami, G. Koretzky, L. Min, K. Mowen, R. Reisfeld, and C. Schmedt for discussions or reading of the manuscript; R. Kay for mice; and C. Dubord-Jackson, M. Young, and the GNF vivarium for mouse handling. Supported by GNF and NIH grant AR048848 (C.D.T.). The protein interactions reported here have been submitted to IMEx under accession numbers IM-8628 (Itk PH domain interactions) and IM-8629 (Itk, LAT, PLC-γ1 interactions).

Supporting Online Material

www.sciencemag.org/cgi/content/full/1138684/DC1
Materials and Methods
SOM Text
Figs. S1 to S7
References

11 December 2006; accepted 29 March 2007
Published online 5 April 2007;
10.1126/science.1138684
Include this information when citing this paper.

A Common Variant in the *FTO* Gene Is Associated with Body Mass Index and Predisposes to Childhood and Adult Obesity

Timothy M. Frayling,[1,2]* Nicholas J. Timpson,[3,4]* Michael N. Weedon,[1,2]* Eleftheria Zeggini,[3,5]* Rachel M. Freathy,[1,2] Cecilia M. Lindgren,[3,5] John R. B. Perry,[1,2] Katherine S. Elliott,[3] Hana Lango,[1,2] Nigel W. Rayner,[3,5] Beverley Shields,[2] Lorna W. Harries,[2] Jeffrey C. Barrett,[3] Sian Ellard,[2,6] Christopher J. Groves,[5] Bridget Knight,[2] Ann-Marie Patch,[2,6] Andrew R. Ness,[7] Shah Ebrahim,[8] Debbie A. Lawlor,[9] Susan M. Ring,[9] Yoav Ben-Shlomo,[9] Marjo-Riitta Jarvelin,[10,11] Ulla Sovio,[10,11] Amanda J. Bennett,[5] David Melzer,[1,12] Luigi Ferrucci,[13] Ruth J. F. Loos,[14] Inês Barroso,[15] Nicholas J. Wareham,[14] Fredrik Karpe,[5] Katharine R. Owen,[5] Lon R. Cardon,[3] Mark Walker,[16] Graham A. Hitman,[17] Colin N. A. Palmer,[18] Alex S. F. Doney,[19] Andrew D. Morris,[19] George Davey Smith,[4] The Wellcome Trust Case Control Consortium,† Andrew T. Hattersley,[1,2]‡§ Mark I. McCarthy[3,5]‡

Obesity is a serious international health problem that increases the risk of several common diseases. The genetic factors predisposing to obesity are poorly understood. A genome-wide search for type 2 diabetes–susceptibility genes identified a common variant in the *FTO* (fat mass and obesity associated) gene that predisposes to diabetes through an effect on body mass index (BMI). An additive association of the variant with BMI was replicated in 13 cohorts with 38,759 participants. The 16% of adults who are homozygous for the risk allele weighed about 3 kilograms more and had 1.67-fold increased odds of obesity when compared with those not inheriting a risk allele. This association was observed from age 7 years upward and reflects a specific increase in fat mass.

Obesity is a major cause of morbidity and mortality, associated with an increased risk of type 2 diabetes mellitus, heart disease, metabolic syndrome, hypertension, stroke, and certain forms of cancer. It is typically measured clinically with the surrogate measure of body mass index (BMI), calculated as weight divided by height squared. Individuals with a BMI ≥ 25 kg/m^2 are classified as overweight, and those with a BMI ≥ 30 kg/m^2 are considered obese. The prevalence of obesity is increasing worldwide, probably as the result of changed lifestyle. In 2003–2004, 66% of the U.S. population had a BMI ≥ 25 kg/m^2, and 32% were obese (*1*).

Twin and adoption studies have demonstrated that genetic factors play an important role in influencing which individuals within a population are most likely to develop obesity in response to a particular environment (*2*). However, despite considerable efforts, there are, as yet, no examples of common genetic variants for which there is widely replicated evidence of association with obesity in the general population. Monogenic forms of obesity at present account for ~7% of children with severe, young-onset obesity (*3*), but as this severity of obesity is only seen in <0.01% of the population, these mutations are rare in the general population. Recent attempts to identify gene variants predisposing to common, polygenic obesity have proven controversial. Initial reports of promising associations between common variants in the *GAD2* (*4*–*7*), *ENPP1* (*5*, *8*, *9*) and *INSIG2* (*9*–*12*) genes and altered BMI have not been widely replicated.

Obesity is a major risk factor for type 2 diabetes, and variants that influence the development of obesity may also predispose to type 2 diabetes. As part of the Wellcome Trust Case

Control Consortium (WTCCC), we recently completed a genome-wide association study comparing 1924 U.K. type 2 diabetes patients and 2938 U.K. population controls for 490,032 autosomal single-nucleotide polymorphisms (SNPs) (Wellcome Trust Case Control Consortium). SNPs in the *FTO* (fat mass and obesity associated) gene region on chromosome 16 were strongly associated with type 2 diabetes (e.g., rs9939609, OR = 1.27; 95% CI = 1.16 to 1.37; $P = 5 \times 10^{-8}$). This association was replicated by analyzing SNP rs9939609 in a further 3757 type 2 diabetes cases and 5346 controls (OR = 1.15; 95% CI = 1.09 to 1.23; $P = 9 \times 10^{-6}$). Analysis of BMI as a continuous trait was possible in the initial diabetes cases and in all replication samples but not in the initial control samples. The diabetes-risk alleles at *FTO* were strongly associated with increased BMI (Table 1). In the replication samples, the association between *FTO* SNPs and type 2 diabetes was abolished by adjustment for BMI (OR = 1.03; 95% CI = 0.96 to 1.10; $P = 0.44$), which suggests that the association of these SNPs with T2D risk is mediated through BMI. The major signal for association with BMI coincides perfectly with that for type 2 diabetes, and rs9939609 represents a cluster of 10 SNPs in the first intron of *FTO* that are associated with both traits (Fig. 1). All BMI-associated SNPs (P ranging from 1×10^{-4} to 1×10^{-5}) are highly correlated with each other (r^2 from 0.52 to 1.0). SNP rs9939609 was used in all further studies, because among the cluster of most highly associated SNPs it had the highest genotyping success rate (100%). The HapMap (haplotype map of the human genome) population frequencies of the rs9939609 A allele are 0.45 in the CEPH (Centre d'Etude du Polymorphisme Humain) Europeans, 0.52 in Yorubans, and 0.14 in Chinese and Japanese.

We studied the association of *FTO* gene variation with BMI and the risk of being overweight and obese in an additional 19,424 white European adults from seven general population-based studies (mean age 28 to 74 years, mean BMI 22.7 to 27.2 kg/m^2) and in 10,172 white European children from two studies (mean age 7 to 14 years, mean BMI 16.1 to 19.2 kg/m^2) [table S1 and supporting online text (*13*)].

In all adult population-based studies, we found that the type 2 diabetes–associated A allele of rs9939609 (frequency 39%) was associated with increased BMI (Table 1) with a median per-allele

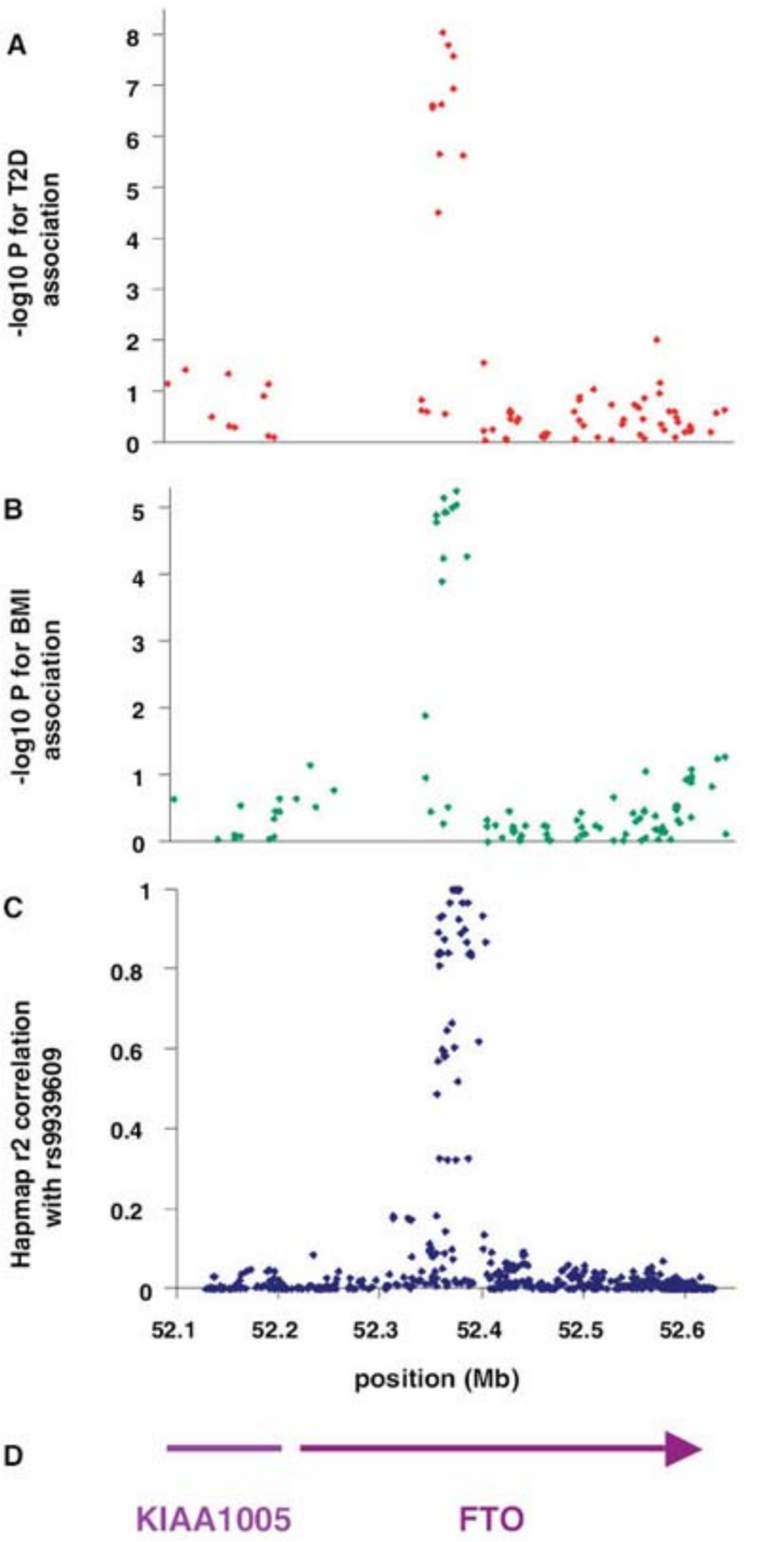

Fig. 1. Associations of SNPs in the *FTO/KIA1005* region of chromosome 16 with (**A**) type 2 diabetes using 1924 cases and 2938 controls and (**B**) adult BMI in type 2 diabetic patients. (**C**) Linkage disequilibrium (r^2) between associated SNP rs9939609 and all other SNPs in HapMap data in Caucasian European samples. (**D**) Gene positions.

[1]Genetics of Complex Traits, Institute of Biomedical and Clinical Science, Peninsula Medical School, Magdalen Road, Exeter, UK. [2]Diabetes Genetics, Institute of Biomedical and Clinical Science, Peninsula Medical School, Barrack Road, Exeter, UK. [3]Wellcome Trust Centre for Human Genetics, University of Oxford, Roosevelt Drive, Oxford, UK. [4]MRC Centre for Causal Analyses in Translational Epidemiology, Bristol University, Canynge Hall, Whiteladies Road, Bristol, UK. [5]Oxford Centre for Diabetes, Endocrinology and Metabolism, University of Oxford, Churchill Hospital, Oxford, UK. [6]Molecular Genetics Laboratory, Royal Devon and Exeter National Health Service Foundation Trust, Old Pathology Building, Barrack Road, Exeter, UK. [7]Department of Oral and Dental Science, University of Bristol Dental School, Lower Maudlin Street, Bristol, UK. [8]Department of Epidemiology and Population Health, London School of Hygiene and Tropical Medicine, London, UK. [9]Department of Social Medicine, University of Bristol, Canynge Hall, Whiteladies Road, Bristol, UK. [10]Department of Epidemiology and Public Health, Imperial College London, Norfolk Place, London W2 1PG, UK. [11]Department of Public Health Science and General Practice, Fin-90014, University of Oulu, Finland. [12]Epidemiology and Public Health Group, Peninsula Medical School, Barrack Road, Exeter, UK. [13]Longitudinal Studies Section, Clinical Research Branch, National Institute on Aging, National Institutes of Health, Baltimore, MD, USA. [14]Medical Research Council Epidemiology Unit, Strangeways Research Laboratories, Cambridge, UK. [15]Metabolic Disease Group, Wellcome Trust Sanger Institute, Hinxton, Cambridge, UK. [16]Diabetes Research Group, School of Clinical Medical Sciences, Newcastle University, Framlington Place, Newcastle upon Tyne, UK. [17]Centre for Diabetes and Metabolic Medicine, Barts and The London, Royal London Hospital, Whitechapel, London, UK. [18]Population Pharmacogenetics Group, Biomedical Research Centre, Ninewells Hospital and Medical School, University of Dundee, Dundee, UK. [19]Diabetes Research Group, Division of Medicine and Therapeutics, Ninewells Hospital and Medical School, University of Dundee, Dundee, UK.

*These authors contributed equally to this work.
†Membership of the Wellcome Trust Case Control Consortium is listed in the Supporting Online Material.
‡These authors contributed equally to this work.
§To whom correspondence should be addressed. E-mail: Andrew.Hattersley@pms.ac.uk

change of ~0.36 kg/m^2 (range 0.34 to 0.46 kg/m^2). In each study, carriers of two A alleles had a higher BMI than heterozygote individuals; when we compared the additive model to a general model in each study, there was no consistent evidence for departure from an additive model. Because there was no evidence of heterogeneity ($I^2 = 0\%$) across the adult studies (*14*), we combined them using the inverse variance method to pool continuous data (*Z* scores) and the Mantel-Haenszel method for binary data. Each additional copy of the rs9939609 A allele was associated with a BMI increase of a mean of 0.10 *Z*-score units (95% CI = 0.08 to 0.12; $P = 2 \times 10^{-20}$), equivalent to ~0.4 kg/m^2. When these data were combined with those from the case-control samples (a total of 30,081 participants), the statistical confidence of the association was further increased ($P = 3 \times 10^{-35}$) (Table 1 and fig. S1). When we applied a Bonferroni correction for the number of tests performed in the initial genome-wide scan (~400,000), the association remained significant ($P = 1.2 \times 10^{-29}$). This association was present in adults of all ages (Table 1) and of both sexes (fig. S1B and S1C), with no difference between males and females ($P = 0.13$).

Although BMI is a continuous trait, standard cut-offs are used to assess the burden of increased body weight on health. Hence, we assessed whether the inheritance of the *FTO* SNP rs9939609 altered the risk of being either overweight or obese compared with being normal weight (<25 kg/m^2). In all the studies, the A allele was associated with increased odds of being overweight (Fig. 2A) and also of being obese (Fig. 2B and table S2). In a meta-analysis of the population-based studies, the per-A allele odds ratio (OR) for obesity in the adult general population was 1.31 (95% CI = 1.23 to 1.39; $P = 6 \times 10^{-16}$); for overweight, it was 1.18 (95% CI = 1.13 to 1.24; $P = 1 \times 10^{-12}$). When participants from the type 2 diabetes case and

Table 1. Association of BMI with rs9939609 genotypes, corrected for sex, in type 2 diabetes cases from genome-wide and replication studies, control participants from replication studies, and adult population-based studies. *P* values represent the change per A allele. BMI presented as geometric means and back-transformed 95% confidence intervals.

Study	Age, years (mean, SD)	Males (%)	*N*	Mean BMI (95% CI) by genotype			*P*
				TT	AT	AA	
Type 2 diabetes							
UK cases (WTCCC)	58.6 (10.3)	58	1913	30.15 (29.69, 30.62)	30.47 (30.12, 30.83)	31.99 (31.39, 32.59)	8×10^{-6}
UK T2D Cases	59.2 (8.6)	58	609	30.89 (30.12, 31.69)	31.14 (30.51, 31.78)	33.46 (32.38, 34.58)	0.001
UKT2D GCC Cases	64.1 (9.6)	57	2961	30.59 (30.24, 30.95)	30.96 (30.67, 31.26)	31.98 (31.48, 32.50)	3×10^{-5}
Combined T2D (I^2)							3×10^{-11} (15.6%)
Nondiabetic controls							
EFSOCH	31.8 (5.6)	51	1746	24.50 (24.21, 24.80)	25.21 (24.95, 25.47)	25.41 (24.92, 25.91)	0.0002
UKT2D GCC Controls	58.8 (11.9)	52	3428	26.25 (26.02, 26.48)	26.34 (26.13, 26.54)	27.07 (26.71, 27.44)	0.001
Population-based studies							
Adult							
ALSPAC (mothers)	28.4 (4.7)	0	6376	22.42 (22.28, 22.56)	22.73 (22.61, 22.85)	23.27 (23.03, 23.51)	3×10^{-10}
NFBC1966 (age 31)	31	48	4435	24.12 (23.94, 24.31)	24.43 (24.26, 24.60)	24.82 (24.53, 25.12)	5×10^{-5}
Oxford Biobank	40.6 (6.1)	55	765	25.48 (25.02, 25.94)	25.36 (24.95, 25.78)	26.43 (25.70, 27.17)	0.09
Older adult							
Caerphilly	56.7 (4.5)	100	1328	26.10 (25.80, 26.40)	26.48 (26.20, 26.76)	26.69 (26.11, 27.28)	0.03
EPIC-Norfolk	59.7 (9.0)	47	2425	25.87 (25.63, 26.11)	26.20 (25.99, 26.42)	26.61 (26.22, 27.01)	0.001
BWHHS	68.8 (5.5)	0	3244	26.77 (26.51, 27.02)	27.33 (27.09, 27.56)	27.58 (27.17, 28.00)	0.0002
InCHIANTI	74.3 (6.9)	45	851	26.99 (26.53, 27.47)	26.99 (26.61, 27.37)	27.84 (27.23, 28.46)	0.06
Combined population studies (I^2)							2×10^{-20} (0%)
Combined population and control studies (I^2)							1×10^{-25} (0%)
All studies (I^2)							3×10^{-35} (0%)

Table 2. Association of BMI (corrected for sex) and birth weight (corrected for sex and gestational age) with rs9939609 genotypes in children. *P* values represent the change in log BMI per A allele. BMI presented as geometric means and back-transformed 95% confidence intervals.

Cohort	Age (years)	Males (%)	*N*	Mean trait value (95% CI) by genotype			*P*
				TT	AT	AA	
Children*							
ALSPAC	7	51	5969	16.00 (15.92, 16.07)	16.11 (16.04, 16.18)	16.31 (16.19, 16.43)	3×10^{-5}
	8	50	4871	16.80 (16.70, 16.90)	17.01 (16.92, 17.09)	17.29 (17.14, 17.45)	1×10^{-7}
	9	50	5459	17.20 (17.08, 17.31)	17.53 (17.43, 17.63)	17.86 (17.69, 18.04)	5×10^{-11}
	10	50	5273	17.66 (17.54, 17.79)	18.05 (17.94, 18.17)	18.37 (18.18, 18.57)	1×10^{-10}
	11	49	5010	18.46 (18.32, 18.61)	18.82 (18.70, 18.94)	19.20 (18.98, 19.42)	7×10^{-9}
NFBC1966 (age 14)	14	47	4203	19.14 (19.02, 19.26)	19.25 (19.14, 19.36)	19.38 (19.19, 19.57)	0.04
Birth†							
ALSPAC	0	51	7477	3438 (3422, 3455)	3452 (3437, 3466)	3454 (3429, 3480)	0.21
NFBC1966	0	47	4320	3523 (3501, 3546)	3538 (3518, 3558)	3536 (3501, 3571)	0.42

*ALSPAC children are offspring of the participants included in the adult study (Table 1), and data are shown at five available ages. NFBC1966 children are the same participants as those in the adult study (Table 1). †ALSPAC birth data are for the same participants as those in the children study. NFBC1966 birth data are for the same participants as those in the children and adult studies. Non-singleton births and individuals born at gestation <36 weeks were excluded from the birth-weight analysis.

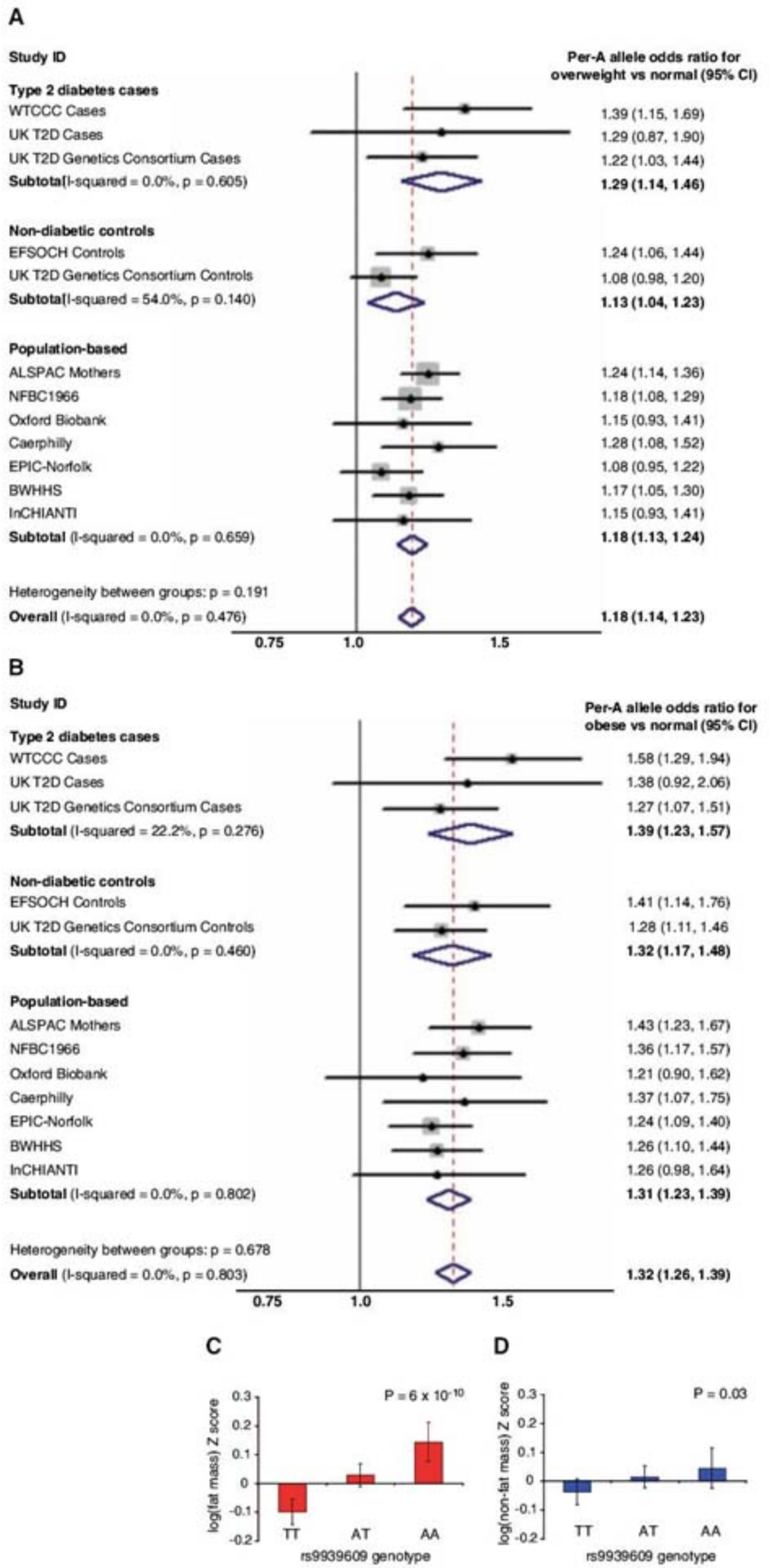

Fig. 2. (**A** and **B**) Meta-analysis plots for odds of (A) overweight and (B) obesity, compared with normal weight in adults for each copy of the A allele of rs9939609 carried. (**C** and **D**) Bar charts showing (C) DEXA-measured fat mass in 9-year-old children and (D) DEXA-measured lean mass in 9-year-old children, both from the ALSPAC study. Error bars represent 95% confidence intervals

control studies were included, the magnitude of the association was unchanged, although the statistical confidence increased (obesity: OR = 1.32; 95% CI 1.26 to 1.39; $P = 3 \times 10^{-26}$; overweight: OR = 1.18; 95% CI = 1.14 to 1.23], $P = 2 \times 10^{-17}$). Individuals homozygous for the A allele at rs9939609 (16% of the population) are at substantially increased risk of being overweight (OR = 1.38; 95% CI = 1.26 to 1.52]; $P = 4 \times 10^{-11}$) or obese (OR = 1.67; 95% CI = 1.47 to 1.89; $P = 1 \times 10^{-14}$) compared with those homozygous for the low-risk T allele (37% of the population). The extent of the variance in BMI explained by rs9939609 was ~1%, and the population attributable risk was 20.4% for obesity and 12.7% for overweight.

Childhood obesity is also increasing rapidly worldwide and is a cause of considerable concern (*15*). To determine the age at which the association of *FTO* SNP rs9939609 with BMI first becomes evident, we analyzed two large birth cohorts for which suitable measures were available from birth to early adolescence. These included 7477 UK children from the Avon Longitudinal Study of Parents and Children (ALSPAC) cohort who had anthropometric measures at birth and at 7, 8, 9, 10, and 11 years of age and 4320 children from the Northern Finland 1966 birth cohort (NFBC1966) with birth measures as well as height and weight available at 14 years. rs9939609 was not associated with birth weight (Table 2) or ponderal index at birth (table S3A) in either cohort. In children from the ALSPAC study, each copy of the rs9939609 A allele was associated with an increase in BMI by 0.08 *Z*-score units (95% CI = 0.04 to 0.12; $P = 3 \times 10^{-5}$; ~0.2 kg/m^2) at age 7, an association maintained up to the most recent assessment at age 11, when the per-allele increase was 0.12 *Z*-score units (95% CI = 0.08 to 0.16; $P = 7 \times 10^{-9}$; ~0.4 kg/m^2) (Table 2). At all ages, the A allele was associated with an increased risk of childhood obesity (e.g., OR per-A allele at age 11 years = 1.35; CI = 1.14, 1.61; $P = 6 \times 10^{-4}$) and of being overweight (e.g., OR per-A allele at age 11 years = 1.27; CI = 1.16 to 1.39; $P = 2 \times 10^{-7}$), as defined by age-specific BMI (table S2). In the Finnish cohort, each copy of the rs9939609 A allele was associated with an increase in BMI by 0.05 *Z*-score units (95% CI = 0.003 to 0.09; $P = 0.04$; ~0.1 kg/m^2) at the age of 14 years (Table 2). We conclude therefore that *FTO* SNP rs9939609 is not associated with changes in fetal growth but is associated with changes in BMI and obesity in children by the age of 7, changes that persist into the prepubertal period and beyond.

BMI is a convenient surrogate measure for obesity, but it may be influenced by changes in height, bone mass, and lean mass, as well as adiposity. We used additional anthropometric measurements available in the study samples to address this issue. In all population-based cohorts, the rs9939609 A allele was associated with higher weight (overall per-A allele increase =

0.09 Z-score units; 95% CI = 0.07 to 0.11); $P = 4 \times 10^{-17}$; ~1.2 kg in adults) (tables S3B and S3C), but there was no difference in height (tables S3C and S3D). Consistent with this observation, we found evidence for higher waist circumference (overall per-A allele = 0.08 Z-score units; 95% CI = 0.05 to 0.11; $P = 4 \times 10^{-9}$; ~1 cm) (table S3E) and higher subcutaneous mass assessed by skinfold measures (per-A allele difference = 0.11 Z-score units; 95% CI = 0.06 to 0.16; $P = 2 \times 10^{-5}$) (table S3F). In the children from the ALSPAC study, dual-energy x-ray absorptiometry (DEXA)–derived measures of fat mass and lean mass were available at age 9. The association of rs9939609 A allele with weight was almost exclusively attributable to changes in fat mass, with a per-allele difference of 0.12 Z-score units (95% CI = 0.08 to 0.16; $P = 6 \times 10^{-10}$), equivalent to a 14% difference across the three genotype groups) (Fig. 2C). Genotype-related differences in lean mass were, in contrast, a modest 0.04 Z-score units (95% CI = 0.005 to 0.08; $P = 0.03$), which is equivalent to a 1% increase across the three genotype groups) (Fig. 2D). Therefore, the association of genetic variation at *FTO* with BMI results from longitudinal changes in fat mass that, on the basis of anthropometric measures, reflect both increased waist circumference and subcutaneous fat.

One important potential source of false-positive associations in genetic studies is population stratification. We do not believe this is likely to be important in the association of the *FTO* SNP with BMI or type 2 diabetes. In all study cohorts, any individuals who were not European whites were excluded. In addition the cohorts were all recruited from single countries, with the majority coming from specific small geographically defined regions, and the analysis for association was done only within individual cohorts. Analysis of the *FTO* signal does not support this association resulting from population stratification. In the original genome-wide association study, the principal component analysis (*16*) implemented in EIGENSTRAT (*17*) made no difference to the evidence for association for type 2 diabetes ($P = 5.3 \times 10^{-8}$ with EIGENSTRAT adjustment and 5.2×10^{-8} without). Similarly, adjusting for the 11 geographic regions did not alter the significance of the *FTO* association for BMI ($P = 9 \times 10^{-6}$ adjusted; 8×10^{-6} unadjusted). The minor allele frequency of rs9939609 differs very little across our studies from Finland, Italy, and many different regions in the UK ranging from 0.38 to 0.40 in all except the second-smallest study, where it was 0.44. We found no significant regional variation in allele frequency in UK type 2 diabetic patients, whether testing 4 ($P = 0.41$) or 11 ($P = 0.22$) geographical regions of residence. For all these reasons, we do not believe that stratification/structure effects provide a realistic interpretation of our findings.

We have shown that common variation in the *FTO* gene is reproducibly associated with BMI and obesity from childhood into old age. SNP rs9939609 lies within the first intron of the *FTO* gene and, based on information from HapMap, is highly correlated ($r^2 > 0.5$), with 45 additional SNPs within a 47-kb region that encompasses parts of the first two introns as well as exon 2 of *FTO*. There are no features to suggest that any of these SNPs represents the functional variant. Linkage disequilibrium between the BMI-associated SNPs and other variants falls rapidly outside the 47-kb region, such that there are no SNPs correlated at $r^2 > 0.2$ outside a 90-kb interval (Fig. 1 and fig. S2). Sequencing of 47 individuals selected for BMI > 40 kg/m^2 has revealed no clear candidate functional variants in the *FTO* coding region and minimal splice sites or 3′ UTR to explain the association (table S4). *FTO* is closely adjacent to a gene of unknown function *KIAA1005* (Fig. 1 and fig. S2), which is transcribed in the opposite direction. This opens up the possibility that genetic variation affects a regulatory element for *KIAA1005*; however, there is no obvious such variant within the 47-kb associated region. We conclude that the 47-kb intron within the *FTO* gene is most likely to contain the predisposing variant(s), but there is, at present, no clear genetic mechanism to explain how this alters the function or expression of *FTO*, *KIAA1005*, or more distant genes.

FTO is a gene of unknown function in an unknown pathway that was originally cloned as a result of the identification of a fused-toe (*Ft*) mutant mouse that results from a 1.6-Mb deletion of mouse chromosome 8 (*18*). Three genes of unknown function (*Fts*, *Ftm* and *Fto*), along with three members of the Iroquois gene family (*Irx3*, *Irx5*, and *Irx6* from the *IrxB* gene cluster), are deleted in *Ft* mice (*18*). The homozygous *Ft* mouse is embryonically lethal and shows abnormal development, including left/right asymmetry (*19*). Heterozygous animals survive and are characterized by fused toes on the forelimbs and thymic hyperplasia but have not been reported to have altered body weight or adiposity (*19*). The fused-toe mutant is a poor model for studying the role of altered *Fto* activity, because multiple genes are deleted. Neither isolated inactivation nor overexpression of *Fto* has been described.

We used reverse transcription PCR to assess the expression of *FTO* and *KIAA1005* in a human tissue panel (*18*). *FTO* was found to be widely expressed in fetal and adult tissues, with expression highest in the brain (fig. S3A). The transcription start site of *KIAA1005* lies only 200 base pairs from the 5′ end of *FTO* and ~61 kb from the 47-kb interval containing the BMI associations. *KIAA1005* is also ubiquitously expressed with relatively high levels in hypothalamus and islet (fig. S3B). The similarity of expression profile between these two transcripts may indicate joint transcriptional regulation but does not provide insights into which of the two genes is more likely to be involved. Further work with both knockout and overexpression models of *FTO* and *KIAA1005* are likely to provide the most fruitful approach to understanding the mechanism and pathways whereby these variants influence the risk of obesity.

References and Notes

1. C. L. Ogden *et al.*, *JAMA* **295**, 1549 (2006).
2. H. H. M. Maes, M. C. Neale, L. J. Eaves, *Behav. Genet.* **27**, 325 (1997).
3. I. S. Farooqi, S. O'Rahilly, *Endocr. Rev.* 10.1210/er.2006-0040 (2006).
4. P. Boutin *et al.*, *PLoS Biol.* **1**, 361 (2003).
5. D. Meyre *et al.*, *Nat. Genet.* **37**, 863 (2005).
6. M. M. Swarbrick *et al.*, *PLoS Biol.* **3**, 1662 (2005).
7. C. J. Groves *et al.*, *Diabetes* **55**, 1884 (2006).
8. M. N. Weedon *et al.*, *Diabetes* **55**, 3175 (2006).
9. A. Herbert *et al.*, *Science* **312**, 279 (2006).
10. R. J. F. Loos, I. Barroso, S. O'Rahilly, N. J. Wareham, *Science* **315**, 179c (2007).
11. D. Rosskopf *et al.*, *Science* **315**, 179d (2007).
12. C. Dina *et al.*, *Science* **315**, 179b (2007).
13. Materials and methods are available as supporting material on *Science* Online.
14. J. P. Higgins, S. G. Thompson, J. J. Deeks, D. G. Altman, *BMJ* **327**, 557 (2003).
15. T. Lobstein, L. Baur, R. Uauy, *Obes. Rev.* **5**, 4 (2004).
16. S. Zhang, X. Zhu, H. Zhao, *Genet. Epidemiol.* **24**, 44 (2003).
17. A. L. Price *et al.*, *Nat. Genet.* **38**, 904 (2006).
18. T. Peters, K. Ausmeier, R. Dildrop, U. Rüther, *Mamm. Genome* **13**, 186 (2002).
19. F. van der Hoeven *et al.*, *Development* **120**, 2601 (1994).

20. Collection of the type 2 diabetes cases was supported by Diabetes UK, British Diabetic Association Research, and the UK Medical Research Council (Biomedical Collections Strategic Grant G0000649). The UK Type 2 Diabetes Genetics Consortium collection was supported by the Wellcome Trust (Biomedical Collections Grant GR072960). The ALSPAC study was supported by the UK Medical Research Council (MRC), the Wellcome Trust, and the University of Bristol. The British Women's Heart and Health Study was funded by the Department of Health and the British Heart Foundation. The Caerphilly study was funded by MRC and the British Heart Foundation. The Caerphilly study was undertaken by the former MRC Epidemiology Unit (South Wales) and was funded by the MRC. The data archive is maintained by the Department of Social Medicine, University of Bristol. The Exeter Family Study of Childhood Health was supported by NHS Research and Development and the Wellcome Trust. The work on the Northern Finland birth cohort study was supported by the Academy of Finland (104781), MRC (G0500539), and the Wellcome Trust (Project Grant GR069224). Oxford Biobank was supported by the British Heart Foundation. The Invecchiare in Chianti (InCHIANTI) study was supported by contract funding from the U.S. National Institute on Aging (NIA), and the research was supported in part by the Intramural Research Program, NIA, NIH. The European Prospective Investigation of Cancer (EPIC)–Norfolk cohort study is supported by program grants from MRC and Cancer Research UK. The EPIC-Norfolk obesity case-cohort study and its genotyping was funded by the Wellcome Trust and MRC. The genome-wide association genotyping was supported by the Wellcome Trust (076113), and replication genotyping was supported by the Wellcome Trust, Diabetes UK, the European Commission (EURODIA LSHG-CT-2004-518153), and the Peninsula Medical School. Personal funding comes from the Wellcome Trust (A.T.H., Research Leave Fellow; I.B., Investigator; E.Z., Research Career Development Fellow; L.R.C., Principal Research Fellow); MRC (J.R.B.P.); Diabetes UK (R.M.F.); and Throne-Holst Foundation (C.M.L.). L.W.H. is a Research Councils UK Diabetes and Metabolism Academic Fellow. M.N.W. is Vandervell Foundation Research Fellow at the Peninsula Medical School. C.N.A.P. and A.D.M. are supported by the Scottish executive as part of the Generation Scotland Initiative. We acknowledge the

assistance of many colleagues involved in sample collection, phenotyping, and DNA extraction in all the different studies. We thank K. Parnell, C. Kimber, A. Murray, K. Northstone, and C. Boustred for technical assistance. We thank S. Howell, M. Murphy, and A. Wilson (Diabetes UK) for their long-term support for these studies. We also acknowledge the efforts of J. Collier, P. Robinson, S. Asquith, and others at Kbiosciences.

Accession numbers for deposited sequence variants from dbSNP are Exon3_A 69374768, 3_UTR_A 69374769, 3_UTR_B 69374770, and 3_UTR_G 69374771.

Supporting Online Material
www.sciencemag.org/cgi/content/full/1141634/DC1
Materials and Methods
SOM Text
Figs. S1 to S3
Tables S1 to S4
References

22 February 2007; accepted 6 April 2007
Published online 12 April 2007;
10.1126/science.1141634
Include this information when citing this paper.

Bat Flight Generates Complex Aerodynamic Tracks

A. Hedenström,[1]* L. C. Johansson,[1] M. Wolf,[1] R. von Busse,[2] Y. Winter,[2,3]† G. R. Spedding[4]

The flapping flight of animals generates an aerodynamic footprint as a time-varying vortex wake in which the rate of momentum change represents the aerodynamic force. We showed that the wakes of a small bat species differ from those of birds in some important respects. In our bats, each wing generated its own vortex loop. Also, at moderate and high flight speeds, the circulation on the outer (hand) wing and the arm wing differed in sign during the upstroke, resulting in negative lift on the hand wing and positive lift on the arm wing. Our interpretations of the unsteady aerodynamic performance and function of membranous-winged, flapping flight should change modeling strategies for the study of equivalent natural and engineered flying devices.

Bats and birds represent two independent evolutionary pathways solving the same problem: powered vertebrate flight. The smaller species show similar wing morphology, kinematics, and flight speeds and operate at similar Reynolds number (*1*). However, the wings of bats and birds also differ in some important respects. For example, the primary feathers of a bird wing can be separated so air can pass through as in a Venetian blind to produce a feathered (and aerodynamically inactive) upstroke. Although bat wing membranes can be actively stretched and collapsed (*2*), they probably cannot be made aerodynamically inactive as easily as bird wing feathers. Flapping wings generate trailing vortices containing information about the time-history and magnitude of the aerodynamic force produced during the wingbeat, and so wake vortices act as an aerodynamic footprint marking the previous passage of the animal through the air (*3*–*10*). The equivalence of forces exerted between a solid object and the surrounding fluid is a consequence of Newton's laws and has long been exploited to estimate drag forces from wake momentum fluxes (*11*, *12*). Similarly, for a lifting body immersed in a uniform flow of speed U, the aerodynamic lift per unit of span can be written as $L' = \rho U \Gamma$, where ρ is air density and Γ is the circulation on the wing section. In the absence of viscosity, vorticity and circulation are conserved according to Helmholtz's laws, and so any change in aerodynamic force (and hence circulation on the wing) must be associated with the shedding into the wake of vorticity of opposite sign, whose circulation matches the change on the wing.

The wake vortices of three bird species have recently been studied in some detail across wide speed ranges (*8*, *10*, *13*), whereas those of bats have received comparatively little attention (*6*). In the one qualitative study of airflows behind bats passing through a bubble cloud (*6*), the bats were reported to generate single vortex loops from each downstroke (with an inactive upstroke) at slow speed, whereas at a faster cruising speed, a pair of undulating vortices trailed the path of the wingtips throughout the wingbeat, implying that the upstroke generated lift. However, kinematic studies show a wingtip reversal during the upstroke during hovering and slow speed in bats (*14*–*19*), suggesting a reversal of the wing circulation during the upstroke, whose signature should be observable in the wake.

We made a systematic and quantitative study of the variation in wake topology and relative down- and upstroke function with flight speed in a small nectar-feeding phyllostomid bat species, *Glossophaga soricina*. Although detailed kinematics data are available for this species across a speed range from 1.2 to 7.5 m/s (*19*), it is impossible to infer the wake vortex distribution from kinematics alone (*19*). The aim was also to test the hypotheses, based on kinematics, that (i) the backward flick of the wing at slow speeds, as inferred on the basis of kinematics, generates lift and thrust (*14*, *16*, *17*, *19*); and (ii) that the negative angle of attack during the upstroke at moderate speeds generates negative lift (*14*, *16*, *19*). Images of the wake were analyzed by means of a digital particle image velocimetry (DPIV) method, and the quantitative measures of wake vorticity and total circulation were used to deduce the magnitude of aerodynamic forces and construct the wake topology (*20*).

We studied the wakes generated by two adult *G. soricina* individuals across the speed range from 1.5 to 7 m/s [body mass, 11 g; wingspan, 0.24 m; aspect ratio, 6.3 (*21*); Reynolds number (Re) $\approx 4 \times 10^3$ to 18×10^3; Strouhal number (St) ≈ 0.27 to 0.81 (*22*)]. Two orientations of the image plane were used: (i) a vertical streamwise plane aligned with the flow at three different positions along the wing span (outer wing, inner wing, and mid-body), and (ii) a cross-stream plane aligned perpendicular to the flow direction (Trefftz plane) (*20*).

We focus our presentation of the wakes on slow (1.5 m/s), medium (4 m/s), and high (6.5 m/s) speeds, which cover the natural range of forward speeds (*19*, *23*). At slow speed (top row of Fig. 1), a strong start vortex, formed at the beginning of the downstroke, can be seen across the span (red blobs at right in Fig. 1, A to C, marked 1 in Fig. 1A). At the transition from downstroke to upstroke, the wing goes through a large supination (pitch-up rotation), so that the wing is flipped upside down. At this point, a combined stop-and-start vortex is shed (blue blob, left side of Fig. 1, A to C). During the upstroke, the wing moves backward faster than the forward speed, with circulation reversed, and the induced flow in the wake is primarily a backward-directed jet. Thus, the net aerodynamic force is forward (thrust) and upward (lift). At the following transition from upstroke to downstroke, the wings pronate rapidly (a pitch-down rotation), to shed a combined start/stop vortex for the next downstroke. This start/stop vortex (2 in Fig. 1A) appears above the previous one (1 in Fig. 1A) because the wake has convected downward in the interim. At the higher flight speed of 4 m/s, illustrated in the next two rows of Fig. 1 (panels D to F for downstroke and G to I for upstroke), the wake structure is quite different. The downstroke generates a strong start vortex (red patches in Fig. 1, D to F). The corresponding stop vortex is weaker and more diffuse, increasingly so as we move from outer wing (Fig. 1D) to inner wing (Fig. 1E) and body (Fig. 1F) image planes. Trace amounts of negative (blue) vorticity can be seen throughout the wingstroke. The associated induced velocity field (vectors in Fig. 1, D to F) shows a downward- and backward-directed momentum

[1]Department of Theoretical Ecology, Lund University, SE-223 62 Lund, Sweden. [2]Department of Biology, University of Munich, Germany. [3]Max-Planck Institute for Ornithology, Seewiesen, Germany. [4]Department of Aerospace and Mechanical Engineering, University of Southern California, Los Angeles, CA 90089–1191, USA.

*To whom correspondence should be addressed. E-mail: anders.hedenstrom@teorekol.lu.se

†Present address: Department of Biology, Bielefeld University, D-335 01 Bielefeld, Germany.

jet whose reaction force on the wings will be lift and thrust.

At 4 m/s, the upstroke generates lift as demonstrated by the downward flow in Fig. 1, H and I. As the wing is flexed on the upstroke, the outer wing image plane (Fig. 1G) now cuts through the outer part of the trailing wingtip vortex, which has a flow curling upward around the trailing vortex. The transition from lifting upstroke to downstroke is marked by a feature seen in Fig. 1, E, F, H, and I, where a substantial upward flow appears to the right of the strong start vortex. At the mid-body position (Fig. 1F), there is also a stronger flow in the flight direction, from right to left. The start vortex is weaker here than at corresponding points in the wing cycle but further out on the wing (Fig. 1, D and E). It is clear that at the inner wing, some kind of secondary vortex shedding has occurred, one that is associated with drag and negative lift.

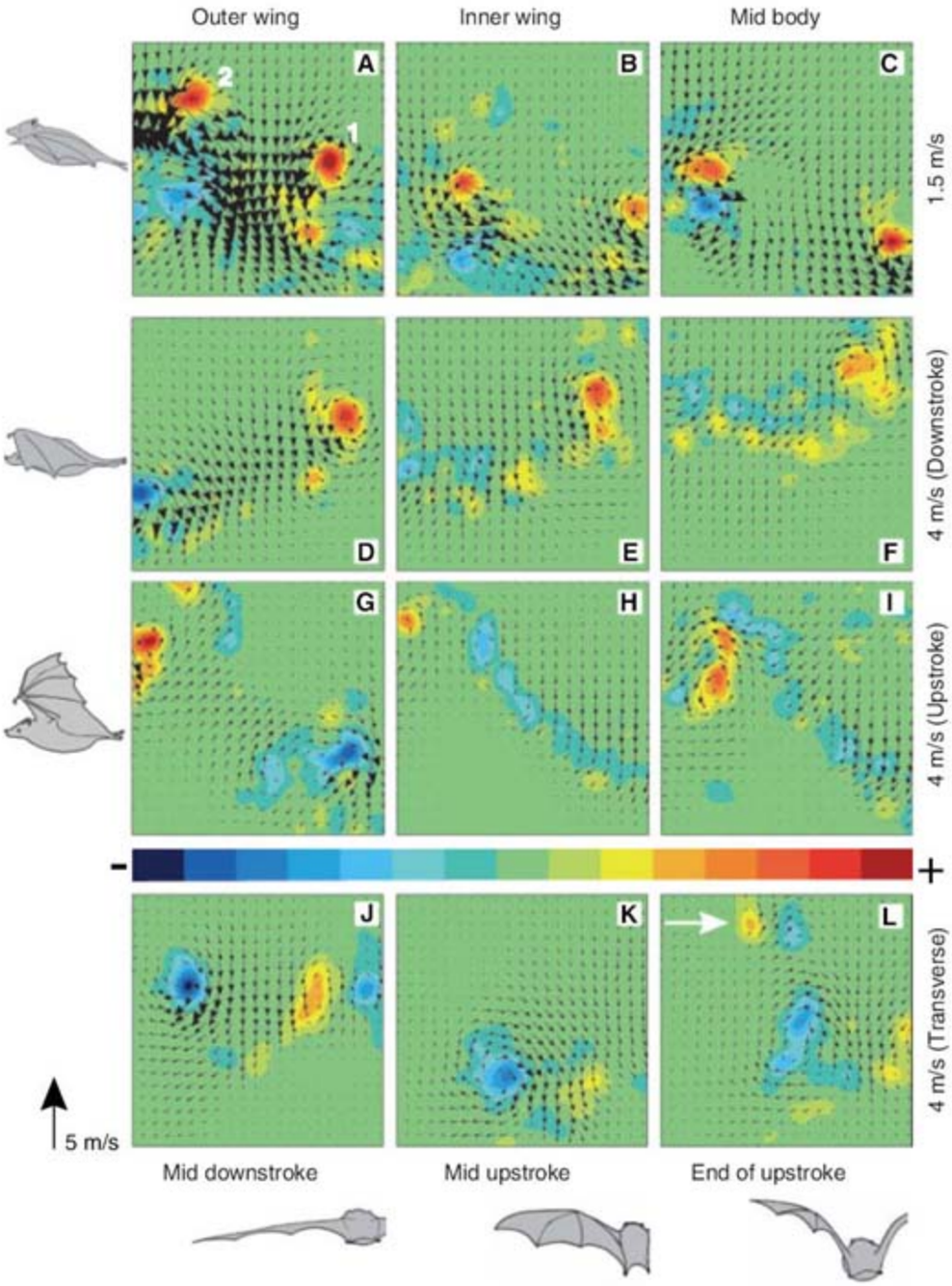

Fig. 1. Color-coded vorticity fields from a bat flying in a wind tunnel (see also fig. S3). Flight direction is from right to left for the upper nine panels, as indicated by the bat silhouettes to the left. The upper nine panels show spanwise vorticity (ω_y) from image planes aligned with the flow [the *x-z* plane (fig. S1)], at positions directly downstream from the outer wing (column 1), inner wing (column 2), and body (column 3), and at 1.5 m/s (**A** to **C**) and 4 m/s (**D** to **I**), respectively (further details in fig. S2). At 1.5 m/s, an entire wingstroke is captured on one frame, but at 4 m/s, separate frames show the downstroke [(D) to (F)] and upstroke [(G) to (I)] because the wingbeat wavelength increases with increasing speed. The bottom row (**J** to **L**) shows streamwise vorticity (ω_x) from the transverse image plane [*y-z* (fig. S1)]. Each transverse image covers the left wing and the body, as indicated by the bat silhouettes below. In (L), a white arrow indicates the vortex shed from the outer wing at the end of the upstroke. The color scale symmetrically represents variation in vorticity (per second) as follows: top row, −450 minimum, 450 maximum; second, third, and fourth rows, −300 minimum, 300 maximum. Velocity vectors are scaled to the reference vector (5 m/s) at bottom left. Each panel covers an area measuring 19.5 × 19.5 cm^2.

Further evidence comes from transverse planes that cut across the wake in Fig. 1, J to L (bottom row). In both mid-downstroke (Fig. 1J) and mid-upstroke (Fig. 1K), although the major feature is an induced downwash that characterizes a lifting body, there is also a streamwise vortex of opposite sign (yellow patch), shed toward the wing root (fig. S3). The horizontal distance between tip vortex (blue) and root vortex (yellow) is reduced as the wings are flexed on the upstroke. At the end of the upstroke, the streamwise vorticity (Fig. 1L) shows another secondary flow at the top of the image (white arrow; see also Fig. 1G above and to the right of the red start vortex). This is a vortex dipole structure with opposite sense to the main vortex: The yellow patch is outboard of the blue patch and the induced flow is upward. The circulation on the outer, hand wing has been reversed, and kinematic measurements show that it has a negative aerodynamic angle of attack here (fig. S4). At a flight speed of 6.5 m/s, the wake is qualitatively similar to that at 4 m/s, but the strength of the vortices is reduced and the wake wavelength is increased (fig. S3).

A full-span transverse image from the mid-downstroke wake (Fig. 2) summarizes one moment in the wingbeat and clearly shows the cores of the wingtip vortices and the opposing vorticity near the wing base. The strength of the wing base vortex is approximately 50% of that of the tip vortex, and it is evident that the three-dimensional wake structure over the entire wingbeat will be substantially more complex than realized hitherto. Nevertheless, certain quantitative measures reveal a quite orderly progression of wake vortex strengths with flight speed.

The magnitude of circulation of the strongest start and stop vortices in the wake decreases monotonically with flight speed (Fig. 3). The continuous variation in circulation with flight speed suggests a commensurate continuous change in wake geometry, which echoes previous findings for birds (*8*, *10*, *13*), and also parallels the continuous change in wing kinematic parameters with varying flight speed in this (*19*) and other (*14*, *16*, *17*) bat species. The measure Γ/Uc, where c is the mean chord, can be interpreted as half the time-averaged lift coefficient (*13*). Under steady conditions, fixed wings of similar aspect ratio and at similar Re can generate lift coefficients up to about 1.6 (*24*), and because $2\Gamma/Uc$ measured for our bats reached values greater than 4 at 1.5 m/s (Fig. 3), it is likely that some unsteady high-lift mecha-

nism is involved at slow speeds (*25*). Also, when U = 1.5 m/s, for example, St (*22*) was approximately 0.8, a comparatively large number that also argues for the importance of unsteady mechanisms (*19*, *26*).

Previous studies on birds showed that the circulation of the primary start or stop vortices alone was insufficient to support the bird's weight at slow speed (*4*, *5*, *8*, *10*, *13*). However, when the additional positive vorticity shed at the transition between down- and upstroke and into the following upstroke was included in the calculation (*8*, *10*, *13*), an approximate (vertical) force balance could be obtained for birds. Following these calculations, we may compare the total wake circulations with a nominal value Γ_1 that would be required if the wake were composed solely of elliptical loops generated during the downstroke (*20*). As in the bird measurements, calculations where the observed circulation Γ_{obs} was confined to main start/stop vortices showed an insufficient wake vortex strength for weight support at 1.5 m/s [$\Gamma_{obs}/\Gamma_1 = 0.23 \pm 0.05$ (mean ± SD) for both individuals]. Only when Γ_{obs} explicitly includes all the diffuse traces of same-signed vorticity (Fig. 1, D to F) does the ratio of measured to required circulation approach 1 [$\Gamma_{obs}/\Gamma_1 = 0.77 \pm 0.17$ (n = 30 observations) and 0.83 ± 0.18 (n = 23 observations)] for both bats. These values are still below 1 ($P < 0.001$, t test) because the upstroke generates lift not accounted for by Γ_1 (Fig. 1, A, B, H, I, and K). Therefore, the wakes of these bats cannot be adequately described by single discrete vortex loops, and the difference due to the aerodynamically active upstroke is more prominent than in the birds studied so far.

Our flow visualization studies demonstrate how the wake signature changes with flight speed and that the upstroke generates a combined lift and thrust at slow speed. These findings support previous hypotheses based on wingbeat kinematics (*14*–*19*, *27*). The upstroke of these bats also generated useful lift at higher speeds but with different mechanisms. At slow speeds, the wing circulation is reversed, whereas at medium and high speeds it has the same sense during both downstroke and upstroke. The circulation drops to 0 at the transition between up- and downstroke, which contrasts with the constant-circulation wake model for birds at cruising speed (*7*, *8*). Our data also provide evidence for a negative lift during the end of the upstroke at medium and high speeds due to rotation (pronation) and a negative angle of attack of the outer wing at this phase (*14*) (fig. S4). This negative lift may be a constraint due to the use of membranous wings, which cannot separate like the wing feathers of birds. Another difference from birds is that here the circulation varies along the wing span (Fig. 1, D to F). Therefore, neither the simple idealized wake models (discrete loops or constant circulation with partially flexed upstroke) nor the more complex patterns based on detailed bird flight measurements (*8*) are directly applicable. Although the wake properties of this bat species

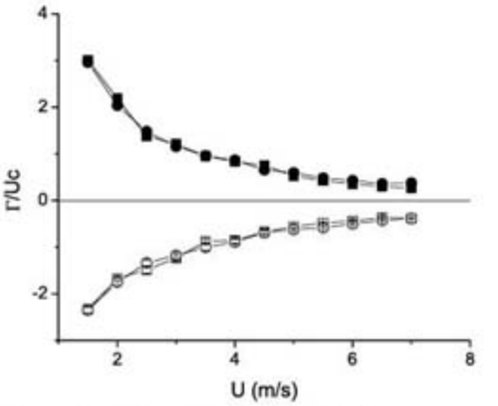

Fig. 3. Variation in circulation Γ of the strongest starting (positive) and stopping (negative) vortices with flight speed (U) for two bats. Γ is nondimensionalized by the mean wing chord c and U. Bat 1 (black squares, start; white squares, stop) and bat 2 (black circles, start; white circles, stop) show statistically indistinguishable values (analysis of variance). Error bars show ± 1 SE.

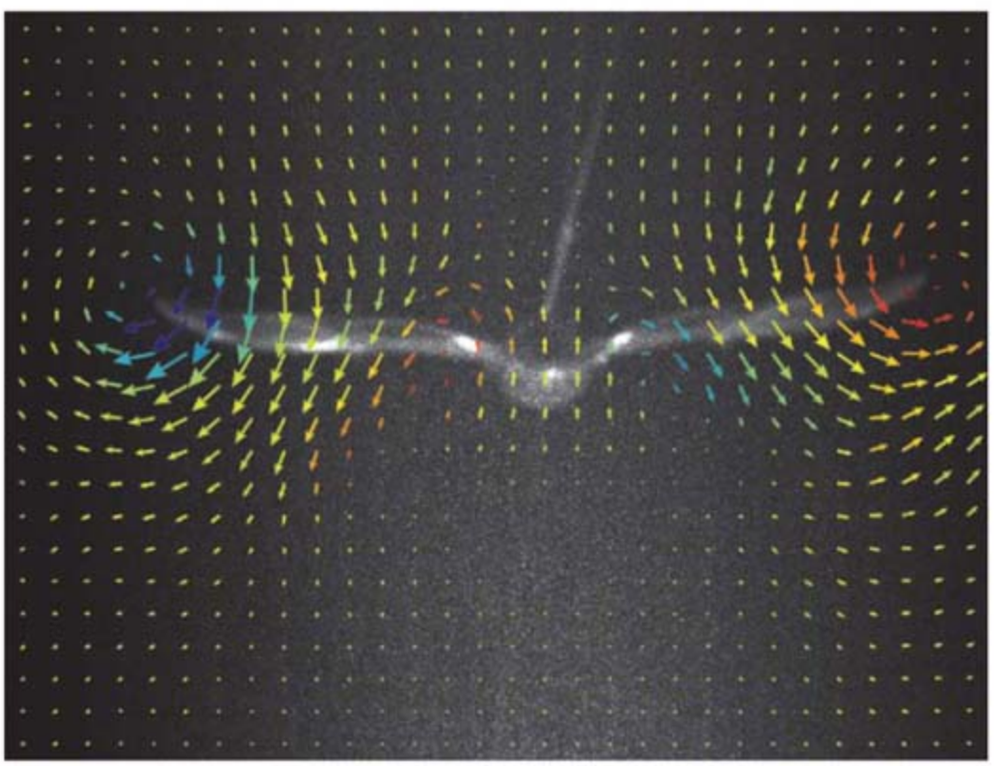

Fig. 2. Velocity field from the transverse (y-z) plane, with a phase- and parallax- corrected image of the bat as seen flying in front of the image plane. The example is from mid-downstroke at 4 m/s, where the two wingtip vortices are clearly seen framing a central induced downwash along the wing's trailing edge. Weaker vortices of opposite sense appear at the wing roots. The colors of the flow vectors indicate the streamwise vorticity magnitude and sign (blue, clockwise and negative; red, anticlockwise and positive).

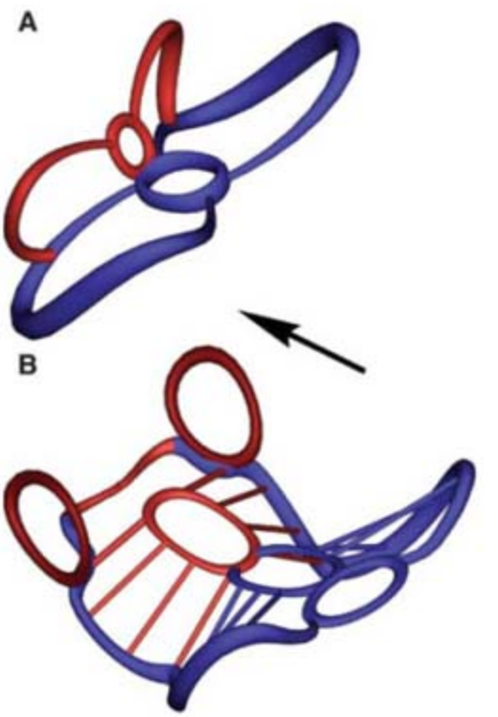

Fig. 4. Cartoons of the (**A**) slow speed (1.5 m/s) and (**B**) medium speed (4 m/s) wakes. Blue denotes vortex structures originating from the downstroke; red from the upstroke. The arrow indicates the flight direction. The slow speed wake has separate vortex loops close to the wing/body junction and a strong signature from the upstroke in red. The medium speed wake has a more continuous shedding of vorticity into the wake, together with reversed-sense vortices produced by the outer wing at the end of the upstroke. This wake also has separate structures shed from the wing roots. The wake at 6.5 m/s (not shown) differs from the wake at 4 m/s by having a longer wavelength, but is otherwise similar. Alternative views are given in fig. S5.

differ in important ways from those of all previously studied passerine birds, the generality of the result is not yet clear. Kinematic parameters vary between different species of bats (*17*), including the presence of features such as the upstroke reversal found in *G. soricina* (*19*). However, based on the similarities among bat species in the variation of wingbeat kinematics with flight speed (*17*), we may predict the presence of similar features in future bat studies.

From the combined evidence of the two perpendicular image planes (Fig. 1 and fig. S3), together with quantitative measures of the vortex sizes and strengths at different stages of the wingbeat and at different spans, we propose conceptual wake models for example flight speeds of 1.5 m/s (low) and 4 m/s (medium) as shown in Fig. 4. These are not discrete models for each speed but are simply representatives from a continuum across the speed range (Fig. 3). The data show that the aerodynamic wake signature is much more complicated than previous flow visualization studies had suggested (*6*), which is due to the higher-spatial-resolution technique we used. The wake models of Fig. 4 suggest how a new vortex-based aerodynamic model of bat flight could be constructed. Future experiments may investigate the detailed flow on the flexible-membrane bat wing itself to establish the link between the lift-generating mechanism and the resulting wake properties reported here. Those results can further be compared with numerical simulations of appropriate model problems in flexible wing aerodynamics (*28*).

References and Notes

1. Re = Uc/ν (where U is the flight speed, c is the mean chord length in the flightwise direction, and ν is the kinematic viscosity) is a measure of the relative importance of inertial forces to viscous forces. For small birds and bats, Re = 5×10^3 to 30×10^3.
2. S. M. Swartz, M. S. Groves, H. D. Kim, W. R. Walsh, *J. Zool.* **239**, 357 (1996).
3. N. V. Kokshaysky, *Nature* **279**, 146 (1979).
4. G. R. Spedding, J. M. V. Rayner, C. J. Pennycuick, *J. Exp. Biol.* **111**, 81 (1984).
5. G. R. Spedding, *J. Exp. Biol.* **125**, 287 (1986).
6. J. M. V. Rayner, G. Jones, A. Thomas, *Nature* **321**, 162 (1986).
7. G. R. Spedding, *J. Exp. Biol.* **127**, 59 (1987).
8. G. R. Spedding, M. Rosén, A. Hedenström, *J. Exp. Biol.* **206**, 2313 (2003).
9. D. R. Warrick, B. W. Tobalske, D. R. Powers, *Nature* **435**, 1094 (2005).
10. A. Hedenström, M. Rosén, G. R. Spedding, *J. R. Soc. Interface* **3**, 263 (2006).
11. L. Prandtl, O. G. Tietjens, *Fundamentals of Hydro- and Aeromechanics* (Dover, New York, 1957).
12. L. Prandtl, O. G. Tietjens, *Applied Hydro- and Aeromechanics* (Dover, New York, 1957).
13. M. Rosén, G. R. Spedding, A. Hedenström, *J. R. Soc. Interface*, 10.1098/rsif.2007.0215 (2007).
14. U. M. Norberg, *J. Exp. Biol.* **65**, 179 (1976).
15. U. M. Norberg, *J. Exp. Biol.* **65**, 459 (1976).
16. H. D. J. N. Aldridge, *J. Exp. Biol.* **126**, 479 (1986).
17. H. D. J. N. Aldridge, *J. Exp. Biol.* **130**, 275 (1987).
18. O. Von Helversen, in *Bat Flight, Biona Report 5*, W. Nachtigall, Ed. (Gustav Fischer, Stuttgart, Germany, 1986), pp. 107–128.
19. U. M. Lindhe Norberg, Y. Winter, *J. Exp. Biol.* **209**, 3887 (2006).
20. See supporting material on *Science* Online.
21. Aspect ratio (AR) = b^2/S (where b is wing span and S is wing area) is a measure of the wing shape. A high AR indicates a relatively long and slender wing, whereas a small AR signals a short and broad wing.
22. St = fA/U, where f is wingbeat frequency, A is tip-to-tip amplitude of the wingbeat, and U is flight speed relative to the air. St measures the relative magnitudes of wingtip and forward flight speed and can be interpreted as an indicator of the relative unsteadiness and efficiency of the vortex generation. In this study, St = 0.27 at U = 6.5 m/s, 0.37 at 4 m/s, and 0.81 at 1.5 m/s.
23. Y. Winter, *J. Exp. Biol.* **202**, 1917 (1999).
24. E. V. Laitone, *Exp. Fluids* **23**, 405 (1997).
25. Alternatively, using the speed of the wingtip (4.41 m/s at U = 1.5 m/s) yields a conservative estimate of the lift coefficient at C_L = 2.1, which is still considerably larger than 1.6. Furthermore, a truly local force coefficient would be based on the small local wing strip area and would be much higher.
26. G. K. Taylor, R. L. Nudds, A. L. R. Thomas, *Nature* **425**, 707 (2003).
27. S. M. Swartz, K. Bishop, M.-F. Aguirre, in *Functional and Evolutionary Ecology of Bats*, A. Zubaid, G. F. McCracken, T. H. Kunz, Eds. (Oxford Univ. Press, New York, 2006), pp. 110–130.
28. Y. Lian, W. Shyy, *J. Aircraft* **42**, 865 (2005).

29. We thank T. Alerstam for his support and comments on the manuscript. This work was supported by grants from the Swedish Research Council, the Swedish Foundation for International Cooperation in Research and Higher Education, the Knut and Alice Wallenberg Foundation, the Crafoord Foundation, the Magnus Bergvall Foundation, the Royal Physiographical Society in Lund, and the Volkswagen Stiftung.

Supporting Online Material

www.sciencemag.org/cgi/content/full/316/5826/894/DC1
Materials and Methods
Figs. S1 to S5
References

8 March 2007; accepted 4 April 2007
10.1126/science.1142281

The After-Hours Mutant Reveals a Role for Fbxl3 in Determining Mammalian Circadian Period

Sofia I. H. Godinho,[1]* Elizabeth S. Maywood,[2]* Linda Shaw,[1]* Valter Tucci,[1] Alun R. Barnard,[1] Luca Busino,[3] Michele Pagano,[3] Rachel Kendall,[1] Mohamed M. Quwailid,[1] M. Rosario Romero,[1] John O'Neill,[2] Johanna E. Chesham,[2] Debra Brooker,[1] Zuzanna Lalanne,[1] Michael H. Hastings,[2] Patrick M. Nolan[1]†

By screening *N*-ethyl-*N*-nitrosourea–mutagenized animals for alterations in rhythms of wheel-running activity, we identified a mouse mutation, after hours (*Afh*). The mutation, a $Cys^{358}Ser$ substitution in Fbxl3, an F-box protein with leucine-rich repeats, results in long free-running rhythms of about 27 hours in homozygotes. Circadian transcriptional and translational oscillations are attenuated in *Afh* mice. The *Afh* allele significantly affected Per2 expression and delayed the rate of Cry protein degradation in Per2::Luciferase tissue slices. Our in vivo and in vitro studies reveal a central role for Fbxl3 in mammalian circadian timekeeping.

Circadian rhythms, oscillations with a period of ~24 hours, are vital for physiological and behavioral homeostasis in multi- and unicellular organisms. In mammals, these biological rhythms are generated by several genetic elements that form autoregulatory transcriptional and translational feedback loops (*1*–*4*). For the clock to function effectively, however, the phase and extent of protein expression must also be tightly regulated. Posttranslational modifications necessary for the accurate timekeeping of this molecular machinery have been described. For example, Per levels depend on phosphorylation by Doubletime in *Drosophila* (*5*) or casein-kinase Iε in mammals (*6*), and sumoylation is a regulator of Bmal1 function (*7*). Circadian roles for ubiquitin E3 ligases containing F-box motifs (*8*) have been described in *Drosophila* for Slimb (*9*) and JETLAG (*10*) and in *Arabidopsis* for ZEITLUPE (*11*, *12*) and FKF1 (*13*). Large families of mammalian F-box proteins have been identified (*14*–*16*), but, apart from mammalian orthologs of *Drosophila* Slimb (β-TRCP) in cultured cells (*17*), none are known to degrade clock proteins in mammals.

To identify previously unknown genetic factors affecting mammalian circadian behavior, we conducted *N*-ethyl-*N*-nitrosourea (ENU) screens for alterations in circadian wheel-running activity in mice (*18*). We identified one mouse with a circadian period (τ_{DD}) of ~24 hours, significantly longer than the population mean (23.63 hours). The phenotype was inherited in a dominant fashion, with τ_{DD} ranging from 23.9 to 24.3 hours. Intercrosses revealed an additional phenotype with a τ_{DD} of ~26.5 hours and a delay in the entrainment phase angle (Fig. 1A). Frequency distribution plots of backcross (n = 264) and intercross progeny (n = 73) indicated semidomi-

[1]Medical Research Council (MRC) Mammalian Genetics Unit, Harwell, Oxfordshire OX11 0RD, UK. [2]MRC Laboratory of Molecular Biology, Neurobiology Division, Hills Road, Cambridge CB2 2QH, UK. [3]Department of Pathology, NYU Cancer Institute, New York University School of Medicine, 550 First Avenue, MSB 599, New York, NY 10016, USA.
*These authors contributed equally to this work.
†To whom correspondence should be addressed. E-mail: p.nolan@har.mrc.ac.uk

nant inheritance of the phenotype, with the latter revealing a group of animals with τ_{DD} ranging from 25.3 to 27.6 hours (Fig. 1B). We named the mutant "after hours" (*Afh*) and mapped the dominant phenotype at low resolution (*18*), selecting 13 mice displaying the most extreme τ_{DD} phenotypes for a genome scan. A single region of linkage was found on mouse chromosome 14, flanked by *D14Mit239* (66.65 Mb) and *D14Mit267* (114 Mb). Using additional polymorphic markers, we refined the nonrecombinant region to 6.41 Mb between 89.65 and 96.06 Mb (Fig. 1C) and confirmed the position by genotyping homozygotes. This region is extremely gene-poor, containing only 25 annotated genes (*19*). We scanned all Ensembl-annotated genes for mutations using denaturing high-performance liquid chromatography and sequencing. Sequencing revealed a point mutation in the coding region of an F-box gene, *Fbxl3*, resulting in a T→A transversion at position 1430 (Fig. 1D). The *Afh* mutation results in the substitution of serine for Cys^{358} (C358S) in Fbxl3 (Fig. 1E). Genotyping allowed us to characterize the behavioral phenotype of mutants systematically (table S1 and fig. S1).

The physiological function of Fbxl3 is unknown. The N-terminal F-box domain implicates this protein in ubiquitination and proteasomal degradation, whereas the C-terminal leucine-rich repeat (LRR) domain is likely to be involved in recognition of phosphorylated targets. Analysis of conserved functional domains (*20*) suggests that C358 is an essential residue in a subclass of LRR, the cysteine-containing LRR (LRR-cc). The Fbxl3 sequence is highly conserved in vertebrates, but there are no invertebrate orthologs. Fbxl3 is ubiquitously expressed, and the protein is predominantly, although not exclusively, nuclear (*14*). In vitro transfection of either wild-type or mutant Fbxl3 tagged with green fluorescent protein (GFP) into COS7 cells confirmed its predominantly nuclear localization with no differences in protein stability (fig. S2A). Furthermore, there was no circadian or genotype effect on gene or protein expression (fig. S2, B and C). Similarly, protein localization was not affected.

To investigate the molecular basis of period lengthening in homozygotes, we examined circadian expression profiles using in situ hybridization, immunohistochemistry, and Western blotting. In the suprachiasmatic nucleus (SCN), the central pacemaker driving circadian rest-activity cycles, *Afh* affected steady-state levels of the principal negative-feedback regulators of the clock, Period genes *Per1* and *Per2*, Cryptochrome gene *Cry1*, and the positive regulator *Bmal1* (Fig. 2A). Although rhythmic with a prolonged period, peak mRNA levels of all four genes were reduced relative to wild-type. Moreover, during late circadian night [circadian time (CT)18 to CT03], *Per1*, *Per2*, and *Cry1* mRNA levels were suppressed for longer than in wild-type mice. These mRNA changes were echoed in cycles of protein expression. For Per1 and Per2, the number of immunoreactive (-ir) nuclei in SCN was severely reduced across circadian time, particularly at the peak around CT12 to CT15. Similarly, the nocturnal peak of Bmal1-ir was lower in mutants. Despite the marked decline in *Cry1* mRNA, however, *Afh* homozygotes showed no apparent alteration in the number of Cry1-ir nuclei (fig. S3). We confirmed and extended the observations in the SCN by quantifying liver mRNA and protein in wild-type and homozygous mice. Peak mRNA levels of *Per1*, *Cry1*, *Rev-erbα*, and the clock-controlled D site albumin promoter–binding protein (*Dbp*) were reduced in homozygotes. *Fbxl3* and *Clock* mRNA levels were nonperiodic and equivalent in wild-type and homozygous mutant liver (fig. S4). Quantification of liver proteins by Western blotting

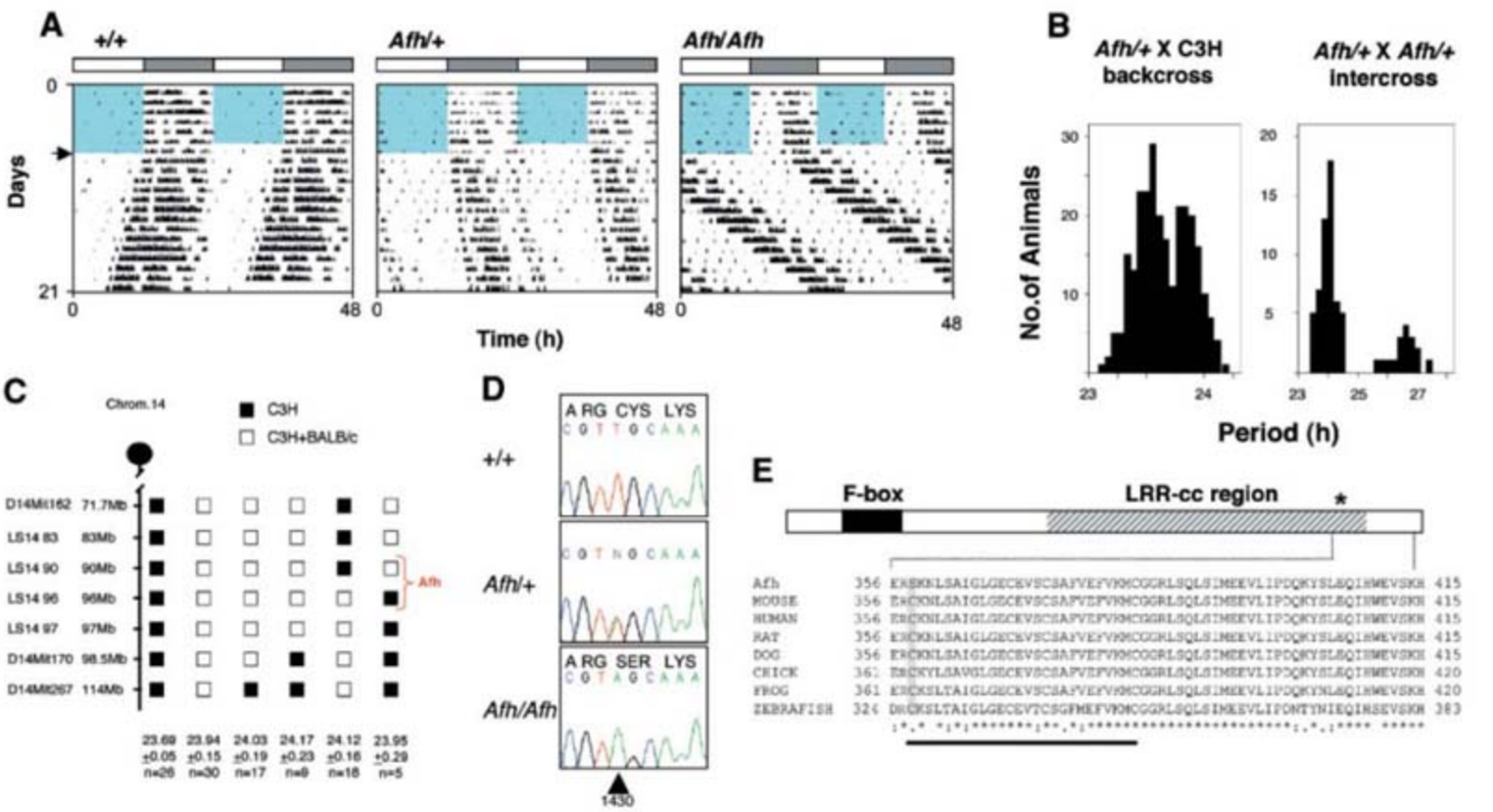

Fig. 1. Mutant phenotype and cloning of the *Afh* mutation. (**A**) Representative activity records of +/+ (τ_{DD} = 23.68 hours), *Afh*/+ (τ_{DD} = 24.23), and *Afh*/*Afh* (τ_{DD} = 26.73) mice. Images show double-plotted actograms of wheel-running activity under light-dark (LD) conditions (days 0 to 7) followed by constant darkness (DD, days 8 to 21). Short, vertical bars represent bouts of wheel-running activity. Periods of light and dark are indicated by horizontal bars above actograms, and the transition from LD to DD is indicated by an arrow. (**B**) Frequency distribution of τ_{DD} in *Afh*/+ backcross and intercross progeny. (**C**) Mapping of the *Afh* mutation to chromosome 14 by haplotype analysis. The number of haplotypes analyzed (*n*) and τ_{DD} (means ± SEM) are indicated. (**D**) Sequence analysis revealing a T→A transversion at nucleotide position 1430 of mouse Fbxl3 in the *Afh* mutant. (**E**) (Top) Schematic representation of Fbxl3 indicating the positions of F-box and LRR-cc regions. The position of the C358S substitution is marked by an asterisk. (Bottom) Protein sequence alignment of the C-terminal end of Fbxl3 in mutant and wild-type mouse and other vertebrate species. The shaded vertical box indicates the position of the C358S substitution, and the bold horizontal line indicates the consensus LRR-cc sequence.

confirmed the suppression of Per1 and Per2 in mutants, whereas Cry1 showed intermediate levels of expression at all time points (Fig. 2, B and C). The levels of Cry protein over the circadian cycle can explain the effect of *Afh* on the clock machinery. Elevated levels of Cry at CT9 to CT12 can enhance the suppression of Clock-Bmal1–dependent transcriptional activation in mutants, whereas reduced levels of Cry at CT18 to CT24 are a consequence of this.

To investigate directly the effect of Fbxl3 on molecular timekeeping within the SCN, the *Afh* mutant was crossed into the Per2::Luciferase (Per2::Luc) reporter line (*21*), and we recorded bioluminescence from SCN slices using a photomultiplier assembly (*22*). SCN from neonatal mice exhibited sinusoidal rhythms of luciferase activity, with a significant lengthening of period in heterozygotes and homozygotes (Fig. 3A). In adult mice, τ_{DD} was determined in vivo by wheel-running, and the period of the SCN molecular cycle was tested in vitro. In slices from wild-type mice, the in vitro period was slightly shorter than the in vivo, but overall, the two methods gave comparable results (Fig. 3, A and B). Peak amplitude in homozygotes was low and variable; there was no significant effect of genotype (Fig. 3C). Finally, alignment of SCN waveforms by peak expression revealed that the principal effect of the homozygous mutation was a prolongation of the circadian nadir of Per2::Luc expression (Fig. 3D). This extension of the negative-feedback phase is consistent with in situ hybridization and immunostaining data and is sufficient to explain the lengthened circadian period. Real-time recordings of Per2::Luc from wild-type and heterozygous kidney, lung, and liver all exhibited well-defined circadian cycles for 4 days (fig. S5). Recordings confirmed that the molecular clock in peripheral tissues is sensitive to the *Afh* allele.

In the accompanying paper (*23*), Busino *et al.* found that Fbxl3 binds and drives the ubiquitination and consequent degradation of Cry1 and Cry2. Thus, we investigated the dynamics of Cry degradation in wild-type and mutant tissue. We treated lung tissue slices from Per2::Luc mice with the protein synthesis inhibitor cycloheximide (CHX) and followed the time course of protein degradation (Fig. 4A). Although peak levels of Per2::Luc were lower in *Afh/Afh* slices (coinciding with the time of CHX treatment), the rate of degradation of Per2::Luc was similar to that of wild-type, with minimal levels detected after 4 hours of CHX treatment. Per2::Luc bioluminescence half-life was 0.54 ± 0.09 hours for wild-type and 0.46 ± 0.07 hours for *Afh/Afh*

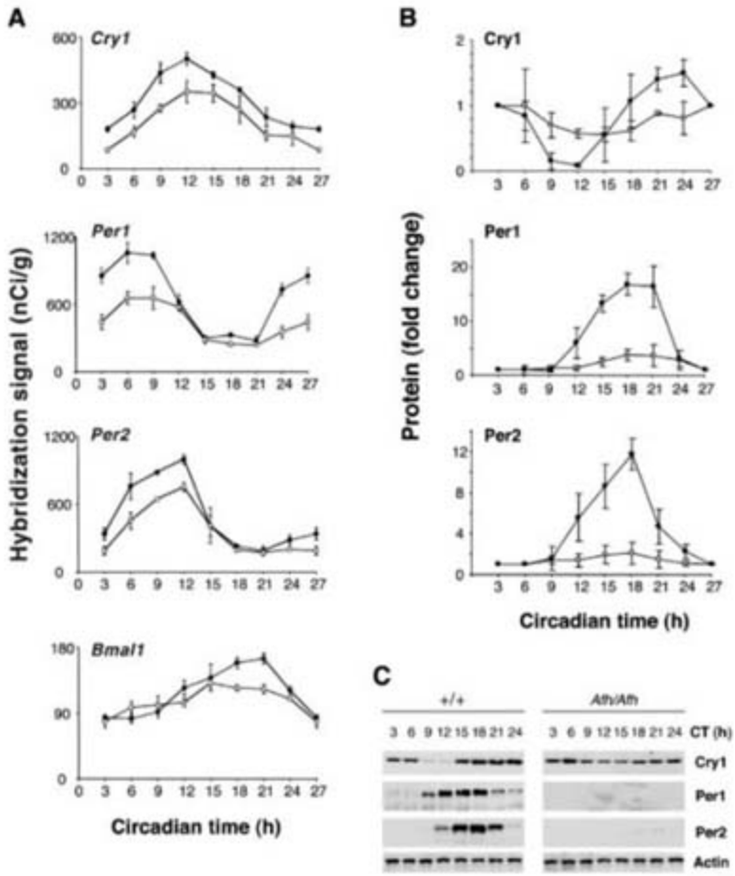

Fig. 2. Suppression of clock gene and protein oscillations in *Afh/Afh* mice. (**A**) Levels of *Cry1*, *Per1*, *Per2*, and *Bmal1* mRNA in SCN of +/+ (solid circles) and *Afh/Afh* (open circles) mice was measured by in situ hybridization. Each value represents the mean ± SEM (n = 3). (**B**) Levels of Cry1, Per1, and Per2 protein in liver of +/+ (solid circles) and *Afh/Afh* (open circles) mice was measured by densitometric analysis of Western blots. Each value represents the mean ± SEM (n = 3). Values are normalized to an internal control (actin) and expressed as the fold change from the value at CT3. (**C**) Representative Western blots of liver from +/+ and *Afh/Afh* mice showing stabilization of Cry1 and suppression of Per oscillations in mutants (*22*).

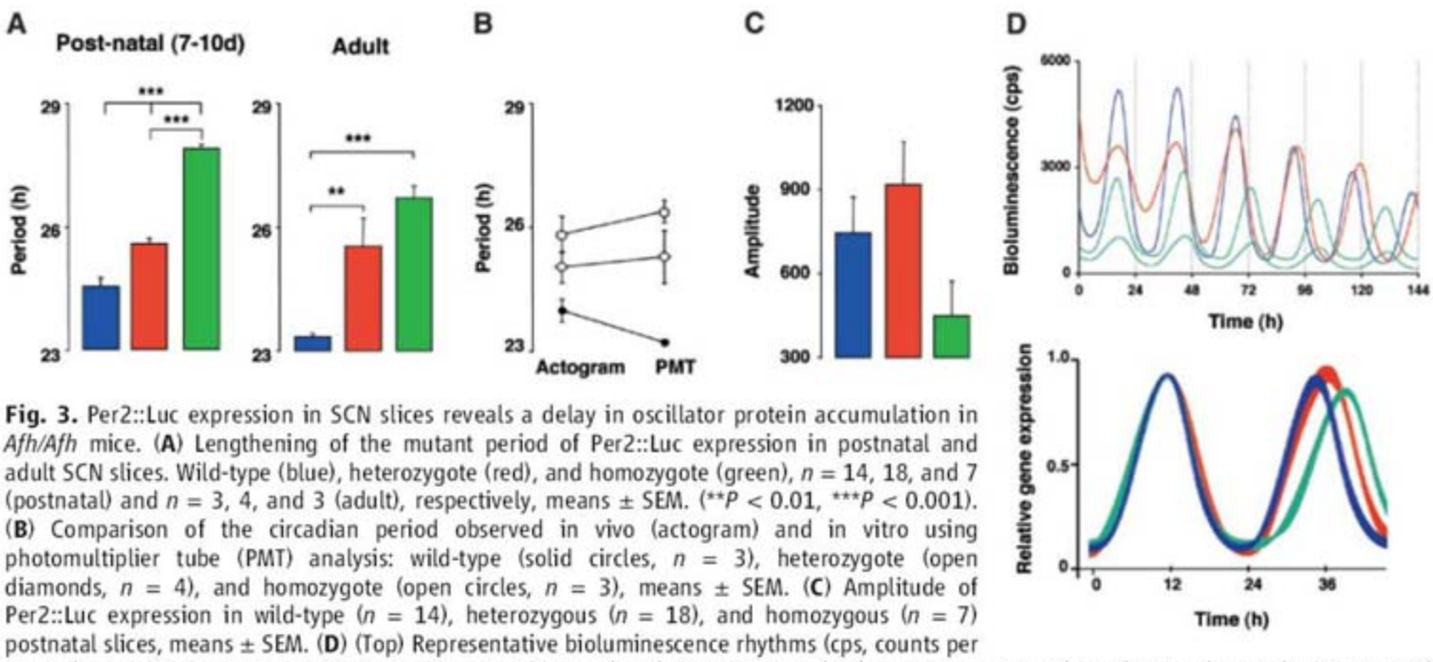

Fig. 3. Per2::Luc expression in SCN slices reveals a delay in oscillator protein accumulation in *Afh/Afh* mice. (**A**) Lengthening of the mutant period of Per2::Luc expression in postnatal and adult SCN slices. Wild-type (blue), heterozygote (red), and homozygote (green), n = 14, 18, and 7 (postnatal) and n = 3, 4, and 3 (adult), respectively, means ± SEM. (**$P < 0.01$, ***$P < 0.001$). (**B**) Comparison of the circadian period observed in vivo (actogram) and in vitro using photomultiplier tube (PMT) analysis: wild-type (solid circles, n = 3), heterozygote (open diamonds, n = 4), and homozygote (open circles, n = 3), means ± SEM. (**C**) Amplitude of Per2::Luc expression in wild-type (n = 14), heterozygous (n = 18), and homozygous (n = 7) postnatal slices, means ± SEM. (**D**) (Top) Representative bioluminescence rhythms (cps, counts per second) recorded from organotypic SCN slices in wild-type (blue), heterozygous (red), and homozygous (green) mice. (Bottom) Alignment of waveforms by peak expression (*22*).

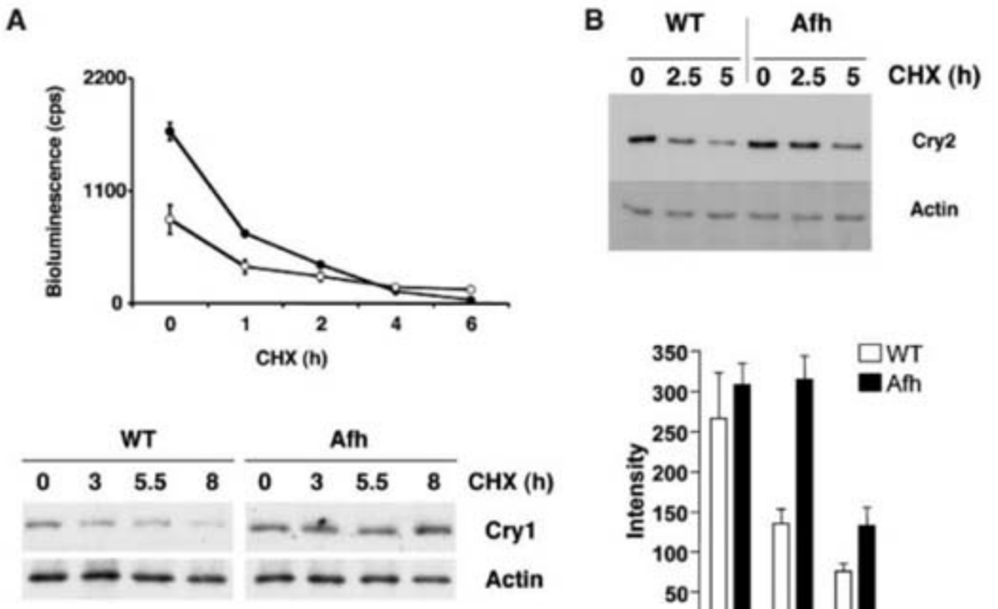

Fig. 4. Increased Cry stability in organotypic tissue slices from *Afh/Afh* mice and in mammalian cells expressing Fbxl3^{Afh}. (**A**) Real-time recording of Per2::Luc (top panel) in isolated lung from +/+ (solid circles) and *Afh/Afh* (open circles) mice, means ± SEM (n = 3). Cycloheximide (CHX, 20 μg/ml) was included in the medium at the peak of Per2::Luc expression, and bioluminescence was recorded after 0, 1, 2, 4, and 6 hours of treatment. Tissue samples were collected after 0, 3, 5.5, and 8 hours of treatment, and protein levels were determined by Western blotting (bottom, WT, wild-type, Afh, homozygous mutant). Blots represent pooled samples from five tissue slice recordings and were repeated to confirm results. (**B**) (Top) Western blots against S-tagged Cry2 expressed in COS7 cells in the presence of either wild-type Fbxl3 or Fbxl3^{Afh} protein. Cultures were treated with CHX (20 μg/ml) and sampled after 0, 2.5, or 5 hours. Group data (bottom, means ± SEM, n = 3) reveal progressive degradation of Cry2 in presence of wild-type Fbxl3. Degradation of Cry2 was significantly delayed in the presence of Fbxl3^{Afh} (*22*).

(means ± SEM, n = 5). Conversely, Cry1 levels, although lower in wild-type samples after 3 hours of treatment, remained high in *Afh/Afh* samples after up to 8 hours of treatment. In a further experiment, we looked at the rate of S-tagged Cry2 degradation in CHX-treated COS7 cells cotransfected with wild-type Fbxl3 or Fbxl3^{Afh} protein (Fig. 4B). Although the dynamic of protein degradation differs from that of native tissue, we detected a significant delay in Cry2 degradation in cells transfected with Fbxl3^{Afh}.

These data provide a role for Fbxl3 in modulating mammalian circadian homeostasis and a biological mechanism whereby this can occur. Fbxl3^{Afh} lengthens τ_{DD} by 3 hours, delaying the rate of Cry protein degradation and prolonging the phase of Cry-mediated negative feedback. As a consequence, peak levels of *Per*, *Cry*, and *Bmal1* mRNA are reduced in homozygotes, as are the corresponding proteins. Despite reduced levels of *Cry* mRNA, protein levels are stabilized in mutants, with an intermediate level of expression. Consequently, the circadian Cry profile in *Afh* mutants reflects a compensatory combination of reduced *Cry* transcription and Cry proteasomal degradation.

References and Notes

1. S. M. Reppert, D. R. Weaver, *Nature* **418**, 935 (2002).
2. M. H. Hastings, A. B. Reddy, E. S. Maywood, *Nat. Rev. Neurosci.* **4**, 649 (2003).
3. S. Yamaguchi *et al.*, *Science* **302**, 1408 (2003).
4. H. R. Ueda *et al.*, *Nature* **418**, 534 (2002).
5. L. Lopez-Molina, F. Conquet, M. Dubois-Dauphin, U. Schibler, *EMBO J.* **16**, 6762 (1997).
6. P. L. Lowrey *et al.*, *Science* **288**, 483 (2000).
7. L. Cardone *et al.*, *Science* **309**, 1390 (2005).
8. C. Bai *et al.*, *Cell* **86**, 263 (1996).
9. H. W. Ko, J. Jiang, I. Edery, *Nature* **420**, 673 (2002).
10. K. Koh, X. Zheng, A. Sehgal, *Science* **312**, 1809 (2006).
11. D. E. Somers, T. F. Schultz, M. Milnamow, S. A. Kay, *Cell* **101**, 319 (2000).
12. P. Mas, W. Y. Kim, D. E. Somers, S. A. Kay, *Nature* **426**, 567 (2003).
13. T. Imaizumi, T. F. Schultz, F. G. Harmon, L. A. Ho, S. A. Kay, *Science* **309**, 293 (2005).
14. C. Cenciarelli *et al.*, *Curr. Biol.* **9**, 1177 (1999).
15. J. T. Winston, D. M. Koepp, C. Zhu, S. J. Elledge, J. W. Harper, *Curr. Biol.* **9**, 1180 (1999).
16. J. Jin *et al.*, *Genes Dev.* **18**, 2573 (2004).
17. E. J. Eide *et al.*, *Mol. Cell. Biol.* **25**, 2795 (2005).
18. Y. Bacon *et al.*, *Genes Brain Behav.* **3**, 196 (2004).
19. Ensembl, Release 28 (NCBI m33 assembly), http://feb2005.archive.ensembl.org/Mus_musculus/index.html.
20. A. Marchler-Bauer *et al.*, *Nucleic Acids Res.* **33**, D192 (2005).
21. S. H. Yoo *et al.*, *Proc. Natl. Acad. Sci. U.S.A.* **101**, 5339 (2004).
22. Materials and methods are available as supporting material on *Science* Online.
23. L. Busino *et al.*, *Science* **316**, 900 (2007).

24. We thank S. Brown, M. Goedert, A. Acevedo, and R. Lucas for comments on the manuscript. Supported by the MRC, U.K. Biotechnology and Biological Sciences Research Council, NIH, the New York State Breast Cancer Research and Education Fund, and the 6th Framework Project EUCLOCK (No. 018741).

Supporting Online Material

www.sciencemag.org/cgi/content/full/1141138/DC1
Materials and Methods
Figs. S1 to S5
Table S1
References

12 February 2007; accepted 18 April 2007
Published online 26 April 2007;
10.1126/science.1141138
Include this information when citing this paper.

SCF^{Fbxl3} Controls the Oscillation of the Circadian Clock by Directing the Degradation of Cryptochrome Proteins

Luca Busino,[1] Florian Bassermann,[1] Alessio Maiolica,[2] Choogon Lee,[3] Patrick M. Nolan,[4] Sofia I. H. Godinho,[4] Giulio F. Draetta,[5] Michele Pagano[1]*

One component of the circadian clock in mammals is the Clock-Bmal1 heterodimeric transcription factor. Among its downstream targets, two genes, *Cry1* and *Cry2*, encode inhibitors of the Clock-Bmal1 complex that establish a negative-feedback loop. We found that both Cry1 and Cry2 proteins are ubiquitinated and degraded via the SCF^{Fbxl3} ubiquitin ligase complex. This regulation by SCF^{Fbxl3} is a prerequisite for the efficient and timely reactivation of Clock-Bmal1 and the consequent expression of *Per1* and *Per2*, two regulators of the circadian clock that display tumor suppressor activity. Silencing of Fbxl3 produced no effect in *Cry1*$^{-/-}$;*Cry2*$^{-/-}$ cells, which shows that Fbxl3 controls clock oscillations by mediating the degradation of CRY proteins.

SCF (Skp1/cullin/F-box protein) ubiquitin ligase complexes mediate the timely proteolysis of important eukaryotic cellular regulators (*1*). In mammals, there are more than 70 SCF ligases, each characterized by a different F-box protein subunit that binds and recruits substrates. Despite the large number of F-box proteins, only five human SCF ubiquitin ligases have been matched to substrates. To identify biologically important substrates of SCF ligases, we have combined immunopurification with analysis by mass spectrometry (*2*, *3*). Here we de-

scribe work on the orphan F-box protein Fbxl3, which we originally identified as an interactor of Skp1 by yeast two-hybrid screening (*4*).

[1]Department of Pathology, NYU Cancer Institute, New York University School of Medicine, 550 First Avenue, MSB 599, New York, NY 10016, USA. [2]European Institute of Oncology, 435 Via Ripamonti, 20141 Milan, Italy. [3]Department of Biomedical Sciences, College of Medicine, Florida State University, Tallahassee, FL 32306, USA. [4]MRC Mammalian Genetics Unit, Harwell, Oxfordshire OX11 0RD, UK. [5]Merck Research Laboratories, 33 Avenue Louis Pasteur, Boston, MA 02115, USA.

*To whom correspondence should be addressed. E-mail: michele.pagano@med.nyu.edu

Fbxl3 was expressed in HeLa-S3 cells and immunopurified (fig. S1). The mass spectrometry analysis of copurified endogenous proteins revealed the presence of two peptides corresponding to Cry1 and three peptides corresponding to both Cry1 and Cry2.

The Cryptochrome proteins, Cry1 and Cry2, are evolutionarily conserved proteins that control the circadian clock (*5*, *6*). A light-regulated master circadian pacemaker in the suprachiasmatic nucleus of the hypothalamus controls sleep-wake cycles and other rhythms (*6*, *7*). In addition, an intrinsic, cell-autonomous circadian clock (light-insensitive) with a rhythm of about 24 hours exists in peripheral tissues to coordinate the timing of basic cellular functions (for example, cell cycle progression and checkpoint activation) (*8*, *9*). The clock machinery is driven by two proteins, Clock and Bmal1, which heterodimerize to form an active transcription complex. Among several clock genes, the Clock-Bmal1 heterodimer drives the transcription of the *Cry* and *Period* (*Per*) genes. In turn, Cry1 and Cry2 inhibit Clock-Bmal1–dependent transcription, creating a negative-feedback loop that is central to the oscillation of the clock. In mammals, CRY proteins

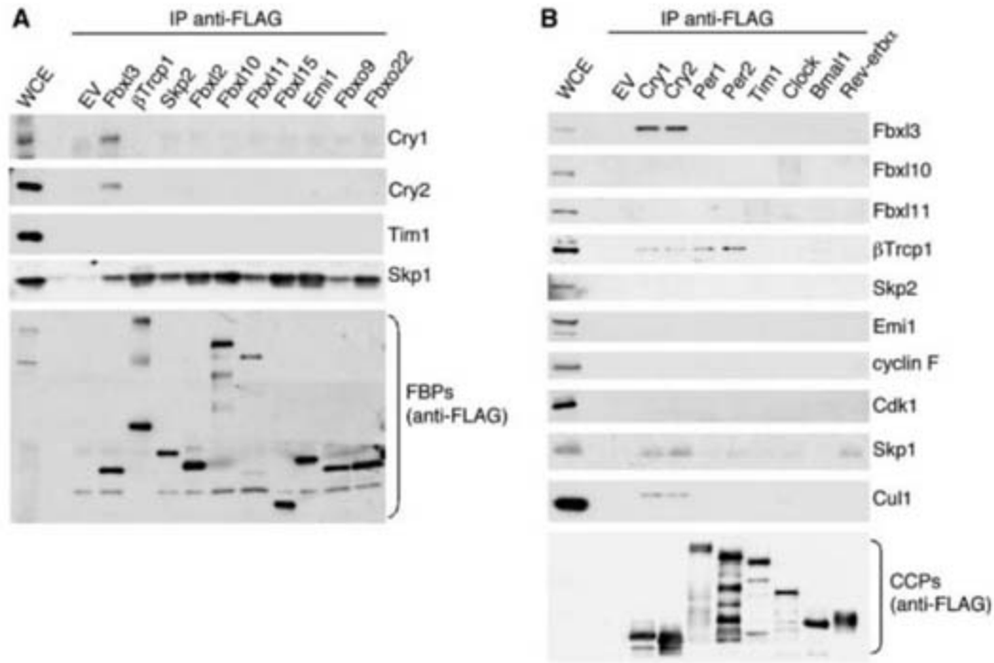

Fig. 1. CRY proteins specifically bind Fbxl3. (**A**) NIH 3T3 cells were infected with retroviruses encoding the indicated FLAG-tagged F-box proteins (FBPs). During the last 6 hours before harvesting, cells were treated with the proteasome inhibitor MG132. Exogenous proteins were immunoprecipitated (IP) from cell extracts with an anti-FLAG resin, and immunocomplexes were probed with antibodies to the indicated endogenous proteins. Lane 1 shows a whole-cell extract (WCE) from cells infected with an empty virus (EV). (**B**) HEK293T cells were transfected with constructs encoding the indicated FLAG-tagged circadian clock proteins (CCPs). Exogenous proteins were immunoprecipitated from cell extracts with an anti-FLAG resin, and immunocomplexes were probed with antibodies to the indicated endogenous proteins. Lane 1 shows a whole-cell extract from cells transfected with an empty vector.

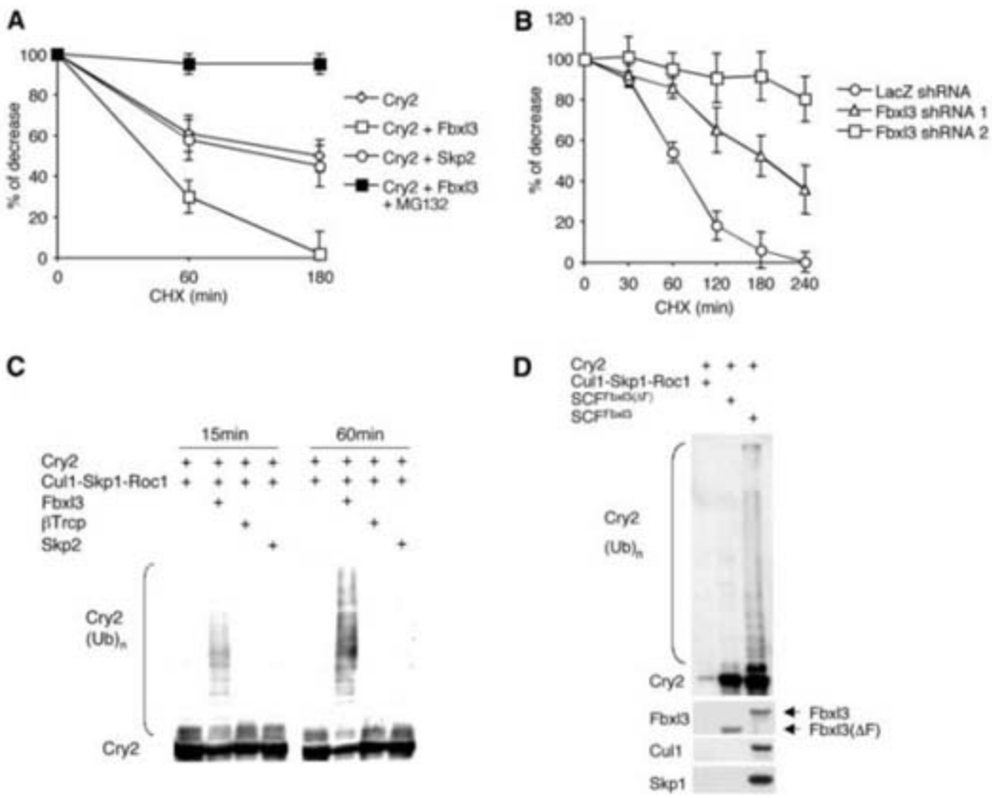

Fig. 2. Fbxl3 controls the degradation and ubiquitination of CRY proteins. (**A**) Fbxl3 promotes the degradation of Cry2. The graph shows quantification of Cry2 half-life in HEK293T cells transfected with Cry2 alone or in combination with either Fbxl3 or Skp2 (with or without MG132). Error bars represent ±SD ($n = 3$). A representative experiment is shown in fig. S2. (**B**) Knockdown of Fbxl3 stabilizes Cry2. The graph shows quantification of Cry2 half-life in HEK293T cells infected with lentiviral constructs that direct the synthesis of two different shRNAs to Fbxl3 or an shRNA targeting LacZ. Error bars represent ±SD ($n = 3$). A representative experiment is shown in fig. S3. (**C**) Fbxl3 ubiquitinates Cry2. In vitro ubiquitination assays of recombinant Cry2 protein were conducted in the presence of the Skp1-Cul1-Roc1 complex plus one of the following recombinant F-box proteins: Fbxl3, Skp2, or βTrcp1, as indicated. Samples were analyzed by immunoblotting with an antibody to Cry2. The bracket at the left marks a ladder of bands corresponding to polyubiquitinated Cry2. (**D**) HEK293T cells were transfected with Cry2, Skp1, Cul1, and Roc1 in the absence or presence of either FLAG-tagged Fbxl3 or a FLAG-tagged Fbxl3(ΔF-box) mutant. After immunopurification with an anti-FLAG resin, in vitro ubiquitination of Cry2 was performed. Samples were analyzed by immunoblotting with an antibody to Cry2. The lower panel shows levels of Fbxl3, Fbxl3(ΔF-box), Skp1, and Cul1 in the immunoprecipitates.

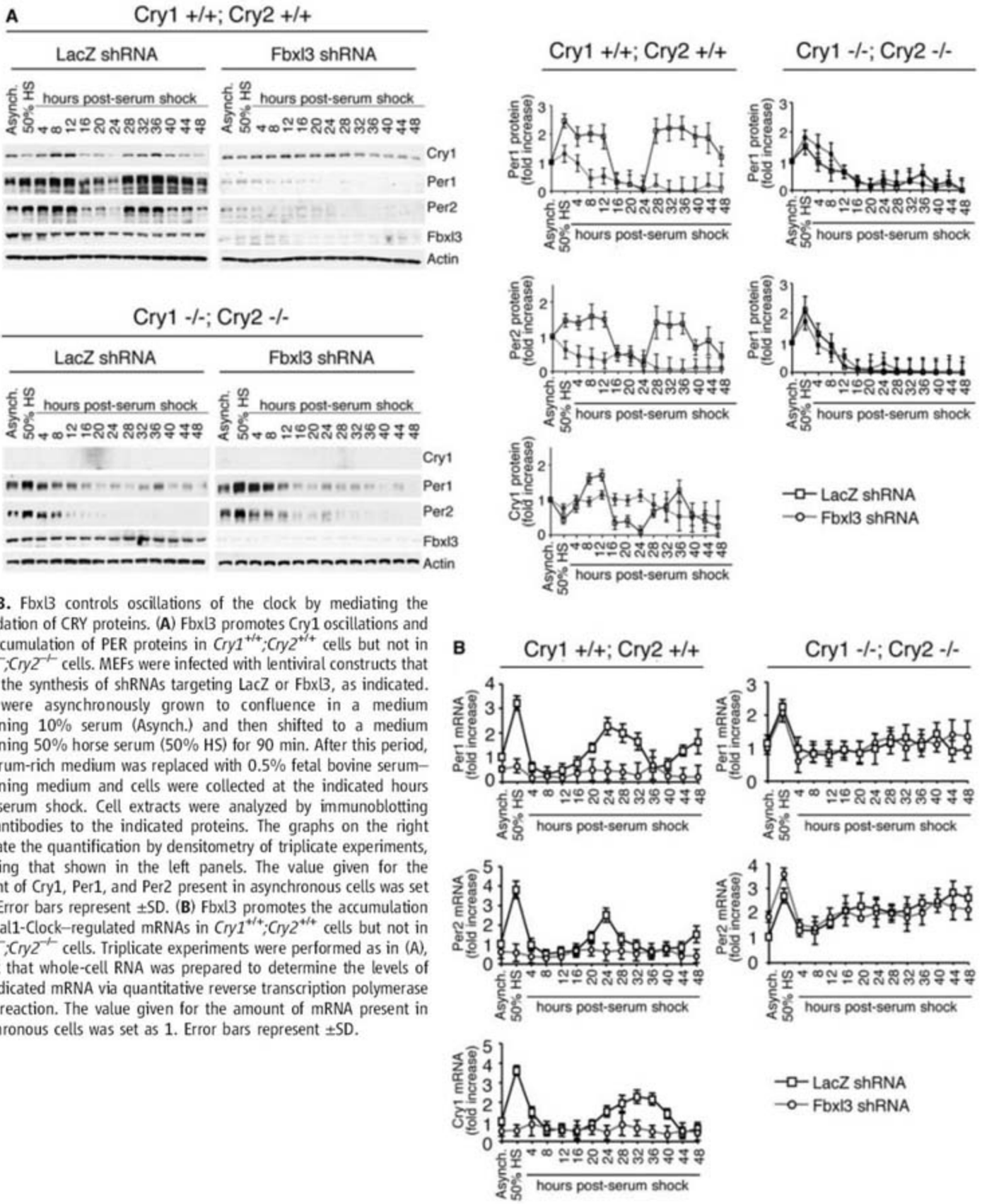

Fig. 3. Fbxl3 controls oscillations of the clock by mediating the degradation of CRY proteins. (**A**) Fbxl3 promotes Cry1 oscillations and the accumulation of PER proteins in $Cry1^{+/+};Cry2^{+/+}$ cells but not in $Cry1^{-/-};Cry2^{-/-}$ cells. MEFs were infected with lentiviral constructs that direct the synthesis of shRNAs targeting LacZ or Fbxl3, as indicated. Cells were asynchronously grown to confluence in a medium containing 10% serum (Asynch.) and then shifted to a medium containing 50% horse serum (50% HS) for 90 min. After this period, the serum-rich medium was replaced with 0.5% fetal bovine serum–containing medium and cells were collected at the indicated hours after serum shock. Cell extracts were analyzed by immunoblotting with antibodies to the indicated proteins. The graphs on the right illustrate the quantification by densitometry of triplicate experiments, including that shown in the left panels. The value given for the amount of Cry1, Per1, and Per2 present in asynchronous cells was set as 1. Error bars represent ±SD. (**B**) Fbxl3 promotes the accumulation of Bmal1-Clock–regulated mRNAs in $Cry1^{+/+};Cry2^{+/+}$ cells but not in $Cry1^{-/-};Cry2^{-/-}$ cells. Triplicate experiments were performed as in (A), except that whole-cell RNA was prepared to determine the levels of the indicated mRNA via quantitative reverse transcription polymerase chain reaction. The value given for the amount of mRNA present in asynchronous cells was set as 1. Error bars represent ±SD.

are the most potent repressors of Clock-Bmal1 (*10*–*13*). An integral component of this feedback loop is the requirement for degradation of CRY repressor proteins, without which the amplitude of the circadian clock oscillations would be inhibited. Although CRY proteins are known to be degraded via the ubiquitin system (*14*), the specific ubiquitin ligase that directs this event has remained unknown.

To investigate the specificity of binding between CRY proteins and Fbxl3, we screened 10 human F-box proteins. FLAG-tagged versions of these F-box proteins were retrovirally expressed in NIH 3T3 cells and then immunoprecipitated to evaluate their interaction with three endogenous clock proteins. We found that the only F-box protein able to coimmunoprecipitate Cry1 and Cry2 was Fbxl3 (Fig. 1A). The Fbxl3-CRY interaction was further confirmed by a complementary experiment in which FLAG-tagged versions of eight clock proteins were expressed in

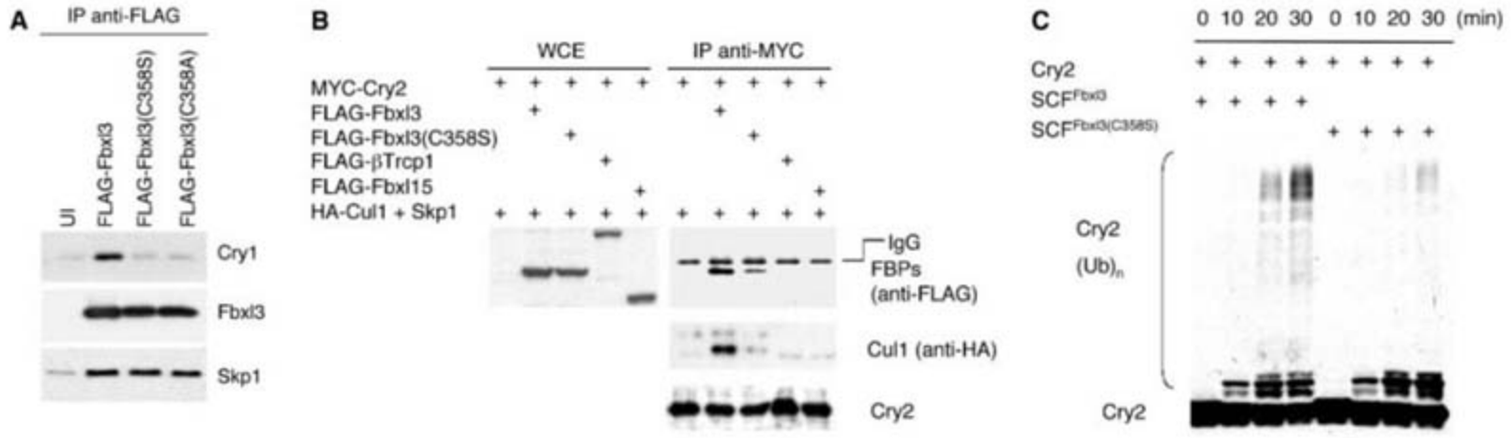

Fig. 4. The Fbxl3(C358S) mutant binds to and ubiquitinates CRY proteins less efficiently than wild-type Fbxl3. (**A**) NIH 3T3 cells were left uninfected (UI) or infected with retroviruses encoding Fbxl3, Fbxl3(C358S), or Fbxl3(C358A) (all FLAG-tagged). During the last 6 hours before harvesting, cells were treated with the proteasome inhibitor MG132. Proteins were immunoprecipitated from cell extracts with anti-FLAG resin, and immunocomplexes were probed with antibodies to the indicated proteins. (**B**) HEK293T cells were transfected with MYC-tagged Cry2 together with vectors encoding the indicated proteins. Cry2 was immunoprecipitated from whole-cell extracts with an antibody to MYC, and immunocomplexes were probed with antibodies to the indicated proteins. (**C**) The experiment was performed as in Fig. 2C, except that Fbxl3(C358S) was also assayed.

human embryonic kidney (HEK) 293T cells, immunoprecipitated, and tested for their ability to coimmunoprecipitate seven endogenous F-box proteins. Only Cry1 and Cry2 interacted with endogenous Fbxl3, but not with Skp2, Fbxl10, Fbxl11, βTrcp1, Emi1, or cyclin F (Fig. 1B).

These results prompted us to test whether Fbxl3 is involved in regulating the stability of CRY proteins. To this end, we transfected HEK293T cells with Cry2 and either Fbxl3 or Skp2. Whereas the expression of Skp2 had no observable effect on Cry2 stability, the expression of Fbxl3 resulted in a decrease in the half-life of Cry2, which was efficiently counteracted by the addition of the proteasome inhibitor MG132 (Fig. 2A and fig. S2). We also used two small hairpin RNA (shRNA) constructs to reduce the expression of Fbxl3 in HEK293T cells. Although both constructs targeted Fbxl3, construct 2 was more efficient in silencing Fbxl3 expression (fig. S3A). Accordingly, both constructs induced an increase in the half-life of Cry2, but construct 2 produced a more robust effect (Fig. 2B and fig. S3B). Stabilization of both Cry1 and Cry2 was also observed as an effect of Fbxl3 knockdown in NIH 3T3 cells (fig. S4).

To test whether CRY proteins are ubiquitinated via the SCF^{Fbxl3} ubiquitin ligase, we reconstituted the ubiquitination of Cry2 in vitro. Cry2 was efficiently ubiquitinated only when Fbxl3 was present (Fig. 2C). Different recombinant F-box proteins, including Skp2 and βTrcp1, were unable to trigger the ubiquitination of Cry2. Addition of methylated ubiquitin to the reaction inhibited the formation of the highest-molecular-weight forms of Cry2 (fig. S5), demonstrating that the high-molecular-weight forms of Cry2 are polyubiquitinated species of the protein. We also used a complementary in vitro ubiquitination strategy using immunopurified Fbxl3 proteins. Fbxl3, but not an inactive Fbxl3(ΔF-box) mutant (*4*), induced the ubiquitination of Cry2 (Fig. 2D), which supports the notion that the effect of Fbxl3 on Cry2 is direct.

To study the biological importance of SCF^{Fbxl3}-mediated proteolysis of CRY proteins, we investigated the effect of Fbxl3 knockdown in cells in which the circadian clock is synchronized. A 90-min pulse with 50% horse serum synchronizes clock oscillators in confluent fibroblasts (*15*, *16*). By synchronizing mouse embryonic fibroblasts (MEFs), we observed periodic oscillations in the levels of Cry1, Per1, and Per2 (Fig. 3A). Silencing of Fbxl3 abolished the oscillations in the levels of Cry1 and produced a decrease in the expression of Per1 and Per2 (Fig. 3A). Similar results were obtained in NIH 3T3 cells with the use of two different shRNA constructs (figs. S6 and S7).

We propose that when Fbxl3 is down-regulated, stabilized Cry1 persistently inhibits Clock-Bmal1, which is responsible for the induction of *Per* and *Cry* genes. In support of this hypothesis, we found that the knockdown of Fbxl3 inhibited the induction and oscillations of Clock-Bmal1–regulated mRNAs (*Per1*, *Per2*, and *Cry1*) (Fig. 3B and fig. S8). Moreover, chromatin immunoprecipitation experiments showed that silencing of Fbxl3 increased the abundance of Cry1 protein at the promoters of the *Per1*, *Per2*, and *Cry1* genes (fig. S9). Because the levels of Fbxl3 do not oscillate (Fig. 3A), it is possible that posttranslational modifications of CRY proteins regulate their recognition by Fbxl3, as is the case for most substrate–F-box protein interactions (*1*).

To determine whether the effects of Fbxl3 knockdown on the circadian clock are dependent on the stabilization of CRY proteins, we silenced Fbxl3 expression in $Cry1^{-/-}$;$Cry2^{-/-}$ MEFs (*12*). No substantial differences in the protein and mRNA levels of Per1 and Per2 were observed in $Cry1^{-/-}$;$Cry2^{-/-}$ MEFs after down-regulation of Fbxl3 (Fig. 3).

In the accompanying report (*17*), Godinho *et al.* used a forward genetic screen to induce mutations in mice that increase the length of the circadian clock and identified a mouse mutation in Fbxl3 [a Cys^{358} → Ser (C358S) substitution] that results in a circadian rhythm of about 27 hours in homozygotes. To investigate whether this mutation interferes with Fbxl3 activity, we generated a Fbxl3(C358S) mutant, as well as a Fbxl3(C358A) mutant (containing a Cys^{358} → Ala substitution). FLAG-tagged versions of Fbxl3 and the two mutants were retrovirally expressed in NIH 3T3 cells and then immunoprecipitated to evaluate their interaction with endogenous Cry1 and Skp1. Whereas all three proteins were able to coimmunoprecipitate Skp1, only wild-type Fbxl3 interacted with Cry1 (Fig. 4A). In a complementary experiment, MYC-tagged Cry2 was expressed in HEK293T cells together with one of the following F-box proteins: Fbxl3, Fbxl3(C358S), Fbxl15, and βTrcp1. After immunoprecipitation, Fbxl3(C358S) was found to bind Cry2 less efficiently than did Fbxl3 (Fig. 4B). Accordingly, expression of Fbxl3(C358S) had no effect on the stability of Cry1 (fig. S10), and Fbxl3(C358S) was less efficient than Fbxl3 in ubiquitinating Cry2 in vitro (Fig. 4C). These results provided evidence that the phenotype observed in mice (*17*) is due to a decreased ability of Fbxl3(C358S) to bind to and induce the proteolysis of CRY proteins.

Our study demonstrates that the SCF^{Fbxl3} ubiquitin ligase controls the oscillations of the circadian clock. Fbxl3-mediated degradation of Cry1 and Cry2 is a prerequisite for the efficient and timely reactivation of Clock-Bmal1 and the consequent transcription of target genes, including *Per1* and *Per2*, two putative tumor suppressors that control fundamental processes such as the timing of cell cycle progression and checkpoint activation (*18*–*21*). Because silencing of Fbxl3 produces no effects in $Cry1^{-/-}$;$Cry2^{-/-}$ cells, we conclude that the effects of Fbxl3 on the clock are largely mediated via regulation of Cry1 and Cry2 stability.

References and Notes

1. T. Cardozo, M. Pagano, *Nat. Rev. Mol. Cell Biol.* **5**, 739 (2004).
2. A. Peschiaroli *et al.*, *Mol. Cell* **23**, 319 (2006).
3. N. V. Dorrello *et al.*, *Science* **314**, 467 (2006).
4. C. Cenciarelli *et al.*, *Curr. Biol.* **9**, 1177 (1999).
5. M. P. Pando, P. Sassone-Corsi, *Sci. STKE* **2001**, re16 (2001).
6. U. Schibler, P. Sassone-Corsi, *Cell* **111**, 919 (2002).
7. S. Hastings, A. Reddy, E. Maywood, *Nat. Rev. Neurosci.* **4**, 649 (2003).
8. H. Okamura, *J. Biol. Rhythms* **19**, 388 (2004).
9. M. Gallego, D. M. Virshup, *Nat. Rev. Mol. Cell Biol.* **8**, 139 (2007).
10. E. A. Griffin *et al.*, *Science* **286**, 768 (1999).
11. K. Kume *et al.*, *Cell* **98**, 193 (1999).
12. L. P. Shearman *et al.*, *Science* **288**, 1013 (2000).
13. T. K. Sato *et al.*, *Nat. Genet.* **38**, 312 (2006).
14. K. Yagita *et al.*, *EMBO J.* **21**, 1301 (2002).
15. A. Balsalobre, F. Damiola, U. Schibler, *Cell* **93**, 929 (1998).
16. E. Nagoshi *et al.*, *Cell* **119**, 693 (2004).
17. S. I. H. Godinho *et al.*, *Science*, in press; published online 26 April 2007 (10.1126/science.1141138).
18. L. Fu *et al.*, *Cell* **111**, 41 (2002).
19. T. Matsuo *et al.*, *Science* **302**, 255 (2003); published online 21 August 2003 (10.1126/science.1086271).
20. S. Gery *et al.*, *Mol. Cell* **22**, 375 (2006).
21. J. Walisser, C. Bradfield, *Dev. Cell* **10**, 539 (2006).

22. We thank L. DiMarcotullio, J. Blau, D. Frescas, J. Rappsilber, and J. Skaar for suggestions; D. Virshup and P. Minoo for reagents; J. Takakashi for *Tim* cDNA and for communicating unpublished results; and T. M. Thor for support. This work was supported by NIH grants R37-CA76584, R01-GM57587, and R21-CA125173, the New York State Breast Cancer Research and Education Fund, the American Italian Cancer Foundation, and the Deutsche Forschungsgemeinschaft.

Supporting Online Material

www.sciencemag.org/cgi/content/full/1141194/DC1
Materials and Methods
Figs. S1 to S10
References

12 February 2007; accepted 18 April 2007
Published online 26 April 2007;
10.1126/science.1141194
Include this information when citing this paper.

How the Brain Translates Money into Force: A Neuroimaging Study of Subliminal Motivation

Mathias Pessiglione,[1,2]* Liane Schmidt,[2] Bogdan Draganski,[1] Raffael Kalisch,[1] Hakwan Lau,[1] Ray J. Dolan,[1] Chris D. Frith[1]

Unconscious motivation in humans is often inferred but rarely demonstrated empirically. We imaged motivational processes, implemented in a paradigm that varied the amount and reportability of monetary rewards for which subjects exerted physical effort. We show that, even when subjects cannot report how much money is at stake, they nevertheless deploy more force for higher amounts. Such a motivational effect is underpinned by engagement of a specific basal forebrain region. Our findings thus reveal this region as a key node in brain circuitry that enables expected rewards to energize behavior, without the need for the subjects' awareness.

Humans tend to adapt the degree of effort they expend according to the magnitude of reward they expect. Such a process has been proposed as an operant concept of motivation (*1*–*3*). Motivational processes may be obvious, as when a prospector spends days in extreme conditions seeking gold. The popular view is that motivation can also be unconscious, such that a person may be unable to report the goals or rewards that drive a particular behavior. However, empirical evidence on this issue is lacking, and the potential brain mechanisms involved in converting expected rewards into behavioral activation are poorly understood.

We developed an experimental paradigm to visualize unconscious motivational processes, using functional magnetic resonance imaging. A classical approach to trigger unconscious processing is subliminal stimulation, which can be implemented by means of masking procedures. The terminology we use in this report is based on a recent taxonomy (*4*), in which a process is considered subliminal if it is attended but not reportable. Successful brain imaging studies of subliminal processes have focused so far on processing words (*5*, *6*) as well as emotional stimuli (*7*, *8*). In our study, the object of masking was an incentive stimulus for a future action, represented by the amount of reward at stake. The question we asked is whether, and how, the human brain energizes behavior in proportion to subliminal incentives.

We developed an incentive force task, using money as a reward: a manipulation that is consistently shown to activate reward circuits in the human brain (*9*–*11*). The exact level of motivation was manipulated by randomly assigning the amount at stake as one pound or one penny. Pictures of the corresponding coins were displayed on a computer screen at the beginning of each trial, between two screenshots of "mask" images (Fig. 1). The reportability of the monetary stakes depended on their display duration, which could be 17, 50, or 100 ms. The perception of the first two durations was determined as subliminal in a preliminary behavioral test, where subjects reported not seeing anything other than the mask. The third duration was consistently associated with conscious perception of the stimuli and their associated amount.

To characterize the effects of the monetary stakes, we recorded not only brain activity but also skin conductance and hand-grip force. Skin conductance response (SCR) is linked to autonomic sympathetic arousal (*12*) and is thereafter interpreted as reflecting an affective evaluation of the monetary stake. Hand-grip force is understood to be a measure of behavioral activation. Online visual feedback of the force exerted was displayed as a fluid level moving up and down within a thermometer depicted on the screen (Fig. 1). Subjects were instructed that the higher the fluid level rose, the more of the monetary stake they would get to keep. At the end of the trial, subjects were given visual

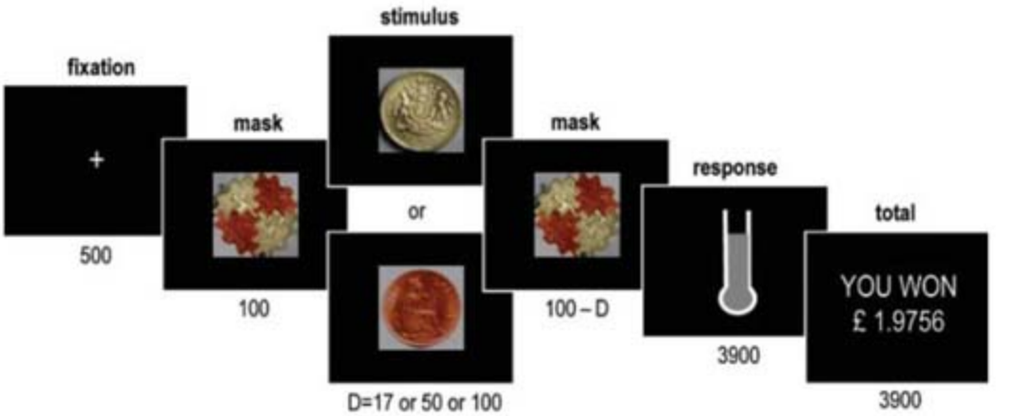

Fig. 1. The incentive force task. Successive screens displayed in one trial are shown from left to right, with durations in ms. Coin images, either one pound (£1) or one penny (1p), indicate the monetary value attributed to the top of the thermometer image. The fluid level in the thermometer represents the online force exerted on the hand grip. The last screen indicates cumulative total of the money won so far.

[1]Wellcome Trust Centre for NeuroImaging, Institute of Neurology, University College London, 12 Queen Square London WC1N 3BG, UK. [2]Institut National de la Santé et de la Recherche Médicale, Unité 610, Centre de Neuroimagerie de Recherche, Groupe Pitié-Salpêtrière, Université Pierre et Marie Curie, 47 Boulevard de l'Hôpital, F-75013 Paris, France.

*To whom correspondence should be addressed. E-mail: pessigli@ccr.jussieu.fr

feedback of the amount of money that they had accumulated. Thus, this cumulative total was increased after every trial, though negligibly so when one penny was at stake.

For the analysis of brain activity, we first examined the main contrast between monetary stakes, in the conscious condition, at the time of stimulus onset (Fig. 2, middle column). After correction for multiple comparisons over the whole brain (family-wise error, $P < 0.05$), the only significant activation was located bilaterally in the basal forebrain, bordering several structures encompassing the ventral striatum, ventral pallidum (VP), extended amygdala, and basal nucleus of Meynert. These structures have been conceptualized as forming output channels for the limbic system, which is devoted to emotional and motivational functions (*13*). According to fiber tracing studies, reward-related information may access these structures either by a subcortical route via the hippocampus and/or amygdala or by a cortical route via the orbitofrontal and/or anterior cingulate areas (*14*–*17*).

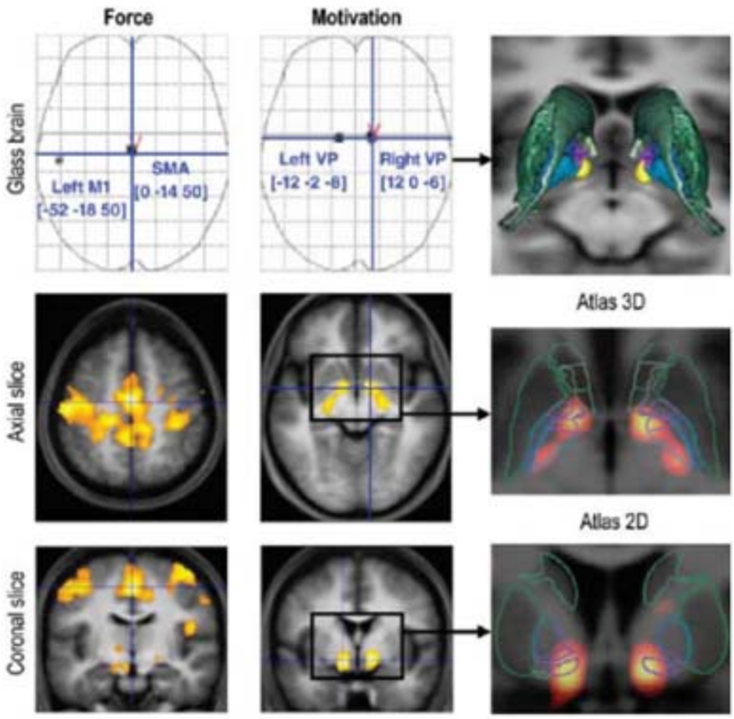

Fig. 2. SPMs of brain activity. Voxels displayed in gray on glass brains showed a significant effect at $P < 0.05$ after correction for multiple comparisons over the entire brain. The [*x*, *y*, *z*] coordinates of the different maxima refer to the Montreal Neurological Institute (MNI) space. Axial and coronal slices were taken at global maxima of interest indicated by red symbols on the glass brains. SPMs are shown at a lower threshold ($P < 0.001$, uncorrected) and were superimposed on the average structural scan to localize significant activations. The images in the left column show regression with the amount of force produced, whatever the condition. The images in the middle column show contrast between conscious pounds and pennies trials (£1 to 1p, 100 ms). For this contrast, SPMs were coregistered with an atlas of the basal ganglia (right column). Caudate, putamen, and accumbens are shown in green; external and internal pallidum are shown in blue, with limbic sectors in violet.

To improve anatomical localization, we coregistered the statistical parametric map (SPM) with a recent histology-based atlas of the basal ganglia, which was designed to distinguish between functional territories (*18*, *19*). Activation foci overlapped with limbic territories of both external and internal pallidal segments (Fig. 2, right column), which together form the VP. The main inputs to the VP come from the ventral striatum, where reward-related activations have been consistently found (*9*–*11*). VP activation might denote engagement of the same ventral striato-pallidal pathway, with a shift in its expression being related to the nature of the upcoming task. More specifically, ventral striatal activity has been linked to reward prediction and reward prediction error during learning (*20*, *21*). Rather than concentrating on learning, our design focused on motivation during effort, which elicited specific processing in the VP. Our finding accords well with evidence in rodents, showing that VP neurons encode rewarding properties of environmental stimuli (*22*), and suggests a role for the VP in incentive motivation. Furthermore, lowering the threshold ($P < 0.001$, uncorrected) revealed that activation extended posteriorly, within nonlimbic territories of the pallidum, pointing out a plausible route by which the VP may influence cortical motor areas (*14*, *15*).

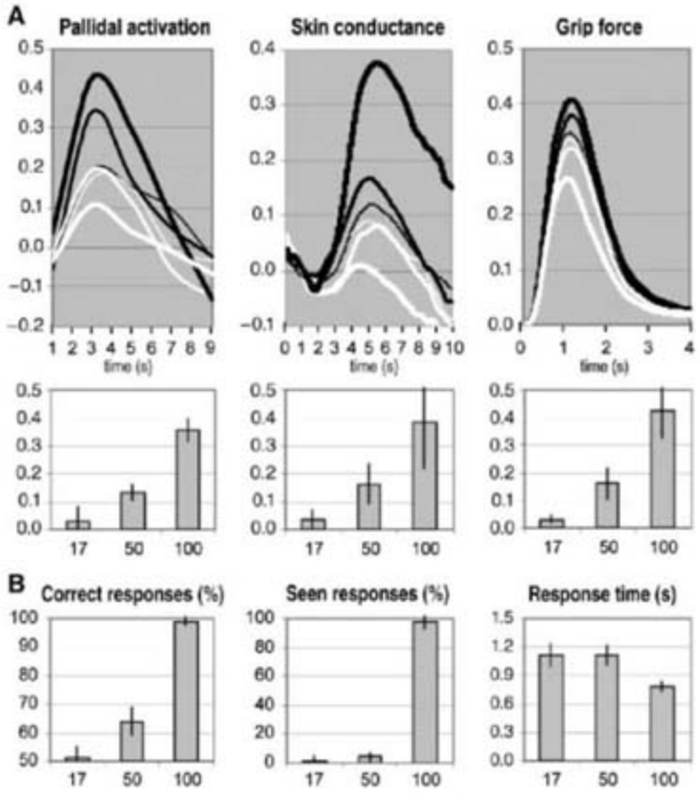

Fig. 3. Main effects of stimulus duration. (**A**) Incentive force task. Time courses were averaged across trials for the different stimuli (black lines indicate £1 and white lines indicate 1p) and durations (thin, intermediate, and thick lines indicate 17, 50, and 100 ms, respectively). Time 0 corresponds to the moment of stimulus display. The histograms indicate the effect of motivation (£1 to 1p), and the error bars indicate SEM. Pallidal activation is expressed as percentage of blood oxygen level–dependent signal change. Force and skin conductance are expressed in proportion of the highest measure. (**B**) Perception task. Stimuli were the same as in (A). Possible responses were "seen £1," "seen 1p," "guess £1," and "guess 1p." A "correct" response means that the subject chose the stimulus that had been displayed. A "seen" response means that the subject perceived all or part of the stimulus. Error bars indicate SEM.

To dissociate motivation per se from force production, we next examined brain activity that was linearly related to the amount of force produced, whatever the condition (Fig. 2, left column). After correction for multiple comparisons over the whole brain (family-wise error, $P < 0.05$), significant activations were found in the supplementary motor area (SMA) and in the primary motor area (M1). Unlike the pallidum, these structures have previously been shown to activate in relation with the amount of force produced (*23*–*25*). Moreover, M1 activation was observed on the left side, which was consistent with the use of the right hand for the task, whereas pallidal activation was bilateral. Thus, in our analysis, the dissociation was clear-cut, probably reflecting the fact that monetary stakes were constant throughout the task, while grip force decreased trial after trial, probably as a result of fatigue (fig. S1). Such dissociation suggests that

motivational processes mediated by the VP include modulation of SMA activity, which in turn drives muscular contractions via M1.

We next asked whether such a circuit was engaged by subliminal incentives. We averaged parameter estimates (Fig. 3A, left panels) over the pallidal voxels that showed significant activation in the previous SPM. The contrast between monetary stakes was significant for 100 and 50 ms (paired t tests, both P values < 0.001) but not for 17 ms. No significant activation was found elsewhere in an SPM estimated for this contrast at 50 ms, even with our liberal threshold ($P < 0.001$, uncorrected). Thus, only the VP appeared in position to modulate behavioral activation according to subliminal incentives and hence to underpin a low-level motivational process, as opposed to a conscious cost-benefit calculation. Again, such a role accords well with experiments on rodents, which show that VP manipulations influence goal-directed behavior, as seen with self-stimulation after electrode implantation in the VP (*26*) or impaired acquisition of conditioned-place preference after the generation of VP lesions (*27*).

We next sought to link our imaging results to simultaneously measured autonomic and behavioral responses. The dynamics of responses recorded from skin conductance electrodes indicated that they were triggered at the time of stimulus display, with a typical SCR profile starting at 2 s post-stimulus and peaking around 5 s (*12*). Comparison between monetary stakes showed significant effects at 100 and 50 ms (paired t tests, both P values < 0.05) but not at 17 ms (Fig. 3A, middle panels). Thus, like fear-relevant stimuli (*28*), subliminal incentives could be evaluated affectively, with subjects being more responsive to images of pounds than to those of pennies. Autonomic responding was not a mere side effect of force production, because it evolved with a different temporal profile throughout the task. Indeed, grip force decreased for consciously perceived pennies, while skin conductance increased for consciously perceived pounds (fig. S1). Regarding grip force, we found similar dynamics, whatever the condition: subjects giving a short squeeze, with peak latency at around 1 s, and relaxing before the next trial (Fig. 3A, right panels). Hence, similar results were found when considering either the height of the peak or the area under the curve. Comparing between monetary stakes, significant effects were found at 100 ms, 50 ms, and even at 17 ms (paired t tests, all P values < 0.01). Thus, the brain could energize behavior in proportion to the reward at stake, even when subjects could not see it.

Finally, we controlled for subjective perception with a forced choice task (Fig. 3B). While still in the scanner, subjects were shown the same masked stimuli and had to report whether they saw a coin, and which coin they thought it was, either from seeing it or from guessing. Based on the percentage of correct responses, the analysis could then be restricted to all situations where subjects guess at chance level about stimulus identity (fig. S2). Even in these situations, pallidal activation and hand-grip force were significantly higher for pounds as compared to pennies (paired t tests, both P values < 0.01). As with the preliminary test, subjects reported seeing almost no stimuli at 17 and 50 ms and almost all stimuli at 100 ms. Compared to the 100-ms condition, subjects also had similarly long response times at 17 and 50 ms, indicating that they were experiencing the same degree of uncertainty about stimulus identity. Thus, subjective perception changed as a function of category, from subliminal to conscious, between 50 and 100 ms. In contrast, objective markers of motivation (pallidal activation, SCR, and hand-grip force) gradually increased with stimulus duration.

These results indicate that motivational processes involved in boosting behavior are qualitatively similar, despite whether subjects are conscious or not of the reward at stake. Consistently, the same basal forebrain region underpinned subliminal and conscious motivation. Such subcortical localization might relate to the simple and repetitive nature of the task, rendering strategic control unnecessary. However, differential sympathetic arousal denoted by SCRs argues against an interpretation in terms of mere stimulus-response habit formation, which is known to involve the basal ganglia (*29*). More generally, our paradigm offers a potential tool to discriminate between motor and affective components of motivation for financial reward in humans, analogous to the dissociation between wanting and liking food reward described in rodents (*30*). Such a tool may be particularly useful in exploring negative symptoms, like those manifested in depression or schizophrenia, involving acute dysfunction within the motivational process.

References and Notes

1. T. W. Robbins, B. J. Everitt, *Curr. Opin. Neurobiol.* **6**, 228 (1996).
2. K. C. Berridge, *Physiol. Behav.* **81**, 179 (2004).
3. W. Schultz, *Annu. Rev. Psychol.* **57**, 87 (2006).
4. S. Dehaene *et al.*, *Trends Cognit. Sci.* **10**, 204 (2006).
5. S. Dehaene *et al.*, *Nature* **395**, 597 (1998).
6. R. Gaillard *et al.*, *Neuron* **50**, 191 (2006).
7. J. S. Morris, A. Ohman, R. J. Dolan, *Nature* **393**, 467 (1998).
8. A. Etkin *et al.*, *Neuron* **44**, 1043 (2004).
9. J. O'Doherty *et al.*, *Nat. Neurosci.* **4**, 95 (2001).
10. R. Elliott *et al.*, *J. Neurosci.* **23**, 303 (2003).
11. B. Knutson *et al.*, *J. Neurosci.* **25**, 4806 (2005).
12. H. D. Critchley, *Neuroscientist* **8**, 132 (2002).
13. L. Heimer, G. W. Van Hoesen, *Neurosci. Biobehav. Rev.* **30**, 126 (2006).
14. G. E. Alexander, M. R. DeLong, P. L. Strick, *Annu. Rev. Neurosci.* **9**, 357 (1986).
15. S. N. Haber, *J. Chem. Neuroanat.* **26**, 317 (2003).
16. S. Lehericy *et al.*, *Ann. Neurol.* **55**, 522 (2004).
17. D. P. Friedman, J. P. Aggleton, R. C. Saunders, *J. Comp. Neurol.* **450**, 345 (2002).
18. J. Yelnik *et al.*, *Neuroimage* **34**, 618 (2007).
19. S. Lehericy *et al.*, *Cereb. Cortex* **16**, 149 (2006).
20. J. O'Doherty *et al.*, *Science* **304**, 452 (2004).
21. M. Pessiglione *et al.*, *Nature* **442**, 1042 (2006).
22. A. J. Tindell, K. C. Berridge, J. W. Aldridge, *J. Neurosci.* **24**, 1058 (2004).
23. C. Dettmers *et al.*, *J. Neurophysiol.* **74**, 802 (1995).
24. T. H. Dai *et al.*, *Exp. Brain Res.* **140**, 290 (2001).
25. D. E. Vaillancourt *et al.*, *Neuroimage* **23**, 175 (2004).
26. G. Panagis *et al.*, *Behav. Brain Res.* **68**, 165 (1995).
27. G. M. McAlonan, T. W. Robbins, B. J. Everitt, *Neuroscience* **52**, 605 (1993).
28. A. Ohman, S. Mineka, *Psychol. Rev.* **108**, 483 (2001).
29. A. M. Graybiel, *Curr. Opin. Neurobiol.* **15**, 638 (2005).
30. K. C. Berridge, *Neurosci. Biobehav. Rev.* **20**, 1 (1996).

31. We thank E. Featherstone for skilful assistance in recording hand-grip data; J. Yelnik and E. Bardinet for having deformed their atlas on SPMs; and G. Lafargue, S. Kloppel, and C. Sergent for helpful discussions. This work was funded by the Wellcome Trust research program grants to C.F. and R.D. M.P. received a grant from the Fyssen Foundation.

Supporting Online Material

www.sciencemag.org/cgi/content/full/1140459/DC1
Materials and Methods
Figs. S1 to S3

26 January 2007; accepted 30 March 2007
Published online 12 April 2007;
10.1126/science.1140459
Include this information when citing this paper.

Multiphoton Laser Scanning Microscope

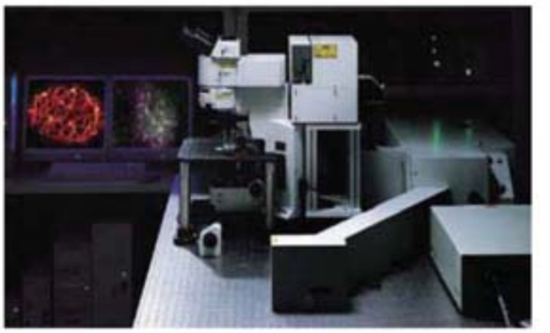

The Fluoview FV 1000-MPE multiphoton laser scanning microscope system is for deep observation and imaging of living or thickly sliced specimens. Neuroscientists and cell biologists can use the system to image dynamic processes up to several hundred microns deep in living cells and tissues without inflicting significant photo-damage on specimens. The system is particularly useful for repeated long-range or time-lapse exposures, and any applications that require deep imaging or extensive fluorescence excitation. The FV1000-MPE incorporates a femtosecond pulsed laser to achieve photon density at the focal plane with minimal damage or photobleaching of living cells. It is optimized for use with near-infrared wavelengths, and a full line of water immersion objectives is available for specimen penetration and imaging. Multiphoton systems allow researchers to achieve thinner optical sectioning and cause less photobleaching and phototoxicity to surrounding areas of the specimen. They are thus suitable for deep, in vivo imaging.

Olympus For information 800-455-8236 www.olympusamerica.com/microscopes

Mutation Surveyor Update

Version 3.01 of Mutation Surveyor DNA variant analysis software includes two additional functionalities: vector masking for use in the quality control of DNA clones and negative single nucleotide polymorphism (SNP) indicator for clinical analysis of sequence traces. The vector masking tool allows users to inform the software of the vector region, which permits the software to use its patented physical trace comparison technology to detect any sequence change from the original sequence trace in up to 400 clone traces in less than 90 seconds. The negative SNP indicator clearly indicates the absence of a nucleotide change in sequence traces.

SoftGenetics For information 814-237-9340 www.softgenetics.com

Transcreener PDE Assay

Transcreener Assays rely on homogeneous immunodetection of nucleotides for robust, generic detection of entire families of drug target. The assay extends nucleotide detection capabilities to include adenosine monophosphate, adenylic acid (AMP) and guanosine 5′-phosphate (GMP) detection. The Transcreener PDE Assay is a far-red, competitive fluorescence polarization immunoassay based on the detection of the hydrolyzed substrates AMP or GMP. Enzyme progress is indicated by a decrease in the fluorescence polarization signal. The simple two-step, endpoint assay can be used for any enzyme class that produces either AMP or GMP.

BellBrook Labs For information 866-313-7881 www.bellbrooklabs.com

Eight-Channel HPLC

The ExpressLC-800 Plus high performance liquid chromatography (HPLC) system features new solvent switching functionality, making up to six solvents available to each of eight LC channels. Solvent switching is easily programmed via the system control software. The ExpressLC-800 Plus is suitable for methods development and high-throughput applications in drug discovery. It allows solvents to be changed automatically with less handling and fewer errors. The system's eight channels offer true multiplexed HPLC for savings in analysis time, labor, and laboratory bench space. The instrument combines advances in gradient delivery and mixing, sample injection, and optical detection to deliver dramatically increased levels of separation resolution and speed.

Eksigent For information 925-560-2637 www.eksigent.com

Proteome Fractionation

FOCUS-Global Protein Extraction kit is a simple, rapid, and reproducible method for extraction of various classes of cellular proteins, both soluble and insoluble. The insoluble protein fractions are further fractionated into various classes of membrane proteins, such as mildly hydrophobic membrane proteins, highly hydrophobic transmembrane proteins, and membrane proteins rich in cholesterol, glycolipids, and glycocylphosphitidylinositol.

G-Biosciences/Genotech For information 800-628-7730 www.GBiosciences.com

Raman Spectrometer

The benchtop RamanStation 400 Raman spectrometer combines research-grade performance with push-button ease-of-use. The RamanStation's dispersive echelle-spectrograph technology allows reliable performance, without the need for moving parts, while enabling detection of the full spectral range at a high resolution in a single acquisition. Raman spectroscopy is a non-destructive technique based on the detection of scattered light to identify and analyze molecular species that has been limited to a narrow sector of highly skilled researchers with special training; the RamanStation is designed to make it accessible to more users. With the push of a button, an operator can obtain high-quality information regarding the identification, composition, and molecular structure of samples.

Perkin-Elmer For information 781-663-6900 www.perkinelmer.com/ramanstation400

Literature

The Analytical Sample Preparation catalog features a regulated methods and applications guide and a filter guide. Products featured include air and liquid monitoring, membrane filters, syringe filters, and water purification systems. The Cell Biology Application and Product Guide showcases a complete range of products to fulfill basic needs, such as cell culture supplies and reagents, as well as more advanced applications, such as stem cell research. The guide also provides membrane-based cell culture protocols, workflows, and application notes. The Immunodetection Application and Product Guide includes optimized protocols for commonly used immunodetection techniques such as immunoprecipitation and protein immunoblotting, as well as protein concentration and antibody purification.

Millipore For information 978-762-5294 www.millipore.com911K

Newly offered instrumentation, apparatus, and laboratory materials of interest to researchers in all disciplines in academic, industrial, and government organizations are featured in this space. Emphasis is given to purpose, chief characteristics, and availability of products and materials. Endorsement by *Science* or AAAS of any products or materials mentioned is not implied. Additional information may be obtained from the manufacturer or supplier.

POSITIONS OPEN

SENIOR RESEARCH ASSOCIATE
Center for Translational Medicine
University of Minnesota

The University of Minnesota is seeking candidates to fill several positions which will direct preclinical laboratory studies utilizing human cells and/or rodent models that will form the basis for Phase I trial testing of cell-based products in the newly created Center for Translational Medicine (CTM). The candidates will be primarily responsible for the development, review/evaluation, and interpretation of experiments that support the translation of basis discovery and research into Phase I clinical trials, as well as preparation of data and reports for regulatory submissions. Candidates will serve as critical members of a liaison team, interacting with leading scientists, clinicians, and the good manufacturing practice production team to help bring novel cell therapy products and strategies to the clinic.

The individual will develop novel experimental strategies and systems to aid in the cell-based, product development process and will be responsible for creating novel protocols to address experimental questions, planning activities, including design and execution of experiments, interpret and analysis the results, ensure data quality, and provide timely insightful reports.

The ideal candidates will be highly motivated and creative, possess strong interpersonal skills with a strong background in research of cellular, pharmacological, molecular, or protein products, and will be extremely detail-oriented, and possess excellent computer, organizational skills, and problem solving abilities. A broad-based understanding of cell biology or biochemistry is essential.

The positions will include responsibility for the direct supervision of other scientific staff, commensurate with the candidate's ability. These positions will report to **Dr. Bruce Blazar, Director of CTM.** As part of the CTM you will benefit from strong leadership, a bold vision, and an empowering culture.

Senior Research Associate is the highest research title at the University of Minnesota, and is recognized as a career position. These positions will enjoy competitive compensation which will be commensurate with experience, as well as a very progressive benefits package. Requirements: Required qualifications: Ph.D. or M.D. degree is required. Minimum of five years of experience conducting research, to include at least three years of supervisory experience in cellular, protein, or pharmacological agent manipulation and testing in biological systems relevant for clinical trial applications. For one of our positions, demonstrable, hands-on experience with animal models is required. Preferred qualifications: Previous experience in a product development environment, and background in stem cell research would be an advantage. Qualified applicants should provide a letter of inquiry, resume, or curriculum vitae, and a list of three professional references. Contact: **Randall Tlachac, e-mail: rtlachac@umn.edu. Telephone: 612-624-0765.**

The USDA, Animal and Plant Health Inspection Service, Foreign Animal Disease Diagnostic Laboratory on Plum Island, New York, is seeking a full-time **SUPERVISORY VETERINARY MEDICAL OFFICER** (GS-15; annual salary of $115,929 to $145,400 plus benefits). Incumbent will serve as the **DIRECTOR** of the facility. *The incumbent must be a U.S. citizen and able to obtain a secret security clearance while employed for the position.* A copy of announcement number 24VS-2007-0175 (open to the public) or 6VS-2007-0223 can be obtained at **website: http://jobsearch.usajobs.opm.gov,** or call **telephone: 515-663-7266** for aplication procedures. This position will be open April 30 through May 29, 2007. *The Federal Government is an Equal Employment Opportunity Employer.*

POSITIONS OPEN

UIC UNIVERSITY OF ILLINOIS AT CHICAGO COLLEGE OF PHARMACY

FACULTY POSITIONS
Department of Biopharmaceutical Sciences
College of Pharmacy
The University of Illinois at Chicago

The Department of Biopharmaceutical Sciences in the College of Pharmacy invites applications for tenure-track positions at the **ASSISTANT, ASSOCIATE, or FULL PROFESSOR** level in the broad field of biopharmaceutical sciences, with an emphasis on novel methods of drug and biopharmaceutical delivery and/or molecular pharmacology. The Department of Biopharmaceutical Sciences has particular interests and strengths in pharmaceutics and pharmacology related to cancer therapy. The College of Pharmacy has complementary strengths in analytical and medicinal chemistry, proteomics, and clinical pharmacy with emphasis on cancer chemoprevention, cardiovascular pharmacology, neuropharmacology, and infectious diseases. We are particularly interested in candidates with research interests that will complement these departmental, College and University research efforts. The successful candidate will have a record of peer-reviewed publications and grant support in these areas, depending on rank, and should be prepared to participate in the teaching programs in the College. Faculty rank and salary will be commensurate with experience and achievements. Applicants must possess a relevant doctoral degree. Women and minorities are encouraged to apply.

The University of Illinois at Chicago (UIC) College of Pharmacy is in the heart of the Illinois Medical District, which includes the UIC Medical Center, College of Medicine, the UIC Hospital, and other health science colleges. The College of Pharmacy is ranked among the top four U.S. colleges of pharmacy in total funding from the National Institutes of Health. The Department of Biopharmaceutical Sciences can offer newly renovated first-class laboratory space and a competitive startup package. For more information about the College of Pharmacy and the Department of Biopharmaceutical Sciences, see **website: http://www.uic.edu/pharmacy/.**

Please submit a letter describing current and proposed research activities, current curriculum vitae, including grant funding history, and three references to:

Hayat Onyuksel, Ph.D.
Professor and Associate Head
Department of Biopharmaceutical Sciences
College of Pharmacy (MC 865)
University of Illinois at Chicago
833 South Wood Street
Chicago, IL 60612-7231

Applications may be submitted electronically to **e-mail: bpssearch@uic.edu.** The positions are available beginning August 15, 2007; review of candidates will continue until the positions have been filled. *The University of Illinois at Chicago is an Affirmative Action/Equal Opportunity Employer.*

STRESS RESISTANCE and AGING in MICE
University of Michigan School of Medicine

POSTDOCTORAL POSITION for studies of stress resistance in cells from long-lived mutant mice. Experience in cell biology, signal transduction, or molecular pathology or toxicology required. Send curriculum vitae, statement of research interests, and names and contact information for three references to: **Richard A. Miller, University of Michigan, P.O. Box 2200, 3001 BSRB, Ann Arbor, MI 48109;** or to **e-mail: millerr@umich.edu.** *An Equal Opportunity Employer.*

INCUBATING INNOVATION: Diversity Efforts Rejuvenate the Life Science Work Force

By Alethea Hannemann

Start with these numbers: African-Americans make up 13 percent of the United States population, but comprise only 5 percent of those employed in the life, physical, and social sciences. Or with this: less than 3 percent of Ph.D.s in biology and chemistry are held by African-Americans. Different statistics pepper various reports, but none dispute the central fact, that African-Americans do not hold life science jobs in numbers commensurate with their representation in the US population. The gap matters not just to African-Americans considering science careers, but to science itself. It raises important questions, such as: How can we address health disparities without researchers from different backgrounds or clinical trials using a range of relevant populations? And how can the US produce world-class scientists without cultivating the ample talent in underrepresented populations, including African-Americans? Esteemed programs such as the National Institutes of Health Minority Access to Research Careers (MARC) have encouraged African-American scientists for years, but it's clear that more efforts are needed. Now some of the best minds in government, academia, and industry are searching for new answers and new strategies, using innovative programs to bolster the life science work force and address disparities from the ground up.

> "The more options and more information students have about career choices, the better career choices they will make."

Clifford Houston

Offering Alternatives for Younger Students

While a knack for science often manifests early—what scientist can't recall a fond memory of an ant farm or a chemistry set?—turning that spark into a sustained career takes years of study, planning, and dedication. So it makes sense that some initiatives focus on early education and exposure, hoping to give African-Americans a strong foundation. At the University of Texas Medical Branch (UTMB) in Galveston, for example, community science programs, including after-school workshops, summer camps and research programs, and career days, start at the prekindergarten level and focus on underserved communities. As **Clifford Houston,** UTMB's associate vice president for educational outreach, points out, "The whole idea is to bring in students who have been ignored or disadvantaged." And those students, once engaged, show a commitment to science studies. Grades almost universally improve, and at the popular UTMB-supported Galveston County Science and Engineering Fair, Houston sees an increasing number of African-American entrants. "Not just presenting but winning, getting first, second, or third place," says Houston. "We can look at winners and say, okay, that person was in our summer science camp." Houston feels the programs create alternatives for local students who may not have considered science otherwise. "What we find is that the more options and more information students have about career choices, the better career choices they will make," he says.

Wayne Bowen, biology professor and co-director of the Molecular Pharmacology, Physiology and Biotechnology Graduate program at Brown University, agrees that reaching African-American students at a young age is crucial. But he thinks that providing good role models is as important as making sure kids learn. "African-American students don't see many people like them in careers like this," he says. "They've seen African-American doctors, maybe, but scientists?" In 2001, Bowen served as the president of NIH's Black Scientists Association (BSA), which works to increase the numbers and visibility of African-American scientists at NIH. In addition to programs such as a seminar series, BSA often brings in continued »

UPCOMING FEATURES

Regional Focus: North Carolina — June 8

International Careers Report: UK and Ireland — June 22

Careers in Chemistry — August 10

"African-American students don't see many people like them in careers like this. They've seen African-American doctors, maybe, but scientists?"
—Wayne Bowen

student groups to publicize science career opportunities. After one presentation, says Bowen, a student came up to the assembled scientists to tell them about his interest in oceanography. "Even though he was at NIH, National Institutes of Health, he saw an opportunity to talk to someone who might know something about oceanography," says Bowen. "There was probably no one at his school who could help him at all."

Building Relationships As Challenges Grow

Not every student who finds an interest in elementary or secondary school, however, will choose to pursue it through a demanding university program. Many students, of all ethnicities, enter college with the intent to study the sciences, and many leave; attrition is not confined to a particular group. "But the problem is multiplied for underrepresented minorities," says **George Langford,** Dean of the College of Natural Sciences and Mathematics at the University of Massachusetts at Amherst (UMass). "When students come into the university, the numbers of white and black students with an interest in the sciences are about the same. However, fewer minority students complete their undergraduate degree in the sciences." One problem is budgetary restrictions: "We don't have sufficient infrastructure to support the numbers of students. It's very expensive to support a professor in the sciences, as compared to the humanities. We have to invest in labs, in faculty." Tighter budgets mean large introductory classes, which can be daunting, particularly when students don't see other African-Americans in the class or more importantly, teaching it. "If I look at UMass," Langford says, "well, I can count the number of minority faculty on my fingers."

Such a homogeneous faculty can lead to lost opportunities. Often, Langford says, African-American students miss out more on what's not in a syllabus than what is. The issue isn't preparation, he says; it's social capital, the culture of science rather than the content. Knowing which professors to approach in a department, and how often to drop into their offices; understanding which publications to bring up in a conversation, or which professional associations to join; assimilating the argot of the industry and separating slang from necessary jargon: all these skills are as important to success as grades and lab technique. "Minority students come in without that; so do white students; but because it's transmitted culturally, it's hard for white faculty to transmit it to black students. Black students study extremely hard, they do well, but they don't always meet the cultural requirements." Langford is working with colleagues in other UMass colleges, such as humanities and fine arts, developing new courses and partnerships to help students and faculty understand the issues they'll face. Facilitating a dialogue between scientists and other scholars, Langford hopes, will help life science faculty realize that not all essential skills can be gauged with an exam.

In an effort to bring more African-American scientists to campus, UMass has also diversified graduate program recruiting and retention strategies. The university leads the Northeast Alliance for Graduate Education and the Professoriate (NEAGEP), a National Science Foundation–funded program that unites large schools such as UMass and the Massachusetts Institute of Technology with minority-serving partner institutions. NEAGEP's orientation, mentoring, and tutoring provide a stable community for African-Americans who choose to study at UMass, while professional development opportunities help them negotiate the first steps in their new career. Since the program's inception, the percentage of new life science doctoral enrollees who are from underrepresented minorities has increased more than fivefold, from 3 percent in 1999 to 15 percent in 2005. Other universities support similar programs. For example, in the Leadership Alliance Summer Research Early Identification Program (SR-EIP), headquartered at Brown, participating students receive a stipend, travel allowance, and housing, and work for eight to 10 weeks with a faculty or research mentor at one of 32 alliance institutions. At the end of the program, students present their findings at a national symposium. The young researchers get valuable lab experience and a great networking opportunity, while faculty can use the program to identify talented African-American students; Brown's Bowen says he often uses the alliance database for recruiting.

Other members of the Leadership Alliance include several historically black colleges and universities (HBCUs), such as Howard University, Spelman College, and Xavier University of Louisiana. HBCUs, of course, produce significant numbers of African-American graduates each year, and many are putting special resources toward science programs. At Morehouse College, for example, **J.K. Haynes,** Dean of the Division of Science and Mathematics, touts the Hopps Research Scholars Program, supported by the US Department of Defense. The Hopps program, in which students do research with chosen mentors from freshman year until they graduate and take special classes focused on graduate school preparation, kicked off in 2006 with about 25 participants, but two recent classes of Packard Scholars followed a similar program. "At least 70 percent of those young men went to graduate school," Haynes says; with the right resources, he hopes to bring that matriculation number up to 85 percent.

Supporting Work Force Breadth and Depth

Support for undergraduate and graduate programs that encourage African-American scientists also comes from industry leaders. Merck, in a partnership with the United Negro College Fund, awards at least 37 scholarships a year to African-American researchers at the undergraduate, graduate, and postdoctoral levels; to date, the program has trained more than 370 scientists. To **Deborah Dagit,** executive director of diversity and work environment at Merck, the UNCF-Merck program is far more than a feeder program for her company. "We seek to prepare students for careers in the pharmaceutical industry, and sometimes with our company, but also in other ways. For example, former fellows can be our partners in clinical research." Increasing the number of African-Americans in biotech will benefit the industry as a whole, she says; whether Merck sees a direct benefit is irrelevant. "We really did this to increase the number of black scientists, not to benefit Merck in particular. If they're working with another health care company to address needs within the African-American community, then we would have accomplished our goal."

continued »

Focus on Diversity

Like Dagit, **Rodney Moses,** vice president of talent acquisition and talent management at Invitrogen, thinks that diversity efforts must work to invigorate the entire industry, rather than a particular company. "We have a day job, which is to meet our customers' needs, but we also need to invest in the pipeline." To that end, Invitrogen is leading a new initiative that uses corporate funds to bolster science education. Called the San Diego Workforce Collaborative, the program is a combined effort by the State of California; a range of local technology and biotechnology employers; and the San Diego Workforce Partnership, an innovative job training and employment program that has pooled state and private resources to rejuvenate the local work force. Invitrogen hopes to augment the funds it already contributes to community development and scholarship opportunities by encouraging other San Diego biotech companies to join the collaborative. "It's an opportunity for the state to generate $1.3 million in scholarship money," says Moses. "That would be a huge win if we could get other companies involved."

Amgen
www.amgen.com

Brown University
www.brown.edu

Invitrogen
www.invitrogen.com

JustGarciaHill
www.justgarciahill.org

Leadership Alliance Summer Research Early Identification Program (SR-EIP)
www.theleadershipalliance.org/matriarch/default.asp

Morehouse College
www.morehouse.edu

National Association for Blacks in Bio
www.nab-bio.org

National Institutes of Health Black Scientists Association
bsa.od.nih.gov/bsaabout.htm

National Institutes of Health Minority Access to Research Careers
www.nigms.nih.gov/minority/marc.html

Northeast Alliance for Graduate Education and the Professoriate
www.neagep.org

San Diego Workforce Partnership
www.sandiegoatwork.com

UNCF• Merck Science Initiative
www.uncf.org/merck

University of Massachusetts at Amherst
www.umass.edu

University of Texas Medical Branch Science Education, Div. of Community Outreach
www.utmb.edu/oeo/Student_Programs

Focusing Resources to Foster Talent

Even the most skilled and talented students, however, can have a hard time finding their way once graduation comes along. Most national science organizations have subgroups that help young African-American scientists navigate career planning, but more targeted organizations include JustGarciaHill, a virtual community that seeks to support minorities entering science careers, and the National Association for Blacks in Bio (NABB), a growing organization that works to create networking and communication opportunities between African-Americans in science careers. **Chad Womack** founded NABB to fill what he describes as a large gap in the work force pipeline. "There's no simple answer," he says of the lack of African-American scientists. "Part of it is recruitment and retention; not just getting people into the pipeline, but getting people in the pipeline out." NABB holds a national event, African-Americans in the Life Sciences (AALS), at the Biotech Industry Organization's annual conference; regional branches will soon provide further networking opportunities, and a new journal will publicize research openings and developments in critical issues such as health disparities. NABB also plans what Womack describes as "a biotech boot camp," a conference to help potential entrepreneurs learn how to contact investors, find financing, and commercialize technology.

Organizations like NABB may make it easier for companies to find talented African-American scientists. But for a company's diversity efforts to thrive, it must support employees internally, providing resources and connections that increase retention and promote talent. At Merck, Diversity Awards highlight the contributions of African-American scientists, among others, and the Black Employee Network offers a range of networking and support opportunities. The company also offers an innovative mentor-matching program, which works similarly to popular online services such as Match.com; it helps interested mentors meet other employees who share their professional goals and interests. Leveraging new technologies to support time-tested career strategies, the system can be a big help to a new employee searching for advice and guidance.

Looking Forward, Reaching Out

Most scientists agree that mentoring, whether formal or informal, is key to professional success. According to Amgen scientist **Karla Savage,** "There's a big transition going from academia to industry; things are a bit more formal and more organized, and mentors can help to figure it out." Like Merck, Amgen has a Black Employee Network (BEN), which provides opportunities for networking and professional development, brings in outside speakers, and helps employees meet other professionals who share their ambitions and experiences. The group also performs outreach, and in this it helps to bring diversity efforts full circle; employees who have benefited from diversity initiatives are eager to pass on what they've learned. In February, for example, the Amgen BEN held a youth summit to discuss the achievements of black scientists with local African-American students. "Young people are always so excited to see people who have impressive jobs," says Savage. "There's more to science than just being a doctor. We can help foster their career exploration as they grow older."

In the end, building a robust, diverse science work force will take vigorous effort from many camps. The good news is that a host of programs in government, academia, and industry are dedicated to increasing the numbers of African-Americans in science. With continued efforts, education and recruiting programs should soon bear fruit, bringing new power to the life sciences. Says Merck's Dagit, "We feel strongly that our internal talent needs to match the marketplace. I think the life sciences have been a little too late to the party on bringing our talents and resources to bear on solving some of the critical issues within a given community. I'm proud to work for a company that feels strongly about that."

Alethea Hannemann is a San Francisco–based freelance writer.


I've got the
science
in me.
Pure Science. It's the building block of life at Invitrogen. That's because a career here requires an unyielding commitment and focus on science. And even though we all have this core value in common, we recognize and embrace our differences. It's the uniqueness of the individual collaborating across teams, across departments, and across cultures that has made us a global biotech leader.
At Invitrogen we understand that creativity and innovation are forged best in an atmosphere of openness where different perspectives, skills, and passions are embraced and encouraged. We're about asking questions and finding answers no matter where the journey takes us. We're about taking risks and fearlessly embracing new frontiers in science – one scientist at a time, one team at a time, one customer at a time.
We invite you to discover life at Invitrogen where the spectrum of opportunity is virtually unlimited.
Visit us online at www.invitrogen.com/careers.
We are proud to be an Equal Opportunity Employer dedicated to hiring a diverse work team.
invitrogen™

NSF-IGERT Opportunities at the University of Wisconsin-Madison

Exceptional students interested in interdisciplinary and international environmental study are invited to apply for traineeship with generous stipend, tuition waver, and health benefits. Opportunities are available in two different programs

Biodiversity Conservation and Sustainable Development in Southwest China

IGERT trainees will address the interactions of ecology, livelihoods, and governance by pursuing a PhD in one of over a dozen departments and participating in IGERT seminars, workshops, language training, and field research in the Himalayas of Yunnan, China - a "biodiversity hotspot." The application deadline for this program is February 1, 2008.

Learn more: **http://www.swchina.wisc.edu**

Certificate on Humans and the Global Environment - the CHANGE IGERT *(Nelson Institute for Environmental Studies)*

CHANGE IGERT fellows acquire a graduate certificate that blends natural science, social science, and humanistic approaches to understanding environmental vulnerability and sustainability as they pursue their PhD. The application deadline for this program is January 2, 2008.

Learn more: **http://www.sage.wisc.edu/igert/**

THE UNIVERSITY of WISCONSIN MADISON

BROAD INSTITUTE

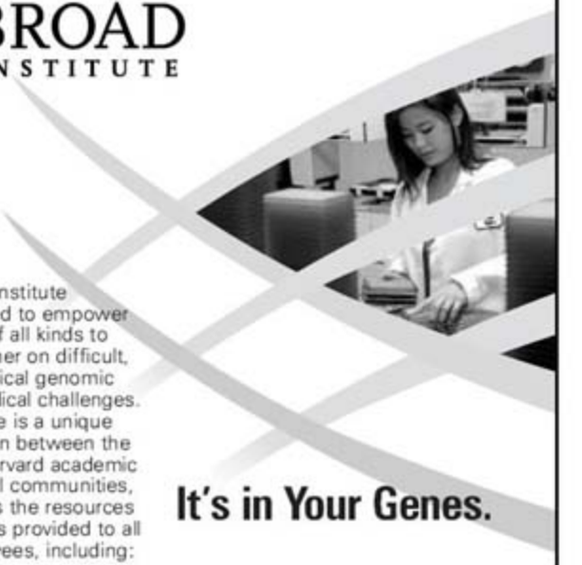

The Broad Institute was founded to empower scientists of all kinds to work together on difficult, diverse, critical genomic and biomedical challenges. The Institute is a unique collaboration between the MIT and Harvard academic and medical communities, and it offers the resources and benefits provided to all MIT employees, including:

- ***Competitive pay***
- ***Medical, dental, life insurance plans***
- ***401(k) plan with matching contributions***
- ***Tuition assistance plan***
- ***Four weeks of vacation after one year***
- ***T-Pass subsidy program***
- ***Athletic and fitness centers***
- ***Child care services***

It's in Your Genes.

Join a team that works the way you've always wanted to work.

Opportunities include: Research Scientists, Research Technicians, Scientific Management, and Computational Scientists and Engineers. Visit our website to view our current opportunities and apply: **www.broad.mit.edu/info/careers**

The Broad Institute is an equal opportunity/affirmative action employer.

MOUNT SINAI SCHOOL OF MEDICINE

DIRECTOR
Mount Sinai Cancer Institute
The Mount Sinai Medical Center
Mount Sinai School of Medicine
Mount Sinai Hospital
New York, New York

Mount Sinai

The Mount Sinai Medical Center is recruiting for an outstanding physician scientist to serve as the Director of the Mount Sinai Cancer Institute. The Mount Sinai Medical Center has recently completed a strategic plan and has embarked on a 1 Billion dollar capital campaign. A major priority of the strategic plan is a major expansion of cancer programs, resulting in a doubling of faculty, research space, and clinical facilities.

The Director will have the opportunity to build an outstanding comprehensive cancer program with an emphasis on translational research leading to therapeutic breakthroughs.

Mount Sinai is currently ranked amongst the top 20 medical schools in NIH funding and places a strong emphasis on the integration of basic and clinical research. The leadership of The Mount Sinai Medical Center is committed to establishing one of the nation's premier cancer programs located in an academic full service medical center. The Medical Center will provide the resources necessary to recruit and retain the highest-quality scientists and clinicians.

The position requires that the candidate have an M.D., or M.D./Ph.D., an outstanding record of scientific accomplishment in cancer research and exceptional leadership ability.

PROCEDURE FOR CANDIDACY – For further information about how to apply for this position, please contact: **Dennis S. Charney, M.D., Dean, Mount Sinai School of Medicine, Executive Vice President for Academic Affairs, The Mount Sinai Medical Center, One Gustave L. Levy Place, Box 1217, New York, NY 10029-6574; Phone (212) 241-5674; Fax. (212) 824-2302; Email: dennis.charney@mssm.edu.**

Assistant/Associate Professor
Department of Pharmacology, Physiology and Therapeutics
University of North Dakota
School of Medicine and Health Sciences

Applications are invited for one full-time tenure-track faculty position at the **Assistant/Associate Professor** level. Applicants for this faculty position must have a Ph.D. or equivalent degree with at least three years of postdoctoral training. Applicants for the position at the Associate Professor level must have evidence of significant independent funding. Preference will be given to those applying mass spectrometric, proteomic and/or modern molecular strategies to areas of existing strength in the Department; namely cellular signaling, neuroscience and aging. A number of our faculty members are supported by a 5-year $10.3 M COBRE (NIH) grant that was recently renewed for a second 5-year period to study "Pathophysiological Signaling in Neurodegenerative Diseases." The successful candidate will be expected to maintain an active extramurally funded research program and participate in team-taught graduate and medical courses.

Please send current curriculum vitae, contact information for at least three individuals willing to serve as references, and descriptions of previous and proposed research as well as teaching experience to: **Dr. Jonathan D. Geiger, Professor and Chair, Department of Pharmacology, Physiology and Therapeutics, Box 9037, University of North Dakota, School of Medicine and Health Sciences, Grand Forks, ND 58203 (Ph. 701-777-2183, Fax 701-777-4490, jgeiger@medicine.nodak.edu)**. Applications will be reviewed as received until the position is filled. The University of North Dakota, with about 13,000 students, is located in Grand Forks, ND, a family-orientated community of over 50,000 people with excellent schools, parks, and abundant year-round outdoor recreational activities.

The University of North Dakota is an Equal Opportunity/ Affirmative Action Employer and invites applications from all qualified individuals.

www.med.und.nodak.edu/depts/pharm

DEPUTY DIRECTOR
National Institute of Diabetes and Digestive and Kidney Diseases
Department of Health and Human Services
National Institutes of Health

THE POSITION: The National Institute of Diabetes and Digestive and Kidney Diseases (NIDDK) is seeking exceptional candidates for the position of **Deputy Director** of the Institute. The incumbent serves as an active partner with the NIDDK Director in the leadership of a $1.8 billion national organization that conducts and supports biomedical and behavioral research. The NIDDK supports and conducts research to understand, treat, and prevent some of the most common and severe diseases affecting the public health, and disseminates research findings and health information to health care professionals, patients and the public through national health information and education programs (**http://www2.niddk.nih.gov/**). This position offers a unique and exciting opportunity for an extremely capable individual to share responsibility in providing strong and visionary leadership to an organization dedicated to uncovering new knowledge and technologies, both basic and clinical. The NIDDK seeks candidates who have a commitment to scientific excellence and the energy, enthusiasm, and innovative thinking necessary to help lead major strategic planning initiatives and their subsequent careful implementation. The Deputy will be expected to represent, and speak on behalf of, the Director and the Institute before Members of Congress and their staffs, high level Government officials, leaders of national voluntary and professional health organizations, and leaders in business, science and academia.

QUALIFICATIONS REQUIRED: Applicants must possess an M.D., Ph.D., or equivalent degree, as well as senior-level research experience or knowledge of research programs in one or more of the following disease areas: diabetes, endocrinology and metabolic diseases; digestive diseases and nutrition; and kidney, urologic, and hematologic diseases. Candidates should be outstanding communicators and known and respected within their professions as distinguished individuals of outstanding competence. Applicants should also demonstrate the ability to think strategically, work collaboratively and use a consultative approach to problem solving and decision making.

SALARY/BENEFITS: Salary is commensurate with experience and a full package of Civil Service benefits is available, including: retirement, health and life insurance, long term care insurance, leave and savings plan (401K equivalent). This position is subject to a background investigation.

HOW TO APPLY: A Curriculum Vitae, Bibliography, and two letters of recommendation must be received by **July 2, 2007**. Application packages should be sent to the **National Institutes of Health (NIH), National Institute of Diabetes & Digestive & Kidney Diseases (NIDDK), 31 Center Drive, MSC 2560, Building 31, Room 9A-16, Bethesda, Maryland 20892.** For further information, please call (301) 594-7772. All information provided by candidates will remain confidential and will not be released outside the NIDDK search process without a signed release from candidates.

DHHS and NIH are Equal Opportunity Employers

CHAIR
Department of Cell Biology
Yale University School of Medicine

Yale University School of Medicine announces a search for Chair, Department of Cell Biology. This department, which was founded by George Palade in the early 1970's, can be arguably considered the birthplace of modern cell biology, and its research has consistently been at the forefront of the field. The successful candidate will be expected to possess an outstanding academic record in research and education, together with demonstrated leadership capacity. He/she must meet the requirements for appointment as Full Professor at Yale.

Interested candidates should send a curriculum vitae and bibliography, a brief statement of programmatic goals, and a list of professional references prior to **July 30, 2007** either electronically (to **darlene.a.smith@yale.edu**) or by mail, to:

Jorge E. Galán, Ph.D.
Chair, Cell Biology Search Committee
c/o Elinor Lutch
Dean's Office, Yale Medical School
333 Cedar Street, C203 SHM
Post Office Box 208055
New Haven, CT 06520-8055

Yale University is an Equal Opportunity, Affirmative Action Employer. Minorities and women are encouraged to apply.

SANTA FE INSTITUTE

Undergrad, Grad, Postdoctoral Fellowship Opportunities

Annual Complex Systems Summer School/Graduate Workshop in Computational Social Sciences/Postdoctoral Fellowships.

Application deadlines vary.

See: **www.santafe.edu**

SFI is a private nonprofit science research and educational center focusing on the common fundamental principles in physical, computational, biological, and social complex systems.

SFI is an equal opportunity employer. Women and minorities are encouraged to apply.

AFFYMETRIX®

Affymetrix, Inc. is a pioneer in creating breakthrough tools that are driving the genomic revolution. We are actively recruiting in our Emeryville, Sacramento, Santa Clara and South San Francisco locations. Positions are available at various levels in the following departments:

- **Research and Development** (Scientists, Research Assistants/Associates)
- **Manufacturing** (Engineers)
- **Finance/IT and Human Resources** (Analysts, Programmers, Accountants)
- **Sales and Marketing**

To apply for one of these positions or to explore other career opportunities with us, please visit Affymetrix online at **http://www.affymetrix.com/corporate/careers/index.affx**.

Affymetrix is an Equal Opportunity Employer.

BASF Conference on Nanomaterials

BASF
The Chemical Company

OCTOBER 21 – 23, 2007 IN SINGAPORE

Nanotechnology is considered to be one of the most important emerging technologies worldwide. Through the controlled manufacture and structuring of materials, it allows the creation of completely new product properties. It is an innovation driver for many industry sectors. BASF is one of the leading companies in the field of chemical nanotechnology.

The BASF conference on Nanomaterials will foster the exchange of ideas, techniques, experiments and applications. A series of lectures will be given in order to match BASF's future vision with current activities of the research institutes in the field of Nanomaterials. Leading scientists from all over the world will be participating in the conference as speakers on the following topics:

1. Nanomodified and nanostructured materials and foams
2. Synthesis and modification of nanoparticles
3. Nanotechnology for electronics
4. Interface of bio- and nanotechnology

Invitation procedure

The conference is open to every young researcher at the PhD, post-doctoral or junior professor level, working in the four fields mentioned above. Full scholarships for participation are available – please send your CV and an abstract for a poster referring to these topics to andreas.a.fechtenkoetter@basf.com by June 30, 2007.

We look forward to meeting you in Singapore.

www.basf.com

NIDDK Tenure-Track Position in Endocrinology and Metabolism and Human Obesity
National Institute of Diabetes and Digestive and Kidney Diseases

We seek an outstanding scientist to direct a vigorous, innovative research program in the Clinical Endocrine Section of the Clinical Endocrinology Branch to advance knowledge in the area of obesity and weight regulation with particular emphasis on the neuroendocrine aspects of weight regulation and the role of sleep in obesity. Applicants must be highly motivated and have a demonstrated track record through publications that address significant contributions to the field of endocrinology and metabolism. The successful candidate is expected to develop an independent, world-class research program complementary to current investigations within the Branch. The position comes with generous start up funds and on-going support.

The Clinical Endocrinology Branch, NIDDK is located on the main NIH campus in Bethesda, Maryland, a suburb of Washington DC. The Branch represents interests similar in range to those of an academic department. There are strong interactions among the independent research groups, and the position offers unparalleled opportunities for interdisciplinary collaboration within NIDDK and throughout NIH. Applicants should submit a curriculum vitae, bibliography, copies of three major publications, a summary of research accomplishments, a brief statement of future research goals, and arrange for three letters of reference to be sent to:

Dr. James Balow, Chair, Search Committee, c/o Glynnis Vance, NIDDK, 9000 Rockville Pike, Building 10-CRC/Room 5-2551, National Institutes of Health, Bethesda, MD 20892.

Application Deadline: **June 8, 2007**

NIDDK Tenure-Track Position in Clinical Research in Diabetes and Kidney Disease
National Institute of Diabetes and Digestive and Kidney Diseases

We seek an outstanding scientist to direct a vigorous, innovative clinical research program in the epidemiology, physiology, and treatment of type 2 diabetes, diabetic nephropathy, and related disorders. Applicants must be highly motivated and have a demonstrated track record through publications that address significant issues of causation, prevention, and treatment of these conditions. Applicants must also be licensed to practice medicine in one of the United States and have substantial experience in community relations, recruitment, and clinical research among US minority groups. The successful candidate is expected to develop an independent, world-class research program complementary to current investigations within the Phoenix Epidemiology and Clinical Research Branch (PECRB). The position comes with generous start up funds and on-going support.

The PECRB, NIDDK is located in Phoenix, Arizona. The Branch represents interests similar in range to those of an academic department. There are strong interactions among the independent research groups, and the position offers unparalleled opportunities for interdisciplinary collaboration within NIDDK and throughout NIH. Applicants should submit a curriculum vitae, bibliography, copies of three major publications, a summary of research accomplishments, a brief statement of future research goals, and arrange for three letters of reference to be sent to:

Dr. James Balow, Chair, Search Committee, c/o Glynnis Vance, NIDDK, 9000 Rockville Pike, Bldg. 10-CRC/Rm. 5-2551, National Institutes of Health, Bethesda, MD 20892.

Application Deadline: **June 8, 2007**.

WWW.NIH.GOV

NIDDK

Tenure-Track Position in Human Energy Metabolism
National Institute of Diabetes and Digestive and Kidney Diseases

We seek an outstanding scientist to direct a vigorous, innovative research program in human energy metabolism and serve as Director of the newly established Metabolic Core Laboratory (MCL), Clinical Endocrinology Branch, NIDDK. The MCL performs a number of analyses including exercise testing, physical activity monitoring, body composition measurement, and 24-hour energy expenditure analysis in health and disease. Applicants must be highly motivated and have a demonstrated track record through publications that address significant contributions in the areas of energy expenditure and physical activity as it relates to metabolism and weight regulation. The successful candidate is expected to develop an independent, world-class research program complementary to current investigations within the Branch and to successfully oversee the functioning of the MCL. The position comes with generous start up funds and on-going support.

The Clinical Endocrinology Branch, NIDDK is located on the main NIH campus in Bethesda, Maryland, a suburb of Washington DC. The Branch represents interests similar in range to those of an academic department. There are strong interactions among the independent research groups, and the position offers unparalleled opportunities for interdisciplinary collaboration within NIDDK and throughout NIH. Applicants should submit a curriculum vitae, bibliography, copies of three major publications, a summary of research accomplishments, a brief statement of future research goals, and arrange for three letters of reference to be sent to:

Dr. James Balow, Chair, Search Committee, c/o Glynnis Vance, NIDDK, 9000 Rockville Pike, Building 10-CRC/Room 5-2551, National Institutes of Health, Bethesda, MD 20892.

Application Deadline: **June 8, 2007**

NCCAM

Diabetes Unit
Postdoctoral Research Positions

Laboratory investigations focus elucidating molecular mechanisms for functional foods and nutritional supplements that may be beneficial for treating diseases such as diabetes and metabolic syndrome that are characterized by reciprocal relationships between insulin resistance and endothelial dysfunction (see *Circulation* 113:1888-1904, 2006). Positions are available for scientists with M.D. and/or Ph.D. degrees and less than five years of postdoctoral experience. Molecular and cellular biology experience and a strong publication record are essential. The salary will be commensurate with your experience.

The Diabetes Unit, NCCAM provides state-of-the-art research facilities in the intramural program at NIH in addition to a collegial and nurturing working environment. Please forward your CV, bibliography, list of three references, and a cover letter stating your scientific interests and experience to:

Michael J. Quon, M.D., Ph.D. (email:quonm@nih.gov. Diabetes Unit, NCCAM, NIH, 10 Center Drive, Building 10, Room 6C-205, Bethesda, MD 20892.

For students, recent graduates, and postdoctoral, research, and clinical fellows.

Your on-line guide to training with the best at the world's largest biomedical research institution.

In Bethesda, Maryland, and at other NIH laboratories.

Office of Intramural Training and Education
Bethesda, Maryland
20892
800.445.8283

opportunity *clicks*

www.training.nih.gov

NIDDK

Tenure-Track Position in Molecular Genetics
National Institutes of Diabetes and Digestive and Kidney Diseases

We seek an outstanding scientist to direct a vigorous, innovative research program in Molecular Genetics in the Genetics and Endocrinology Section/Metabolic Diseases Branch. Applicants must have a demonstrated track record of significant publications that address identification and mechanisms of action of tumor genes. The successful candidate is expected to develop an independent, world-class research program complementary to current investigations within the Branch. The position comes with generous start up funds and on-going support.

The Metabolic Diseases Branch of NIDDK is located on the main NIH campus in Bethesda, Maryland, a suburb of Washington DC. The Branch represents interests similar in range to those of an academic department with groups studying G-proteins and hormone-secreting tumors including those mediated by the MEN1 or HRPT2 genes in man. There are strong interactions among the three independent research groups, and the position offers unparalleled opportunities for interdisciplinary collaboration within NIDDK and throughout NIH. Applicants should submit a curriculum vitae, bibliography, copies of three major publications, a summary of research accomplishments, a brief statement of future research goals, and arrange for three letters of reference to be sent to:

Dr. Dan Camerini-Otero, Chair, Search Committee, c/o Linda Robinson, NIDDK, 9000 Rockville Pike, Building 5/Room 201, National Institutes of Health, Bethesda, MD 20892.

Application Deadline: **June 15, 2007**.

NIDDK

Tenure-Track Position in Human Molecular Genetics
National Institute of Diabetes and Digestive and Kidney Diseases

We seek an outstanding scientist to direct a vigorous, innovative research program in the molecular genetics of human type 2 diabetes and/or obesity, in particular as these diseases relate to the Pima Indian population of Arizona. Applicants must be highly motivated and have a demonstrated track record through publications that address significant issues of discovery of genetic susceptibility factors to these conditions in human populations. The successful candidate is expected to develop an independent, world-class research program complementary to current investigations within the Phoenix Epidemiology and Clinical Research Branch (PECRB). The position comes with generous start up funds and on-going support.

The PECRB, NIDDK is located in downtown Phoenix, Arizona. The Branch represents interests similar in range to those of an academic department. There are strong interactions among the independent research groups, and the position offers unparalleled opportunities for interdisciplinary collaboration within NIDDK and throughout NIH. Applicants should submit a curriculum vitae, bibliography, copies of three major publications, a summary of research accomplishments, a brief statement of future research goals, and arrange for three letters of reference to be sent to:

Dr. Dan Camerini-Otero, Chair, Search Committee, c/o Linda Robinson, NIDDK, 9000 Rockville Pike, Building 5/Room 201, National Institutes of Health, Bethesda, MD 20892.

Application Deadline: **June 15, 2007**.

WWW.NIH.GOV

NIDDK

POSTDOCTORAL FELLOWSHIPS IN MOLECULAR AND CELL BIOLOGY
National Institute of Diabetes and Digestive and Kidney Diseases (NIDDK)

We are seeking outstanding postdoctoral candidates holding a PhD, an MD or an MD-PhD with a background in molecular and cell biology and genetics interested in the following research topics:

A) IDENTIFICATION OF NOVEL REGULATORS OF MESENCHYMAL STEM CELL SPECIFICATION

The laboratory studies the transcriptional regulation of adipogenesis and is currently interested in the characterization of novel molecules that can influence adipocyte cell lineage specification. If you would like to apply for a postdoctoral position in this laboratory, please send your curriculum vitae with a cover letter to Dr. Elisabetta Mueller (elisabettam@niddk.nih.gov). To learn more about our research, please visit our lab website at **http://intramural.niddk.nih.gov/research/faculty.asp?People_ID=1702**

B) SKELETAL MUSCLE STEM CELL REGULATION

Our laboratory studies the role of TGF-beta family members in skeletal muscle development and metabolism. A postdoctoral position is available to study the regulation of adult skeletal muscle stem cell quiescence and activation. Please send your curriculum vitae with a cover letter to Dr. Alexandra McPherron (mcpherrona@niddk.nih.gov). To learn more about our research, please visit our lab website at **http://intramural.niddk.nih.gov/research/faculty.asp?People_ID=1701**

C) BIOLOGY OF SPHINGOLIPID SIGNALING

The laboratory studies the signaling functions of sphingolipids, a diverse group of cellular lipids, with focus on their roles in immunity and inflammation. If you would like to apply for a postdoctoral position in this laboratory, please send your curriculum vitae with a cover letter to Dr. Richard Proia (proia@nih.gov). To learn more about our research, please visit our lab website at **http://intramural.niddk.nih.gov/research/faculty.asp?People_ID=1533**

Applications will be reviewed upon receipt. The selected candidates will be contacted for an interview within a month from the application.

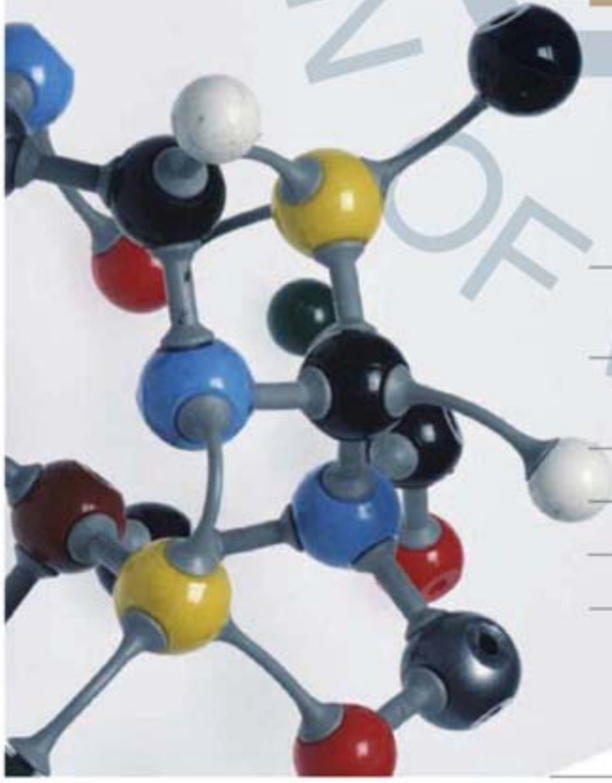

Postdoctoral Research Training at NIH

Launch a career to improve human health

Work in one of 1250 of the most innovative and well-equipped biomedical research laboratories in the world

Explore new options in interdisciplinary and bench-to-bedside research

Develop the professional skills essential for success

Earn an excellent stipend and benefits

Click on www.training.nih.gov

Office of Intramural Training and Education

Chief Scientist to head new theoretical biology or bioinformatics laboratory
Permanent Position, RIKEN

RIKEN invites applications for the position of Chief Scientist (Laboratory Director) to head a new laboratory for theoretical biology or bioinformatics. Applications from overseas are welcome. The successful candidate will be responsible for the laboratory's overall management and research strategy, directing research projects and contributing to more general aspects of RIKEN's management and research planning activities.

Laboratory - RIKEN Discovery Research Institute (DRI) will establish a new laboratory for biology research focusing on *in silico* biology. One of the directions taken by the life sciences in the post-genome era is the *in silico* reconstitution of biomolecules, cells, and tissues using theoretical and mathematical approaches. Related to this is bioinformatics, the processing of massive volumes of omics databases.

Job title and number of positions - Chief Scientist, one person

Qualifications - Applicants should have ability and experience equivalent to that of a professor who manages research at a university graduate school, and appropriate research experience supported by a distinguished research record and the ability to play a pivotal role in these areas. This position is open to all nationalities.

Location - RIKEN, 2-1 Hirosawa, Wako, Saitama, 351-0198, JAPAN

Status - The post is a permanent appointment, subject to RIKEN's mandatory retirement age of 60. However, it is possible, depending on evaluation results, to continue research after the age of 60 (73 maximum) as a Distinguished Senior Scientist. Terms and conditions of employment shall include a director-level salary, annual salary system, and bonuses, and be in accordance with RIKEN's procedures for appointing Chief Scientists.

Deadline and documents to be submitted - Applicants should send a full curriculum vitae and photograph; list of publications; one copy each of five key publications; a statement (about 5 A4-size pages) explaining former research experience and proposals for research at RIKEN; and the names and addresses of three referees. Please write to the address below for further details. All applications should reach RIKEN by September 30, 2007.

Personal information - Submitted documents will be handled in accordance with the RIKEN rules concerning personal information, and only used for screening applications for this position. Personal information will not be disclosed, transferred, and lent to any third party without a justifiable reason.

Starting date - April 1, 2008 or as soon as possible after then.

Notes - Submitted documents will normally not be returned. Information about RIKEN and its procedures for appointing Chief Scientists is available on the RIKEN website: http://www.riken.jp/engn/r-world/info/recruit/index.html

Inquiries, and where applications should be submitted - Dr. Minoru Yoshida, Head of the Chief Scientist Nominating Committee, Chemical Genetics Laboratory, RIKEN, 2-1 Hirosawa, Wako, Saitama, 351-0198, JAPAN Tel.: +81-48-467-9516 / Fax: +81-48-462-4676 / E-mail: yoshidam@riken.jp

University of Heidelberg

The **Faculty of Medicine Mannheim, University of Heidelberg** offers the position of a

Full Professor (W3) of Urology
(formerly held by Prof. Dr. Peter Alken).

The Full Professorship will be a tenured position. The successful candidate should have a distinguished record of qualifications in all areas of urology. The Department of Urology should secure highest level patient care in all clinical in- and outpatient areas. It should furthermore have a special focus on Uro-Oncology. The successful candidate should actively take part in established and developing research programs of the Faculty in the field of oncology, medical technology, vascular medicine and/or neuronal plasticity. He/she should actively participate in restructuring the undergraduate curriculum at the faculty (MaReCuM).

The successful candidate should be a board certified urologist and should have high ranking, internationally acknowledged academic qualifications commensurate with the rank of a full professor with life-time tenure including extraordinary clinical and teaching skills, a distinguished record of original research, administrative experience and an understanding of departmental financing in universities.

The successful candidate will fulfil his/her clinical duties with the University Medical Centre Mannheim; to this end he/she will be appointed Chairperson of the Dept. of Urology at University Medical Centre Mannheim. In this respect, he/she will negotiate a separate contract with the University Medical Centre Mannheim.

The position is available unlimited. In case that the successful candidate has not been appointed to a professorship position before, State law regulation demands under chapter 50 of the University law to fill the position as a tenure track position for 3 years. Exceptions are possible for candidates from abroad or from non-university institutions if candidates cannot be attracted otherwise. When the position is tenured after the tenure track period, the formal application process need not be repeated.

The University of Heidelberg is an Equal Opportunity/Affirmative Action Employer.

Interested candidates should submit a full CV with copies of certificates, publication list and selected reprints (according to the structured listing: http://www.ma.uni-heidelberg.de/dekanat/berufungen/) within 4 weeks of publication of this advertisement to **Prof. Dr. Dr. h.c. K. van Ackern, Dean of the Faculty of Medicine Mannheim, University of Heidelberg, University Medical Centre Mannheim, 68167 Mannheim, Germany.**

Open Rank
Tenure Track Position

The University of North Carolina at Chapel Hill, Department of Genetics, in conjunction with the Carolina Vaccine Institute, is searching for individuals with promising or established research programs in the broadly defined area of genetics of pathogenesis and its application to vaccine design.

Candidates should have a Ph.D., D.V.M. and/or M.D. with a strong record of recent accomplishments as a postdoctoral fellow or sustained productivity as an established faculty member. Candidates chosen will be placed in a tenure track position at The University of North Carolina at Chapel Hill.

Applicants should send a curriculum vitae, a description of research plans, and the names of three references to:

Robert E. Johnston, Ph.D.
Director, Carolina Vaccine Institute
University of North Carolina
at Chapel Hill
Campus Box #7292
Chapel Hill, NC 27599
or email to
rjohnst@med.unc.edu

We strongly encourage applications from women and minorities. The University of North Carolina at Chapel Hill is an Equal Opportunity Employer.

HOWARD HUGHES MEDICAL INSTITUTE

HHMI Investigator Competition

The Howard Hughes Medical Institute invites applications for investigator positions from scientists who have demonstrated originality and productivity in biomedical research and who show exceptional promise for future contributions.

Eligibility

- Ph.D. or M.D. (or the equivalent)
- Tenured or tenure-track position as an assistant professor or higher academic rank (or the equivalent) at an eligible U.S. institution
- Four to 10 years of experience since appointment as an assistant professor
- Principal investigator on one or more active national peer-reviewed research grants with a duration of at least three years

Application deadline: June 13, 2007

Application information:
www.hhmi.org/investigator2008/sci

HHMI investigators are among the most creative and promising biomedical scientists in the nation. They rigorously pursue significant biological questions, develop innovative research tools and methods, and lead their scientific fields into new areas of inquiry. Working to push the boundaries of fundamental knowledge and ultimately to improve human health, HHMI investigators forge links between basic biology and medicine.

The Institute seeks to appoint to its investigator program approximately 50 outstanding scientists. This competition will enable HHMI to strengthen its community of researchers and bring innovative approaches to the study of biological problems not only in the biomedical disciplines but also in adjacent fields, such as chemistry, physics and biophysics, biomedical engineering, and computational biology. Candidates should apply directly to HHMI; prior institutional endorsement is not part of the application process.

HHMI, a nonprofit medical research organization, plays a powerful role in advancing biomedical research and education in the United States. The investigator program rests on the conviction that scientists of exceptional talent, commitment, and imagination will make fundamental biological discoveries for the betterment of human health if they receive the resources, time, and freedom to pursue challenging questions. The Institute's investigators, selected through rigorous national competitions, include 11 Nobel Prize winners and 115 members of the National Academy of Sciences.

The Howard Hughes Medical Institute is an equal opportunity employer. Women and members of racial and ethnic groups traditionally underrepresented in the biomedical sciences are encouraged to apply.

HHMI
HOWARD HUGHES MEDICAL INSTITUTE

Neuroscience Faculty

Stony Brook University and the Department of Neurobiology and Behavior are pleased to announce a major initiative in Neuroscience beginning with the recruitment of multiple tenure-track faculty members at the Assistant Professor level in 2007.

Successful candidates will join an active and diverse group of neuroscientists at Stony Brook University and its affiliated institutions, and will participate in the Department's educational mission of undergraduate, graduate, and medical school teaching. Outstanding candidates in all fields of neuroscience will be considered, but those engaged in a multidisciplinary approach to neural circuits and behavior are especially encouraged to apply. Applicants must have a Ph.D. or equivalent degree and postdoctoral experience.

Review of applications starts immediately and will continue until all positions are filled. Exceptional packages include state-funded salary and benefits, newly renovated lab space, and generous start-up funding.

Interested individuals can apply online at *www.stonybrook.edu/cjo* or send C.V., statement of research interests, and contact information for three references to:
Faculty Search Committee, Department of Neurobiology and Behavior, Life Sciences Building, Stony Brook University, SUNY Stony Brook, NY 11794-5230

Reference Number: F-4043-07-04

Equal Opportunity/Affirmative Action Employer. Women, people of color, individuals with disabilities, and veterans are encouraged to apply.

STONY BROOK

Director for the Thomas Jefferson National Accelerator Facility (Jefferson Lab)

Jefferson Science Associates, LLC (JSA) – the Southeastern Universities Research Association and Computer Sciences Corporation/Advanced Technologies Division Joint Venture that serves as the management and operations contractor for the U.S. Department of Energy's Thomas Jefferson National Accelerator Facility (Jefferson Lab) in Newport News, Virginia – invites nominations and applications for the position of Lab Director. The JSA Board seeks a strong and visionary scientific leader with effective management skills who enjoys stature among peers in the scientific and lab communities.

The successful candidate will be responsible for leading and managing all Lab initiatives and activities in support of a world-class research facility, including its strategic and long-range planning and its building of a comprehensive external relations program to serve and promote the interests of the Lab and its users. Reporting to the JSA Board, the Lab Director is also the President of JSA and is responsible for the Lab's 700-plus staff and total annual budget of approximately $100 million.

Jefferson Lab (**www.jlab.org**) is a national laboratory for nuclear physics research. As a user facility for more than 2000 scientists worldwide, its primary mission is to conduct basic research to advance the understanding of the fundamental constituents of the atomic nucleus and their interactions. The tools for probing the structure of the nucleus are the Lab's Continuous Electron Beam Accelerator Facility (CEBAF) and the advanced particle-detection and ultra-high-speed data-acquisition equipment in three experimental halls. Currently operating at 6 GeV, the Lab is in the project engineering and design phase of a $ 300 M upgrade of the electron accelerator to 12 GeV that includes the addition of a fourth experimental hall to investigate the origins of quark confinement through the study of exotic mesons.

The Lab has achieved US leadership and world-class status in its core competency in superconducting radio frequency accelerator technology. It has applied this capability by building the superconducting linac of the Spallation Neutron Source as one of six partner labs and it seeks to position itself similarly for future Office of Science accelerator construction projects. By partnering with industry, government and universities, the Lab developed the world's most powerful Free Electron Laser, thereby providing an opportunity to explore diversification into other scientific arenas.

Nominations, applications, and inquiries should be directed to: **Dr. Jerry Draayer, 1201 New York Ave., NW; Suite 430; Washington, DC 20005; draayer@sura.org**. For timely consideration, submit a resume and outline of qualifications/accomplishments by **15 June 2007**. **Dr. Thomas Appelquist** of Yale University and **Dr. Ernest Moniz** of MIT are, respectively, chair and vice-chair of the Search Committee.

JSA is an Equal Opportunity/ Affirmative Action Employer.

averajobs.org

Healthcare

Research Scientist & Research Technician
Behavioral Genetics Research

Avera McKennan in Sioux Falls, South Dakota, is seeking applications for the following positions. These positions will be responsible for studying the molecular genetics of behavioral disorders.

Research Scientist/Post-doctoral Researcher - *Req. #2339*
A degree in biological science and a PhD in molecular genetics or a related area with post-doctoral study is required. Candidates for this position will need the ability to work independently with minimum supervision. Responsibilities include serving as a group leader and overseeing the day-to-day activities of the laboratory while supervising a group of researchers and bioinformatics analysts.

Research Associate/Technician - *Req. #2340*
A BS in molecular genetics with several years of experience, preferably including an MS in human genetics, is required.

Extensive knowledge and experience in the operation of ABI genetic sequencing and analysis equipment is an essential requirement for both positions. Laboratory experience in genetic linkage and association studies including genotyping of SNP's, microsatellites, DNA pooling analysis and basic statistical approaches are also required. Experience of Affymetrix gene chip technology is preferred.

Applicants will also need to demonstrate a strong interest and record of achievement in researching the genetic mechanisms of complex diseases including a strong publication record in peer reviewed journals.

South Dakota offers an outstanding family oriented environment with plenty of activities for the young and young at heart. The city's low cost of living – with no state income tax and low taxes overall – and cosmopolitan atmosphere provide a pleasant contrast with the idyllic rural setting of the South Dakota countryside.

Avera McKennan offers competitive compensation, benefits and professional growth opportunities in a caring working environment. Positions are open until filled.

Avera McKennan Hospital & University Health Center
Human Resources
email: hr@mckennan.org
www.averajobs.org

Avera McKennan

Equal Opportunity Employer

Does your next career step need direction?

There's only one place to go for career advice if you value the expertise of *Science* and the long experience of AAAS in supporting career advancement - ScienceCareers.org. The pages of *Science* and our website ScienceCareers.org offer:

- Thousands of job postings
- Funding information
- Career advice articles and tools
- Networking opportunities

www.sciencecareers.org

CONFERENCE

8th Annual HBCU-UP National Research Conference

Science and Technology: Knowledge Generators for Global Competitiveness

OCTOBER 4-7, 2007 ▸ WASHINGTON, DC
Grand Hyatt Hotel, 1000 H Street, NW

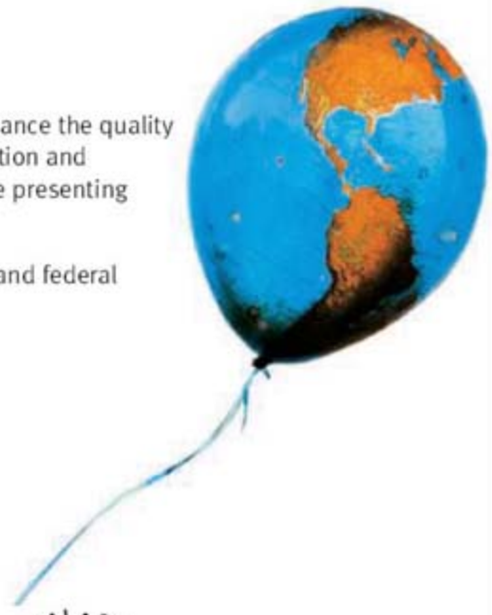

A national gathering of more than 700 students and faculty working together to enhance the quality of undergraduate science, technology, engineering, and mathematics (STEM) education and research at the nation's Historically Black Colleges and Universities. Students will be presenting research in more than 8 STEM fields.

This is an excellent opportunity for representatives from universities, corporations, and federal agencies to promote:

- ▸ Undergraduate Research Opportunities
- ▸ Graduate School Opportunities
- ▸ Fellowship & Internship Opportunities
- ▸ Faculty Research Opportunities

Exhibitor and recruiter information is available at:

www.HBCU-UP.org

The HBCU-UP National Research Conference is organized by AAAS for the National Science Foundation.

NATIONAL SCIENCE FOUNDATION

AAAS
ADVANCING SCIENCE, SERVING SOCIETY

POSITIONS OPEN

CIC nanoGUNE
nanoscience cooperative research center

The Nanoscience Cooperative Research Center **CIC nanoGUNE Consolider (www.nanogune.eu)** invites applications and nominations for three positions as

Group Leaders

CIC nanoGUNE Consolider, located in San Sebastian, Basque Country (Spain), is a R&D center created recently with the mission of conducting basic and applied world-class research in nanoscience and nanotechnology, fostering training and education excellence, and supporting the growth of a nanotechnology-based industry.

The Group Leaders of nanoGUNE will be responsible for the design, management, and operation of their respective Research Area and laboratories. At the present time, nanoGUNE is welcoming applicants in the following disciplines:

- Nanofabrication and nanostructure assembly (#001)
- Synthesis of nanomaterials and nanostructures (#002)
- Biological nanostructures and nanobiotechnology (#003)

Candidates should have an outstanding track record of research, with an orientation to nanoscience and nanotechnology, a proven ability to obtain competitive research funding, and a proven record of technological transfer initiatives. Proficiency in spoken and written English is compulsory; knowledge of Spanish is not a requirement. An attractive remuneration will be offered.

Applicants should forward their CV, a summary of research interests, and a list of at least three references to director@nanogune.eu

Closing date: 30 June 2007

AWARDS

RANBAXY RESEARCH AWARDS 2006

RESEARCH FOR LIFE
RANBAXY
SCIENCE FOUNDATION

Nominations are invited from Heads of Research Institutions, Universities and Medical & Pharmaceutical Colleges, for the Ranbaxy Research Awards-2006. There are four Awards of Rs. 1 lakh each, for excellence in original research, in Medical and pharmaceutical Sciences.

Medical Sciences
One Award each for Basic Research, Medical Research and Clinical Research.

Pharmaceutical Sciences
One Award

The sponsored work of Indian scientists, both in India and abroad, together with their bio-data, research achievements, awards received in the past and papers published, may be forwarded (in 12 bound sets) to the Ranbaxy Science Foundation by July 2, 2007.

Details of the procedure are being circulated to nominators and are also available from the office of the Foundation and on **our Website**. A panel of judges, comprising eminent scientists, will review the research work. Non-resident Indian scientists are also eligible for these awards.

Dr. O.P. Sood
Member-Governing Council
RANBAXY SCIENCE FOUNDATION
77B, Sector 18, IFFCO Road, Udyog Vihar Industrial Area, Gurgaon-122 015 (Haryana) India
Phone : 91-124-2341477 (D) 2342001-10, 4012501-10
Fax : 91-124-2342018, 2342017
E-mail : omprakash.sood@ranbaxy.com
Website : http://www.ranbaxysciencefoundation.com

POSITIONS OPEN

ASSISTANT or ASSOCIATE PROFESSOR (Neurobiology)

The Department of Veterinary Biosciences in the College of Veterinary Medicine at the University of Illinois at Urbana-Champaign invites applications for Assistant or Associate Professor as a **NEUROBIOLOGIST.**

Candidates must possess a Ph.D. or equivalent degree from an accredited institute. Postdoctoral training and neurobiology teaching experience are desirable. Candidates with a research focus in neuroendocrinology, neuropharmacology, neurotoxicology, or neuroimaging or who hold the D.V.M. or equivalent degree are preferred.

The successful candidate will develop a research program which complements existing Department and campus strengths in reproductive biology, neuroscience, and environmental toxicology; full information about the Department is available at **website: http://www.cvm.uiuc.edu/vb/index.cfm** and about the campus Neuroscience Program at **website: http://www.life.uiuc.edu/neuroscience/.** The successful candidate will teach neurobiology in the veterinary curriculum, participate in graduate instruction, and develop an independently funded research program. Academic and other service is also expected.

Appointment will be full-time, tenure-track (nine-month) on an academic-year basis with the possibility of supplementing salary from extramural research grants for up to three summer months. The appointment is expected to begin on or after August 16, 2007.

Salary and rank are negotiable and commensurate with qualifications.

Qualified applicants should electronically submit a cover letter, curriculum vitae, and contact information for three references to: **Linda Swett, Search Coordinator (e-mail: lswett@uiuc.edu).** Questions may be directed to **Dr. Paul Cooke, Chair; e-mail: p-cooke@uiuc.edu** or **telephone: 217-333-6825.**

In order to ensure full consideration, applications must be received by June 15, 2007. *Minority, women, and other designated classes are encouraged to apply. The University of Illinois is an Equal Opportunity Employer.*

THE UNIVERSITY of CHICAGO

The University of Chicago's Department of Radiation and Cellular Oncology and the Ludwig Center for Metastasis Research is seeking applicants for full time **RESEARCH ASSOCIATE, JUNIOR RANK** (Instructor, Assistant Professor) positions. The primary activity of a Research Associate is research in association with a faculty member or team. Candidates are required to possess a Doctorate degree and prior research experience in the field of molecular and cellular biology and/or models of metastasis. Compensation is dependant on qualifications. The University provides a generous package of fringe benefits.

Interested candidates should submit curriculum vitae, bibliography, a statement of research, and contact information for three professional references to: **Dr. Weichselbaum, c/o Janet Riley, Department of Radiation and Cellular Oncology, 5758 S. Maryland Avenue MC9006, Chicago, IL 60637** or via **e-mail: jriley@radonc.uchicago.edu.** For information about the University of Chicago please consult **website: http://uchicago.edu.**

The University of Chicago is an Affirmative Action/Equal Opportunity Employer.

POSITION ANNOUNCEMENT
University of Connecticut

ASSISTANT PROFESSOR: MOLECULAR BIOLOGIST specializing in crop improvement.

For details see: Department of Plant Science, position search #2007102 **(website: http://www.hr.uconn.edu/jobs-fac.html).**

We encourage applications from underrepresented groups, including minorities, women, and people with disabilities.

POSITIONS OPEN

ASSISTANT DIRECTOR, FLOW CYTOMETRY AND CELL SORTING CORE

Applications are invited for Assistant Director, Flow Cytometry and Cell Sorting (FACS) Core Facility in the University of South Carolina School of Medicine Instrumentation Resource Facility **(website: http://dba.med.sc.edu/price/irf/irf.htm).** This will be a full-time research track faculty position that will involve 50 percent time towards development of FACS Core and 50 percent time dedicated to development of an individual's own research program. The FACS Core will be a service facility developed to assist other Principal Investigators and their laboratories in experiments that involve analysis and cell-sorting technologies. A strong background in immunology, experience in hands-on operation of a FACS system, and interpretation of FACS data are essential. A background in stem cell biology is desirable. The candidates can have research experience in any area of biomedical sciences although preference will be given to those interested in cancer, HIV/AIDS, or cardiovascular development and disease. Review of applicants will begin immediately and continue until the position is filled. Applicants should submit their curriculum vitae, future research plans, and three letters of reference to: **Dr. Robert Price, Director, Instrumentation Resource Facility, University of South Carolina School of Medicine, Columbia, SC 29208. E-mail: price@med.sc.edu.** *The University of South Carolina is an Affirmative Action, Equal Opportunity Institution.*

DIRECTOR, Division of Viral and Rickettsial Diseases (DVRD), the National Center for Zoonotic, Vectorborne and Enteric Diseases (NCZVED), CDC, is seeking an exceptional candidate for the position of Director, DVRD. The mission of DVRD is to prevent illness and death caused by viral and rickettsial infectious diseases of public health importance in the United States and throughout the world. The Division fully integrates modern laboratory and epidemiologic science for the accomplishment of it mission; disease surveillance and epidemiologic field investigations are integrated with microbiologic and molecular biological laboratory technologies and many special reference diagnostic services. These programs are national and international in scope and involve laboratory research, surveillance, medical, and epidemiology service activities. The Director oversees complex scientific and epidemiological programs in the field of viral and rickettsial diseases, and working with DVRD staff, conceives and establishes program plans and objectives and provides overall direction in their accomplishment, and provides guidance in program development and identification of scientific goals.

Inquiries made before May 14, 2007, may be directed to **Dr. Mark Eberhard, Chair, Search Committee,** at **e-mail: meberhard@cdc.gov.** *CDC is an Equal Opportunity Employer.*

POSTDOCTORAL RESEARCH SCIENTIST
Tissue Engineering and Regenerative Medicine Laboratory (TERML)
Columbia University Medical Center

We seek a self-motivated individual (Ph.D.) with expertise in molecular biology and molecular genetics and previous documented experience in transgenic models with previous publication record in these areas. Ability to work collaboratively with stem cell biologists, bioengineers, and computer-aided design and computer-aided manufacturing engineers, with a common goal to engineer biologically derived tissues and organs. Position is grant-funded and is available immediately; salary commensurate with experience.

Applicants should send a statement of career goals, specific research interest, contact information for three references, and full-length curriculum vitae to **Sarah Kennedy (e-mail: sk2848@columbia.edu).**

Columbia University is an Affirmative Action/Equal Opportunity Employer.

RAMON MARGALEF prize in ecology and environmental sciences

The Autonomous Government of Catalonia (Spain) launches the 2007 edition of the 100,000 International Ramon Margalef Prize in Ecology

THE PRIZE

- The main objective is the recognition of a scientific career or a discovery in ecology or another environmental science which has significantly contributed to scientific knowledge.
- It is awarded to living individuals, to legal entities or to groups from all over the world.
- The prize is worth 100,000.

NOMINATIONS

- Nominations can be submitted by qualified representatives of universities, higher institutions of learning, research centres, winners of the Prize in previous years or former members of the Jury.
- They should be submitted through a letter or statement of well reasoned justification, accompanied by a curriculum vitae of the candidate.
- The nominations should be addressed to the Technical Secretariat of the Prize, Presidency Office of the Autonomous Government of Catalonia (Generalitat de Catalunya).

For detailed information please refer to:
www.gencat.cat/premiramonmargalef

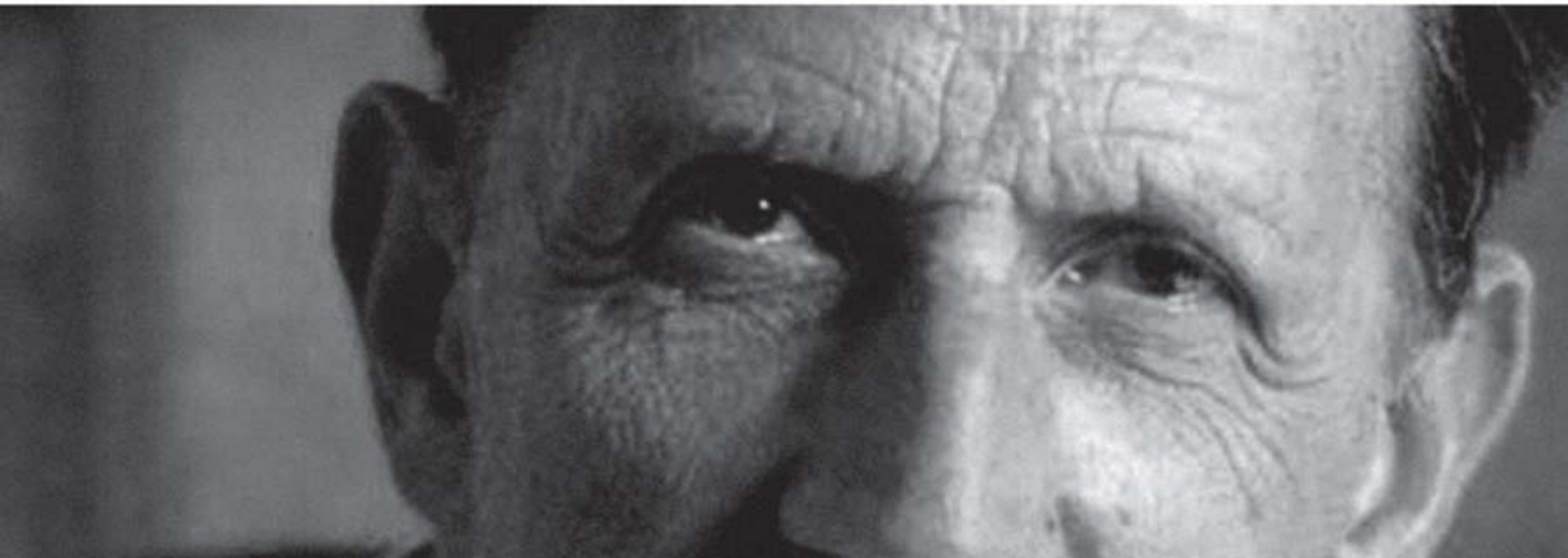

POSITIONS OPEN

POSTDOCTORAL POSITION

A Postdoctoral position is available immediately in the Schubiger Laboratory, with NIH funding for four years. The Laboratory is investigating regeneration in *Drosophila* imaginal discs and we have recently identified three genes necessary for the location and timing of blastema formation. These genes all have vertebrate homologues. Our work addresses a fundamental question in developmental biology and will provide an opportunity for the candidate to build a career in this area. Applicants should have a Ph.D., have experience in molecular genetics, be able to work independently, and have a strong publication record. Applications should include curriculum vitae and three references. It is expected that candidates will apply for their own funding during the first year.

Applications should sent to: **Gerold Schubiger, Department of Biology, P.O. Box 351800 University of Washington, Seattle, WA 98195-1800. Telephone: 206-543-8158, e-mail: gerold@u.washington.edu.**

The University of Washington is an Affirmative Action, Equal Opportunity Employer. The University is building a culturally diverse faculty and staff and strongly encourages applications from women, minorities, individuals with disabilities, and covered veterans.

INSTITUE of HUMAN VIROLOGY
University of Maryland School of Medicine
Baltimore, Maryland

The Institute of Human Virology is seeking to fill a **TENURE-TRACK FACULTY POSITION** with an investigator with the ability to establish an independent research program centering on the molecular biology/virology of human papilloma virus and its interactions with host cell factors, especially those relevant to cancer. The successful candidate will have a demonstrable track record of relevant publications in peer-reviewed journals and of attracting peer-reviewed funding, preferably related to cancer. The level of appointment will be commensurate with the candidate's experience. Interested applicants are requested to forward curriculum vitae in PDF format to: **Chairperson, IHV Faculty Search Committee, Institute of Human Virology, 725 W. Lombard Street, Baltimore, MD 21201.**

The University of Maryland, Baltimore, is an Equal Opportunity, Affirmative Action Employer.

RESEARCH TRAINING FELLOWSHIP
Yale University School of Medicine

Underrepresented minority openings for a two to three-year NIH-supported postdoctoral training program in vascular biology (molecular and translational) with rolling admission at the Yale University School of Medicine. Interested candidates should be M.D.s, Ph.D.s, or M.D./Ph.D.s, may have completed clinical training, and *must be U.S. citizens or permanent residents.* Contact:

Jeffrey R. Bender, M.D.
Yale University School of Medicine
Anlyan Center for Medical Research, S-469A
300 Cedar Street
P.O. Box 208017
New Haven, CT 06510
E-mail: jeffrey.bender@yale.edu

RESEARCH ASSOCIATE/SENIOR RESEARCH ASSOCIATE

T cell and APC signaling and T cell function. Candidates will build upon new insights concerning cooperation between innate/adaptive immunity. Well-funded and highly productive Laboratory of 14 with four faculty. Contact: **M. Edward Medof, M.D., Ph.D. E-mail: mxm16@case.edu.**

RESEARCH ASSOCIATE (multiple positions) with experience in mass spectrometry. Send resume to: **J. Schenkel, Case Western Reserve University, School of Medicine, 10900 Euclid Avenue, BRB933, Cleveland, OH 44106.** Must reference job code FF4007.

Seeking **POSTDOCTORAL RESEARCH FELLOW** in Winston-Salem, Forsyth County, North Carolina. Requires knowledge in biochemical, histopathological and heratological research. Perform sodium dodecyl sulfate-polyacrylamide gel electrophoresis and Western blot analysis on samples from transgenic mouse facility and from tissue cultures. Care and maintain stable CHO Apo A-1 mutant cell lines in tissue culture as well as HepG2 and COS cells. Requires experience in protein expression using *E.coli* hosts and the purification of thee proteins using classical biochemical techniques. Requires use of these expressed protein in preparing discoidal recombinant lipid protein complexes, lipid extraction, trypsin digestion and mass spectroscopy in order to map the tertiary structure of the lipid binding apoprotein. Requires Ph.D. in biology or biochemistry. Requires: knowledge and use of mass spectrometer; two years of experience with mass spectrometer machines; and use of high performance liquid chromatography machines. Salary $48,298 a year. Work schedule: Monday through Friday, 8:30 a.m. to 5 p.m. Send resumes by **fax: 484-270-1600** or by mail to: **Backlog Elimination Center, Employment and Training Administration, Division of Foreign Labor Certification, 1 Belmont Avenue, Suite 220, Bala Cynwyd, PA 19004.** Reference ETA case number P-05152-49230wo15 in replies. *Affirmative Action/Equal Opportunity Employer.*

THREE-YEAR POSTDOCTORAL FELLOWSHIP
for Work on Human ES Cell-Derived Motor Neurons

We seek a Postdoctoral Fellow with experience in working with human ES cells to join a privately funded laboratory in Manhattan associated with Columbia University. The candidate will use motor neuron derived from new ES cell lines to study disease mechanisms in amyotrophic lateral sclerosis and spinal muscular atrophy. The work will be carried out in collaboration with scientists at the Harvard Stem Cell Institute and the Memorial Sloan-Kettering Cancer Center. The fellowship is for three years. Salary in excess of $45,000, commensurate with experience.

Applications consisting of full curriculum vitae and covering letter with details of at least two references should be sent to:

Mary Lee
Project ALS/Jenifer Estess Laboratory for Stem Cell Research
E-mail: projectals.employ@gmail.com
Website: http://www.projectals.org

THE UNIVERSITY of CHICAGO

The University of Chicago/Department of Radiation and Cellular Oncology and the Ludwig Center for Metastasis Research is seeking applicants for full-time **POSTDOCTORAL SCHOLAR POSITIONS.** The primary activity of a Research Associate is research in association with a faculty member or team. Candidates are required to possess a Doctorate degree and prior research experience in the field of molecular and cellular biology and/or models of metastasis.

Interested candidates should submit curriculum vitae, bibliography, a statement of research, and contact information for three professional references to: **Dr. Weichselbaum, c/o Janet Riley, Department of Radiation and Cellular Oncology, 5758 S. Maryland Avenue MC9006, Chicago, IL 60637** or via **e-mail: jriley@radonc.uchicago.edu.**

The University of Chicago is an Affirmative Action/Equal Opportunity Employer.

POSTDOCTORAL POSITION available at the University of California, Los Angeles, to study Regulatory T cells development and function *(Nature Immunology.* **8**:359-68, 2007, *Journal of Immunology* **178**:2961-72, 2007). Experience in molecular biology and immunology desirable. Send curriculum vitae, a brief description of research experience, and names of three references to **Dr. Talal Chatila (e-mail: tchatila@mednet.ucla.edu).**

POSTDOCTORAL POSITIONS
Molecular Microbiology and Pathogenesis of Bacterial and Viral Infections

National Institute of Allergy and Infectious Diseases training grant-funded Postdoctoral positions are available at the University of Colorado Health Sciences Center to study molecular mechanisms of bacterial infections (with **Randall Holmes, Michael Schurr, Michael Vasil, Andres Vazquez-Torres,** or **Martin Voskuil**), molecular aspects of viral infections (with **David Barton, Thomas Campbell, Robert Garcea, Donald Gilden, Kathryn Holmes, Jerome Schaack, Kenneth Tyler,** or **Linda Van Dyk**), molecular basis of innate immunity (**with Charles Dinarello, Sonia Flores,** or **Andres Vazquez-Torres**), or structural biology of microbial pathogenesis (with **Mair Churchill**). See **website: http://www.uchsc.edu/sm/microbio/** for information about many of our research programs. Research facilities, grant funding, and training environment are excellent. Candidates with Ph.D. or equivalent research degrees must have experience in microbiology, bacteriology, virology, immunology, molecular biology, genetics, biochemistry, cell biology, structural biology, or a related field. Candidates with M.D., D.V.M., or equivalent clinical degrees must have demonstrated competency for research related to our program. Individuals from underrepresented groups in the biomedical sciences are encouraged to apply. Compensation is determined by NIH policies. *Applicants for these positions must be citizens or permanent residents of the United States.* Submit curriculum vitae, bibliography, and names of three professional references to: **Training Program Director, UCHSC at Fitzsimons, Microbiology Department, Mail Stop 8333, P.O. Box 6511, Aurora, CO 80045** or **e-mail randall.holmes@uchsc.edu.** *The University of Colorado Health Sciences Center is committed to Equal Opportunity and Affirmative Action.*

DIRECTOR, Neuroscience Imaging and Physiology Facility, University of Vermont. Duties: maintain systems, train users, design experiments, collect data. Opportunities: collaborate with researchers and teach optical imaging course. Facility includes: BioRad Radiance multiphoton microscope, Applied Precision Deltavision restoration microscope, Nikon total internal reflection microscope, ratiometric imaging system and Noran laser scanning confocal microscope, and electrophysiology equipment. Minimum qualifications: Master's degree in related science and three to five years of experience in confocal, multi-photon, and deconvolution microscopy as applied to cell biological problems required, or an equivalent combination. Ideal: neuroscience background, computer expertise, excellent interpersonal and communication skills. Apply online, **website: http://www.uvmjobs.com.** *The University of Vermont is an Equal Opportunity/Affirmative Action Employer. Applications from women and people from diverse racial, ethnic, and cultural backgrounds are encouraged.*

MARKETPLACE

Tools for Cell Biology Research

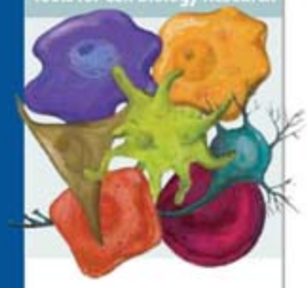

R&D Systems Proteome Profiler™ Arrays

Simultaneously detect multiple proteins in a single sample.

R&D Systems offers these Array Kits:

- Human Cytokine Array Kit, Panel A
- Human Phospho-Immunoreceptor Array Kit
- Human Phospho-Mitogen-Activated Protein Kinase (MAPK) Array Kit
- Human Phospho-Receptor Tyrosine Kinase (RTK) Array Kit

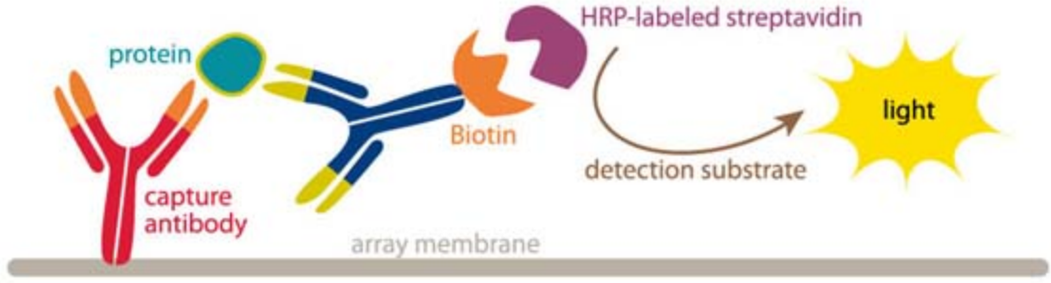

Proteome Profiler Arrays enable the measurement of the relative levels of phosphorylation or abundance of multiple proteins in a single serum, plasma, or cell culture supernatant sample. Proteome Profiler kits contain buffers, detection antibodies, and membranes spotted in duplicate with capture antibodies carefully selected for their specificity. And with chemiluminescent detection, no specialized equipment is necessary.

Rapid | **Highly specific** | **Sensitive** | **Efficient**

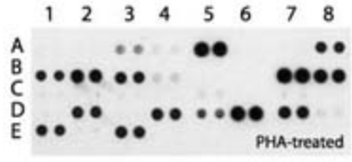

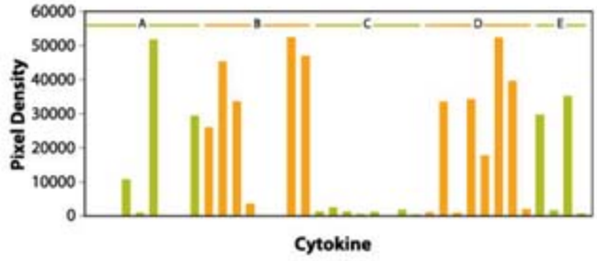

Sample data for **R&D Systems Human Cytokine Array, Panel A** demonstrating high-throughput multi-analyte profiling of 36 cytokines, chemokines, and acute phase proteins in a single sample of PBMC supernatant.

For more information visit our website at **www.RnDSystems.com/go/ProteomeProfiler**

U.S. & Canada
R&D Systems, Inc.
Tel: (800) 343-7475
info@RnDSystems.com

Europe
R&D Systems Europe Ltd.
Tel: +44 (0)1235 529449
info@RnDSystems.co.uk

Selection expanding weekly—visit www.RnDSystems.com to sign up for weekly new product updates.

R&D SYSTEMS®